


Title	Monitoring and modelling the morphodynamic evolution of a breached barrier beach system
Author(s)	O'Shea, Patrick Michael
Publication date	2015
Original citation	O'Shea, P. M, 2015. Monitoring and modelling the morphodynamic evolution of a breached barrier beach system. PhD Thesis, University College Cork.
Type of publication	Doctoral thesis
Rights	© 2015, Patrick Michael O'Shea. http://creativecommons.org/licenses/by-nc-nd/3.0/ 
Embargo information	No embargo required
Item downloaded from	http://hdl.handle.net/10468/3359

Downloaded on 2018-08-23T18:02:56Z



UCC

University College Cork, Ireland
Coláiste na hOllscoile Corcaigh

Ionad Taighde Hiodráilice agus Mara,
Rionn na hInnealtóireachta Sibhialta agus Timpleallachta,
Coláiste na hOllscoile Corcaigh,



Monitoring and Modelling the Morphodynamic evolution of a breached barrier beach system

Patrick Michael O'Shea

A thesis submitted for the Degree of Doctor of Philosophy

In the School of Engineering
Department of Civil and Environmental Engineering
National University of Ireland, Cork

Supervisors: Dr. Jimmy Murphy & Prof. Tony Lewis,
Hydraulics & Maritime Research Centre,
Dept. Civil & Environmental Engineering,
University College Cork,
Ireland.

Head of School: Prof. Nabeel Riza

Table of Contents

Abstract.....	vii
Acknowledgements.....	ix
List of Figures	vii
List of Tables.....	xviii
Nomenclature.....	xix
Acronyms.....	xx
1 Introduction.....	1
1.1 Introduction.....	1
1.2 Environmental Setting.....	3
1.3 Scope of Research	5
1.4 Outline of Theses.....	6
1.4.1 Chapter 2.....	6
1.4.3 Chapter 3.....	7
1.4.4 Chapter 4.....	7
1.4.5 Chapter 5.....	7
1.4.6 Chapter 6.....	8
1.4.7 Chapter 7.....	8
1.4.8 Chapter 8.....	8
1.5 Publications	8
2 Literature Review	10
2.1 Introduction.....	10
2.2 Coastal Zone Processes.....	11
2.2.1 Coastal Zone Hydrodynamics	11
2.2.2 Sediment Transport.....	15

2.3 Coastal Morphology	19
2.3.1 Beach Morphology Classification	19
2.3.2 Barrier Beaches.....	22
2.3.3 Barrier Beach Breaching	24
2.3.4 Dune Erosion.....	33
2.3.5 Inlet dynamics	34
2.4 Coastal Morphodynamic Monitoring Techniques.....	45
2.4.1 Coastal Hydrodynamic Monitoring.....	45
2.4.2 Sediment Transport Monitoring	60
2.5 Numerical Modelling of Coastal Processes	75
2.5.1 Profile evolution models	75
2.5.2 Coastal Area Models	77
2.5.3 Long-term Morphodynamic Modelling	82
2.6 Previous Studies of Dingle Bay	87
2.6.1 Formation and Geological Studies	87
2.6.2 Wave Climate and Morphology	91
2.6.3 Wave and Storm Impact Modelling.....	96
2.7 Conclusions	102
3 Coastal Evolution of Dingle Bay	104
3.1 Introduction.....	104
3.2 Long term evolution of Dingle Bay	104
3.3 Recent Evolution.....	111
3.4 Cross-sectional Analysis.....	114
3.5 Tidal Inlet and ebb Tidal Bar Evolution	122
3.6 Sediment Transport Analysis	128
3.7 Conclusions	134
4 Wind, Wave and Hydrodynamic Monitoring.....	135

4.1	Introduction.....	135
4.2	Field Data Collection.....	136
4.2.1	Wave Data.....	136
4.2.2	Tidal Current Data	149
4.2.3	Morphological Analysis of Hydrodynamic Field Data.....	154
4.2.4	Sediment Dye Test	156
4.2.5	Sediment Fencing	157
4.2.6	Aeolian Sediment Transport Measurement	160
4.3	Bathymetry	164
4.3.1	Previous Bathymetric Surveys in Dingle Bay.....	164
4.3.2	Design of PWC Surveyor.....	166
4.3.3	Error analysis of PWC Survey Craft	167
4.3.4	Bathymetry Survey of March 2013	169
4.3.5	Bathymetry Survey of September 2013.....	170
4.3.6	Morphodynamic analysis of near shore Bathymetric Surveys	171
4.4	Sediment Trend Analysis.....	181
4.4.2	Sediment sampling	181
4.4.3	Sediment sieving analysis	183
4.4.4	Grain Size Trend Analysis Results	185
4.5	Conclusions	191
5	Dingle Bay Ocean Radar Trial.....	193
5.1	Introduction.....	193
5.2	Dingle Bay Radar Setup	194
5.3	Wave Radar Results.....	198
5.3.1	Validation of Results.....	198
5.3.2	Surface Current Mapping	201
5.3.3	Wave Height Mapping	207

5.4 Error analysis.....	212
5.4.1 Error Identification	212
5.4.2 Transect method	216
5.5 Error Analysis Results	219
5.6 Critique of HF ocean radar	223
5.7 Conclusions	225
6 Morphodynamic Modelling.....	227
6.1 Introduction	227
6.2 Numerical Model Set up	228
6.2.1 Model Domain and Boundary Conditions	228
6.3 Model validation.....	230
6.3.1 Tidal height and current validation.....	231
6.3.2 Wave height and Wave Period validation	233
6.3.3 Sediment Transport and Morphology	234
6.4 Morphodynamic Modelling Approach.....	236
6.5 Morphodynamic Modelling – Stage 1.....	238
6.5.1 Stage 1 Approach.....	238
6.5.2 Stage 1 Results	238
6.5.3 Conclusions from Stage 1	247
6.6 Morphodynamic modelling – Stage 2.....	249
6.6.1 Stage 2 Approach.....	249
6.6.2 Stage 2 Results	250
6.6.3 Conclusions from Stage 2	255
6.7 Morphodynamic modelling – Stage 3.....	256
6.7.1 Stage 3 Approach.....	256
6.7.2 Stage 3 Results	256
6.7.3 Conclusions from Stage 3	263

6.8 Comparison with sediment trend analysis	264
6.8.1 General.....	264
6.8.2 Results	265
6.8.3 Conclusions on GSTA and Numerical Modelling Comparison....	266
6.9 Conclusions	267
7 Predicting the Evolution of Inner Dingle Bay	269
7.1 Introduction.....	269
7.2. Summary of Findings.....	270
7.3 Critical Components to establishing Timescale of Evolutionary Cycle	272
7.3.1 Quantifying limits of Breach Width Erosion.....	272
7.3.2 Ebb Tidal Bar migration and Channel Infilling.....	274
7.3.3 Aeolian driven dune regeneration.....	278
7.4 Flood risk.....	283
7.5 Intervention Strategy.....	289
7.5.1 Stage 1 – Beach Nourishment / Dredging	289
7.5.2 Stage 2 Sediment Fencing	292
7.5.3 Stage 3 Sediment Fencing	293
7.5.4 Summary	294
7.6 Conclusion.....	295
8 Conclusions	297
8.1 Introduction.....	297
8.2 Innovative Aspects of Study	298
8.3 Characteristics of Governing Coastal Processes on Rossbeigh.....	300
8.4 Sediment Transport Pattern.....	301
8.5 Long Term Behaviour	302
8.6 Assessment of Experimental techniques	303

8.7 Further Research Recommendations	305
8.7.1 Field Data and Numerical Modelling.....	305
8.7.2 Wave Radar	305
8.7.3 Intervention.....	305
8.7.4 Flood protection.....	306
8.8 Closure	307
References.....	308

Declaration

I hereby declare that this thesis is my own work and effort and that it has not been submitted either at university College Cork or elsewhere for any award.

Where other sources of Information have been used, they have been acknowledged.

Signature:.....

Date:.....

Abstract

Predicting the evolution of a coastal cell requires the identification of the key drivers of morphology. Soft coastlines are naturally dynamic but severe storm events and even human intervention can accelerate any changes that are occurring. However, when erosive events such as barrier breaching occur with no obvious contributory factors, a deeper understanding of the underlying coastal processes is required. Ideally conclusions on morphological drivers should be drawn from field data collection and remote sensing over a long period of time. Unfortunately, when the Rossbeigh barrier beach in Dingle Bay, County Kerry, began to erode rapidly in the early 2000's, eventually leading to it breaching in 2008, no such baseline data existed. This thesis presents a study of the morphodynamic evolution of the Inner Dingle Bay coastal system. The study combines existing coastal zone analysis approaches with experimental field data collection techniques and a novel approach to long term morphodynamic modelling to predict the evolution of the barrier beach inlet system. A conceptual model describing the long term evolution of Inner Dingle Bay in 5 stages post breaching was developed. The dominant coastal processes driving the evolution of the coastal system were identified and quantified. A new methodology of long term process based numerical modelling approach to coastal evolution was developed. This method was used to predict over 20 years of coastal evolution in Inner Dingle Bay. On a broader context this thesis utilised several experimental coastal zone data collection and analysis methods such as ocean radar and grain size trend analysis. These were applied during the study and their suitability to a dynamic coastal system was assessed.

Acknowledgements

Completing this PhD thesis would not have been possible without the help and advice of many people.

Firstly, I would like to thank my supervisor, Dr Jimmy Murphy, for all his guidance and support over the past 4 years. Without him, I simply would not have been able to complete this thesis. I would also like to thank my co-supervisor Prof. Tony Lewis, who afforded me the opportunity to work and study at the Hydraulics and Maritime Research Centre.

I have received great support from my colleagues at the HMRC, especially from Mr. Thomas Walsh, Mr. Niall O'Sullivan, Dr. Keith O'Sullivan and Mr. James Kelly without whom the field work would not have been possible.

I would like to thank the CMRC and the Department of Geography in U.C.C., and in particular Mr. Jeremy Gault for the use of equipment during this research. I would also like to acknowledge the advice I received from Professor Mal Heron of Cooke University, Australia on ocean radar analysis and Dr Max Kozyachenko and Dr. Emmanuel Poizot, on sediment analysis.

I would like to thank the Marine Institute for providing the recording current meters and ocean wave data and also travel funding for WERA training required for this research.

Finally, I would like thank my parents, Colette and Leo for encouraging me to pursue this Phd, my sisters Aoife and Alanna who both served their time as assistants on Rossbeigh, and my fiancée Annette, for her patience and understanding over the last four years.

List of Figures

Figure 1.1 Study Area	3
Figure 2.1 Spatio-Temporal Scales of Coastal Change (Steve et al., 2001).....	11
Figure 2.2 Wave Refraction (source: http://piru.alexandria.ucsb.edu)	12
Figure 2.3 Breaker Types (Chadwick & Morfett, 1998)	13
Figure 2.4 Longshore Currents (Source: www.srh.noaa.gov)	14
Figure 2.5 Rip Currents (MacMahan et al., 2006)	15
Figure 2.6 Beach Morphological zones (CEM, 2002).....	19
Figure 2.7 Beach Morphology Classifications (Masselink & Short, 1993)	21
Figure 2.8 Barrier Beach Classifications (Cope, 2004)	23
Figure 2.9 Transition from DAS to SAB through macro cannibalisation (Stephan, 2009)	25
Figure 2.10 Development of micro Cannibalisation (Orford et al., 1996)	26
Figure 2.11 Cannibalisation in Rio Chico (Isla et al., 2000)	27
Figure 2.12 Little Pikes Inlet (Terchunian et al., 1995).....	28
Figure 2.13 Belongil beach (Baldock et al., 2008).....	29
Figure 2.14 Nauset Barrier Beach System (Giese et al., 2007)	31
Figure 2.15 Conceptual model of the evolution of Nauset beach (Giese et al., 2009).....	32
Figure 2.16 Historical breaches in Bartra Barrier (Cooper et al., 2011)	33
Figure 2.17 DUNERULE Schematic (Van Rijn, 2009).....	34
Figure 2.18 Escoffier diagram of maximum velocity and equilibrium velocity versus inlet cross-sectional area (Escoffier, 1940, amended).....	35
Figure 2.19 Model 1 of FitzGerald's classification (FitzGerald et al., 2000)	36
Figure 2.20 Model 2 of FitzGerald's classification (FitzGerald et al., 2000)	37
Figure 2.21 Model 3 of FitzGerald's classification (FitzGerald et al., 2000)	38
Figure 2.22 Model 4 of FitzGerald's classification (FitzGerald et al., 2000)	39
Figure 2.23 Model 5 of FitzGerald's classification (FitzGerald et al., 2000)	40
Figure 2.24 Model 6 of FitzGerald's classification (FitzGerald et al., 2000)	41
Figure 2.25 Four stage conceptual model (Vila-Concejo, 2007)	42
Figure 2.26 Two stage conceptual model (Michel et al., 1997)	43
Figure 2.27 Morphological cycle of Five Finger strand (Cooper et al., 2007)	44
Figure 2.28 Waverider buoy (Courtesy Of Marine Institute).....	46

Figure 2.29 Fugro Wave scan PRH buoy (Courtesy Marine Institute)	47
Figure 2.30 Valeport Bottom Mounted Pressure Sensor Wave Gauges	48
Figure 2.31 CODAR installation in California (UC Davis Bodega Laboratory)	50
Figure 2.32 Frequency modulated continuous radar chirp (www.helzel.com).....	51
Figure 2.33 WERA TX array (www.helzel.com)	52
Figure 2.34 WERA RX array (www.helzel.com).....	52
Figure 2.35 Bragg scattering effect (WERA 2008)	53
Figure 2.36 Doppler Spectrum of backscattered radar (Helzel, 2006)	54
Figure 2.37 WERA Beam formed range vs frequency	55
Figure 2.38 Range resolution vs transmission bandwidth	55
Figure 2.39 Comparison of Radar, ADCP and simulated tidal currents (Cochin, 2006)	57
Figure 2.40 RCM 8 rotor based current meter (Source: www.aanderra.com).....	58
Figure 2.41 Propeller type current meter (Source: www.Valeport.co.uk)	59
Figure 2.42 Electromagnetic current meter (Source: www.Valeport.co.uk).....	59
Figure 2.43 Bottom Mounted ADCP (Source: www.awi.de).....	60
Figure 2.44 Schematic of side mounted ADCP (Courtesy of Sontek)	60
Figure 2.45 Dispersion results of sediment dye tracer experiments (Bertin et al., 2007).....	62
Figure 2.46 OBS surf zone rig (Masselink, 2007)	63
Figure 2.47 Delft Bottle Sampler (Dijkman 1978).....	64
Figure 2.48 Bed load Transport meter (Delft Hydraulics, 1958).....	65
Figure 2.49 Helley-Smith bed load sampler (Helley et al., 1971)	65
Figure 2.50 Sediment trend analysis pre and post dredging (Poulus et al., 2010).....	68
Figure 2.51 FB+ Case in Cadiz (Poizot, 2008).....	69
Figure 2.52 Conceptual model of foreshore trend variation (Poizot, 2008)	69
Figure 2.53 Wedge Shaped Aeolian Sediment Trap (Nickling et al., 1995)	70
Figure 2.54 Modified MWAC vertical sediment profiler	72
Figure 2.55 Anemometer and Camera set up (Delgado-Fernandez, 2013)	73
Figure 2.56 Moisture profile mapping process (Delgado-Fernandez, 2013)	74
Figure 2.57 Airflow simulations over dune blowout (Smyth, 2011).....	74
Figure 2.58 X-beach model of Trabucador barrier beach system (Gracia, 2013).....	76

Figure 2.59 Model Architecture of Delft 3D (Delft 3D Manual)	77
Figure 2.60 Flexible Mesh from DHI Mike 21	78
Figure 2.61 Erosion/Deposition rates of spring tide and spring to neap on Arklow Bank (Panigrahi, 2009).....	80
Figure 2.62 Morphodynamic model module flow chart (Mason & Garg, 2001)	81
Figure 2.63 Simulated sediment transport (Herling & Winter, 2013)	82
Figure 2.64 a. Differential bathymetry 1995-2000 and b. Simulated 5 year bed evolution (Villaret, 2012)	85
Figure 2.65 Mid ebb and mid flood velocity vectors and suspended sediment concentration after 30 year simulation (XI et al., 2009).....	86
Figure 2.66 Location of samples used in Luminescence dating (Wintle et al., 1998).....	88
Figure 2.67 Cross-section of test locations on Inch (Wintle et al., 1998)	88
Figure 2.68 Salt marsh accretion rate measurement locations (Duffy & Devoy, 1998).....	91
Figure 2.69 Division of Rosbeigh (Sala, 2010).....	92
Figure 2.70 Currents in Dingle Bay (Admiralty, 2006).....	93
Figure 2.71 Seasonal storm events from 1958 to 1994 with increasing average frequency (black line) (Sala, 2010)	94
Figure 2.72 Wave gauge data compared to offshore wave buoy (Vial, 2008).....	95
Figure 2.73 Conceptual model of breaching at Rossbeigh (Sala, 2010)	96
Figure 2.74 Distribution of Wave Energy under A) Modal swell and B) 90 th Percentile storm (Cooper et al., 2011) - Darker shades indicating larger wave energy.....	97
Figure 2.75 Wave orbital velocities of A) Modal Swell and B) Hurricane Debbie wind-generated waves (Cooper et al., 2011) - Darker shades indicating higher velocities	97
Figure 2.76 Significant wave height simulated for 1 in 100 year storm (Vial, 2008).....	99
Figure 2.77 Hs at high tide post-breaching phase (Sala, 2010)	100
Figure 2.78 Mid ebb flows (Sala, 2010)	100
Figure 2.79 Mid flood flows (Sala, 2010).....	101
Figure 3.1 Historical Map of Inch and Rossbeigh 1842 (OSI)	105
Figure 3.2 Historical Map of Inch and Rossbeigh 1884 (OSI)	106

Figure 3.3 Aerial Photograph of Rossbeigh 1977 (OSI)	107
Figure 3.4 Centennial Scale Shoreline Change	108
Figure 3.5 DVL variations since 2006 on Rossbeigh	112
Figure 3.6 Evolution of beach orientation on Rossbeigh over a decade	113
Figure 3.7 Location of beach profiles	114
Figure 3.8 Profile analysis of Hinge point.....	116
Figure 3.9 Profile analysis of Drift aligned Dunes	117
Figure 3.10 Vegetation in breach zone	118
Figure 3.11 Profile analysis of Breach	120
Figure 3.12 Profile analysis of Island	121
Figure 3.13 Decadal Evolution of Rossbeigh, ebb Tidal Bar and Inlet	123
Figure 3.14 Ebb tidal bar evolution	126
Figure 3.15 Channel between ebb tidal bar and drift aligned shore of Rossbeigh.....	127
Figure 4.1 Burst details of Valeport Wave Gauge	136
Figure 4.2 Onshore Valeport Wave Gauge on custom steel raft.....	137
Figure 4.3 Wave Gauge Locations.....	138
Figure 4.4 Scatter plot of Wave data recorded offshore of Rossbeigh in August 2011	139
Figure 4.5 Hs plot at breach location	140
Figure 4.6 Hs plot at Edge of Dune location	140
Figure 4.7 Hs plot at Drift aligned shoreline location.....	141
Figure 4.8 Hs plot at Drift/Swash Boundary	141
Figure 4.9 Hs plot in Swash aligned zone	142
Figure 4.10 Wave Direction variations over tidal cycle on Swash and Drift Aligned Zones.....	143
Figure 4.11 Wave direction at A) lower and B) higher tides incident on Rossbeigh.....	145
Figure 4.12 Wave gauge location during wave radar trial	146
Figure 4.13 Measured significant wave height (Valeport)	147
Figure 4.14 Measured peak wave direction (Valeport).....	147
Figure 4.15 Measured mean current magnitude at instrument (Valeport).....	148
Figure 4.16 Measured mean current direction at instrument (Valeport)	148
Figure 4.17 Measured depth of water at instrument (Valeport)	149

Figure 4.18 Tidal current data collection points.....	150
Figure 4.19 Tidal current velocity at A)mid flood and B) mid ebb.....	151
Figure 4.20 Time series of tidal current recording at Location 1 (RCM8 measurement).....	152
Figure 4.21 Time series of tidal current recording at Location 2 (RCM8 measurement).....	152
Figure 4.22 Time series of tidal current recording at Location 3 (RCM8 measurement).....	153
Figure 4.23 Time series of tidal current recording at Location 4 (Valeport measurement).....	153
Figure 4.24 4 Stage Morphodynamic Conceptual Model of Rossbeigh	155
Figure 4.25 Dyed sand injection point.....	156
Figure 4.26 Dyed sediment sample grid with outliers along beach	157
Figure 4.27 Location of sediment fencing and aeolian measuring stations.....	158
Figure 4.28 Sediment fencing in Location 2.....	159
Figure 4.29 MWAC sediment profiles (Goosens, 2000).....	161
Figure 4.30 Aeolian recording equipment at Station 2	161
Figure 4.31 Outer Dingle Bay Bathymetry (Courtesy of Infomar).....	165
Figure 4.32 Survey of Rossbeigh and Inlet August 2011	166
Figure 4.33 PWC Survey Craft.....	167
Figure 4.34 Bathymetry Survey of Rossbeigh March 2013.....	170
Figure 4.35 Contour of ebb tidal bar and drift aligned shoreline from successive bathymetric surveys.....	172
Figure 4.36 Change in Bathymetry between A) August 2011 and March 2013 and B) March 2013 and September 2013	173
Figure 4.37 Trends identified from bathymetry survey analysis	174
Figure 4.38 Plan of Survey long sections.....	175
Figure 4.39 Long Section Profile at Southern Channel Entrance (Profile 1)	177
Figure 4.40 Long Profile in Channel (Profile 2)	177
Figure 4.41 Long Profile in Northern end of Channel (Profile 3)	178
Figure 4.42 Plan of shore parallel channel area calculation polygon	180
Figure 4.43 Sediment sample locations	182
Figure 4.44 FP+ trend.....	188
Figure 4.45 FB- trend.....	188

Figure 4.46 FB+ trend.....	189
Figure 4.47 FP- trend.....	189
Figure 5.1 Station locations	194
Figure 5.2 South site radar setup looking towards Rossbeigh	195
Figure 5.3 North Site radar station setup looking toward Inch	196
Figure 5.4 Comparison of recorded and WERA measured tidal current	199
Figure 5.5 Comparison of recorded and WERA measured Hs.....	201
Figure 5.6 Data cell grid of Combined Radar results	202
Figure 5.7 Surface currents at Spring tide mid flood	204
Figure 5.8 Surface currents at Spring high tide with low wave energy sea state	205
Figure 5.9 Surface currents Spring tide mid ebb.....	206
Figure 5.10 Surface currents at spring low tide.....	207
Figure 5.11 Mild wave climate at low tide	208
Figure 5.12 Mild wave climate at high tide	209
Figure 5.13 Large wave climate at low tide	210
Figure 5.14 Large wave climate at high tide	211
Figure 5.15 Radar derived surface current velocity vectors overlaid on simulated velocity vectors	213
Figure 5.16 Uneven Doppler shift	214
Figure 5.17 Side lobe impact on grid cell data	215
Figure 5.18 Land echo interference	216
Figure 5.19 Transect of entire grid.....	217
Figure 5.20 Side lobe energy contribution	217
Figure 5.21 Transect flagging method	218
Figure 5.22 High Tide tidal current plot original (upper) and reprocessed (lower).....	219
Figure 5.23 Mid ebb tidal current plot original (upper) and reprocessed (lower).....	220
Figure 5.24 Low tide tidal current plot original (upper) and processed (lower).....	221
Figure 5.25 Mid flood tidal current plot original (upper) and reprocessed (lower).....	222
Figure 6.1 Model Domain.....	229
Figure 6.2 Recorded and simulated tidal current velocity in drift aligned zone	232

Figure 6.3 Recorded and simulated tidal current velocity in drift aligned zone	232
Figure 6.4 Modelled Vs Recorded Tz in Dingle Bay.....	233
Figure 6.5 Modelled vs recorded Hs in Dingle Bay	234
Figure 6.6 Volume comparison locations	235
Figure 6.7 Initial Bathymetry of drift aligned section Stage 1 (2013)	239
Figure 6.8 Bathymetry at end of Year 1 Stage 1 (2014).....	239
Figure 6.9 Bathymetry at end of Year 2 Stage 1(2015).....	240
Figure 6.10 Significant wave height in drift aligned zone in Year 1 Stage 1 (2014)	241
Figure 6.11 Significant Height at high tide in drift aligned zone in Year 2 Stage 1(2015)	241
Figure 6.12 Mean wave direction in drift aligned zone in Year 1 Stage 1(2014)	242
Figure 6.13 Mean wave Direction at high tide in drift aligned zone in Year 2 Stage 1(2015)	242
Figure 6.14 Mid flood drift aligned zone in Year 1 Stage 1(2014)	243
Figure 6.15 Mid flood drift aligned zone in Year 2 Stage 1(2015)	243
Figure 6.16 Mid ebb in drift aligned zone in Year 1(2014)	244
Figure 6.17 Mid ebb in drift aligned zone in Year 2(2015)	244
Figure 6.18 Accumulated Sediment transport vectors at end of Year 1(2014).....	245
Figure 6.19 Accumulated Sediment transport vectors at end of Year 2(2015).....	246
Figure 6.20 Bathymetry at start of Stage 2 (2025)	250
Figure 6.21 Bathymetry at end of Stage 2 (2026)	251
Figure 6.22 Significant wave height at high tide Stage 2 (2026)	251
Figure 6.23 Mean wave direction at high tide Stage 2(2026)	252
Figure 6.24 Mid flood Stage 2 (2026).....	253
Figure 6.25 Mid ebb Stage 2(2026)	253
Figure 6.26 Cumulative sediment transport vectors at end of year 1 Stage 2(2026)	254
Figure 6.27 Bathymetry at Beginning of Stage 3(2034)	257
Figure 6.28 Bathymetry at end of Stage 3(2036)	257
Figure 6.29 Significant wave height year 2 Stage 3(2036).....	258
Figure 6.30 mean wave direction year 1 Stage 3(2035)	258
Figure 6.31 mean wave direction year 2 Stage 3 (2036)	259

Figure 6.32 Mid flood year 1 Stage 3 (2035).....	259
Figure 6.33 Mid flood year 2 Stage 3(2036).....	260
Figure 6.34 Mid ebb year 1 stage 3(2035)	260
Figure 6.35 Mid ebb year 2 stage 3(2036)	261
Figure 6.36 cumulative sediment transport vectors end of year 1 in Stage 3(2035)	262
Figure 6.37 cumulative sediment transport vectors end of year 2 in Stage 3(2036)	262
Figure 6.38 GSTA Fp + case	264
Figure 6.39 Simulated Accumulated Sediment transport vectors for GSTA comparison	265
Figure 7.1 Breach width – Dune Termination points over time on Rossbeigh.....	273
Figure 7.2 Ebb Tidal Bar migration	275
Figure 7.3 Channel area used in volume calculation	276
Figure 7.4 Windrose for Valentia Weather Station (Met Eireann)	279
Figure 7.5 Simulated Data Locations	284
Figure 7.6 Simulated water level at Behy Estuary, Cromane Upper, Dooks, and Back Barrier	285
Figure 7.7 Simulated water level heights at Cromane Lower.....	286
Figure 7.8 Hs at high tide for pre Breach bathymetry (2000)	287
Figure 7.9 Hs at high tide for present bathymetry (2013).....	287
Figure 7.10 Hs at high tide for simulated future bathymetry (2030-2035)	288
Figure 7.11 Proposed borrow pit for beach nourishment of Rossbeigh	290
Figure 7.12 Percentage loss of dredged material (Matias et al. 2004).....	291
Figure 7.13 Cutter suction dredger suitable for Rossbeigh beach nourishment	292
Figure 7.14 Aeolian fencing trials on Rossbeigh	293
Figure 7.15 5 Phase evolution of Rossbeigh and Inner Dingle Bay	295

List of Tables

Table 1.1 Tidal statistics for Inner Dingle Bay relative to Chart Datum (Vial, 2008).....	4
Table 2.1 Calculated ages of sediment samples on Inch (Wintle, 1998).....	89
Table 2.2 Tidal statistics for Inner Dingle Bay relative to Chart Datum (Vial, 2008).....	93
Table 3.1. Cross-shore Dune Recession Analysis (Van Rijn)	131
Table 3.2. Annual Alongshore Transport	133
Table 4.1 Guelph trap results.....	163
Table 4.2 Typical MWAC results on Rossbeigh	163
Table 4.3. Volumetric difference between surveys within polygon	180
Table 4.4 Sediment Sample Statistics	183
Table 4.5 Summary stats by location	185
Table 6.1 Final model parameter values	231
Table 6.2 Directional spreading index (DHI Software, 2007)	231
Table 6.3 Volume comparison of morphodynamic simulations	235
Table 6.4 Morphodynamic simulation stage timeline	236
Table 6.5 Volume calculations for Stage 1 simulations.....	247
Table 6.6 Volume calculations for Stage 2 simulations.....	254
Table 6.7 Volume calculations for Stage 3 simulations.....	263
Table 7.1 Median Termination widths	272
Table 7.2 Ebb Tidal Bar migration rate	275
Table 7.3 Channel Infilling Rates	276
Table 7.4 Yearly rate of aeolian sediment accumulation.....	279
Table 7.5 Yearly Weight and Volume per m width of Dune.....	280
Table 7.6 Calculation of monthly dune height increase.....	280
Table 7.7 Comparison of Dune Height increase rates	281

Nomenclature

The main symbols used in this thesis are listed below.

A1	Fitting parameter depending on λ_0 [-]
A2	Fitting parameter depending on λ_0 [-]
Ac	Inlet cross-sectional flow area [m ²]
As	Stable cross-sectional area [m ²]
Au	Unstable cross-sectional area [m ²]
B	Dune height above mean sea level [m]
C	Wave celerity [ms ⁻¹]
d	Sphere diameter [m]
d ₅₀	Median grain diameter [m]
D _{HIGH}	Dune crest height [m]
D _{LOW}	Dune base height [m]
G	Acceleration due to gravity [m/s ²]
h _b	Water depth at wave breaking [m]
H _b	Wave height when waves break [m]
H _c	Closure depth [m]
H _{sx}	Non-breaking significant wave height that is exceeded 12hr per year [m]
H _s	Significant wave height [m]
k	Wave number [rad/m]
K	Dimensionless parameter [-]
L ₀	Deepwater wave length [m]
m	Beach slope [-]
p	In-place sediment porosity [-]
Q	Longshore sediment transport [m ³ /s]
T	Wave period [s]
t	Time [s]
T _e	Non-breaking significant wave period that is exceeded 12hr per year[s]
T _p	Peak wave period equal to the largest spectral peak of the spectrum[s]
T _z	Mean wave period between zero downward or upward crossings [s]
U	Mean velocity over a half tidal cycle [m/s]
V _e	Equilibrium velocity [m/s]
V _m	Maximum velocity [m/s]
Ws	Fall velocity [m/s]
λ	Wavelength [m]
λ_0	Deepwater wavelength [m]

Acronyms

ADCP	Acoustic Doppler Profiler
ADV	Acoustic Doppler Velocimeter
BP	Before Present
CEM	Coastal Engineering Manual
CERC	Coastal Engineer Research Centre
CMRC	Coastal and Marine Resources Centre
DAB	Drift Aligned Barrier
DEM	Digital Elevation Model
DVL	Dune Vegetation Line
FMCW	Frequency Modulated Chirp Wave
GIS	Geographical Information System
GPS	Global Positioning System
HAT	Highest Astronomical Tide
HMRC	Hydraulics and Maritime Research Centre
LAT	Lowest Astronomical Tide
LIDAR	Light Detection and Ranging
MHWL	Mean High Water Level
MHWN	Mean High Water Neap
MHWS	Mean High Water Spring
MORFAC	Morphological Speed up Factor
MSL	Mean Sea Level
MSR	Mean Spring tidal Range
OBS	Optical Backscatter Sensor
OD Malin	Ordinance Datum Malin
OTH	Over The Horizon
RTK	Real Time Kinematic
RTR	Relative Tide Range
SAB	Swash Aligned Barrier
SAC	Special Area of Conservation
SLR	Sea Level Rise
SWAN	Simulating Waves Nearshore
TIN	Triangulated Integrated Network
UCC	University College Cork

1 Introduction

1.1 Introduction

Barrier beach systems perform a critical role in coastal zone dynamics. Their primary function is to protect vulnerable coastlines from open ocean forcing such as waves, wind and tidal currents. In combination with inlets, barrier beaches also form a dynamic flow regulation system. Adapting to changes in the coastal zone the barrier system follows a morphological cycle of erosion and aggradation. It is common for barrier beaches to move along the coastline and Inlets to move or even multiply as part of a cycle. In certain cases the cycles can change abruptly and a period of significant dynamic instability ensues, before the system reverts to gradual change again. Such events are rare and difficult to predict without continuous monitoring as morphodynamic cycles of barrier beach systems can be at a centenary scale and significant dynamic events can last only years.

When abrupt changes to the morphology of a barrier beach system, such as barrier breaching, occur, the response of coastal management authorities in the past has been ineffectual and even detrimental to the local coastal zone. Solutions to breaching have previously focussed on short-term stop gap measures to prevent damage to infrastructure e.g. groynes, and sea walls. These solutions have typically not considered the long-term behaviour of the coastal system or the consequences of intervention in response to a single event i.e. breaching.

To formulate a comprehensive solution that considers both the long term and short term benefits of intervention, an understanding of the governing hydrodynamics and crucially the morphodynamics of barrier systems is essential.

This thesis presents an in depth study of the morphodynamic evolution of the mid-bay barrier beach system of Inner Dingle Bay, Co. Kerry, Ireland. The system has been under observation by the Hydraulics and Maritime

Research Centre (HMRC) of University College Cork since 2008 when the Rossbeigh barrier breached. The study utilises numerical modelling, field data collection and remote sensing to understand the coastal processes driving the system's evolution.

Experimental coastal analysis techniques and novel data collection methods are also trialled as part of this research. As there is no directly identifiable anthropogenic cause of the accelerated erosion and breaching, Inner Dingle Bay is an ideal case study site. This natural breaching event presents a rare opportunity to assess the validity and accuracy of coastal monitoring practices and coastal morphological theory.

1.2 Environmental Setting

The barrier beach system, figure 1.1, is situated in Dingle Bay, County Kerry, Ireland, and consists of three mid-bay barriers. Sandy dune barriers, Inch and Rossbeigh, extend across the bay divided by a tidal inlet: Inch extends from the north to south across the bay and is approximately 5 Km long; Rossbeigh is located seaward of Inch and is over 4 Km in length and runs in the opposite direction propagating from the south coast running north. The low-lying barrier, Cromane, is located further inshore in the estuarine Castlemaine Harbour. The two outer barriers act as a flexible defence of the harbour from the Atlantic Ocean.

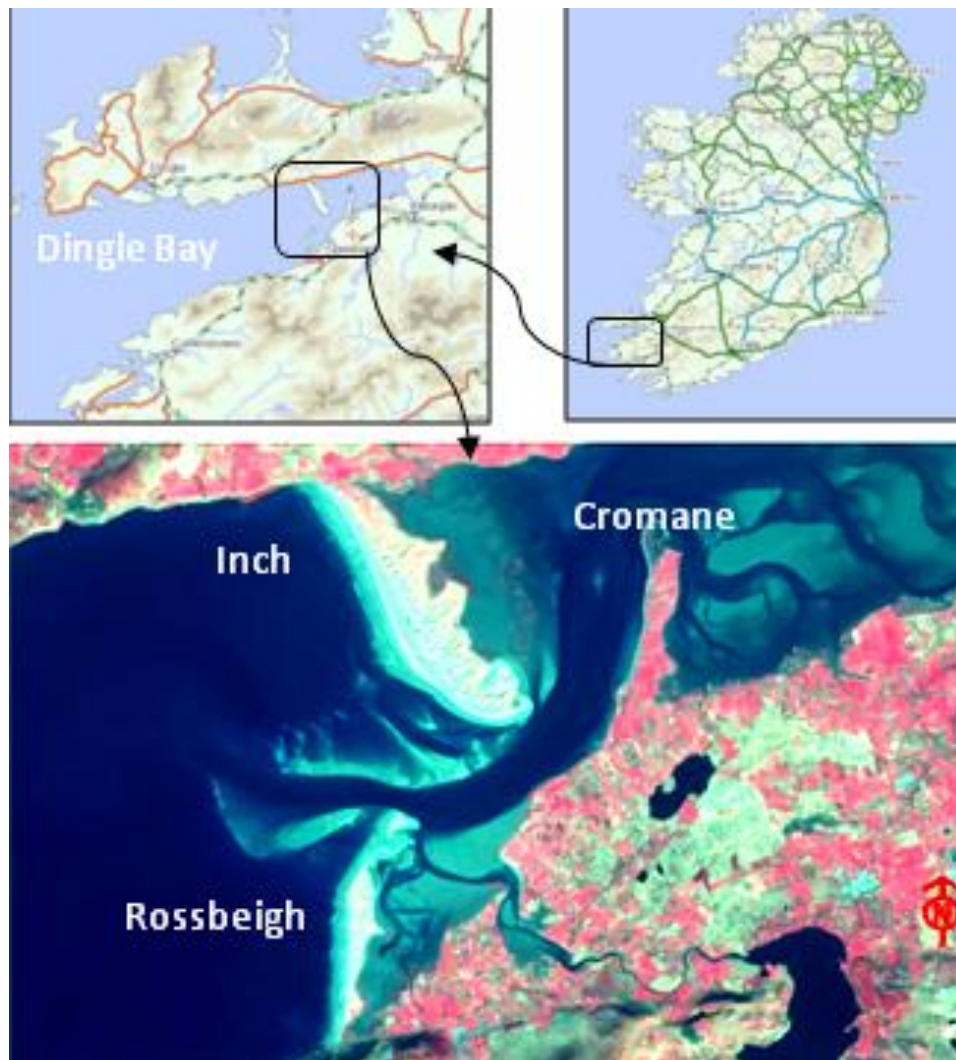


Figure 1.1 Study Area

The spring tidal range is approximately 3.2 m, Table 1.1. The mean significant wave height (H_s) is 2.8 m and an average wave period (T_z) is 7 s

based on 50 years of storm data analysis (Sala, 2010). Dingle Bay is relatively narrow and is bounded by two rocky headlands; the direction of wave forcing affecting morphology is narrow banded ranging from 230° to 280°. Because of this narrow incident wave directionality, it can be classed as a self-contained coastal cell, i.e. sediment transport is conserved within the bay. The tidal inlet that separates Inch and Rossbeigh acts as an important sediment transport driver with tidal currents reaching over 1 m/s at peak flood. It has been classified as mixed wave/tide dominated to tide dominated.

Table 1.1 Tidal statistics for Inner Dingle Bay relative to Chart Datum (Vial 2008)

Highest Astronomical Tide	+4.36 m
Mean High Water Spring	+3.76 m
Mean High Water Neap	+3.15 m
Mean Sea Level (0m at Malin Head)	+2.30 m (Ordnance Datum)
Mean Sea Level	+2.15 m
Mean Low Water Neap	+ 1.17 m
Mean Low Water Spring	+ 0.58 m
Lowest Astronomical Tide	0 m

The barrier dunes protect Castlemaine Harbour, which is a brackish low-lying area of approximately 5300 Ha. Protection of the harbour is vital as it is both commercially and environmentally significant. It is a designated Special Area of Conservation (SAC) and wildfowl reserve as well as being a valuable clam, mussel, and salmon fishery. The beaches, which are both blue flag status, are an important tourist resource for the local economy.

The dune system had been in a state of dynamic equilibrium with shorelines eroding and prograding seasonally; however, a breach in the Rossbeigh dunes occurred in the winter of 2008 and has since widened to over 900 m. The impact this breaching has on the surrounding environment is multifaceted and potentially of significant economic impact. The loss of amenity and habitats is already occurring with the removal of protected dune; the change in sediment transport patterns is increasing sedimentation in the back barrier area and affecting aquaculture.

It is the reported (Kerry Co. Co, 2009) increase in flooding since the breaching event, however, that is potentially the greatest impact of the erosion in Rossbeigh. Approximately 100 homes and businesses are located on the low-lying (ground level, <10 m OD Malin) coastline directly behind the barrier beach.

Anecdotal evidence (KerrysEye, 2010) suggests that recent storm surge flooding corresponds to the emergence of the breach in the barrier beach. If present erosion trends continue, it is feared that flood risk in the back barrier will increase, thus increasing the potential economic loss.

1.3 Scope of Research

It is apparent that a comprehensive examination of the entire coastal cell of Inner Dingle Bay is required before the extreme erosion occurring on Rossbeigh and consequently the morphodynamics of the barrier beach system can be understood.

There is a paucity of the type of field data required to undertake such analysis. Predicting the evolution of the barrier beach system post breaching requires long term regular shoreline details, seasonal wave and tidal current data and accurate nearshore bathymetry.

This research project must address several key factors including:

- Gaining a deeper understanding of shoreline changes on Rossbeigh and Inch by examining alternative data sources such as satellite imagery.
- Undertaking regular topographic surveys to document the evolution of the breach area and Rossbeigh.
- Characterising the wave climate and tidal current regime of Dingle Bay.
- Conduct seasonal bathymetry surveys to identify where sediment is being transported to.

- Undertake an assessment of the sediment transport regime on Rossbeigh with respect to the established Coastal Sediment Transport Formulae.
- Performing an assessment of the influence of Aeolian transport in the morphology of Dingle Bay's Barrier Beaches.
- Investigate the applicability of novel and experimental methods on Inner Dingle Bay's Barriers such as Grain Size Trend Analysis, Surface Wave Radar Monitoring and Sediment Dye Testing.
- Developing a robust numerical modelling tool that can predict the evolution of erosion in the Barrier Beach system and quantify the effects future evolution has on the surrounding low lying back barrier areas.

1.4 Outline of Theses

This thesis is presented in 8 chapters, including this introductory chapter. The flow of the thesis approximately mirrors the chronology of the research undertaken. A review of relevant literature and publications on coastal barrier breaching was followed by an initial investigation of the previous work conducted in Dingle Bay. The next chapter investigated remotely sensed datasets from the area. This work then informed the structure of field work undertaken during the course of this study. The analysis of field work and trials of coastal monitoring techniques were presented in the latter chapters along with a detailed discussion of the numerical modelling undertaken during the study. The penultimate chapter collated the work of the preceding chapters to develop a clear and concise theory of the coastal evolution of the inner Dingle Bay barrier beach system, while conclusions on all facets of the research were made in the final chapter.

1.4.1 Chapter 2

This chapter provides a review of the essential literature and recent publications undertaken in the fields of research most relevant to the current study. These fields include traditional coastal monitoring, experimental

coastal monitoring techniques such as GSTA and Wave Radar, and numerical modelling studies. The emphasis on this review was to provide information from similar case studies, i.e. breaching barrier beach / inlet systems to use as a comparison with the Inner Dingle Bay. Recent studies of Dingle Bay from a range of fields including geology, hydrodynamics and sedimentology are also discussed in this chapter including an introduction to the breaching event on Rossbeigh.

1.4.3 Chapter 3

The initial research into the evolution of Dingle Bay is described in Chapter 3. This includes examining the long term evolution of both Inch and Rossbeigh. An examination of the recent breaching and the change in beach alignment is also identified in this chapter. Finally a study of sediment transport formulae for both cross shore and long shore transport on Rossbeigh are compared for a 3 year dataset.

1.4.4 Chapter 4

The collection and analysis of the majority of the field work undertaken during this research is presented in this chapter. Wave, tidal current, aeolian sediment transport, sediment fencing, sediment dye testing, bathymetric surveying and sediment sampling are all discussed. The analysis of this field work resulted in the formulation of a conceptual model to describe the processes during the coastal erosion in Dingle Bay. The conceptual model is described in detail in this chapter. The short comings in terms of spatial coverage of wave and tidal current monitoring identified in this chapter form the basis for the proceeding chapter, the wave radar trial.

1.4.5 Chapter 5

The wave radar trial undertaken as part of this study is documented in this chapter. This includes the equipment set up, analysis results, error analysis and post processing attempts. The merits and demerits of the technology and specifically the errors in the data produced by wave radar are also discussed. A new methodology for reducing the error in data plots produced by the radar system is developed and detailed.

1.4.6 Chapter 6

While the numerical modelling outputs are referenced throughout the thesis, this chapter contains the main body of the numerical modelling undertaken as part of the research. This chapter contains a description of the software used, a validation of the model with field collected data as well as a description of the several stages of modelling undertaken. The evolution of Dingle Bay is simulated in several scenarios representing 2 years, 13 years and 21 years of evolution from the base year of 2013.

1.4.7 Chapter 7

The results from the preceding chapters are collated in this chapter to form definitive conclusions on the evolution of Inner Dingle Bay. A 5 phase model describing the morphodynamic evolution of the area from its present erosive climate back to a stable morphological climate similar to the pre breaching phase is developed. The key processes influencing this model are addressed and quantified. The flood risk due to the evolution is also examined with significant implications for flooding of the back barrier area identified. An intervention strategy involving dredging and shore nourishment to speed up the natural cycle of evolution is also discussed.

1.4.8 Chapter 8

The final chapter presents the main conclusions from this research with emphasis on the main aims of the study as stated in Chapter 2. An assessment of the experimental coastal monitoring techniques trialled as part of this research is provided. Finally several recommendations for further research on key aspects of the research are made.

1.5 Publications

The research undertaken as documented in this thesis has contributed to several publication and conference presentations, including IEEE Oceans '11, Santander, EGU 2012, Vienna, Environ 2012, Dublin. In addition to the publications listed, two further publications are being prepared, one on Wave radar, as detailed in Chapter 5 and one on numerical modelling and GSTA as detailed in Chapter 6 and Chapter 4 respectively. The following is a list of the publications directly related to this research

- “Investigating the Hydrodynamics of a Breached Barrier Beach” by M. O’Shea and Dr. J. Murphy EGU2012 Vienna, 2012.
- "Monitoring the Morphodynamic Behavior of a Breached Barrier Beach System and its Impacts on an Estuarine System" OCEANS'11 *IEEE* Conference, Santander, Spain, 2011.
- “Predicting and Monitoring the Evolution of a Coastal Barrier Dune System Post breaching”. Michael O’Shea and Jimmy Murphy. *Journal of Coastal Research*: Volume 29, Issue 6a: pp. 38 – 50. 2013.
- Heron, M.L.; O’Shea, M.; Murphy, J.; Petersen, L.; Mollaghan, D.; Prytz, A., "Interpretation of VHF radar echoes from a complex flow field," *Oceans - San Diego, 2013* , vol., no., pp.1,4, 23-27. 2013.

2 Literature Review

2.1 Introduction

Developing an understanding of the morphodynamics of a coastal system is critical to predicting the long term behaviour of such systems. The underlying theoretical concepts that drive coastal evolution and specifically, wave action, tidal currents and sediment transport are detailed. The classification of coastal systems, identification of Inlet types, beach morphology modes and barrier alignment characteristics are also discussed.

The methodology used to collect data that informs theoretical concepts on coastal morphology is examined. The methodologies include field based coastal hydrodynamic monitoring techniques and both water and air driven sediment transport. The role of numerical models in predicting the evolution of coastal systems is discussed with particular reference to coupled morphological modelling strategies. A review of previous work undertaken on the study site is presented at the end of the chapter.

2.2 Coastal Zone Processes

The coastal zone is subject to various processes that drive its morphology. The following is a description of the most significant processes to consider when examining coastal change at the Meso and Macro temporal scales, figure 2.1, as is the case for barrier beach and tidal inlet evolution.

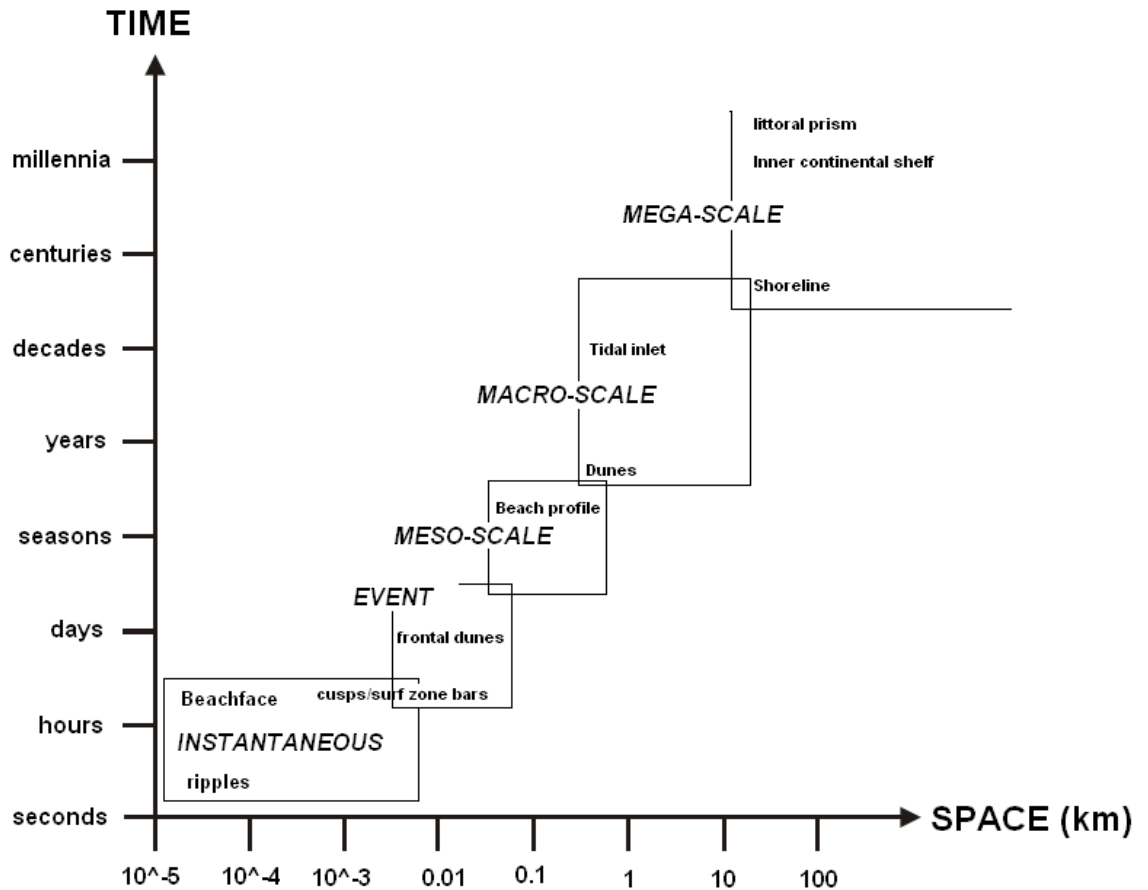


Figure 2.1 Spatio-Temporal Scales of Coastal Change (Steve et al., 2001)

2.2.1 Coastal Zone Hydrodynamics

Predominantly in the coastal zone, evolution is driven by sediment transport. The two drivers of marine sediment transport in the coastal zone are wave action and tidal currents. The associated hydrodynamic processes of these drivers are outlined.

Wave Refraction

When waves approach a coastline with an uneven bed level, there is a variation in phase speed along the crest of the wave. This is due to the relationship of wave speed with water depth (1) according to linear wave theory:

$$c = \sqrt{\frac{g}{k}} \tanh(kd) \quad (1)$$

Where c = wave celerity

h = water depth

This disparity in speed along the wave crest results in the wave turning towards the shallower water as shown in figure 2.2.

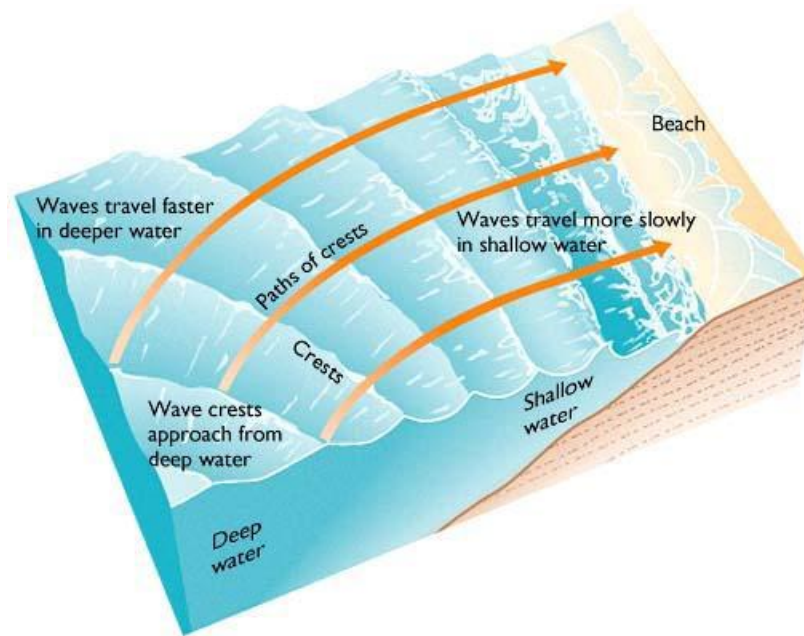


Figure 2.2 Wave Refraction (source: <http://piru.alexandria.ucsb.edu>)

Wave Breaking

As a wave propagates shoreward the wave height increases and wavelength decreases. The wave steepness increases until the wave breaks. As the wave breaks, nearshore currents are created. These currents are responsible for significant sediment transport in the coastal zone.

Types of wave breaking have been categorised by Battjes (1974) based on wave height, water depth and wave steepness. The following formula called the surf similarity parameter (2) is used to define the type of breaker:

$$\xi_0 = \frac{\tan(\beta)}{\sqrt{\frac{H_0}{L_0}}} \quad (2)$$

Where β = Beach slope

H_0 = Deepwater wave height

L_0 = Deepwater wave length

The breakers are categorised into 3 main types, spilling, plunging and surging breakers, Figure 2.3. In terms of sediment transport, plunging type breakers are considered the most effective as they have greatest impact on seabed and thus entrain the most sediment during breaking.

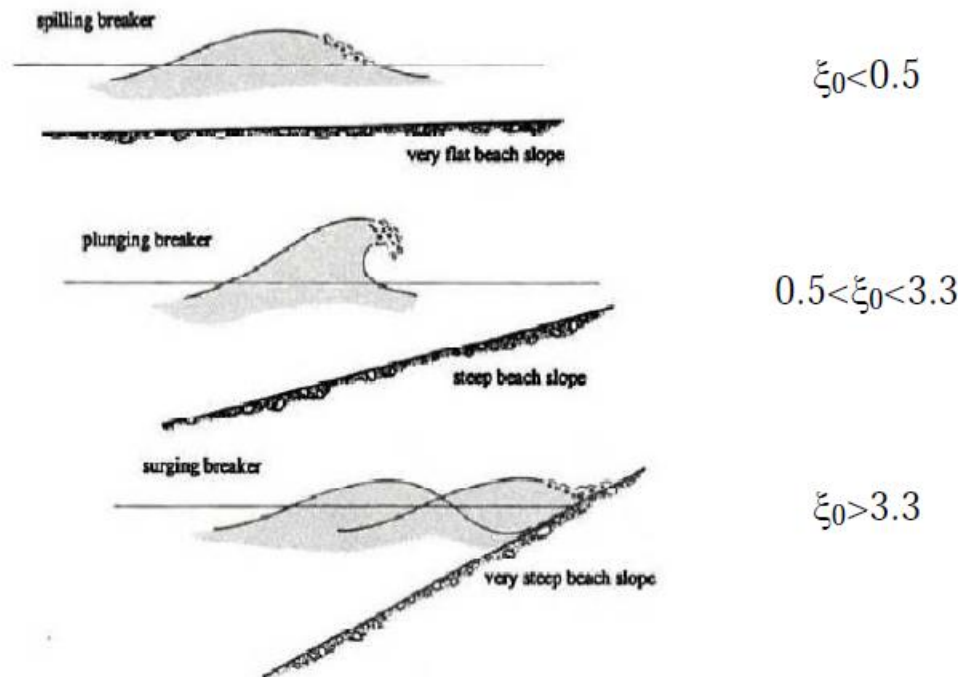


Figure 2.3 Breaker Types (Chadwick & Morfett, 1998)

Wave Induced Currents

There are two modes of wave induced current that impact the coastal zone sediment transport, long-shore and cross-shore currents. The long shore currents are generated due to the incident waves travelling at an angle to the shoreline; this can be due to refraction or oblique offshore incident wave direction. This current transports sediment in a shore parallel direction and is active only in the surf zone to swash zone, figure 2.4.

Longshore Current

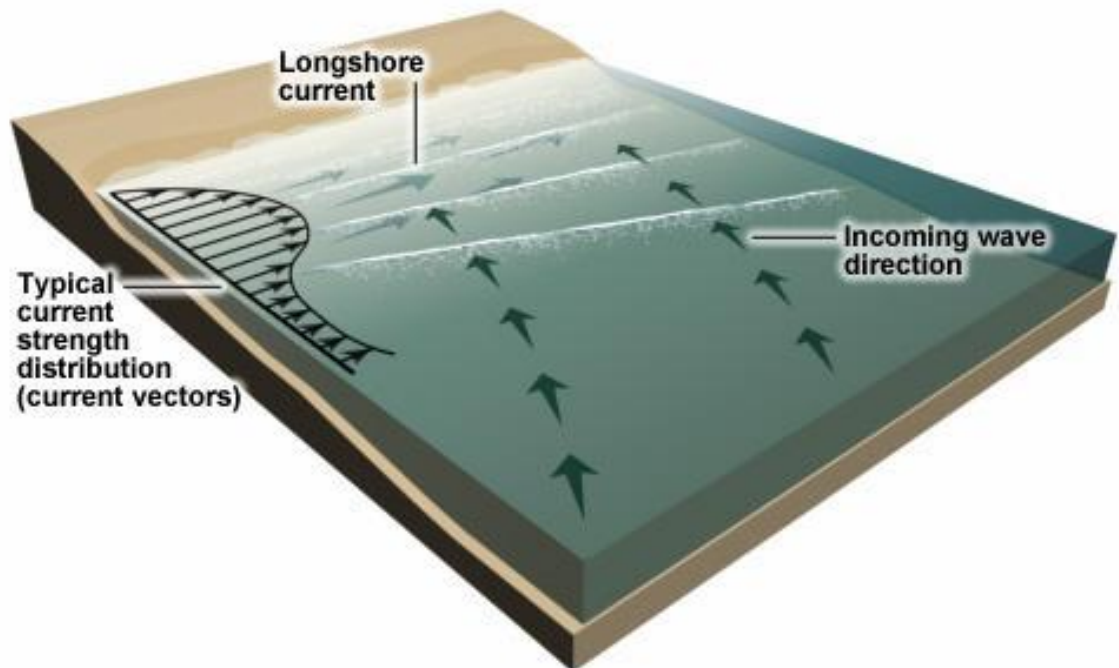


Figure 2.4 Longshore Currents (Source:www.srh.noaa.gov)

Cross-shore currents occur as a result of wave breaking and can be divided into two sub-types, undertows and rip currents. An undertow is the response to surface shoreward moving current generated by wave breaking. To compensate for this a residual offshore current is generated in the lower section of the water column. An undertow can be responsible for large sediment transport in an offshore direction during storm conditions. Rip currents are another response to residual shoreward wave breaking currents. They are currents that form via channels and flow seaward toward the breaker zone from the shoreline, figure 2.5.

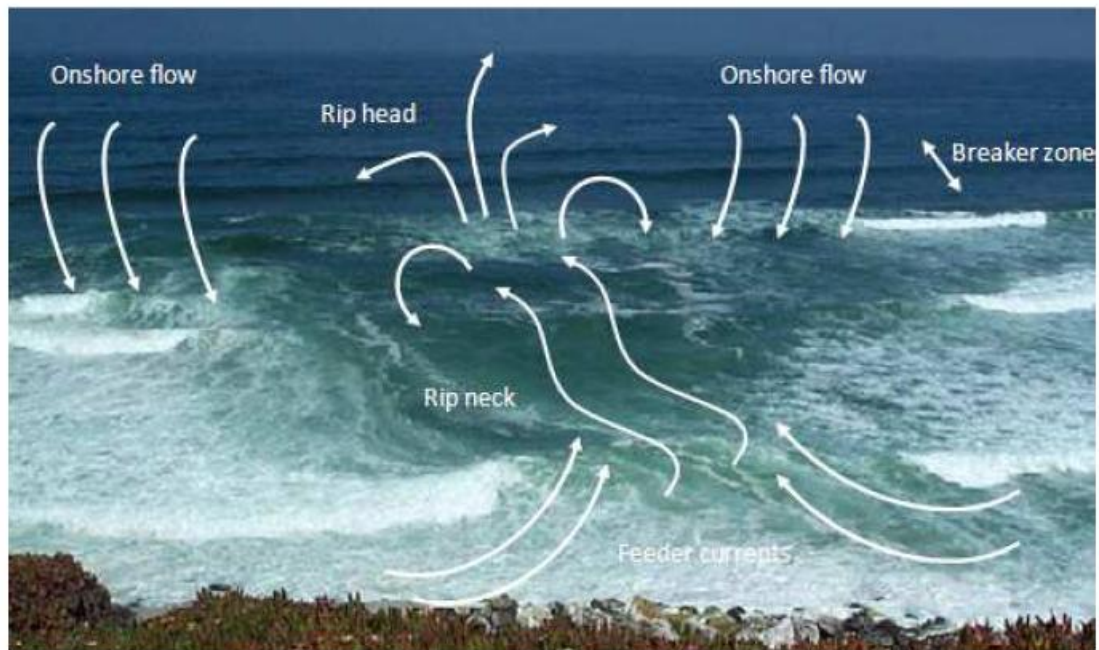


Figure 2.5 Rip Currents (MacMahan et al., 2006)

Tidal currents

Tidal currents can have a significant impact on the morphological climate of a coastal cell. Tidal currents driven by the rise and fall of the tide and are typically bi-directional in the coastal zone. The two forms of tidal currents are flood-tidal and ebb-tidal. The former is generated on the rising tide with a peak velocity at mid flood tidal height and a shoreward direction, while the latter is initiated on the falling tide and has a peak velocity at mid ebb tidal height and is typically in a seaward direction, depending on the bathymetry and tidal signal of the coastal cell in question.

The influence of tidal currents on wave induced currents, sediment transport and geomorphology is complex, multi faceted and difficult to quantify. The relationship between tidal current features and geomorphology are discussed in Section 2.3.

2.2.2 Sediment Transport

Sediment transport can be divided by sediment type, cohesive and non-cohesive sediments. This study does not consider cohesive sediment transport as the coastal zone of the study site is dominated by sandy coastline. Non-cohesive sediments such as sand and gravel in the coastal

zone can be driven by a variety of sources including hydrodynamic, as described in section 2.2.1 and also by wind or aeolian sediment transport. This section describes the key characteristics of coastal sediment transport.

Modes of Sediment Motion

There are three main modes of sediment movement, sliding, saltation and suspended sediment transport.

Sliding is the movement of sedimentary particles inside the bed boundary layer. The transport is via collision of particles.

Saltation occurs when the driving force is increased and sediment particles begin to bounce along the bed layer.

Suspended sediment transport is the suspension of the particles in the fluid (air or water) and there is no contact with the bed layer.

Typically in the water deeper than the wave breaking zone, bed load transport (Sliding & Saltation) is the main mode of transport. This is due to low tidal currents compared to wave action in deeper water. The main features of the bed load dominated transport is small ripple forms and sand bars. In the surf zone and shallower, breaking waves results in a larger amount of sediment being suspended (stirring). This entrained sediment is then transported by wave induced and tidal currents which are largest in the surf zone.

Aeolian Sediment Transport

In sand-dune areas of the coastline, aeolian transport is a significant driver of morphology. The modes of aeolian sediment transport are the similar to hydrodynamic driven sediment transport. The rate of transport is a function of available sediment, fetch length and wind speed. The mode of transport is dependent on the size and moisture content of the particles. The lighter dryer particles become entrained and suspended in wind with heavier grains

saltating. The wetter sand is cohesive and resists initiation of motion until its moisture content is reduced due to drying.

Fall Velocity

The fall velocity of transported sediment particles is an important metric in determining sediment transport trends. The fall velocity is a function fluid viscosity, sediment density and particle diameter and is given as (3):

$$w_s = \frac{10\nu}{d} \left[\left(1 + \frac{0.01 \left(\frac{\rho_s}{\rho_w} - 1 \right) g d^3}{\nu^2} \right)^{0.5} - 1 \right] \quad (3)$$

Where

ν = Kinematic viscosity

d = diameter of grain

ρ_s = sediment density

ρ_w = fluid density

g = acceleration due to gravity

Long-shore Sediment Transport

As described in Section 2.2.1, the wave induced and tidal currents can act in a shore parallel direction. In doing so, these hydrodynamic forcings move sediment in an alongshore direction. Predicting the rate of long shore sediment transport is a difficult proposition as there are several modes and drivers of sediment transport involved. This includes both bed load and suspended load driven by a combination of wave breaking, wave induced currents and tidal currents. Several formulae have been developed to predict the sediment transport. Three of the most widely used are discussed below:

CERC Formula

This is formula based on empirical data was developed by the US Army Corp of Engineers. The formula (4) has several limitations it assumes an unlimited sediment supply and does not include sediment grain size. The formula is given as

$$Q_t = K \left(\frac{\rho_w \sqrt{g}}{16\gamma_b^{\frac{1}{2}} (\rho_s - \rho_w) (1 - \rho)} \right) H_b^{5/2} \sin(2\alpha_b) \quad (4)$$

Where:

K = dimensionless coefficient

ρ_s = sediment density
 ρ_w = water density
 α_b = angle between wave front and shoreline
 p = porosity
 H_b = breaking wave height

Kamphius

This formula (5) developed by Kamphius (1991) considers wave period, sediment grain size and beach slope in its derivation of transport rates. However, tidal current driven transport is not included.

$$Q_t = 2.33(T_p)^{1.5} (\tan\beta)^{0.75} (H_b)^2 (d_{50})^{-0.25} (\sin(\alpha_b))^{0.6} \quad (5)$$

Where:

T_p = peak wave period
 $\tan\beta$ = beach slope (breaker line to still water beach line)
 d_{50} = is the mean sediment grain size
 H_b = breaking wave height

Van Rijn

Van Rijn (2002) developed a comprehensive formula (6) to predict along shore transport rates including tidal current forcing, beach slope and grain size characteristics. The formula contains several coefficients empirically derived during beach studies and flume tests.

$$Q_t = K_0 K_{swell} K_{grain} K_{slope} (H_b)^{2.5} V_{eff,L} \quad (6)$$

Where:

$K_0 = 42$
 K_{swell} = swell correction factor for swell waves <2m, $K_{swell} = T_{swell}/T_{ref}$
 K_{grain} = particle size correction factor
 K_{slope} = bed slope correction factor
 $V_{eff,L}$ = effective longshore velocity for tidal velocity component and wave induced velocity component.

2.3 Coastal Morphology

The characteristics and features of coastal morphology are described in the following section. The classification of beach morphology and significance of barrier beach alignment is documented as well as the various types of tidal inlet configurations. Assessing the rates of Dune erosion and modes of barrier breaching are also discussed.

2.3.1 Beach Morphology Classification

The changes on a beach due to hydrodynamic and aeolian forcing do not act uniformly across the beach. There are distinct differences in morphology between the sub tidal and the supra tidal areas of a beach. The various generalised morphological zones on a beach are described in the Coastal Engineering Manual, as shown in figure 2.6

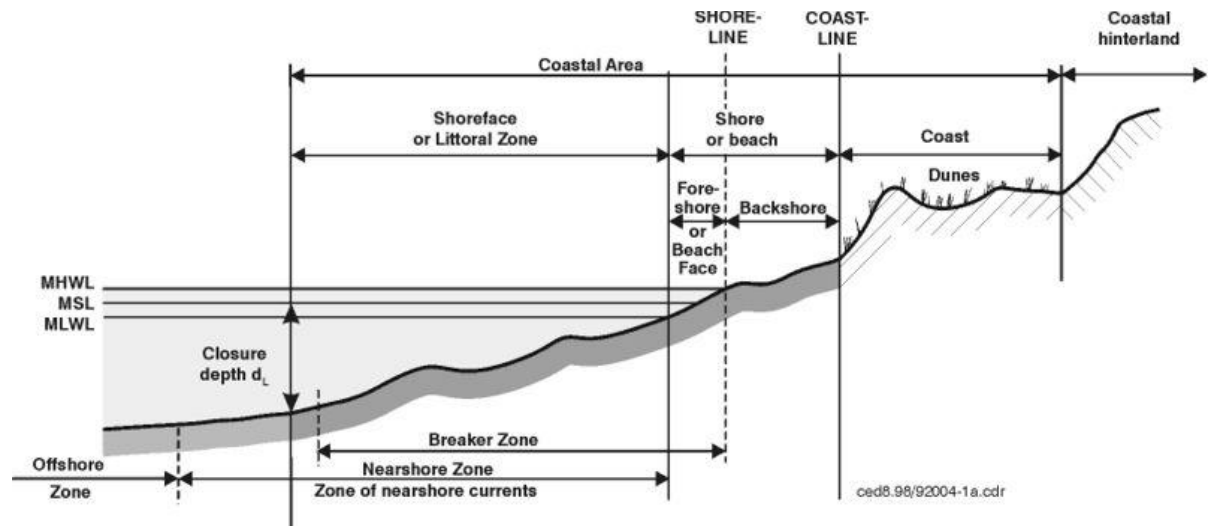


Figure 2.6 Beach Morphological zones (CEM, 2002)

In this classification the seaward boundary is termed the closure depth. It is the minimum depth at which no significant wave induced sediment transport occurs. This in effect bounds the coastal cell. Hallermeier (1981) estimated the annual average closure depth to be (7):

$$h_c \approx 2.28H_{sx} - 68.5 \left(\frac{H_{sx}^2}{gT_e^2} \right) \quad (7)$$

Where:

H_{sx} = non breaking significant wave height 12 hours per year

T_e = the associated wave period

As discussed in Section 2.2 Fall velocity is an important parameter in sediment transport and in particular when examining morphological climate of a given beach. The dimensionless fall velocity (Dean's parameter Ω) is a metric developed by Gourlay (1968) and Dean (1973) to define whether a beach is dissipative (>5) or reflective (<3). This is given by (8):

$$\Omega = \frac{H_b}{w_s T} \quad (8)$$

Where:

H_b = breaker height

W_s = sediment fall velocity (m/s)

T = wave period

Masselink and Short (1993) refined this classification further by introducing relative tidal range, (RTR), given by (9);

$$RTR = \frac{TR}{H} \quad (9)$$

Where

TR = tidal range

H = modal wave height

A classification was created using data from beaches in Queensland, Australia. It concluded that low RTR and Ω values coincided with highly reflective beaches, coasts with low RTR and high Ω produced barred dissipative morphology, high RTR and low Ω gave a low tide terrace effect on the beach profiles while highly dissipative beaches possessed high RTR and a high Ω . A notable finding was that for bar morphology to develop surf zone processes should dominate 25% of time in a lunar cycle.

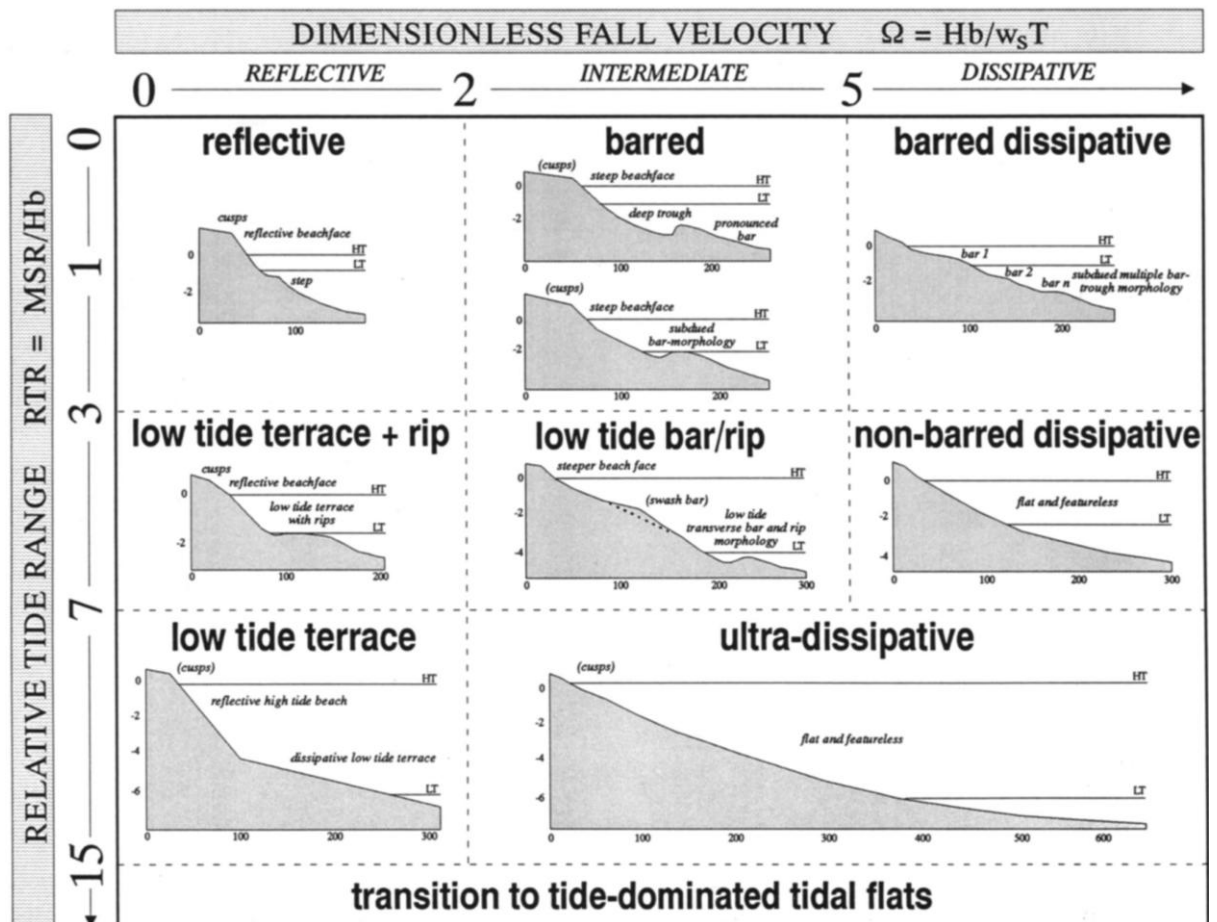


Figure 2.7 Beach Morphology Classifications (Masselink & Short, 1993)

However, this classification system has been disputed notably by Sanderson et al. (1999) who suggests that the model does not take account for complications such as near shore reefs. Jackson et al. (2005) examines the accuracy of classification techniques of morphology in beaches, namely Dean's parameter and RTR. Twenty five beaches from Northern Ireland are studied utilising grain size and sediment sampling and topographical surveys. The morphodynamic state was then predicted for each beach using Dean's parameter and RTR. Correlation between the measured and calculated of most parameters was poor, tidal range and beach slope, RTR and beach slope, Tidal range and breaking wave height (H_b), Dean's and RTR and H_b and RTR included.

However, good correlation between beach slope and Ω was recorded since grain size is included in Dean's and also factored in slope. H_b and RTR also displayed good correlation, as expected since H_b is a component of RTR.

Many cases show a marked difference especially beaches that are not actually in the dissipative state. Geological control factors are highlighted as not being accounted for and hence the inaccuracies. Mean grain size was 0.125 mm to 0.250 mm. Sediment supply and underlying geological conditions have a strong influence on morphology but are not accounted for fully in the RTR or Dean's parameter. It was also suggested that RTR may also mask hydrodynamic variability especially in 5 m plus tide ranges.

Walstra et al. (2007) investigated the effects that bed slope and wave skewness had on sediment transport and hence morphology using Delft 3D (Section 2.4.2) numerical modelling software. Three factors were examined: phase lag effects, skewness and bed slope effects. A phase lag is when sediment is stirred up and does not respond to orbital wave motion as it takes time to fall back to the bed. This can decrease or sometimes change direction of transported sediment. It was found that depending on the F_p (phase lag function) suspended sediment could change direction and hence the direction of bar migration. It was found that acceleration skewness was more dominant than velocity skewness in the surf zone. This has implications for sediment transport both bed load and suspended sediments.

Karunaratna et al. (2009) studied beach profile evolution with the aim of using beach observations to solve beach profile evolution equation, using historic beach profiles from Christchurch Bay in Dorset, UK. The Bay is bounded by a head and a spit at either side. The survey data was processed to ensure even temporal and spatial spacing occurred, necessary for the source function recovery. The source function predicted formation and disappearance of near shore features such as bars, however, strong noise and interference may limit this method.

2.3.2 Barrier Beaches

The defining characteristic of what constitutes a barrier beach is a beach with a distinct crest that divides the seaward beach face and back barrier zone. The back barrier zone typically contains a water body (estuary or lagoon), or previously contained one. Cope (2004) has developed a general

classification of barrier beaches, figure 2.8, based on the plan shape of the beach relative to the surrounding coastline.

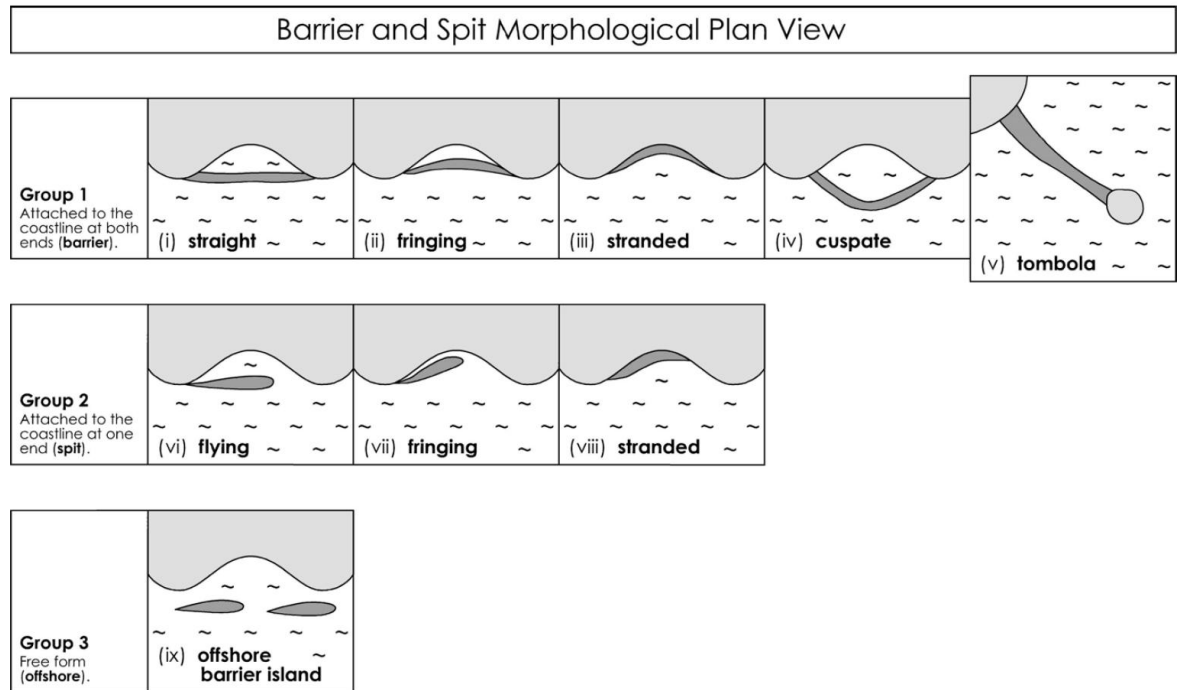


Figure 2.8 Barrier Beach Classifications (Cope, 2004)

The alignment of a barrier beach is a key indicator of the morphological climate.

There are two distinct modes of alignment a barrier beach may take based on the beach contours alignment to the dominant wave front. These are swashing aligned (SAB) and drift aligned (DAB). The swash aligned barrier is aligned to the wave front incident on the beach whereas the drift aligned barrier is aligned at a significant angle to the dominant incident wave front.

The variation in alignment of a barrier beach is driven by longshore drift rates or lack thereof. A swash aligned beach has a very low or even zero net alongshore sediment transport rate calculated on an annual or decadal scale, while cross shore transport rates dominate. The drift aligned beach usually has a significant alongshore sediment transport rate. On a drift aligned beach the direction is typically from the “proximal” end (side of beach attached to main land mass) towards the “distal” end (free end of beach).

Some barrier beaches can be composites of both drift and swash alignment, while other beaches change alignment depending on the dominant wave direction.

2.3.3 Barrier Beach Breaching

Monitoring the evolution and specifically the breaching of coastal barrier systems has been conducted at various locations around the world. The extent of the monitoring has ranged from large scale, long term remote sensing approaches to short term, intensive field campaigns and combinations of both.

The orientation and evolution of alignment of barrier beaches Orford et al. (1996) in Nova Scotia has been subject to an intensive research programme. The study links the change from stable drift aligned gravel barrier to unstable swash aligned gravel barrier. High sediment supply, growth and spatial stability is associated with a drift aligned barrier where as breakdown, migration and spatial instability are associated with gravel barrier changing orientation to swash aligned.

The processes of micro- and macro- cannibalisation of dune systems are also introduced, figure 2.9 and figure 2.10, as the method in which barriers change orientation.

- Macro-cannibalisation is experienced through the whole length of a barrier; it is due to a change in the sediment supply regime. It is an indication that over all beach orientation is changing from drift aligned to swash aligned barrier.
- Micro scale cannibalisation is symptomatic of the breakdown phase; it is usually as a result of changes in alongshore transport pattern. The erosion is localised in sub cells and breaching is a common result of micro scale cannibalisation.

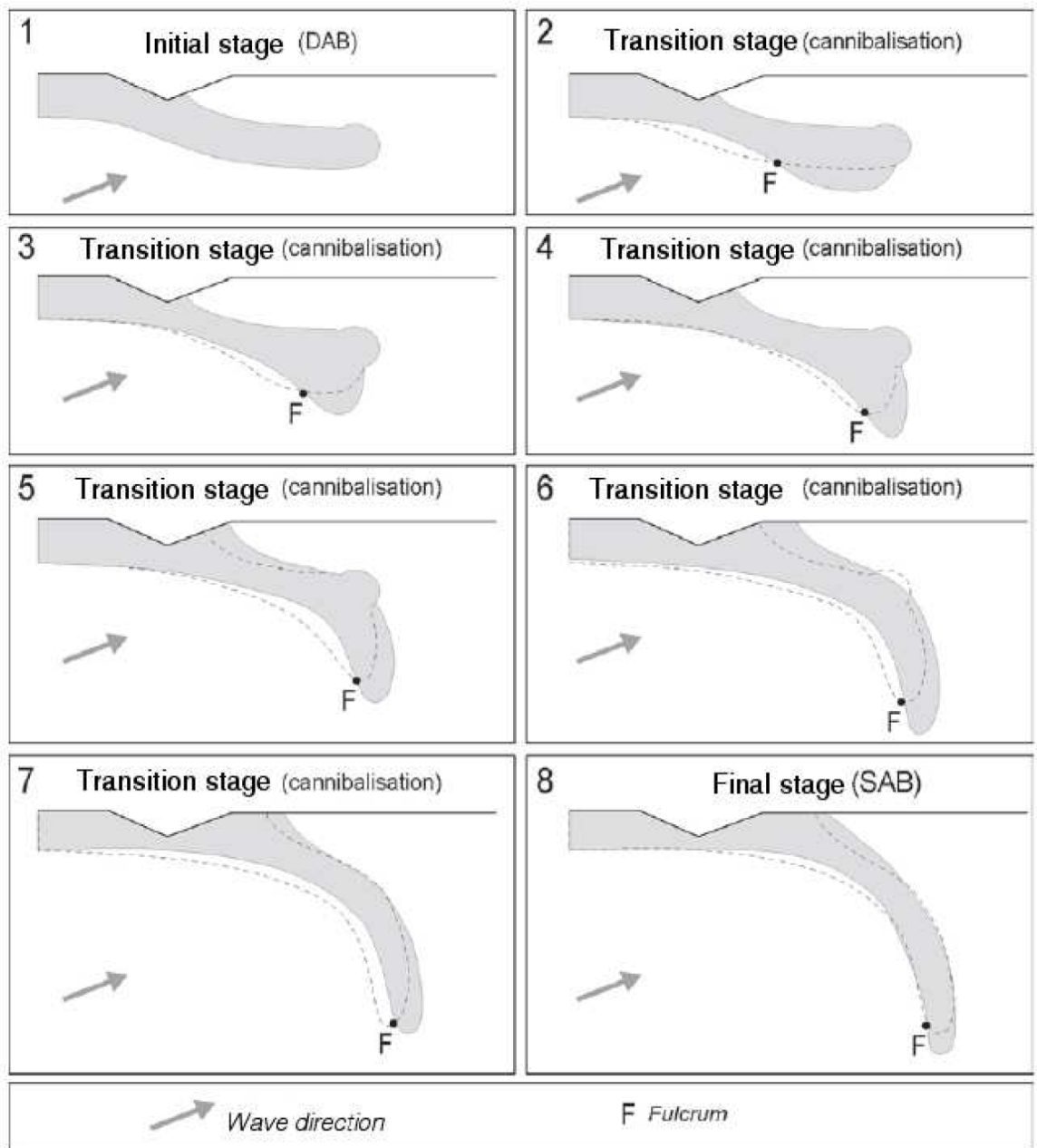


Figure 2.9 Transition from DAS to SAB through macro cannibalisation (Stephan, 2009)

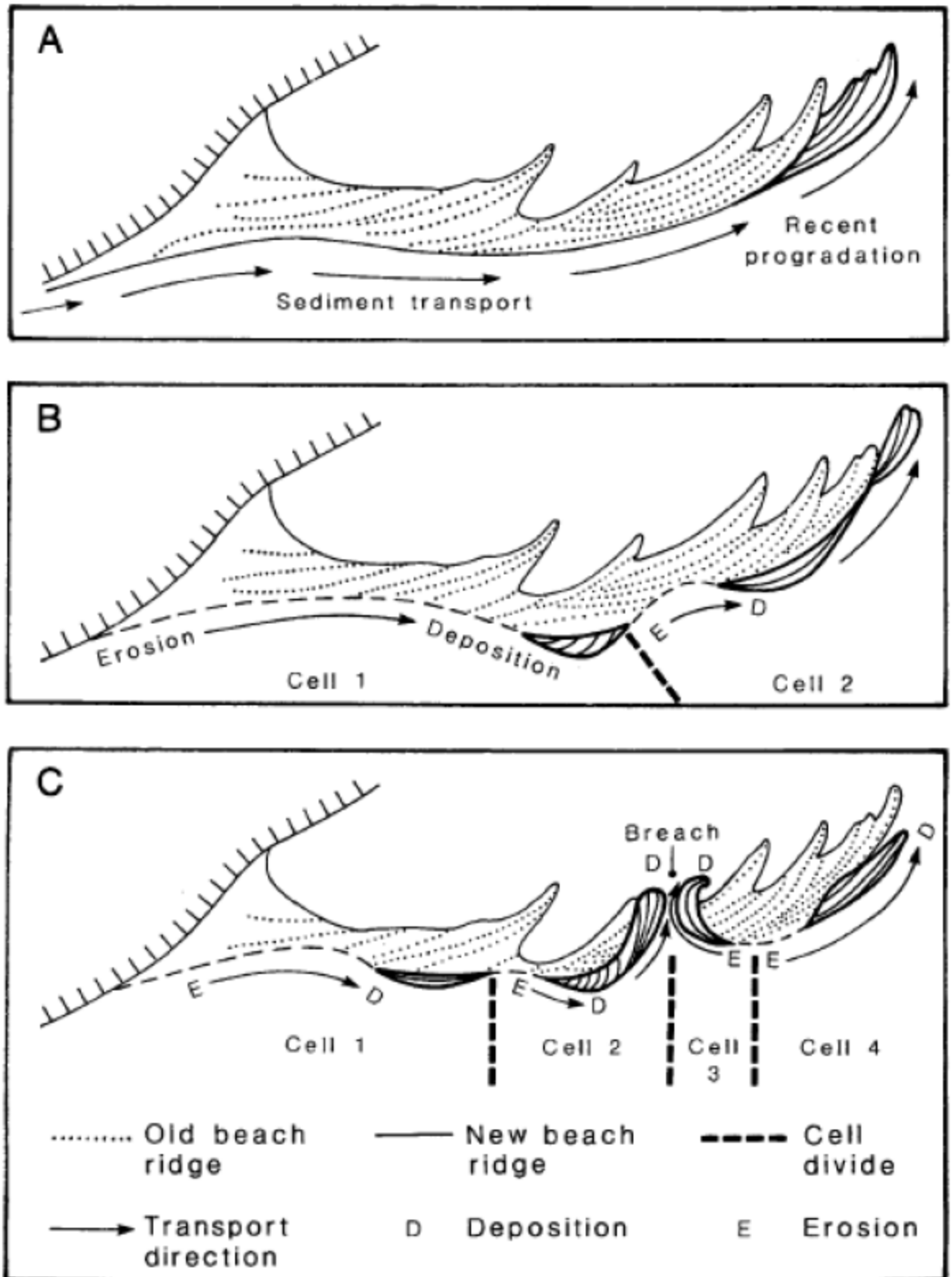


Figure 2.10 Development of micro Cannibalisation (Orford et al., 1996)

Similar cannibalisation is reported by Isla et al. (2000) in Rio Chico, Tierra del Fuego, Argentina. The elongation of a gravel spit is maintained by cannibalisation of the gravel bank further down shore, figure 2.11

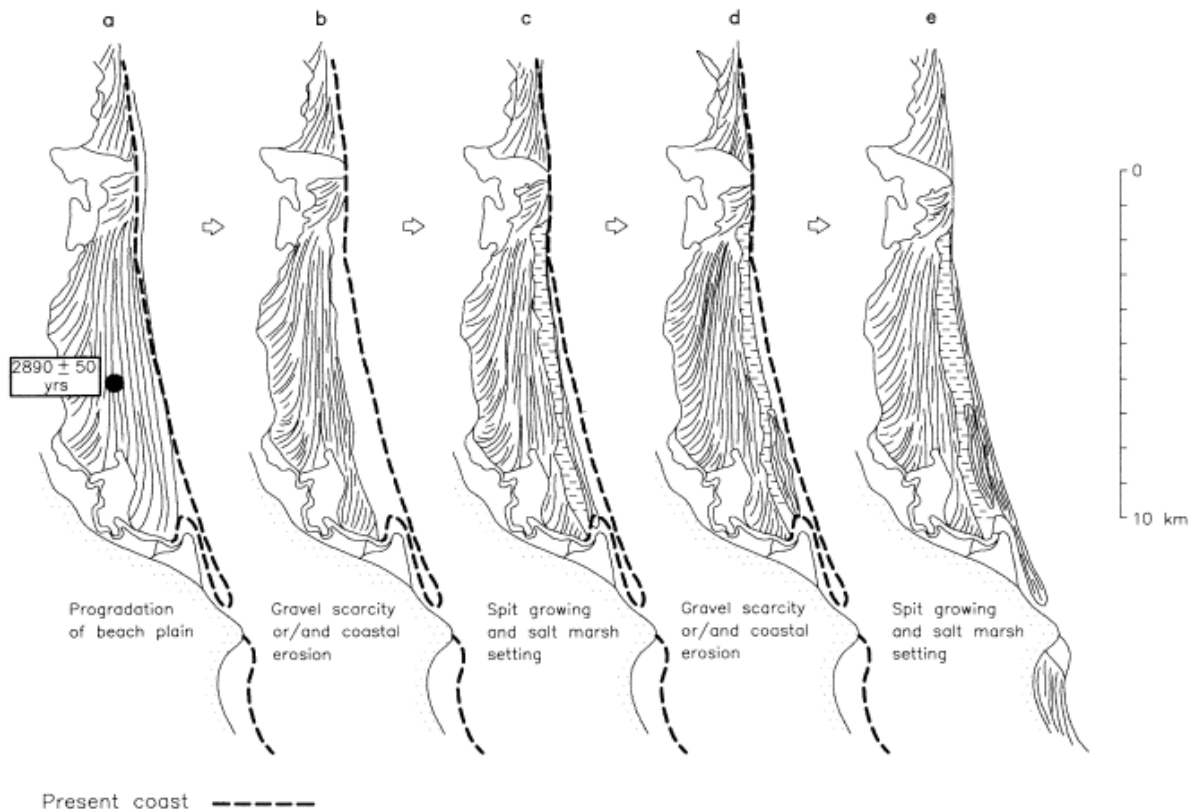


Figure 2.11 Cannibalisation in Rio Chico (Isla et al., 2000)

Terchunian et al. (1995) monitored the breaching and closure of two inlets after a storm in winter of 1992 in Long Island, NY, USA. The breaches occurred downdrift of groynes which restricted the barrier's ability to regenerate. The initially larger breach, Pikes inlet, was 250 m wide and closed within two months of breaching. This was achieved both by mechanical means and also the fact that it was far enough (1.4 Km) down drift of the nearest groyne for sediment flow to accrete. Little Pikes inlet, figure 2.12, initially only 30 m in width grew to a breach length of 1.5 Km.

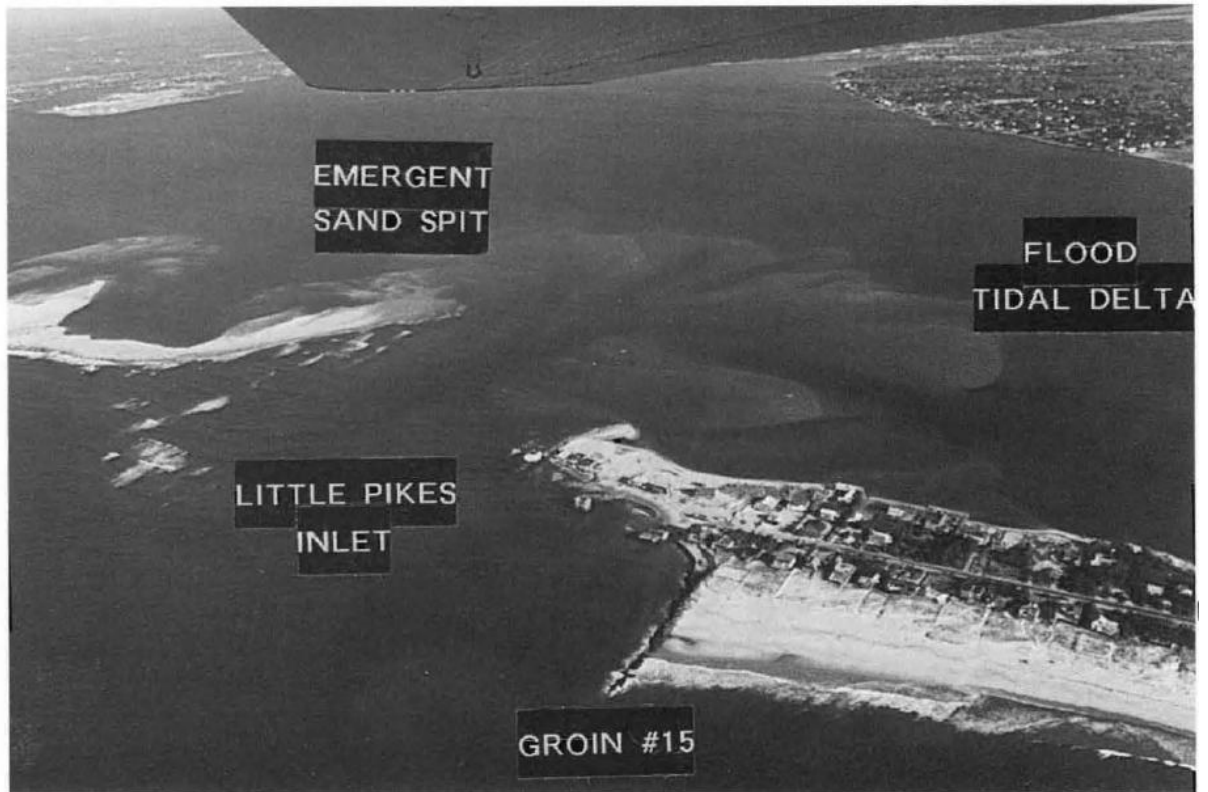


Figure 2.12 Little Pikes Inlet (Terchunian et al., 1995)

This was primarily because it was within the shadow of the last groyne and therefore was receiving very little sediment transfer. The channel deepened and flow became bidirectional. This led to the formation of ebb and flood tidal deltas. The inlet was eventually closed after emergency works 8 months later. Steel sheeting was combined with extensive beach nourishment from an offshore source. It took over 1 million m³ of sand to fill the inlet.

Barrier breaching in a seaward direction from the lagoon side has also received some examination. A breaching event occurred at Stone Lagoon, California in 2002 and was analysed by Krauss et al. (2002). Using site and aerial photography the morphology of the barrier was studied post breaching. The breach was steep sided and had a minimum width of approximately 91 m. The formation of ebb and flood shoals was recorded as well as the development of wing spits. Low tide closure occurred within one week of initial breach and the ebb shoal welded to the shoreline. The beach orientation was altered due to the effects of infilling by the longshore

transport. The flood shoal and wing spits were covered within a month of breach closure.

Baldock et al. (2008) studied the evolution of a berm in a coastal lagoon, figure 2.13, after it had been breached mechanically at Belongil Beach, New South Wales, Australia. The lagoon entrance intermittently opens and closes. Natural opening occurs after heavy rains in the catchment build up on the lagoon side of the berm. Wave and tidal forcing close the entrance rapidly during dry periods. The Berm is mechanically breached on occasion by the local authority to prevent flooding and also maintain water quality within the lagoon.

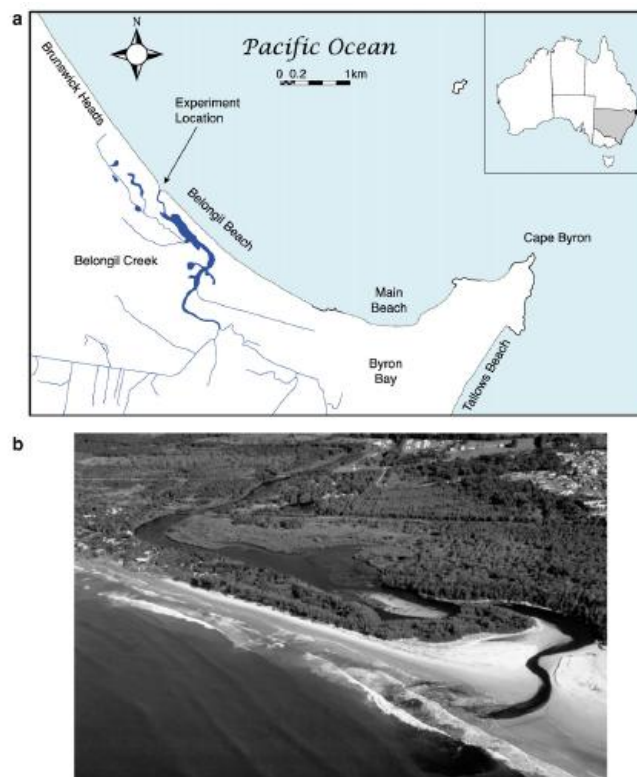


Figure 2.13 Belongil beach (Baldock et al., 2008)

After one such breaching a monitoring campaign was conducted. The lagoon entrance, the beach face and an area 100 m in length each side of the berm were surveyed daily. Wave run up on the berm was measured using shore normal array of pressure sensors deployed below sand surface. The offshore wave characteristics were obtained from Cape Byron waverider buoy, with the root mean square offshore wave height varying from 0.45 m to 1.35 m and the significant period ranged from 4 to 9.5 s. Longshore currents in the

inner surf zone were recorded by an ADV but were found to be very weak and the tidal range of 1.4 m was recorded for the duration of the test campaign.

Sediment analysis of the beach indicated that the mean grain diameter was 23 mm. It was recorded that the entrance was sealed to tidal flows 4 days after breaching. Analysis of the berm regrowth found that vertical growth was dominant with almost no progradation in the horizontal axis.

The response of barrier islands to extreme storms is documented by Houser et al. (2008) using Santa Rosa barrier Island Florida as a case study. The research applies statistical methods of cross correlation and co spectral analysis. Several conclusions on the response and evolution of barrier dunes are made. Erosion rates were correlated with bathymetry. The erosion rates were largest at the crest of inter and sub-tidal sand ridges. These locations also coincided with the lowest dune heights onshore. The area with most dissipative offshore bathymetry corresponded to the largest on shore dune heights onshore. Unfortunately the exact hydrodynamic effect the ridge has on waves during storms is not examined.

Nauset beach, figure 2.14, in Cape Cod, MA, in the USA is a dynamic system of barrier beaches that undergoes significant cyclical morphological change and has been the subject of coastal monitoring programmes for several decades. The barrier beach has historically varied from being a single inlet to dual inlet system feeding a shallow estuarine system of 6,500 ha.

A breach in the dune system in April 2007 and its subsequent development into an inlet prompted the latest research Giese et al. (2009). The location of the inlets were tracked using historical survey information from as early as the 17th Century, this was combined with recent cartography to create a conceptual model of the evolution of Nauset beach. Analysis of the results agrees with the quasi-cyclic evolution of Nauset barrier presented in earlier research.



Figure 2.14 Nauset Barrier Beach System (Giese et al., 2007)

The model describes the system's evolutionary cycle in two phases, figure 2.15. Firstly, an Inlet development phase begins with a breaching of the barrier at an updrift location, causing a period of instability with multiple inlets forming and tidal changes. The tidal range increases and tidal phase lag decreases in the bay between coast and barrier beach. Downdrift of this inlet instabilities continue while updrift the spit undergoes recurving. In this phase the tidal current is dominant over alongshore sediment transport.

After several years of instability and multiple inlets, the updrift inlet becomes stable, dominant and then the only inlet as the barrier system migrates down drift.

The inlet migration phase commences after several decades of single inlet stability, the inlet moves downdrift as the barrier spit elongates in a down drift direction. This phase is wave dominated with the downdrift driven by alongshore transport. The tidal range decreases and phase lag increases in the bay area. In this phase remnants of the barrier weld to the shoreline.

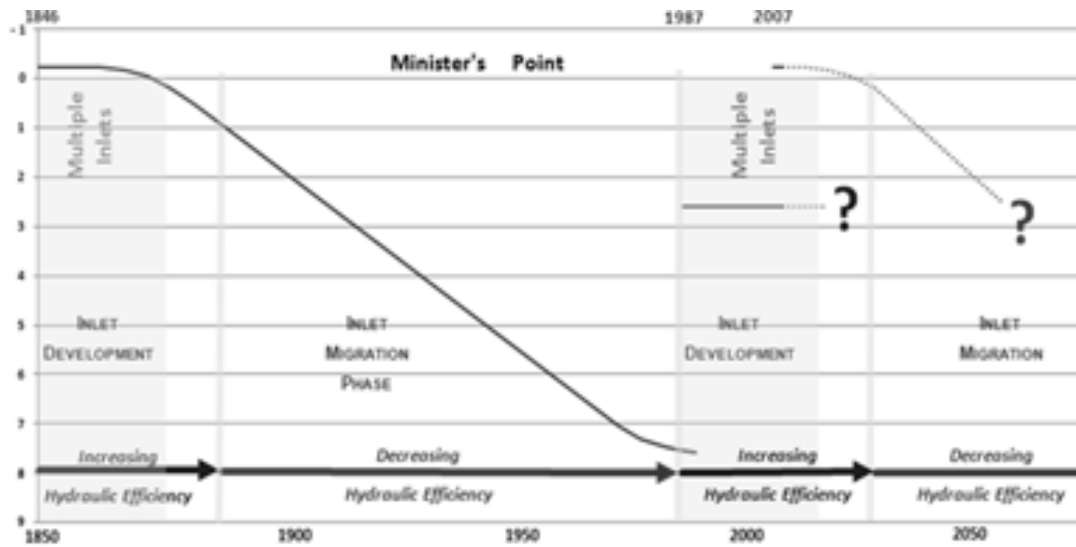


Figure 2.15 Conceptual model of the evolution of Nauset beach (Giese et al., 2009)

The use of ground penetrating radar (GPR) in combination with vibrocoring analysis (Buynevich & Donnelly, 2006) enabled the identification of breaching events and inlet formations previously undocumented in Massachusetts, USA. Sediment over wash due to storm events from 900AD was preserved in the back barrier areas. Similar techniques were applied to Bartra barrier island in Kilalla bay, Co. May, Ireland (Cooper et al. 2011).

The study focuses on the behaviour of the system over a decadal timescale from a breaching event in the 1950's to 2002. The breaching can be related to the position of an inlet in the 1950's when it was running along the margin of the dunes. This enabled the fast moving inlet stream to remove sediment from the dunes at this location thus reducing the dune's capacity for post storm repair.

The inlet channel began to migrate in the 1970's leaving a large sand swash plane which contributed to the infilling of the breached area. The sealing of the breach began with successive sand ridges extending out and becoming vegetated. These recurves are clearly visible from the GPR, figure 2.16

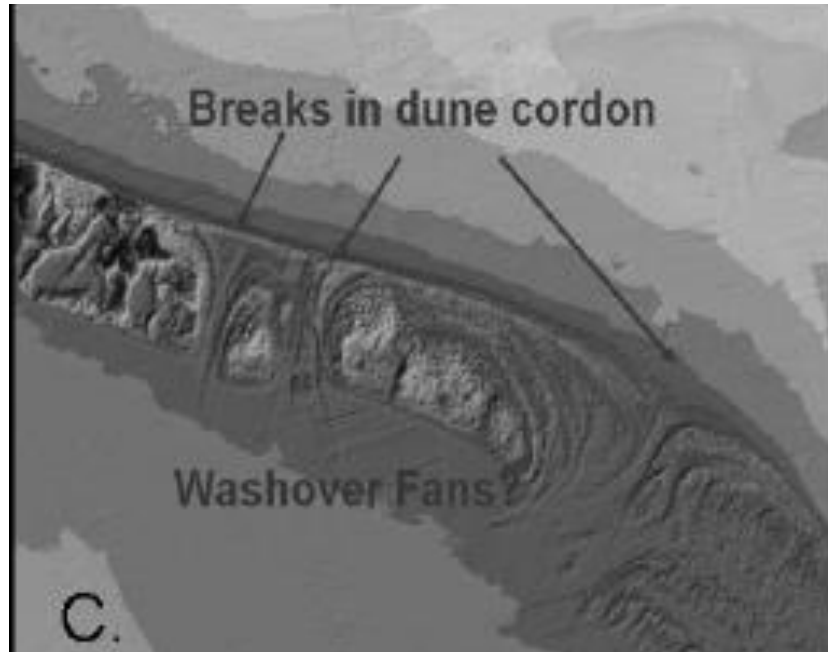


Figure 2.16 Historical breaches in Bartra Barrier (Cooper et al., 2011)

2.3.4 Dune Erosion

Dune erosion which is closely related to barrier breaching has been quantified by Van Rijn (2009). The DUNERULE formula (10) was developed using results from experimental modelling and mathematical modelling of dune erosion. This includes output from the wave by wave cross shore profile model, CROSMOR-model and both large and small scale physical modelling in wave flumes. A sensitivity study showed that the most influential input parameters for the DUNERULE formulae are storm surge and sediment grain size diameter. A schematic of the formulae is presented in figure 2.17.

$$A_{d,t=5} = A_{d,ref} (d_{50,ref} / d_{50})^{\alpha_1} (S/S_{ref})^{\alpha_2} (H_{s,o}/H_{s,o,ref})^{\alpha_3} (T_p/T_{p,ref})^{\alpha_4} (\tan\beta/\tan\beta_{ref})^{\alpha_5} (1 + \theta_o/100)^{\alpha_6} \quad (10)$$

with:

$A_{d,t=5}$ dune erosion area above storm surge level after 5 h (m^3/m),

$A_{d,ref}$ dune erosion area above storm surge level after 5 h in Reference Case=170 (m^3/m),

S storm surge level above mean sea level (m),

S_{ref} storm surge level above mean sea level in Reference Case=5 m,

$H_{s,o}$ offshore significant wave height (m),

$H_{s,o,ref}$ Offshore significant wave height in Reference Case=7.6 m,

T_p peak wave period (s),

$T_{p,ref}$ peak wave period (s) in Reference Case=12 s,
 d_{50} median bed material diameter (m),
 $d_{50,ref}$ median bed material diameter in Reference Case=0.000225 m,
 $\tan\beta$ coastal slope gradient defined as the slope between the -3 m depth contour (below mean sea level) and the dune toe (+3m),
 $\tan\beta_{ref}$ coastal slope gradient defined as the slope between the -3m depth contour and the dune toe (+3 m) for the Reference Case=0.0222 (1 to 45),
 θ_o offshore wave incidence angle to the coast normal (degrees),
 α_1 exponent=1.3,
 α_2 exponent=1.3 for $S > S_{ref}$ and $\alpha_2=0.5$ for $S < S_{ref}$,
 $\alpha_3 \alpha_4 = \alpha_6 = 0.5$ (exponents), α_5 exponent=0.3.

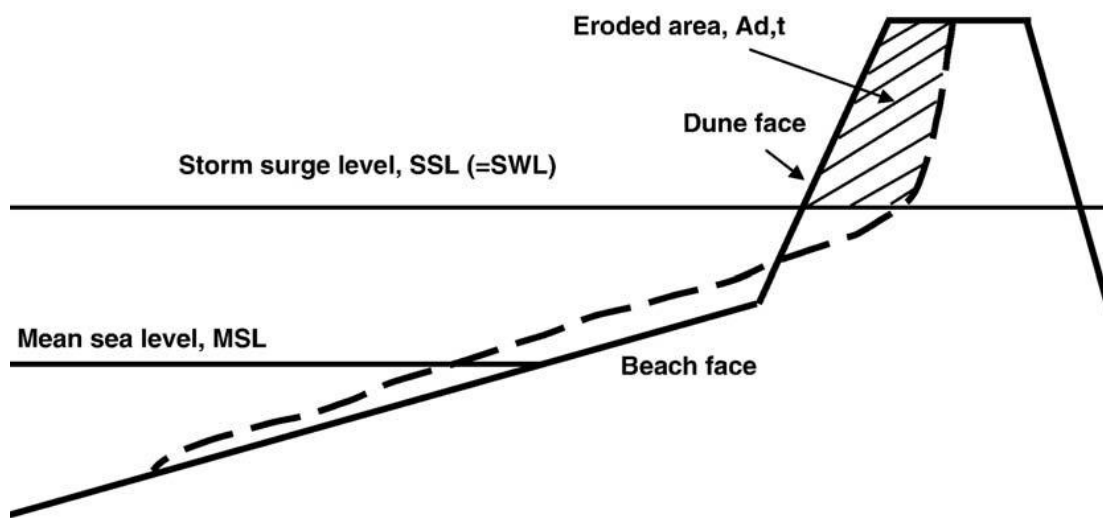


Figure 2.17 DUNERULE Schematic (Van Rijn, 2009)

2.3.5 Inlet dynamics

Tidal inlet dynamics are an important factor when considering morphology of a coastal cell. Examining the evolution patterns of tidal inlet channels enhances the understanding of the morphological drivers on inlet/barrier coastal systems and also provides points of reference for future morphological responses of the barrier beach system.

Determining the stability of tidal inlets has been the subject of several equations the most notable being Escoffier's (1940). The peak velocity (V_m) and cross-sectional area of an inlet is plotted as a semi empirical closure curve and stability is based on the curve's intersection with a line representing the equilibrium velocity (V_e , which is based on the grain size of

sediment) at which point sediment from the inlet bed is transported by the current, figure 2.18.

If the peak velocity, V_m , is less than V_e , the channel tends to fill and if V_m is greater than V_e than the channel will erode. However, stability is not to be confused with stationary cross sectional area ($V_e = V_m$). A typical Escoffier curve will have one unstable and one stable root.

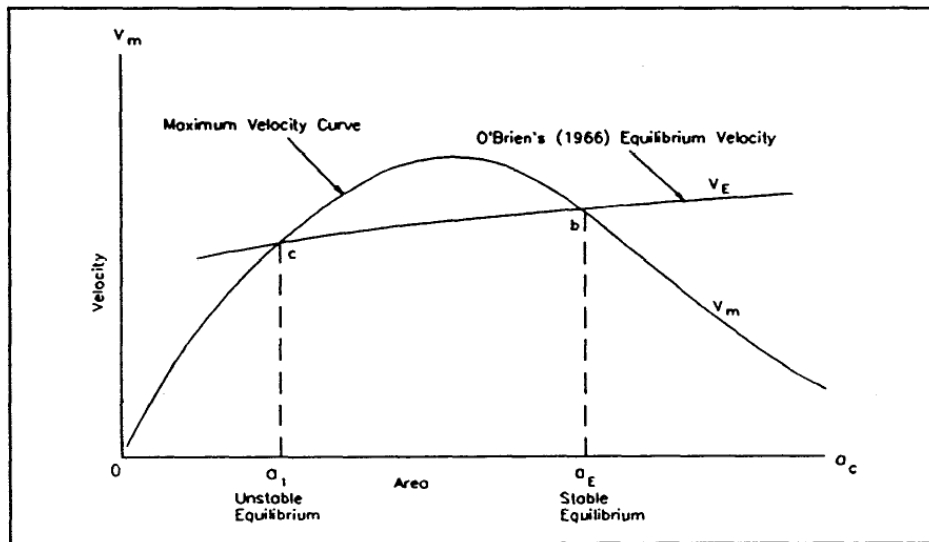


Figure 2.18 Escoffier diagram of maximum velocity and equilibrium velocity versus inlet cross-sectional area (Escoffier, 1940, amended)

The various mechanisms of sediment bypassing at inlets have been documented by FitzGerald, Kraus et al. (2000) and categorised into 6 typical conceptual models of natural inlet sediment bypassing behaviour, plus 3 artificial jettied (manmade) models, not discussed here due to relevance.

Model 1, figure 2.19, describes an inlet migration and spit breaching process where ebb delta migration and spit accretion from the up drift to down drift causes the inlet to infill. This is followed by updrift barrier breaching and closure of original inlet due to the landward migration of ebb tidal bars.

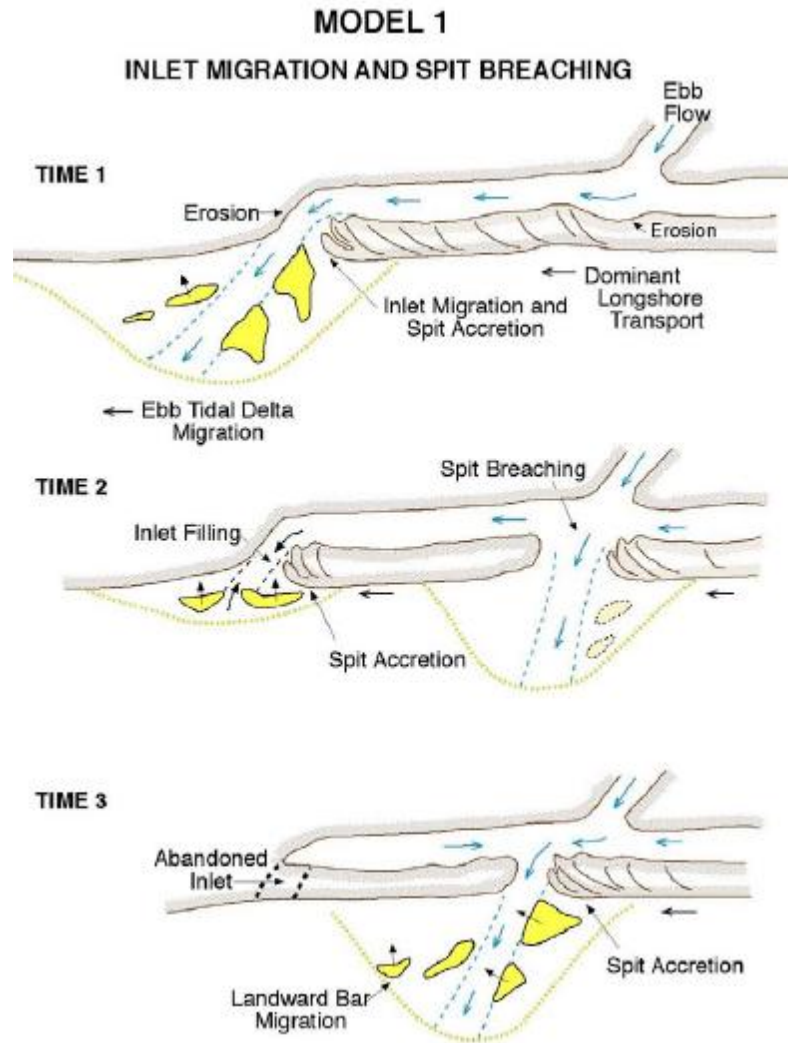


Figure 2.19 Model 1 of FitzGerald's classification (FitzGerald et al., 2000)

Model 2, figure 2.20, describes the stable inlet processes when an inlet is usually geologically fixed and main ebb tidal channel does not tend to migrate. Accumulation and shoreward migration of swash bars occurs on the ebb tidal delta. These bars eventually weld with incipient spits formed by large deposition on the distal end of barrier. These large swash platforms induce wave refraction which can locally force the sediment transport regime in the opposite direction to the dominant downdrift direction.

MODEL 2
STABLE INLET PROCESSES

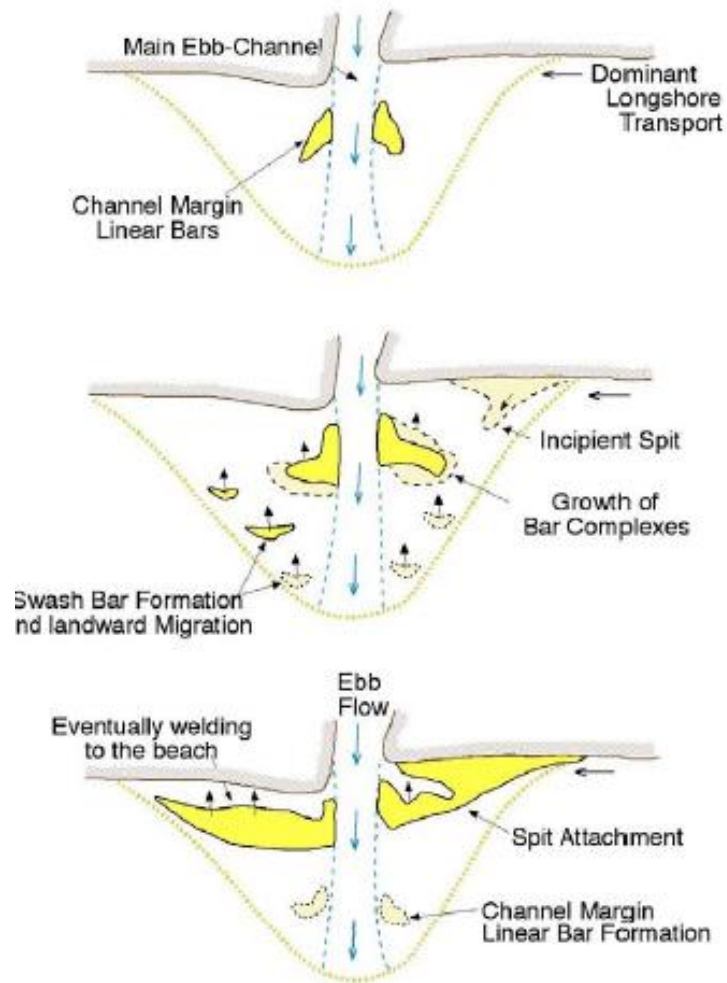


Figure 2.20 Model 2 of FitzGerald's classification (FitzGerald et al., 2000)

The ebb tidal delta breaching model, figure 2.21, occurs when the tidal inlet's throat position is stable but the ebb channels migrate in a downdrift direction. The main ebb channel is deflected in a downdrift direction as a result of accumulated sediments on the updrift side of the inlet. As the inlet is deflected erosion occurs on the down drift shore line. The deflection angle of the channel reaches a critical point whereby it becomes hydraulically inefficient. The ebb tidal delta is breached to form a more direct pathway seaward by the inlet resulting in the migration shoreward of the remnants of the ebb tidal delta bars. Bar welding occurs in the down drift shoreline as the updrift ebb tidal delta begins to accrete again.

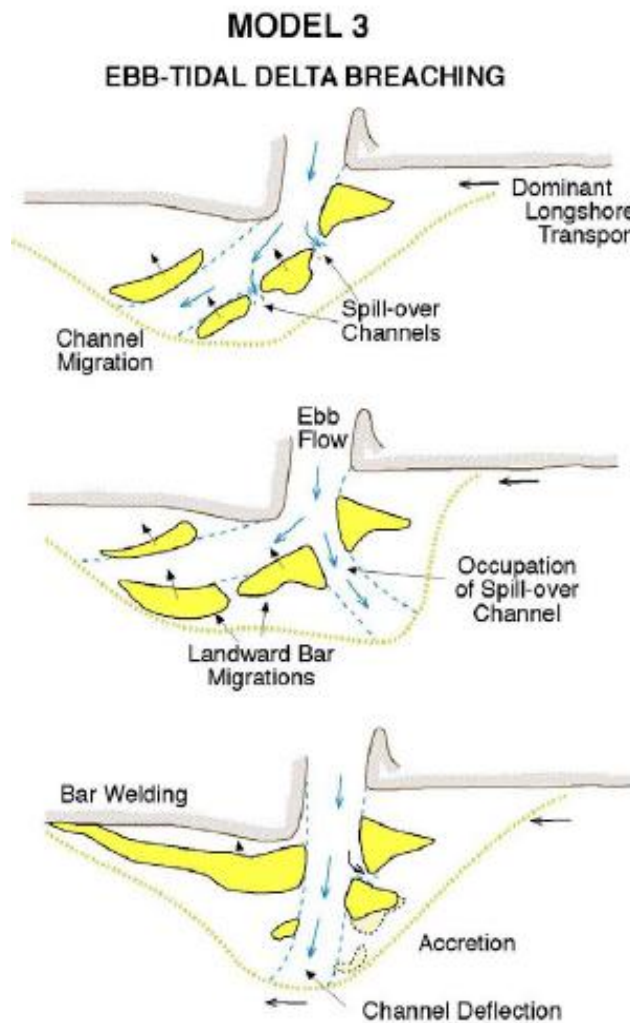


Figure 2.21 Model 3 of FitzGerald's classification (FitzGerald et al., 2000)

The Outer Channel Shifting Model, Model 4, figure 2.22, is similar to Model 3 but only involves the outer seaward section of the channel. The inner portion of the tidal inlet channel remains fixed as the outer portion deflects in a downdrift direction. Subtidal shoals are created as the inlet is deflected. Eventually a channel is cut through the ebb tidal delta, this divides the ebb tidal delta and allows for a portion, typically 5,000 – 50,000 m³ of sediment to migrate to the down drift shoreline.

MODEL 4 OUTER CHANNEL SHIFTING

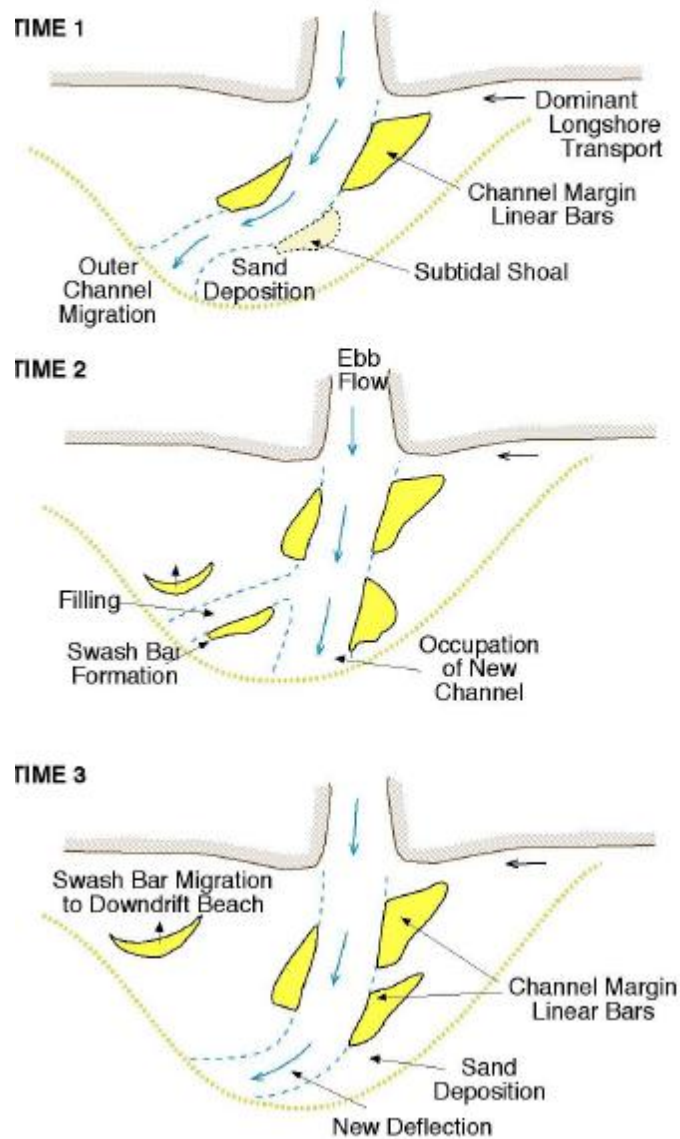


Figure 2.22 Model 4 of FitzGerald's classification (FitzGerald et al., 2000)

Spit platform breaching, Model 5, figure 2.23, is a process that occurs when the spit platform on the down drift side extends into the main inlet channel. The major channel in the back barrier usually runs parallel to the downdrift side close to the inlet channel entrance. As the spit grows out into the main channel, secondary channels are formed closer to the updrift side to provide a short cut route to the ocean from the backbarrier. A secondary channel gradually deepens and becomes the main inlet channel. The portion of the

spit platform on the downdrift side of the new channel migrates downdrift and eventually fills the original channel entrance.

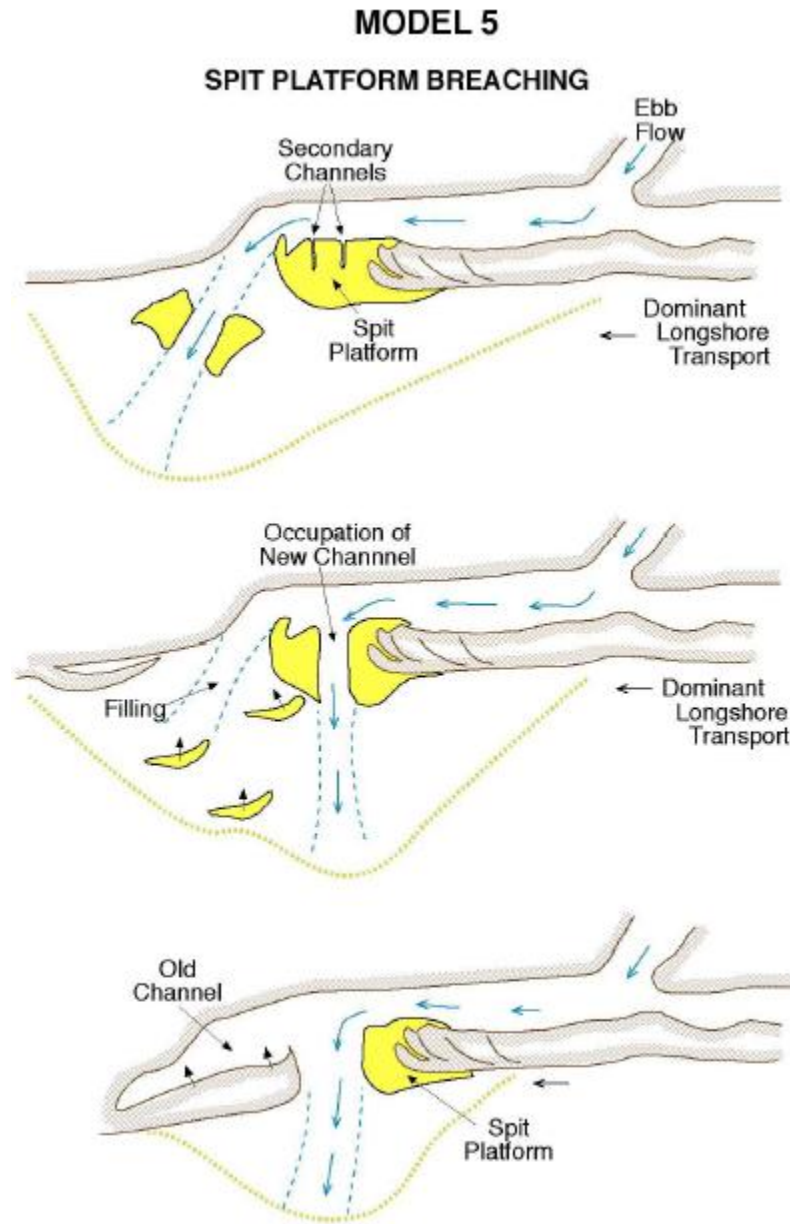


Figure 2.23 Model 5 of FitzGerald's classification (FitzGerald et al., 2000)

The final model of natural sediment bypassing of inlets, Model 6, figure 2.24, describes the wave dominated inlet. When wave driven sediment transport dominates over tide driven, the inlet channel tends to be less than 200 m wide with shallow ebb channels. The ebb tidal deltas are close to shore and generally exposed at low tide. Sediment bypassing is a continuous process driven by surf zone processes rather than event driven tidal forced bypassing.

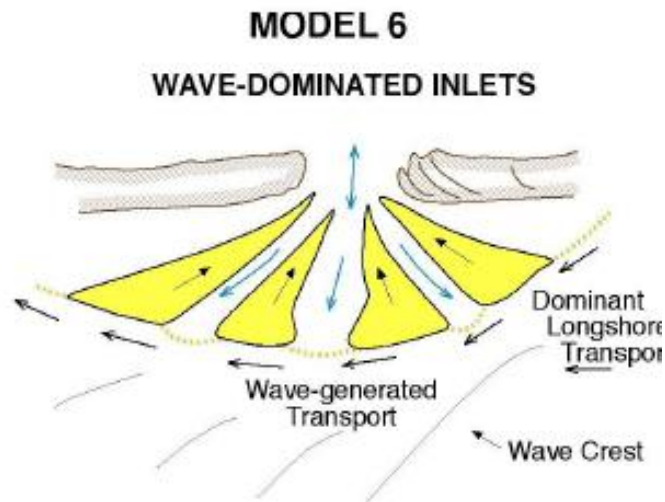


Figure 2.24 Model 6 of FitzGerald's classification (FitzGerald et al., 2000)

The evolution of inlets in the Ria Formosa barrier island system in southern Portugal has been well documented notably by Balouin et al. (2001), Vila-Concejo et al. (2003) and Vila-Concejo et al. (2007).

Balouin et al. (2001) described the evolution of the barrier system with a model corresponding to FitzGerald et al's (2000) classification model of inlet migration and spit breaching. The evolution was governed by winter storms. The inlet channel moved downdrift with progress dependent on onshore drift rates and storm frequency.

Vila-Concejo et al. (2007) developed a 4 stage conceptual evolution model, figure 2.25, of the breaching process on Ria Formosa. The model is based on volumetric analysis of an artificially opened inlet and surrounding morphological features such as ebb and flood tidal deltas. It was observed that after two years of opening, the inlet entered a mature phase, Stage 3, figure 2.25, with fully developed deltas and inlet migration and sediment bypassing began. This stage was periodically interrupted thereafter by storm conditions, Stage PS (Post Storm), figure 2.25.

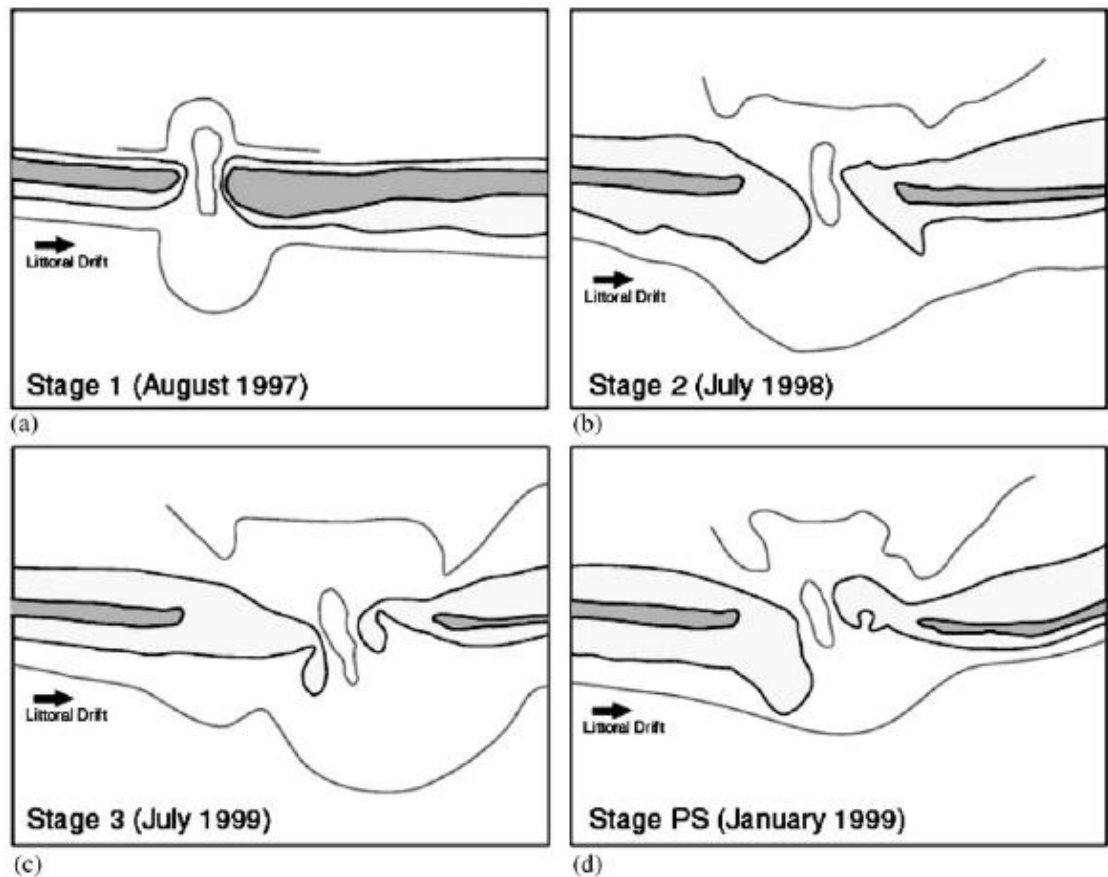


Figure 2.25 Four stage conceptual model (Vila-Concejo, 2007)

Michel et al. (1997) developed two stage conceptual model, figure 2.26, of the evolution of the Arcachon tidal inlet in south west France. The model describes the evolution of a single channel inlet system to a dual inlet system that connects the open sea to the Arcachon's tidal lagoon.

Initially, a single channel is present in the south with the ebb tide delta eroding and the up drift and down drift coasts prograding, Stage 1, figure 2.26. A northern channel breaks through the delta and changes the processes, with the coasts eroding and the ebb tidal delta growing. Two inlet channels are formed and begin moving away from each other, Stage 2, figure 2.26.

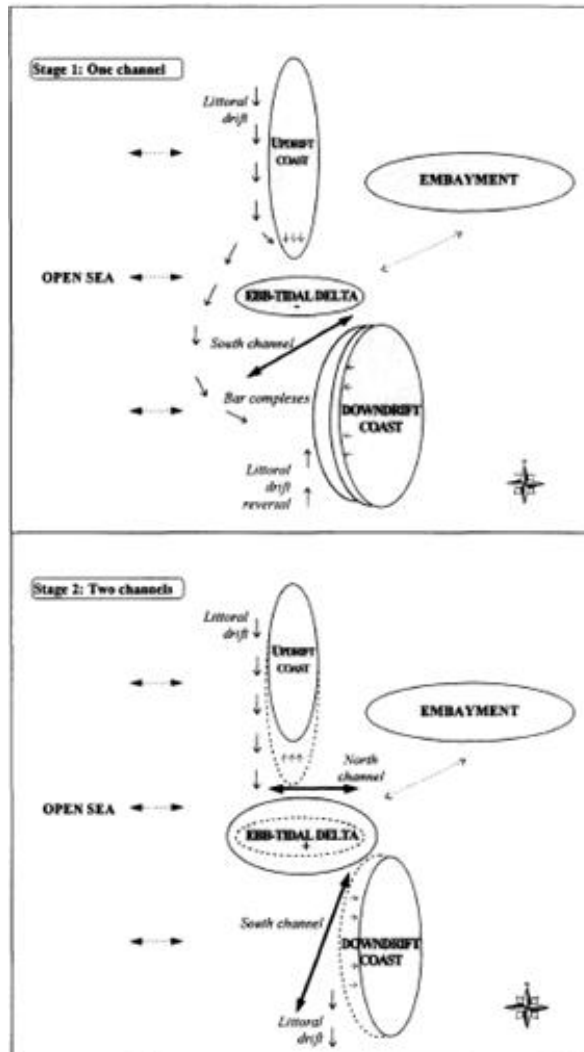


Figure 2.26 Two stage conceptual model (Michel et al., 1997)

Cooper et al. (2007) studied the evolution of an embayed tidal inlet with no external sediment budget. The site, Five Finger Strand, Co. Donegal, Ireland, is significant, in that it is relatively free of the major drivers of coastal morphology (storms, sediment supply). It was found that the location of the ebb channel and its ebb tidal delta had alternated on a north-south axis over a decadal scale with zones of accretion and erosion varying in response to the location of the channel and delta.

The cycle, figure 2.27, is driven by the balance between ebb currents and wave energy. When sediment in the southern ebb tidal delta has built up enough by wave action, the ebb tidal channel begins to change direction, B, figure 2.27. As the ebb channel migrated away from the southern beach, bar welding of the delta occurred, re-nourishing that barrier beach.

When the ebb channel has migrated to the northern side an ebb tidal delta is formed there at the expense of the sand on the northern barrier beach causing dune scarping and erosion. The northern ebb tidal delta eventually becomes large enough that it diverts the ebb tidal channel to the south again.

The migration begins from north to south with the northern ebb tidal delta worked back onshore replenishing the erosion that occurred on the northern barrier beach, C, figure 2.27. An important conclusion from this study was the regular occurrence of erosion at high tide in the absence and independent of storms. It was determined that traditionally assumed drivers were not necessary to implement coastal change and that it can occur in the absence of these drivers.

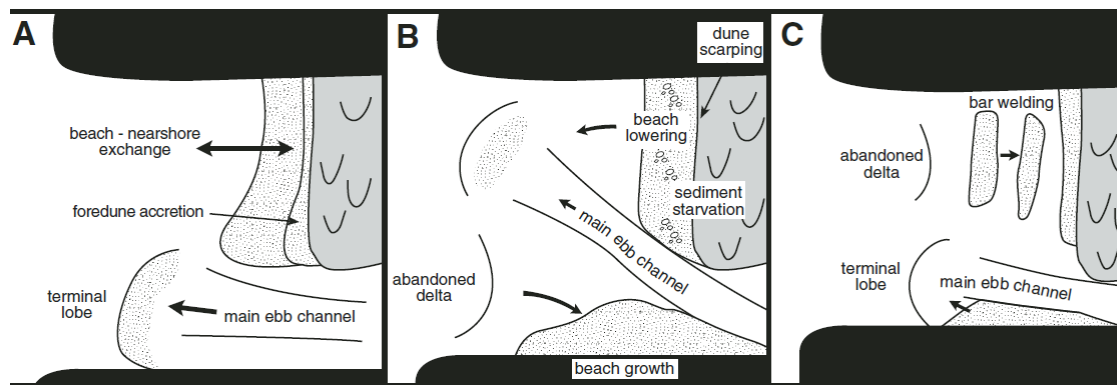


Figure 2.27 Morphological cycle of Five Finger strand (Cooper et al., 2007)

2.4 Coastal Morphodynamic Monitoring Techniques

The previous sections have outlined the various factors influencing coastal morphodynamics, particularly as applied to barrier structures. When examining the previous work on barrier beach tidal inlet morphological studies, it becomes clear what parameters are required and how these parameters clarify the unknowns relating to formation and the future of coastal morphology. Typically datasets required include information on wind, waves, tidal currents, water level, topography, bathymetry, geology and sometimes even site vegetation, hydrology and seismology.

Established methods of coastal zone monitoring include topographical surveys, deploying wave and tidal current recording equipment, sediment sampling and tracer studies.

This section, however, also provides, a review of experimental coastal monitoring techniques. These experimental monitoring techniques include aeolian sediment transport monitoring, grain size trend analysis or GSTA, detailed in Chapter 4, a trial of a HF Ocean Radar system, detailed in Chapter 5.

The monitoring methodologies can be broken into two general types those relating to hydrodynamic data collection and those relating to sediment transport monitoring.

2.4.1 Coastal Hydrodynamic Monitoring

There are several established methods used to record wave and tidal current data in the coastal zone. Established wave data recording technology include several types of floating buoys and bottom mounted pressure sensors. While more recently seismic plates, satellite and HF Ocean radar are being developed to record wave data. The range of tidal current recording instruments include impellor base type, acoustic Doppler and electromagnet current meters. The following is a description of the most relevant devices for recording wave and tidal current data in a marine environment;

Particle Following Buoys

Particle following buoys such as the Datawell Directional Waverider Buoy (Datawell BV 2010), figure 2.28, are small (typically diameter < 1 m) moored floating buoys that traditionally operated utilising accelerometers fixed on a stabilised platform within the buoy. The heave motions of the buoy were deduced by double integrating vertical accelerations and directionality was calculated based on horizontal and vertical acceleration data. Recently, accelerometers have been replaced by RTK GPS systems that record the motion directly and are much lighter than accelerometers. The correct mooring of this type of buoy is critical for accurate data recording. If incorrectly laid the mooring line can limit the motion of the buoy and sometimes induce motion unrelated to the sea state.



Figure 2.28 Waverider buoy (Courtesy Of Marine Institute)

Pitch-Roll-Heave Buoys

The Pitch-Roll-Heave (PRH) is a floating buoy that are larger than the particle following buoys, sizes ranging from 3 m up to 12 m in diameter. Unlike the particle following, which are excited by wave orbital motion the larger PRH buoys follow the slope of the wave surface. As well as heave data, the pitch and roll motion is also recorded to give wave directionality. Due to their large size these wave buoys are usually fitted with other metocean sensors to measure wind speed and direction, air pressure, relative humidity, salinity and sea surface temperature. The M3 offshore wave data used in this research was recorded on a Fugro Wavescan buoy, a PRH type buoy similar to the one shown in figure 2.29.



Figure 2.29 Fugro Wave scan PRH buoy (Courtesy Marine Institute)

Bottom Mounted Pressure Sensors

These instruments are deployed on the seabed and measure the changes in pressure caused by wave action. These sensors are depth limited due to the attenuation of the pressure signal from waves with depth. The Valeport Midas bottom mounted wave gauge, figure 2.30, which is used extensively during the course of this research, is limited to depths shallower than 20 m. Deeper than this and waves under 7s period are not recorded. Care must be taken when deploying these sensors as they can become buried easily if located far enough inshore of the closure depth of the coastal cell. Several bottom mounted pressure sensors have been lost in previous studies of Dingle Bay due to the burial (Vial, 2009). However, for coastal and inshore studies they are a mobile and cost effective solution. Electromagnetic Tidal current meters, discussed later, are usually installed within the Valeport unit to give tidal current data at 0.1 m above the unit.



Figure 2.30 Valeport Bottom Mounted Pressure Sensor Wave Gauges

Satellite Measurement

Recently, satellite measurements of the sea surface are being used to derive wave statistics. The backscatter of high frequency pulses from the ocean surface is analysed by altimeters to produce wave height maps of large areas of the ocean surface. This method has been applied over a long duration to compare with hindcast global wave models (GlobWave Project, 2012). Due to its focus on wave statistics at a global level this method is more suited to large spatial scale applications such as forecasting and wave resource assessments rather than specific coastal studies which are undertaken on a much smaller spatial scale.

Seismic Correlation

An experimental method of deriving significant wave heights from seismic land based coastal seismic recording locations is being developed by University College Dublin. A seismic signal is generated on the seabed by wave action (Micro-seism) which is detectable on land in the background

seismic noise of these recorders. By comparing micro-seisms to offshore measurement buoy wave data, a methodology of extracting significant wave height was developed (Moni et al, 2012). Although in its early stages this methodology could provide a legitimate source of wave height validation for other instruments deployed in the coastal zone as well as calibrating numerical coastal models.

HF Ocean Radar

Ocean data (surface currents, wave heights and wind direction) can be acquired by interpreting the backscatter signal from radar transmitted out over a water surface. This technology offers the advantage over single point measurement of being able to capture wave and surface current statistics over a large area of sea surface instantaneously. The systems are usually land based which allows ease of access for maintenance and deployment. Until recently the radar systems have been used in open ocean settings to record ocean surface currents and wave statics over a long range (100 km) and low spatial resolution (1 km grids).

There are two commonly used methods of ocean radar, differentiated by the method in which the azimuth is resolved, beam forming and direction finding.

Direction finding systems such as CODAR, figure 2.31, is a combined transmit and receive system in one unit. The system transmits a signal then waits for the back scatter, this is known as chirp. This delay results in a cut off of the first 2 km in front of the unit. The signal is received by two internal antennae set at 90° to each other. The software calculates the signal direction from the difference between these two antennae. Its advantages are its compactness and greater than 180° angular range. However, it is more unreliable in high energy sea states and has a higher angular uncertainty than beam forming phase arrays systems.



Figure 2.31 CODAR installation in California (UC Davis Bodega Laboratory)

The Beam Forming method utilised by WERA, transmits frequency modulated continuous wave radar chirp (FMCW), figure 2.31. A continuously swept radar signal is transmitted. The reflected signal has a frequency offset

compared to the actual transmitted signal, thus the distance is frequency encoded.

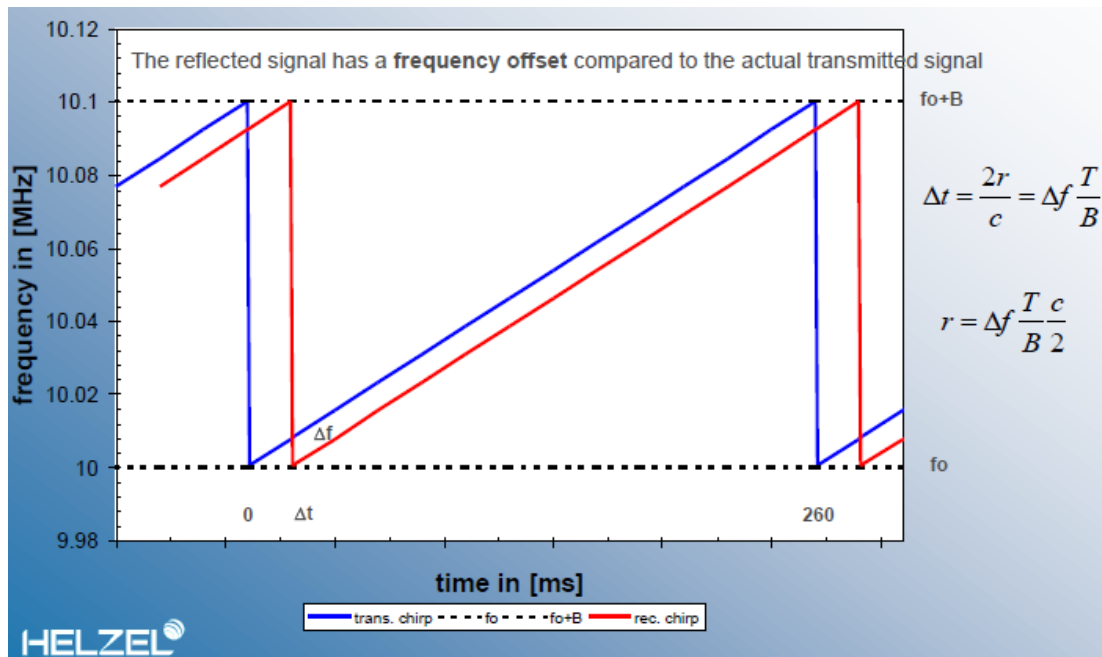


Figure 2.32 Frequency modulated continuous radar chirp (www.helzel.com)

The beam is sent over a defined angular range; typically 120° via 2 or 4 antennas transmit arrays (TX), figure 2.33. An array of receive antennas (RX) usually 12 or 16, figure 2.34, are decoupled from the transmission array.



Figure 2.33 WERA TX array (www.helzel.com)



Figure 2.34 WERA RX array (www.helzel.com)
Ocean Radar Theory

Ocean radar technology is based on converting the backscattered radar signal into surface current and wave statistics using the Bragg effect theory.

The Bragg effect or Bragg scattering principle first documented for ocean surface by Crombie (1955) states that radar signals are backscattered by moving surface waves at exactly $\frac{1}{2}$ the wavelength of the radar wavelength λ_{radar} , figure 2.35.

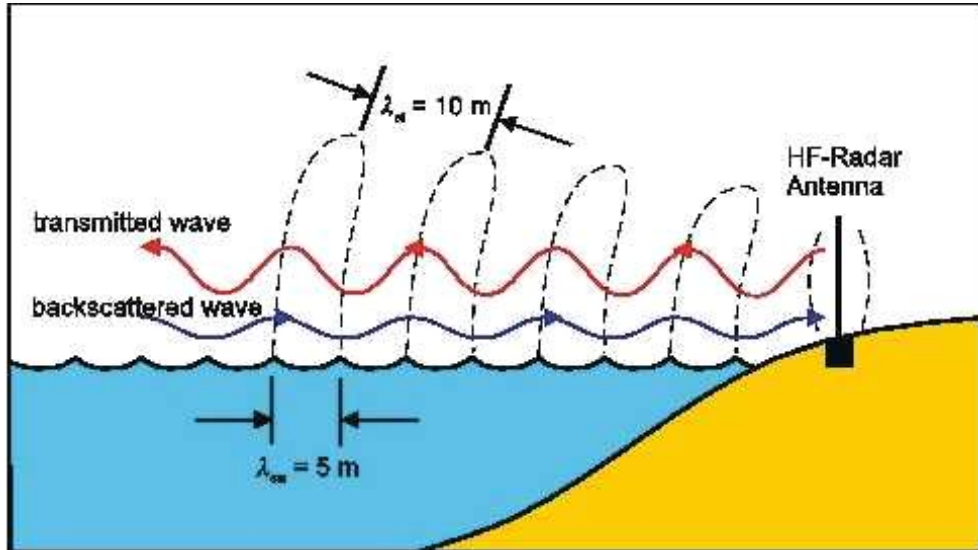


Figure 2.35 Bragg scattering effect (WERA 2008)

The back scattered radar is integrated over time and an energy spectrum is produced. The Bragg effect produces two dominant peaks in the echo Doppler spectrum, figure 2.36, symmetrically positioned about the radar frequency. If there is no surface current the Bragg peaks are offset about the radar frequency on the spectrum by a known frequency, called the “Bragg frequency” and given by (11);

$$f_B = \sqrt{\frac{g}{\pi \lambda_{\text{radar}}}} \quad (11)$$

Where f_B = Bragg frequency
 λ_{radar} = Radar signal wave length

If a surface current exists, the Bragg peaks shift from the theoretical “Bragg Frequency”. This shift is known as the Doppler frequency shift, Δf . The radial component of the surface current velocity Δv , is calculated from the Doppler frequency shift using (12). At least two radar stations are required to calculate a surface current vector. The accuracy of the surface current extraction is maximised when radar beams intersect at 90° .

$$\Delta v = \frac{\lambda_{\text{radar}}}{2} \Delta f \quad (12)$$

Analysis of the second order Bragg backscatter peaks, figure 2.36, can yield information of the ocean wave energy spectrum. Several techniques of inversion integration have been used to extract wave height and direction statistics from backscattered radar data most notably Barrick (1972) and Wyatt et al. (1999).

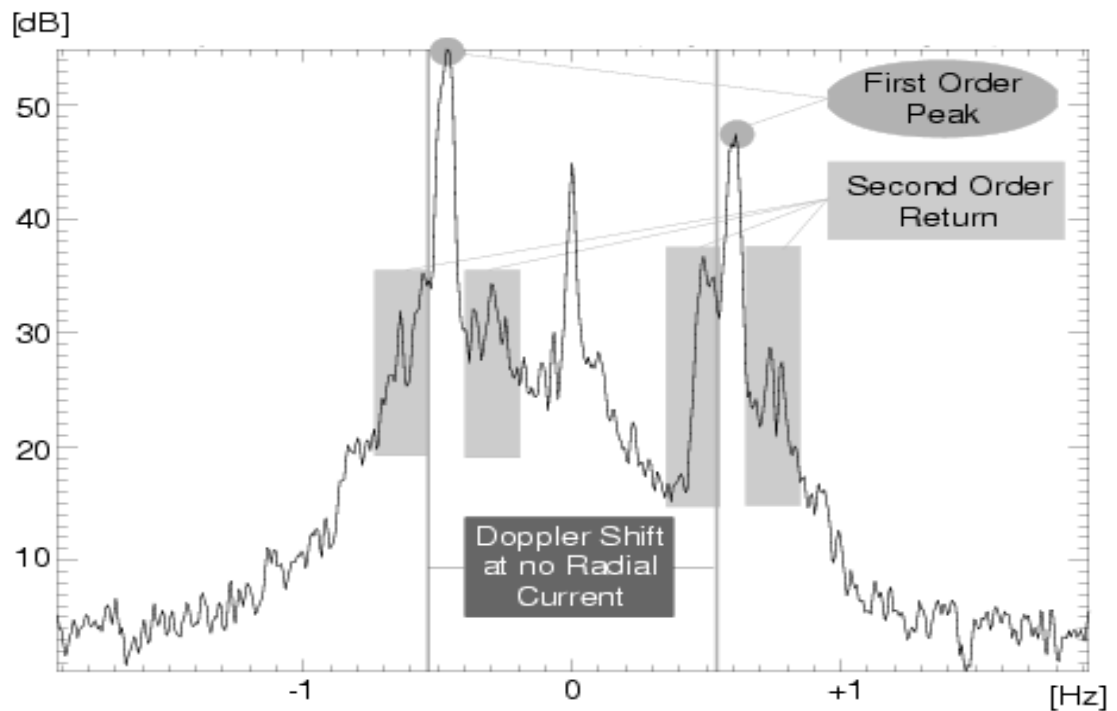


Figure 2.36 Doppler Spectrum of backscattered radar (Helzel, 2006)

The frequency range of the transmitted signal dictates the distance of the beam forming and hence the distance that ocean data is recorded. Because ocean radar follows the surface of the ocean it can extend beyond the horizon, this is known as “over the Horizon radar”, or OTH radar. WERA radars can detect surface currents up to 250 Km, figure 2.37. As a result of this range, this technology has also been adapted as an early warning system to detect tsunamis and as a ship tracking system.

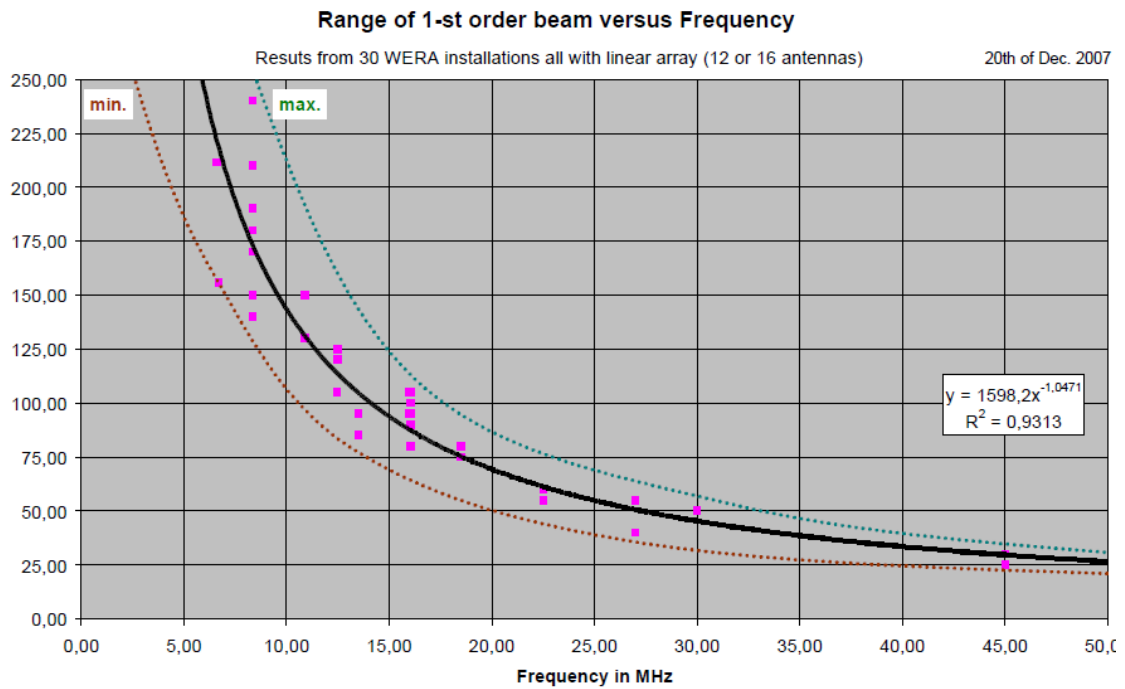


Figure 2.37 WERA Beam formed range vs frequency

The bandwidth of the transmitted radar signal dictates the range resolution. The greater the bandwidth the higher the resolution, figure 2.38. This can be subject to licensing restrictions depending on the country of transmission. The other restriction to operating over a broad frequency is the processing power required to analyse the data.

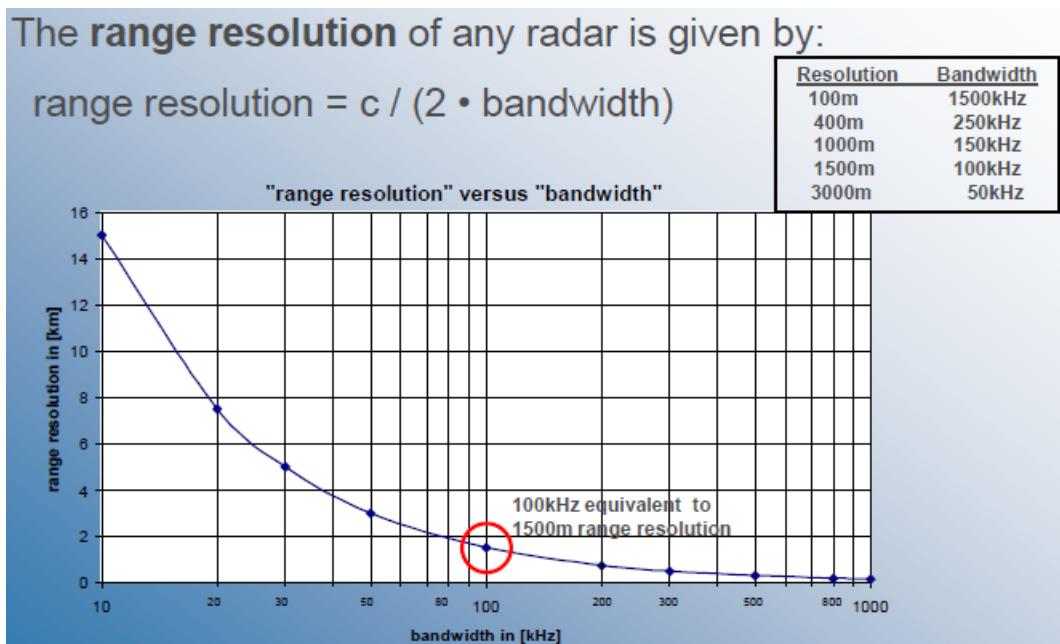


Figure 2.38 Range resolution vs transmission bandwidth

A two station radar setup operating over 500 kHz bandwidth from 45 MHz was used to describe transport processes in the Gulf of La Spezia Haza et al. (2010). The surface current results showed good agreement with physical drifter deployments. A similar experiment was undertaken in two southern Californian locations using the direction finding radar Sea-Sonde at 1-2 Km grid square resolution by Ohlmann et al. (2007). The maximum RMS error between current velocities recorded using radar and drifter were found to be greater than 13 cm/s.

The performance of the beam forming based COSMER radar system was validated against both Acoustic Doppler Current Profiler (ADCP) and numerical modelling (Telemac 2D) results in an environment of highly tidal range and velocity Cochin et al. (2006). The two station radar system was set up to cover an area of 25km² of the Normand Breton Gulf in France at a 1 km grid resolution. The systems operated at 45MHz and 47.8 MHz respectively. While good agreement was achieved between model, field and radar results, figure 2.39, two limitations were observed. The radar plotting smoothed out eddies recorded by the ADCP and spurious non Bragg peaks in the energy spectrum added errors to the radar data. Time frequency analysis of the entire dataset was suggested as a solution to eliminate the spurious peaks.

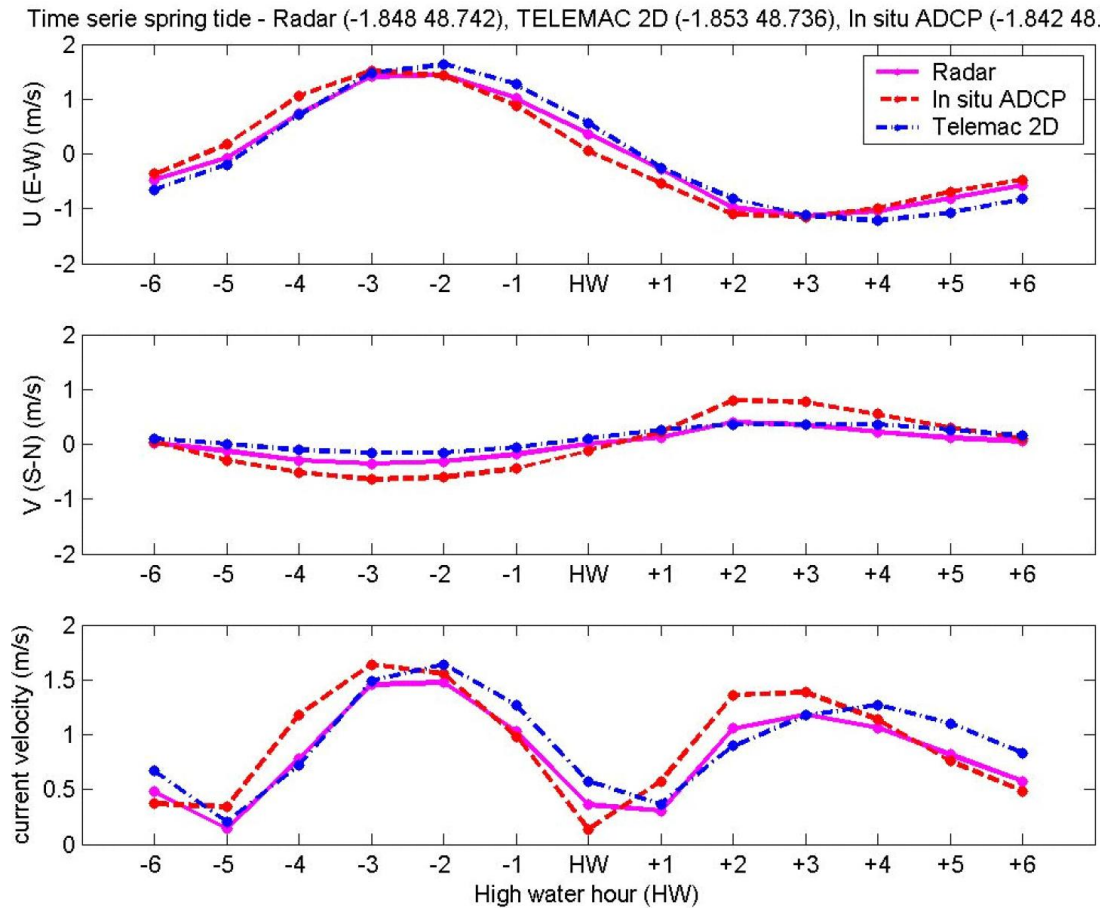


Figure 2.39 Comparison of Radar, ADCP and simulated tidal currents (Cochin, 2006)

Although open ocean surface current studies using HF radar have been successfully validated, the application of this technology at finer spatial resolution suitable for coastal processes studies is at an experimental stage. As noted, the technology struggles to record more dynamic features of the water surface at a 1 Km grid resolution. However, with a larger transmitting bandwidth, theoretically all the features of the ocean's surface currents can be captured using this technology.

Rotor/Impellor Type Recording Current Meters

Rotor and impellor, figures 2.40 and figure 2.41, are the oldest types of marine current recording instruments. The rate of revolutions of the rotor or impellor is used to calculate the speed of the current. The instruments are typically free standing and directed into the current direction using a vane or fins. The RCM 8, figure 2.40, also contains a compass to record current directionality.

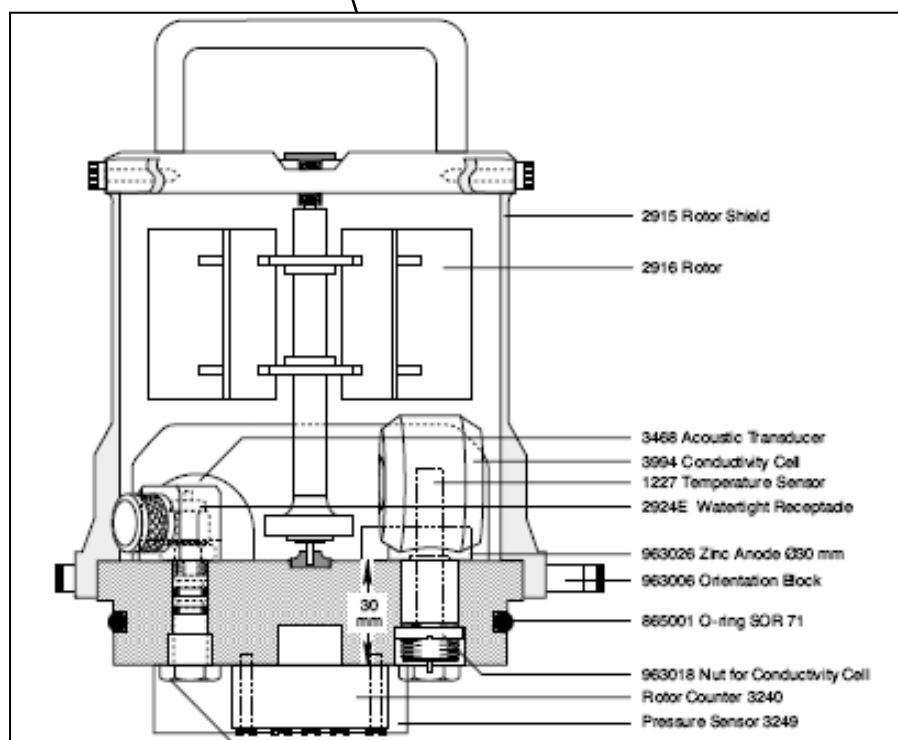
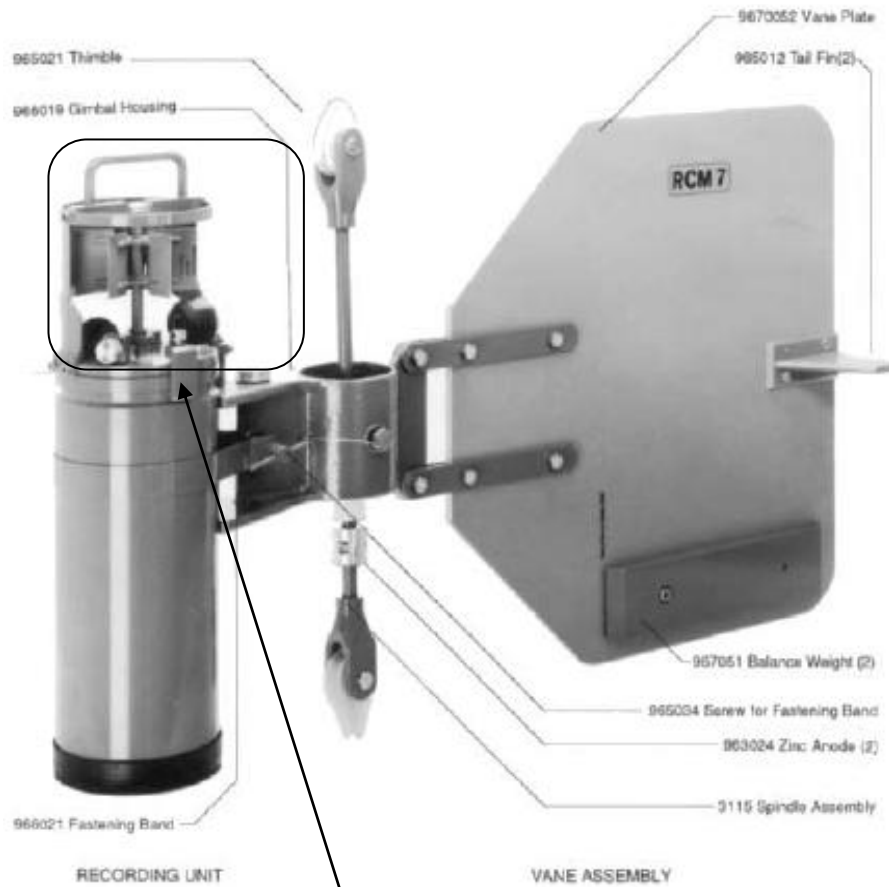


Figure 2.40 RCM 8 rotor based current meter (Source: www.aanderra.com)



Figure 2.41 Propeller type current meter (Source: www.Valeport.co.uk)

Electromagnetic Current Meter

This type of recording current meter is based on Faraday's law of electromagnetic induction. The instrument contains a probe that creates a magnetic field in the water column. The voltage change induced by the flow velocity of the water is measured by electrodes in the probe and this is converted into tidal current velocity. The Valeport Midas and 760 bottom mounted wave gauges both possess an electromagnetic current meter similar to that shown in figure 2.42.



Figure 2.42 Electromagnetic current meter (Source: www.Valeport.co.uk)

Acoustic Doppler Current Meters and Profilers

These instruments measure change in frequency of acoustic signals that are reflected by small particles such as air bubbles in the flow. The change in wavelength due to the Doppler Effect is converted to velocity. Unlike the single point acoustic Doppler current velocimeter (ADV), the acoustic Doppler current profilers (ADCP) measures the water column in discrete cells to give a current profile velocity. Typically ADCPs are mounted on the seabed looking upward, figure 2.43, or on a fixed vertical structure looking horizontally into the water column, figure 2.44.

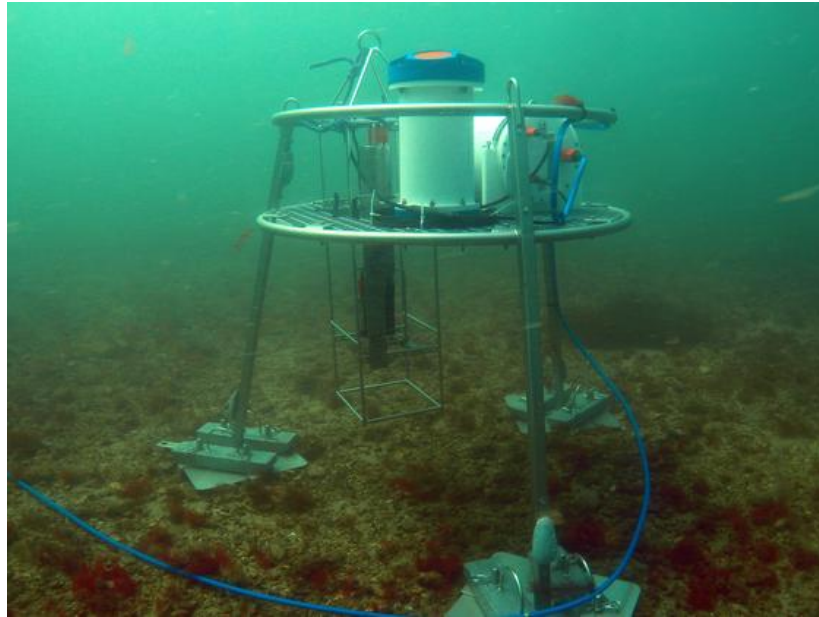


Figure 2.43 Bottom Mounted ADCP (Source: www.awi.de)

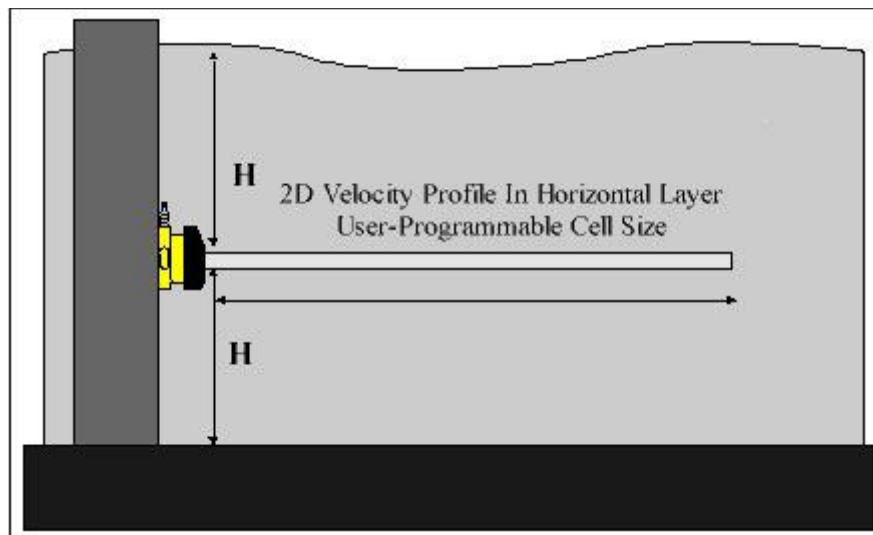


Figure 2.44 Schematic of side mounted ADCP (Courtesy of Sontek)

2.4.2 Sediment Transport Monitoring

Tracking sediment transport in the coastal zone has traditionally proven a difficult task due to the dynamic action of waves and tidal currents combined with large volumes of entrained sediment. Issues with equipment stability and security have usually prevented comprehensive investigation particularly in the surf zone when undertaking coastal process studies. The need for data in this area is often critical to erosion and beach evolution studies, as most of the initial movement occurs in this zone.

Several methods of monitoring sediment transport exist and have varying degrees of success depending on the study sites characteristics. These

methods include sediment dye tracers, optical and acoustical sensors to measure suspended sediment, impact sensors, sediment traps for both hydrodynamic and aeolian driven sediment transport. An experimental method of identifying sediment pathways has been established recently called Grain Size Trend Analysis (GSTA). It is based on identifying transport trends from the variation of sediment grain characteristics within a defined study area.

Sediment Dye Tracer Studies

The dying and tracking of sand has been one of the most common methods of sediment transport tracking for several decades. Typically sediment from the study site is dyed with Rhodamine or alternatively a tracer with similar properties to that of the site under investigation is placed in the intertidal zone at known locations. Sediment samples are then taken in grid format from the study site to assess where the dyed sand has been transported to.

McComb and Black (2005) undertook a study of littoral transport processes using an artificial sediment tracer in New Zealand. Two different coloured fluorescent tracers were used to assess the natural bypassing of a port entrance and the movement of sediment from dredged sand mounds. Samples were released at depths of 6 m to 10 m and tracked for 10 months. The experiment found that very little trace was found within the harbour suggesting that sediment bypassing is occurring. The spreading rates of the sediment were calculated to be in the region of $0.01 \text{ m}^3/\text{s}$ to $0.288 \text{ m}^3/\text{s}$.

Bertin et al. (2007) experimented with the location of injection point of fluorescent point on Arcay spit in western France. Natural sand from the test location was dyed with three different colours for three injection points. The mixing depth was calculated for the various locations on the beach where the dyed sand was injected in accordance with recommendations of White (1998). The sediment was sampled with a 25 cm PVC pipe and analysed at three different depths within the sand column.

The sediment tracer results, figure 2.45, shows the variation of sediment transport across the shore. On the lower shore the residual sediment at the surface layer (0-3 cm) is minimal with most of the dyed sediment being transported alongshore and out of the sample area. This effect is amplified in the lower layers. On the upper shore, a slug of the dyed sediment is still visible along the sampling grid; this slug is reduced in definition and concentration in the lower layers also. While not accurate enough to derive annual longshore sediment transport rates from, this method could provide a validation for a numerical sediment transport model.

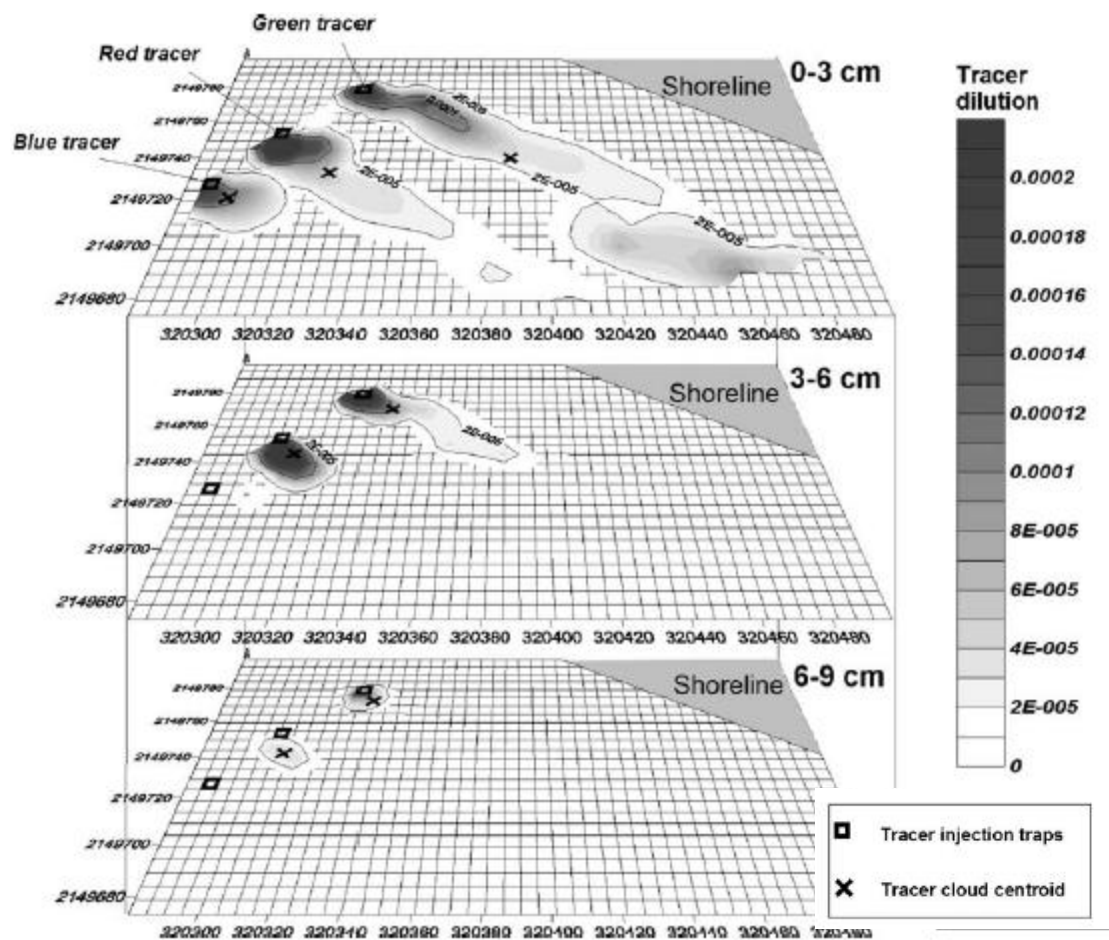


Figure 2.45 Dispersion results of sediment dye tracer experiments (Bertin et al., 2007)

Optical and acoustical sampling methods

The measurement of suspended sediment in the surf zone has been achieved using both acoustic and optical sampling methods. An optical backscatter point sensor (OBS) can measure the turbidity and suspended solids concentrations by detecting infra-red light scattered from suspended matter.

Masselink (2007) monitored the drivers of bed evolution of intertidal bars in Truc ver, France. A set of ADCPs and a frame containing OBS sensors, figure 2.46, were deployed. The OBS measured suspended sediment concentrations deployed at 15 cm from bed. The custom rig of vertically integrated sensors was used in one location. Parameters recorded included mean cross shore velocity, max wave orbital velocity, vertically integrated suspended sediment flux was obtained from custom rig. The custom rig was not affected by interferences from bubbles and hence velocity data quality was good.

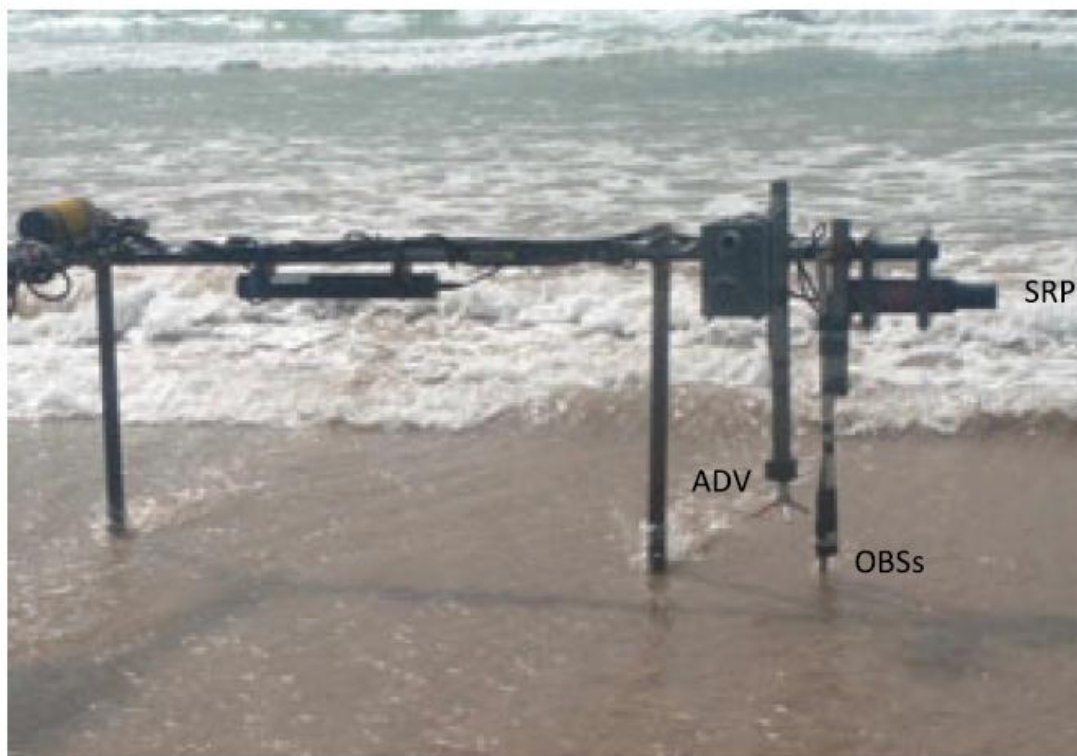


Figure 2.46 OBS surf zone rig (Masselink, 2007)

Acoustic sediment sensors work in a similar way to OBSs but using shift in frequency of backscattered acoustic signals. Similar to acoustic current meters, it is possible to have single point recorders, acoustics sand transport monitor (ASTM), and acoustic backscatter profile sensors, which produce a profile of suspended sediment velocities.

Other Suspended Load Measuring Instruments

Impact probes rely on recording the force at which sediment grains hit the sensor to measure the density of suspended sediment in the water column.

These probes are fixed in place and orientated in the direction facing the flow to achieve maximum impact coverage of suspended sediment. The sand concentration can be deduced from the impact rate and the velocity of the surrounding water, which must be measured separately, usually by ADCP.

Bottle and bag samplers are some of the earliest mechanical forms of measuring suspended sediment. These devices, such as the Delft Bottle sampler, figure 2.47, operate on the flow through principle, where the water is allowed to flow through but suspended sediment is retained and measured. Large inefficiencies can exist in this type of measurement due to flow interference and unaccounted for sediment collection during deployment and extraction. The non-invasive sensors, such as the acoustic and optical offer a more accurate and reliable form of suspended sediment measurement.

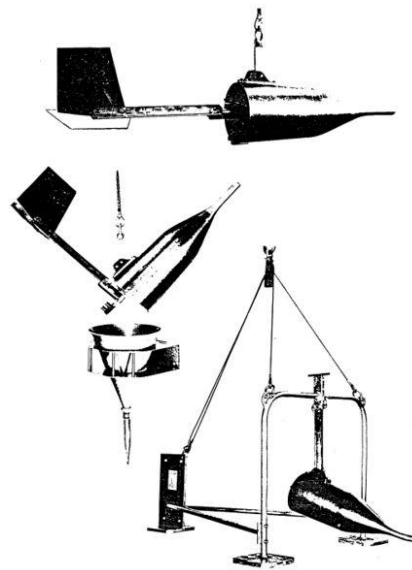


Figure 2.47 Delft Bottle Sampler (Dijkman 1978)

Bed Load Sediment Transport Monitoring

The measurement of bed load sediment transport can be undertaken in two ways: recording of the change of bed levels over time usually with topographic surveying instruments such as RTK GPS and trap type samplers. Topographic surveying is discussed in detail in Chapter 3. Mechanical trap samplers capture sediment particles transported along the seabed. There are several instruments designed to undertake bed load

sampling including the Bed load transport meter Arnhem (BTMA), figure 2.48 and the Helley-Smith sampler (HS), figure 2.49.

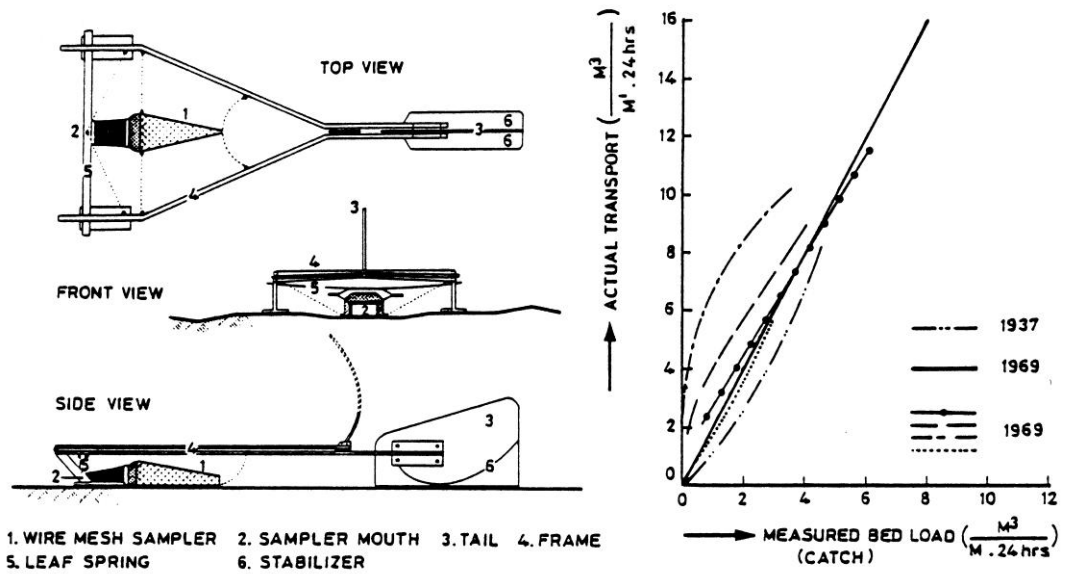
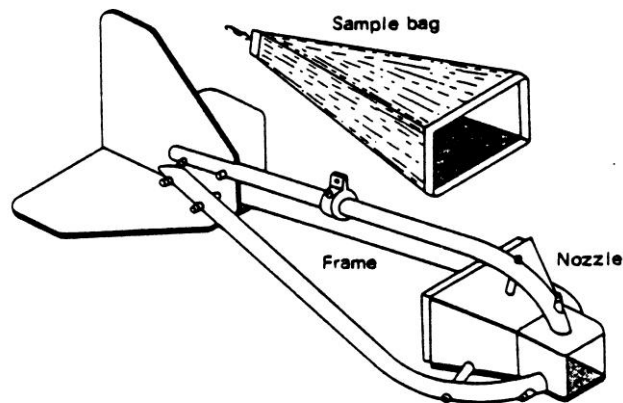


Figure 2.48 Bed load Transport meter (Delft Hydraulics, 1958)



Sketch of the Helley-Smith bedload sampler.

Figure 2.49 Helley-Smith bed load sampler (Helley et al., 1971)

Both instruments have a nozzle that is orientated into the flow by means of fins. The nozzle is connected to a sampling container, usually a polyester bag. The captured sediment is compared to a calibration curve that has been formulated for the specific device. The accuracy of the trap type bed load sampler is heavily dependent on the accuracy and suitability of the calibration curve. The Helley–Smith device has an advantage in that its calibration curve is based on over 10,000 sample results

Grain Size Trend Analysis

The basic theory behind grain size trend analysis (GSTA) is inferring sediment transport pathways from variations in sediment grain size characteristics sampled within the study area. The assumption is that the difference in grain size characteristics from one location to the next is due to the action of sediment transport in that direction. The method requires an initial assumption of the direction of sediment transport in the study area. This assumption is usually validated through prior knowledge of the study site such as bathymetry, hydrodynamic data or numerical models of the site

Deriving sediment transport pathway trends by analysing sediment grain characteristics was initially investigated by Pettitjohn et al. (1938). They looked at the geographic variation of mean grain size of sediment samples and related it to a sediment transport pathways. This was improved upon by McLaren (1981) who added skewness and sorting. These parameters are statistically derived from the grain size distribution curve of a sediment sample. Sorting is a function of the second moment and skewness a function of the third moment.

Until recently, these parameters have been time consuming to derive, especially for a large database on samples. Blott (2000) developed Gradistat, a spreadsheet based tool that has the capability to calculate the Mean grain size, sorting coefficient and skewness for a large data base. McLaren (1981) suggested that although 8 cases are possible the trend analysis should only consider 2 cases, those being; finer, better sorted and negatively skewed (FB-) or coarser, better sorted and positively skewed (CB+), as most transport trends follow one or the other trend. Gao et al. (1992) proposed expanding the analysis to all 8 cases:

1. Finer, Better Sorted, Positively Skewed (FB+)
2. Finer, Poorer Sorted, Negatively Skewed (FP-)
3. Finer, Better Sorted, Negatively Skewed (FB-)
4. Finer, Poorer Sorted, Positively Skewed (FP+)
5. Coarser, Better Sorted, Positively Skewed (CB+)
6. Coarser, Poorer Sorted, Negatively Skewed (CP-)
7. Coarser, Better Sorted, Negatively Skewed (CB-)

8. Coarser, Poorer Sorted, Positively Skewed (CP+)

This method is a two dimensional vectorial method expanding on the point to point 1-dimensional method of McLaren (1981). This method includes the filtering of noise by specifying a characteristic distance, d_{cr} . The points within this distance are used in the analysis of each point. Trend vectors are summed to produce a single vector then this is averaged to form a residual pattern. If patterns are similar then a pathway is defined.

Le Roux (1994) argued against the filtering step and developed a method using trend analysis from the 4 closest neighbours. Since then, studies have used both methods with the Gao et al. (1992) method proving the more popular. The majority of trends on beaches have coincided with the original cases specified by McLaren (1983) (FB- and CB+). These trends are usually supported by other monitoring activities in the coastal zone such as dye testing, bed form surveying and morphological modelling.

Poulus et al. (2010) utilised the Gao and Collins method to examining the effect of a dredged pit had on the sediment transport regime on the Kwinte Bank, southern North Sea. Sediment samples were taken pre and post dredging, and sediment trend analysis conducted. The results, figure 2.50, show a by-passing effect caused by the dredging.

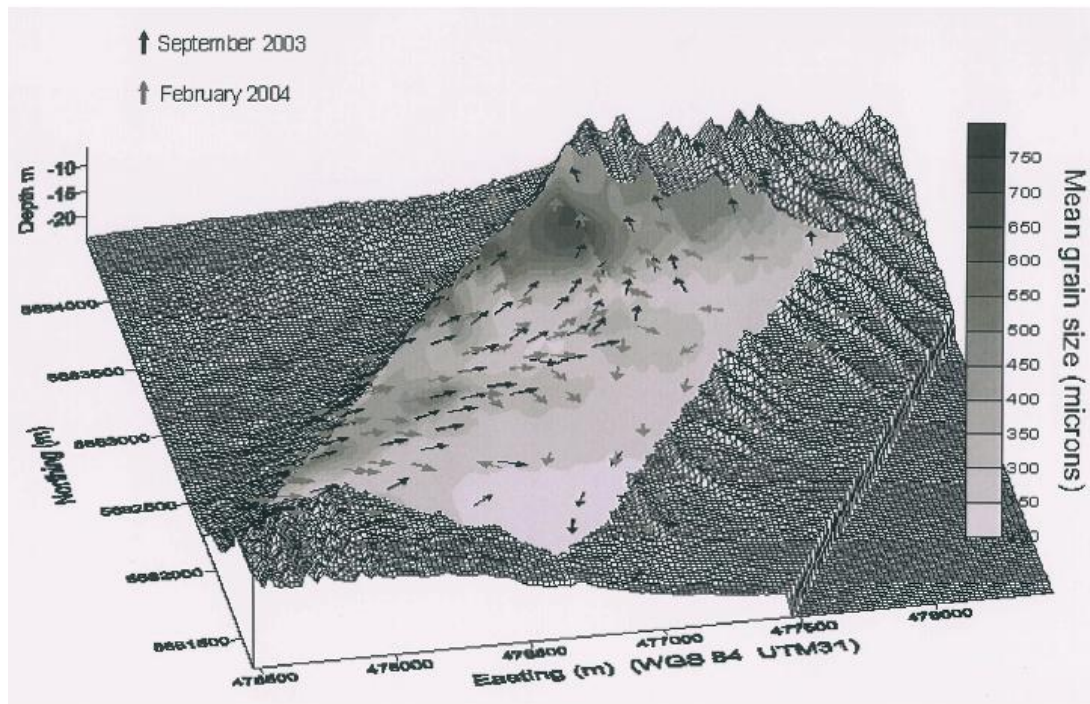


Figure 2.50 Sediment trend analysis pre and post dredging (Poulus et al., 2010)

However, other cases have also been identified such as FB+, figure 2.51, by Poizot et al. (2008), in Cadiz Spain. This work goes further and suggests that two cases can occur on the same beach. A conceptual model is developed based on this theory proposing that FB+ dominates in the upper foreshore and FB- case is the dominant trend in the lower foreshore, figure 2.52.

Poizot (2013), has recently developed a GIS based GSTA tool called Gis Sed trend. This tool incorporates all of the various GSTA methodologies and the 8 different case tests previously mentioned. It allows the user to input data and vary parameters such as d_{cr} . There is also a facility to statistically test each result and display the trend vectors in a GIS format. This tool was used extensively in developing the GSTA plots presented in Section 4.4.

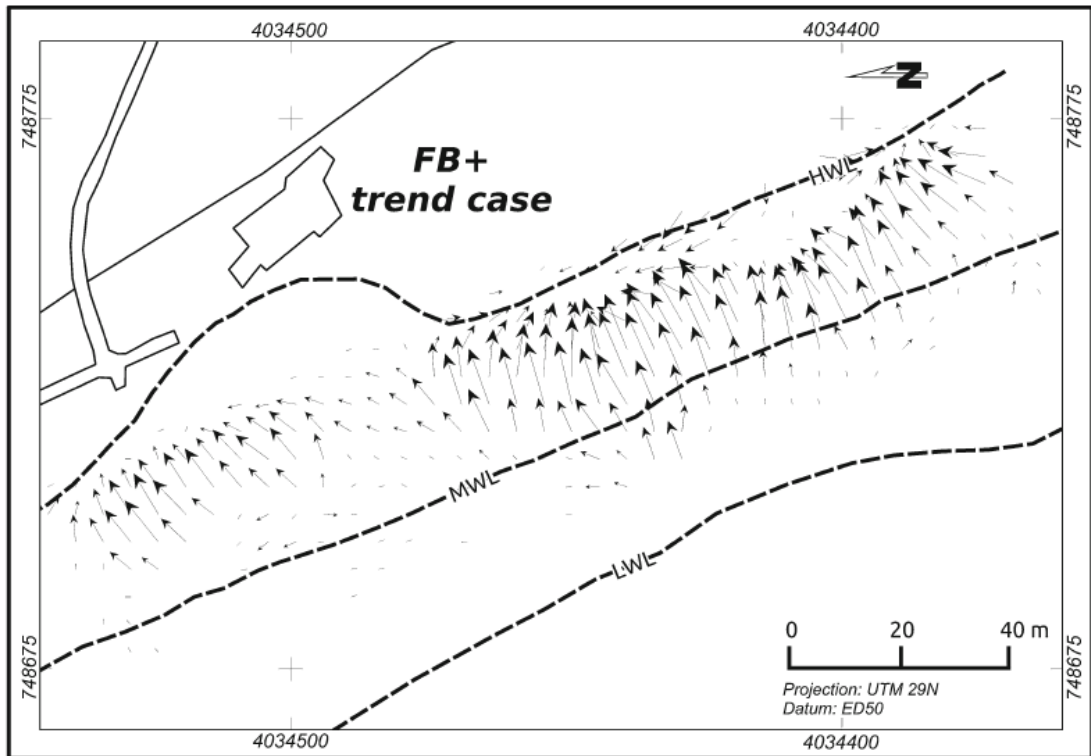


Figure 2.51 FB+ Case in Cadiz (Poizot, 2008)

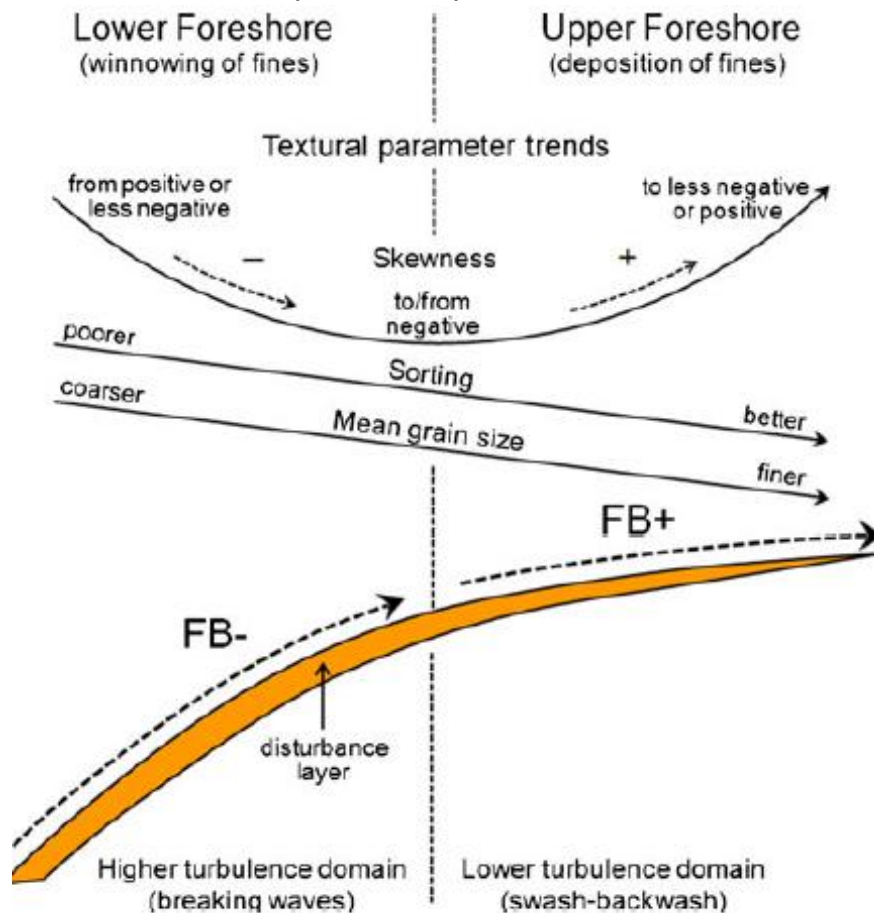


Figure 2.52 Conceptual model of foreshore trend variation (Poizot, 2008)

Aeolian Sediment Transport Measurement

The methodologies developed to characterise the transport potential of wind on beaches are similar to the trap type instruments used in hydrodynamic sediment transport. A typical aeolian transport experiment has multiple traps that capture bed load, saltating and suspended sediments as well as wind speed and moisture content instrumentation.

Nickling et al. , (1995) designed and tested a low cost sediment trap, figure 2.53. The trap was constructed of aluminium and has a fine stainless steel mesh in a wedge shape with a narrow opening orientated into the wind direction. The trap underwent testing in a wind tunnel and was found to have a 90% sampling efficiency for sediment capture over a range of wind speeds. The efficiency is evaluated relative to a settling chamber in a wind tunnel which captures all the particles entrained in the wind column.

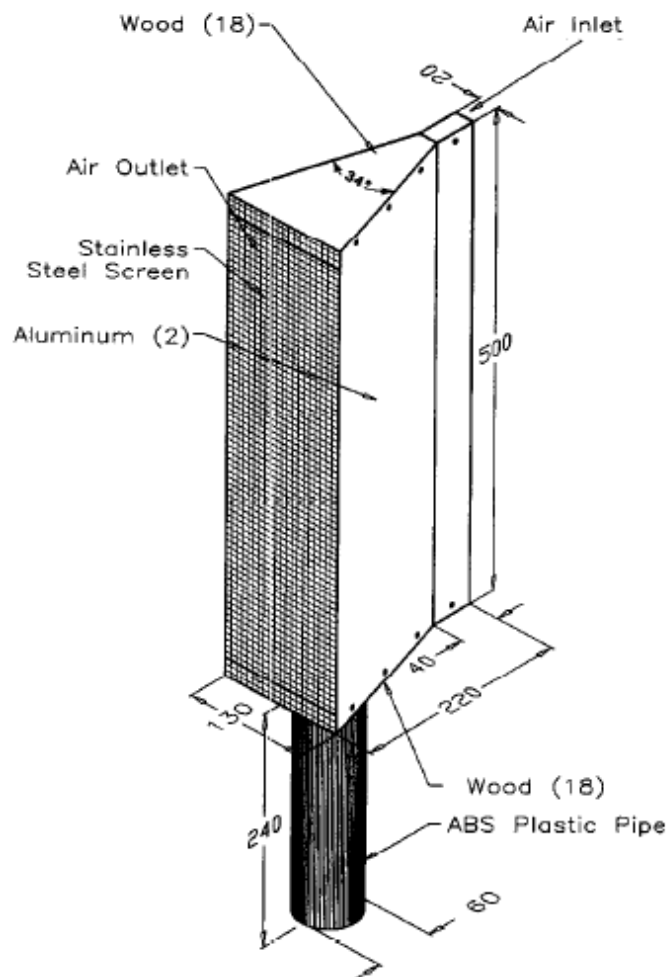


Figure 2.53 Wedge Shaped Aeolian Sediment Trap (Nickling et al., 1995)

The trap also called a Guelph trap was found to be very sensitive to incident wind direction. High scouring around the narrow trap inlet was recorded when incident angles were greater than 5 degrees. It was concluded that while efficiency is high these types of traps should only be used for short term studies and in environments where the variation incident wind direction is minimal. This type of trap is particularly suitable to capturing saltating sediment transport.

Goosens et al. (2000) evaluated the efficiency of five aeolian samplers and traps in both field and wind tunnel experiments. The five samplers were the Big Spring Number Eight (BSNE) sampler, the Modified Wilson and Cooke (MWAC) sampler, the Suspended Sediment Trap (SUSTRA), the Pollet catcher (POLCA), and the saltiphone. The traps were tested in a wind tunnel at 3 different sand types and 5 different wind velocities.

The traps were also assessed in the Negev desert in Israel over a two week period. The MWAC, figure 2.54, performed the best of the five traps in both wind tunnel and field experiments with efficiencies' of over 90% recorded. The MWAC consists of a plastic holding bottle with two glass tubes, an inlet and outlet. The testing also showed that the MWAC's performance was independent of wind speed, making it suitable for use in locations with variable wind speed.

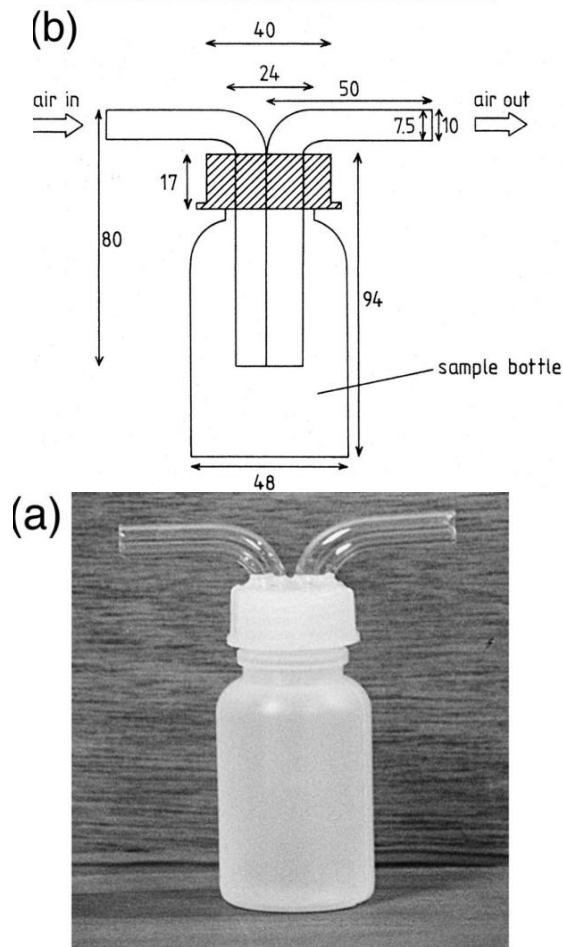


Figure 2.54 Modified MWAC vertical sediment profiler

De Vries et al. (2013) attempted to model Aeolian driven deposition and erosion on a beach through remotely sensed video imaging of beach surface profile mapping. The conceptual model is based on the Bagnold (1954) dimensional model and is presented in the form (13):

$$\frac{\partial C_c}{\partial t} + u \frac{\partial C_c}{\partial x} = \frac{\min(C_u - \frac{C_c S_e}{h})}{T}$$

Where:

$$\frac{\partial C_c}{\partial t} = S_s - \frac{\min(C_u - \frac{C_c S_e}{h})}{T}$$

And:

$$C_u = u^2 \tag{13}$$

Where C_u = wind driven equilibrium transport concentrations

S_s = maximum sediment which can be ejected from the bed into transport

C_c = sediment concentration,
 S_e = the amount of erodible sediment at the bed
 h = is the height of the transport layer.
 u = wind speed

The model produced some encouraging results but the limitations in morphological feedback prevent the accurate simulation of measured beach surface changes. The characterisation of sediment supply also requires further refinement with the need to account for effect of surface moisture and sediment sorting.

Delgado-Fernandez (2013) examined the use of moisture maps in aeolian transport modelling at Greenwich Dunes, Prince Edward Island National Park, Canada. A pixel coarsening method was developed to derive moisture maps from digital images taken from a height of 14 m above the beach, figure 2.55 and figure 2.56.

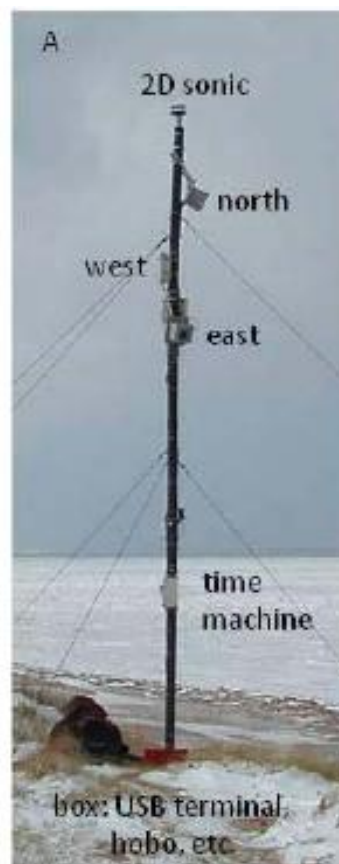


Figure 2.55 Anemometer and Camera set up (Delgado-Fernandez, 2013)

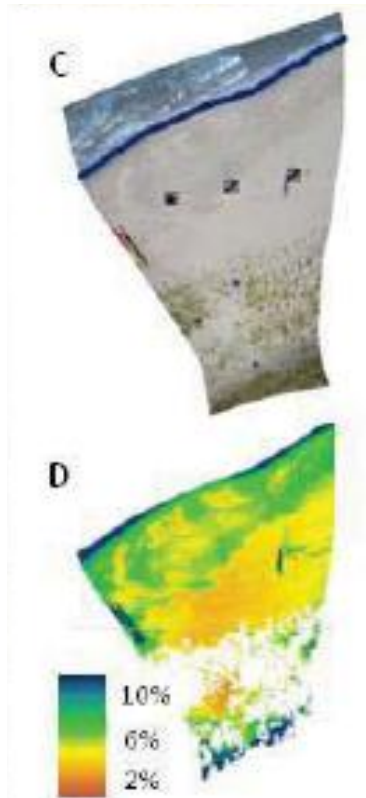


Figure 2.56 Moisture profile mapping process (Delgado-Fernandez, 2013)

Smyth et al. (2011) modelled an aeolian driven enlargement of a dune blowout using fluid dynamics software OpenFOAM. The airflows of two wind events were modelled in 3D on a coastal foredune in Bellmullet peninsula. A light (4 m/s) and moderate (9 m/s) wind were simulated and their patterns over the dune examined, figure 2.57. This model is a useful tool when attempting understand the behaviour of aeolian transport and erosion on dune systems, but requires more comprehensive validation with anemometers. The model under predicted the retachment rate of streamlines in the lee of the dune.

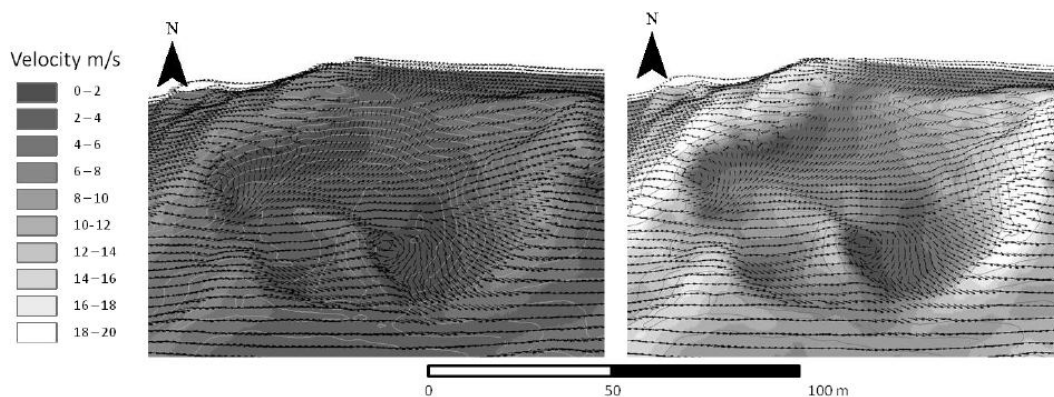


Figure 2.57 Airflow simulations over dune blowout (Smyth, 2011)

2.5 Numerical Modelling of Coastal Processes

Numerical modelling can be a very powerful tool when applied to the coastal zone. Wave, current, sediment transport and morphological processes can all be simulated numerically. A correctly validated coastal morphodynamic model can be used to predict changes in the coastal zone. Important conclusions on the future of a coastal cell can also be drawn from scenario modelling approaches such as simulating extreme storm events and morphological speed up techniques.

A large number of coastal morphodynamic numerical models have been developed; ranging from 1 and 2 dimensional profile evolution models to fully coupled 3 dimensional morphological models.

2.5.1 Profile evolution models

Several models have been developed to represent the evolution of coastal systems in simplest terms of elevation and cross-shore distance, (1-D). These models such as S-Beach (Sommerfield et al. , 1996) have been superseded by 2 dimensional profile models that expand the evolution model an alongshore direction (2-D) such as X-Beach (Unesco-IHE) and LitPack (DHI). These models predict the change in bed level and movement of sediment. Such models usually require a time series wave input from the nearshore zone and sediment characteristics. The X-beach model solves the equations for wave propagation (14) & (15) and the Soulsby Van Rijn formula (16) for sediment transport as this is applied to a bed updating algorithm which results in a change in bed profile.

$$\frac{\partial A}{\partial t} + \frac{\partial C_x A}{\partial x} + \frac{\partial C_y A}{\partial y} + \frac{\partial C_\theta A}{\partial \theta} = -\frac{D}{\sigma} \quad (14)$$

Where A = wave action density

C = wave celerity

D = wave energy dissipation

θ = Wave angle

$\bar{\omega}$ = Intrinsic wave frequency

Wave Action is given by;

$$A(x, y, \theta) = \frac{E(x, y, \theta)}{\sigma(x, y)} \quad (15)$$

The Soulsby Van rijn formula for sediment transport is given as

$$q_{st} = A_s \cdot U_c \cdot \left[\sqrt{\left(U_c^2 + \frac{0.018}{C_d} \cdot U_{wrms} \right) - U_{cr}} \right]^{2.4} \cdot (1 - 1.6 \cdot \tan(\alpha)) \quad (16)$$

Where U_c = current velocity

U_{wrms} = root mean square wave orbital velocity

α = local bottom slope

C_d = drag coefficient

U_{cr} = threshold velocity

A_s = total load = ($A_{sb} + A_{ss}$)

A_{sb} = bed load

A_{ss} = suspended load

Where h = water depth

ρ = water density

D_{50} = mean sediment grain size

D = dimensionless grain diameter

Austin and Brown (2009) created an X-beach model to examine the effect of cross over a rip channel and a shoal of a transverse rip bar system. The breaching of Trabucador barrier beach system, figure 2.58 in the Spanish Mediterranean Coast was modelled using X-Beach by Gracia (2013). The study successfully reproduced 3 breaching events from the previous 25 years. The simulated breaching all occurred within an 8 hour timeframe and at high water.

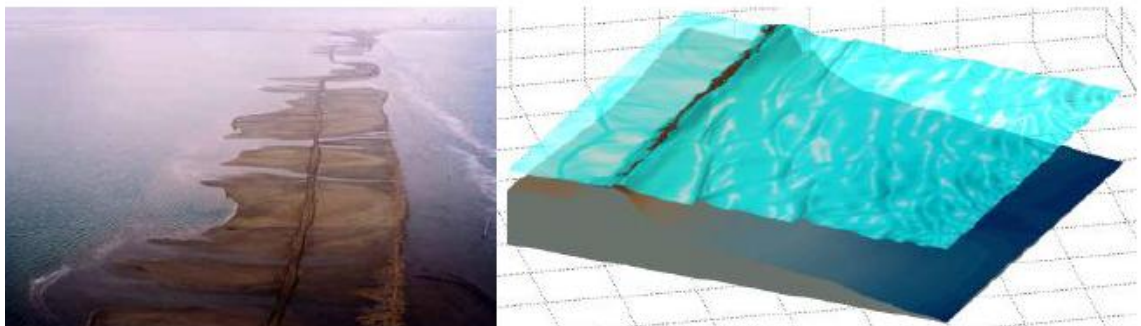


Figure 2.58 X-beach model of Trabucador barrier beach system (Gracia, 2013)

2.5.2 Coastal Area Models

Coastal area models such as DHI Mike 21 (DHI, 2008), Delft 3D (Deltares 2010) and Telemac typically simulate coastal processes on a Cartesian or curvilinear grid that represents the bathymetry of the study site. The various processes that drive coastal evolution (wind, wave, tidal elevation, sediment transport, and morphology) are separated into individual modules, like the architecture of Delft 3D, figure 2.59. After a specified time step the individual module outputs are then coupled and fed back to one another, to account for the effect of each module process on the others. These models are typically driven by spectrally resolved waves and 2 dimensional depth integrated flow.

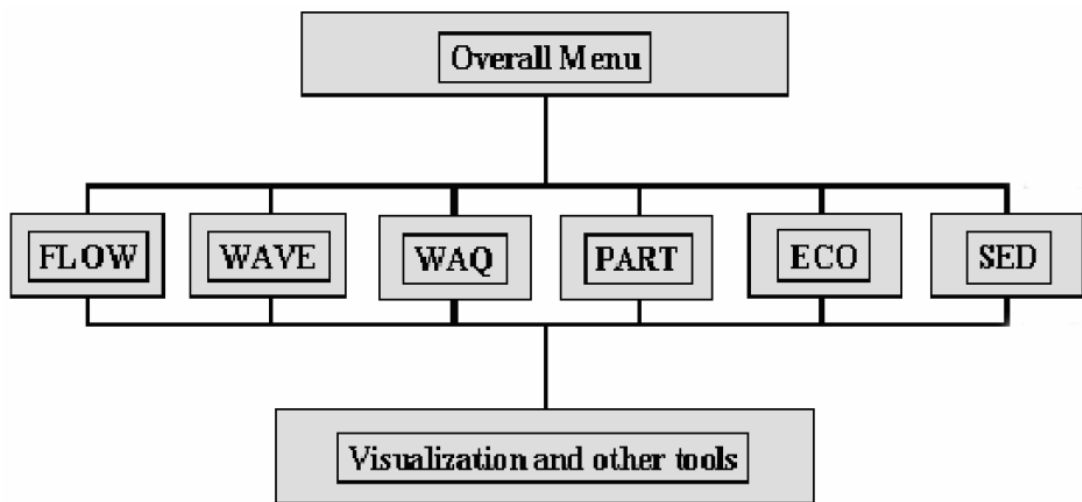


Figure 2.59 Model Architecture of Delft 3D (Delft 3D Manual)

DHI Mike 21 (DHI, 2008) modelling software package consists of separate modules that compute wave forcings (SW), hydrodynamics (HD), sediment transport and morphology (ST) combined into one coupled model. The bathymetry of the model domain is represented on an unstructured mesh of quadrilateral and triangular shaped cells, figure 2.60. The various model outputs are calculated at nodes in the centre of these cells.

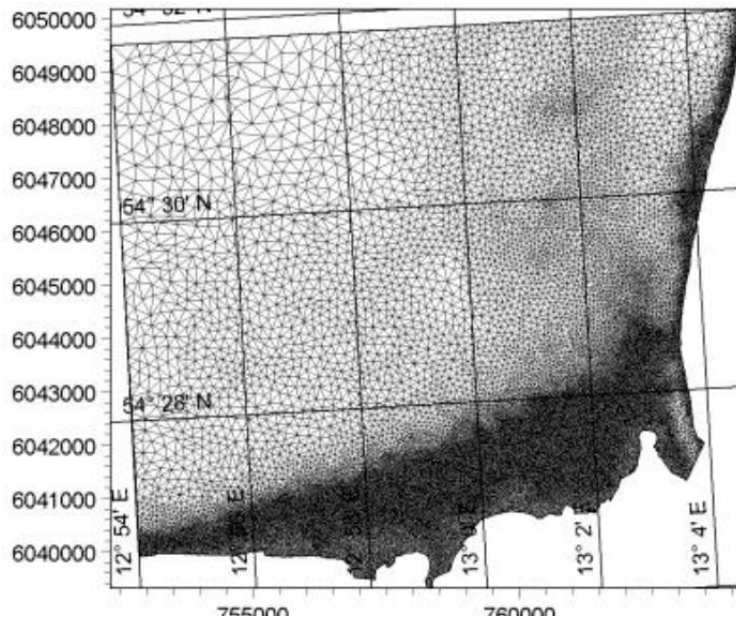


Figure 2.60 Flexible Mesh from DHI Mike 21

The SW module calculates wave forcings based on the wave action conservation formulae (17) and solves the wave energy transfer function from initial boundary condition across the mesh using a finite volume method at the cell centres. Wind swell can also be incorporated in this module. This method is similar to the one used for the Delft 3D wave module SWAN (SWAN User Manual). Detailed information on the driving equations can be found in the manual (DHI, 2008):

$$\frac{\partial N}{\partial t} + V \cdot (vN) = \frac{S}{\sigma} \quad (17)$$

Where $N(x, \sigma, \theta, t)$ = action density

t = time

$x = (x, y)$ Cartesian co=ordinates

$v = (cx, cy, c\sigma, c\theta)$ the propagation velocity of a wave group in four dimensional space

S = the source term for energy balance equation

V = is the four dimensional operator in the x, σ, θ -space

The HD module calculates hydrodynamic forcings (tidal elevation and currents) utilising Navier stokes equations (18) and applying a finite volume method similar to the SW module to solve the boundary condition of a tidal signal across the mesh. The coupling of these modules on the same mesh

enables the simulation of current and wave interactions on the sediment transport and ultimately the morphology.

$$\frac{\partial u}{\partial x} + \frac{\partial v}{\partial y} + \frac{\partial w}{\partial z} = S \quad (18)$$

Where x,y,z = Cartesian co ordinates

u,v,w = flow velocity components

The sediment transport and morphology module (ST) applies the wave and hydrodynamic forcings generated at each node to drive sediment transport formulae (Van Rijn, Section 2.2.2). The ST module requires several key inputs such as sediment particle size and morphological update frequency. The ST Module updates the bathymetry based on the sediment transport calculations in the model domain and effectively feeds back into the HD and SW modules during a simulation. To reduce computation time and increase model time scale a morphological speed up factor can be applied.

Panigrahi (2009) used the DHI Mike 21 morphological modelling software suite to assess the morphodynamic trends on the Arklow Bank off the East coast of Ireland. The aim of the modelling was to identify stable areas of the sand bars suitable for offshore wind turbine foundations. A probability of occurrence approach to modelling was adopted. A run matrix with the percentage yearly occurrence was modelled for a spring neap tidal cycle.

The results, figure 2.61, show that erosion only occurs for depths under 5 m. The average rate of accretion/erosion is less than 8 cm /day. It was noted that wave height variation had little effect on erosion rates and tidal current magnitude having a strong impact.

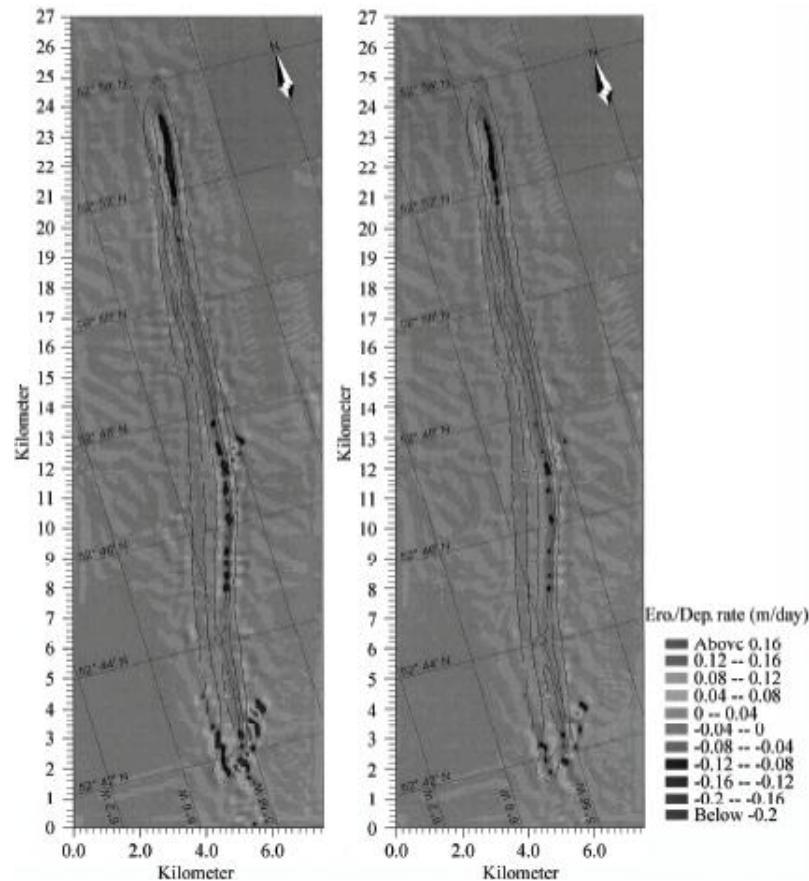


Figure 2.61 Erosion/Deposition rates of spring tide and spring to neap on Arklow Bank (Panigrahi, 2009)

Mason and Garg (2001) constructed a morphodynamic model of Morecambe Bay, England. The model was developed by combining several modules, figure 2.62, and shows the layout of the model system. 2 dimensional depth integrated flows are simulated, the wave heights were inputted based on water depth, wind speed and wind fetch, using equations from the Shore Protection Manual (1997). The Soulsby-Van Rijn formula (Soulsby 1997) was used to predict total sediment load and bed update was calculated based on the net transport in and out of a grid cell.

The model was calibrated from remotely sensed tidal heights detected using radar over a 3 year period and run for a 3 year morphodynamic simulation. The model results failed to show accurately the changes in bathymetry and consequently could not be used as a predictive tool. The authors suggested several steps to improve the accuracy of the model including an increased grid resolution, a grid cell of 240 m was deemed to coarse to effectively

model changes in tidal circulation, the use of extensive data sets in the model calibration sets, and the discretisation of spatially varying grain size specification.

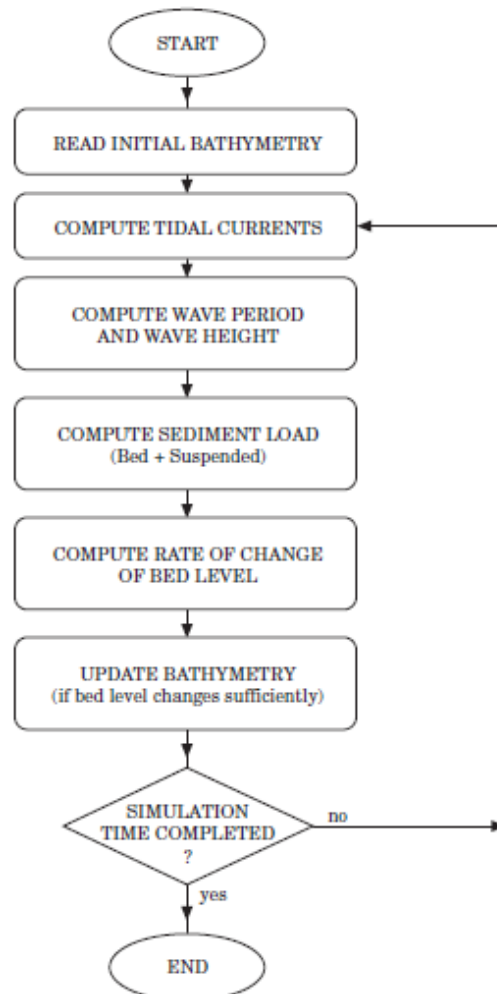


Figure 2.62 Morphodynamic model module flow chart (Mason & Garg, 2001)

Delft 3D has the capability to model processes in 3 dimensional space. This differs from the 2-d depth integrated method that other coastal area models employ. The 3D option is composed of a series of discrete horizontal layers in the water column across the model domain. The impact of wave breaking and mixing is accounted for vertically through these layers by incorporating a vertical and horizontal velocity component in each cell. While this method may enhance the accuracy of suspended sediment mixing the computational cost is very high. Due too the processing demands this method is restricted to small domain areas.

Herling and Winter (2013) modelled the morphological response of the East Frisian barrier islands of Langeoog and Spiekeroog in the southern North Sea using Delft 3D. The software is used to model the hydrodynamics and sediment transport characteristics of the ebb tidal delta and tidal inlet between the two barriers. The sediment grain size distribution is discretised to investigate the sedimentological features of ebb tidal bar morphology.

The response of the barrier system is simulated under both fair-weather and storm conditions. The bed load of the ebb tidal delta was found to move onshore during storm conditions, figure 2.63, with wave forcing being the dominant driver. Medium grain sized sediment is found around the ebb tidal delta and the inlet throat. The model successfully simulates sediment by-passing around the inlet. The re-circulation of sand in a semi-circular pathway to the side of the ebb tidal delta is also reproduced in the simulations.

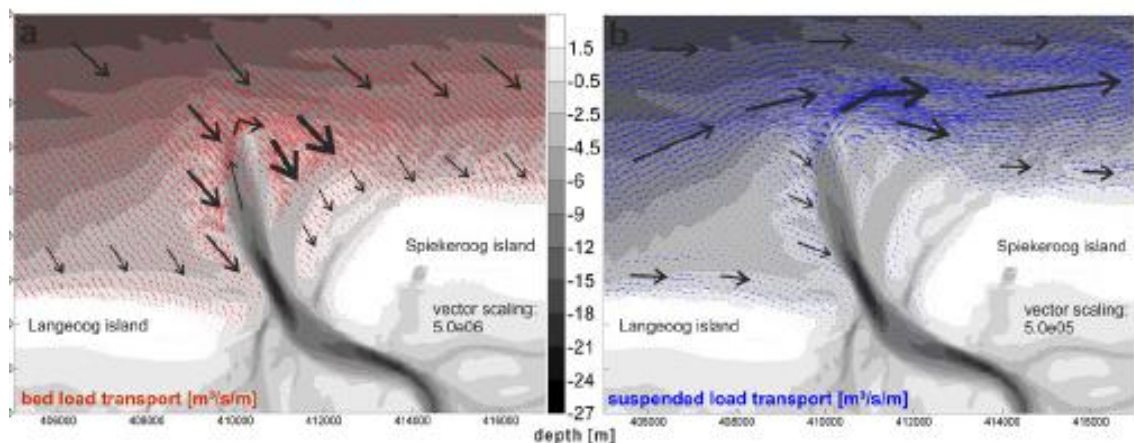


Figure 2.63 Simulated sediment transport (Herling & Winter, 2013)

2.5.3 Long-term Morphodynamic Modelling

Two approaches to long term morphodynamic modelling have been suggested by De Vriend (1993), behaviour based and process based.

The behaviour based approach relies on empirical relationships established between parameters but unaware of the fundamental processes responsible for such relationships. While useful in identifying trends of coastal evolution, this approach lacks the confidence of the process based method.

The process based approach requires an understanding of the driving physical processes. However, detailing every process in its entirety would produce unfeasibly bulky and time consuming models. The process based approach requires the simplification of these processes i.e. to reduce the model inputs to the limit where no relevant features are lost. This schematisation of inputs could be for example, utilising depth integrated flow instead of simulating fully 3 dimensional flows.

There are several factors to consider when selecting the features to schematise in a long term morphodynamic model. The use of a morphological scaling factor, the effect of tidal variation and variation of the numerical time step are common methods.

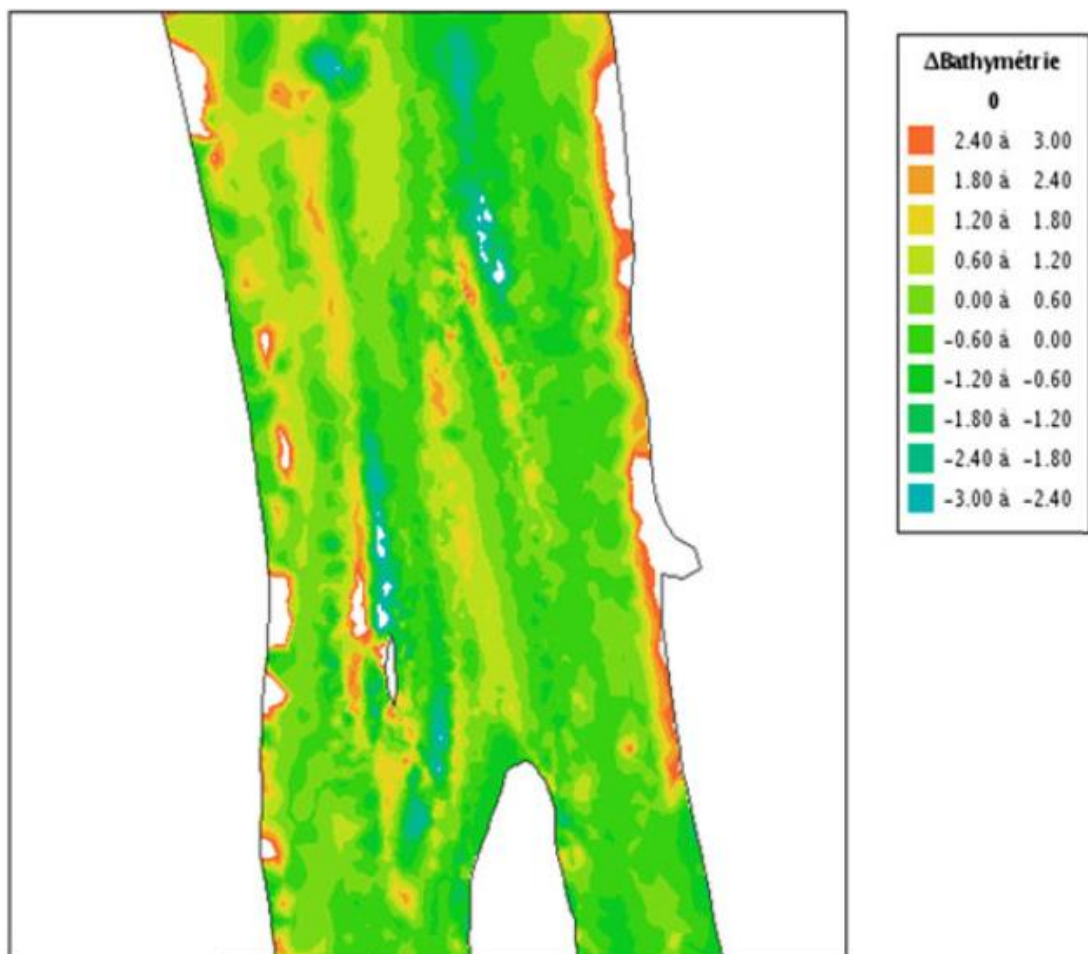
As hydrodynamic and wave processes occur on a much shorter timescale than morphology, a morphological response scaling factor (MORFAC) can be implemented. The original morphological response of the model due to the wave and tidally driven sediment transport is multiplied by a factor to represent a longer term response than was simulated.

Latteux (1995) successfully simulated morphological bed changes of 19 years on a single tidal diurnal tidal cycle, thus greatly reducing the time length of the model. The schematised tidal input was formulated based on a tidal elevation signal that produced a percentage of the peak spring tidal velocities.

The variation of morphological time step relative to the hydrodynamic process time step is another method of schematising a long term morphological model. By setting the bed update time step to a multiple of the numerical time step, efficiencies in computation can be achieved with little or no loss in morphological response accuracy. However, prior to any attempted schematising, a sensitivity study should be conducted and validated.

Cayocca et al. (2001) documents a 2DH long term model of 160 Km² tidal Inlet, in the Archaron Basin, France. The model consists of a wave module, 2 dimensional depth integrated current module a sediment transport module and a bed level module. Long term trend simulation utilised representative tides and wave conditions, while extreme events were modelled separately from long term trends models. The morphological time step was stretched to avoid negligible bottom change.

Villaret et al. (2012) developed a Telemac model of the Gironde estuary in France, including morphodynamic evolution simulation. The model couples hydrodynamic flow module with a sediment transport model. The model was run for a 5 year evolution with a time step of a 1000 s. The evolution of the bed levels are compared to differential bathymetry from between 1995 and 2000, figure 2.64. The overall trends of evolution for the 5 year frame are relatively similar.



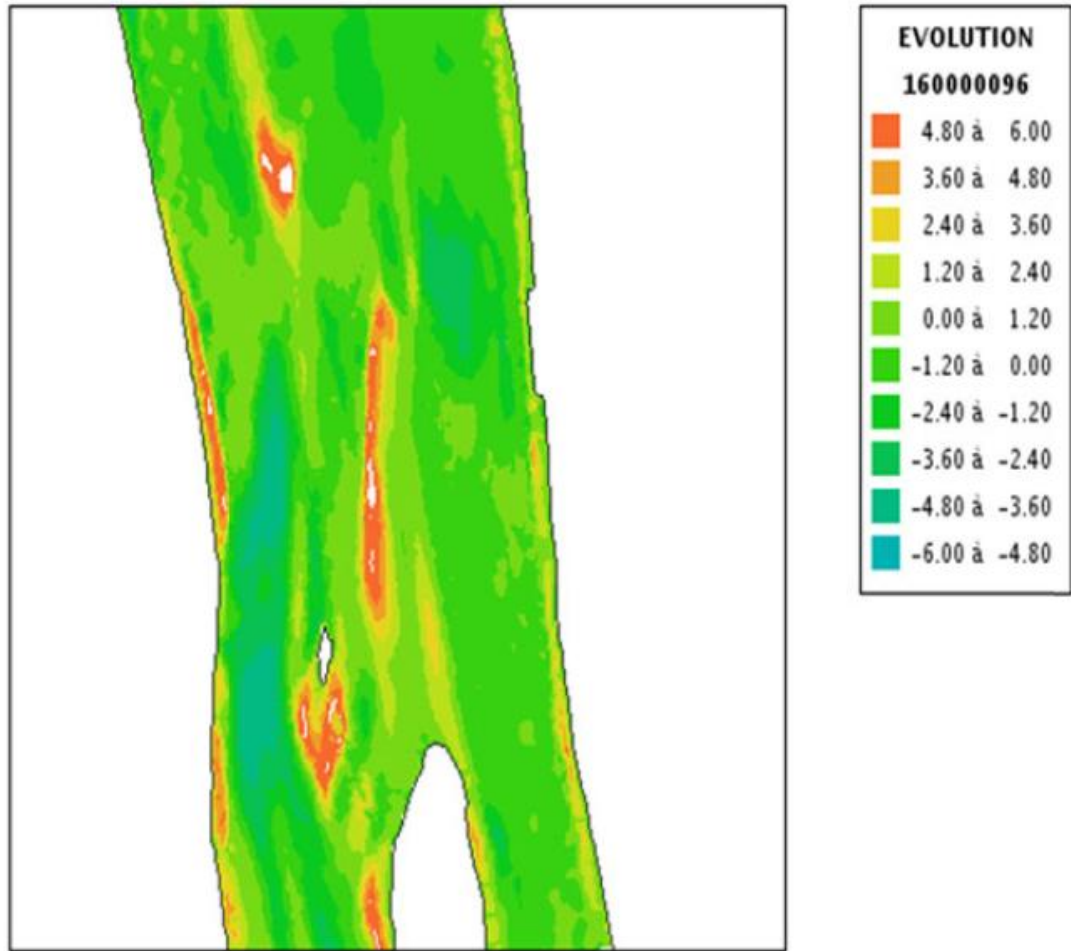


Figure 2.64 a. Differential bathymetry 1995-2000 and b. Simulated 5 year bed evolution (Villaret, 2012)

Xie et al. (2009) used Delft 3D to simulate the emergence of two tidal inlets in Hangzhou bay, China, figure 2.65. The model successfully modelled sediment transport of cohesive sediments. The formation of the present day inlets took a simulation time frame of 30 years.

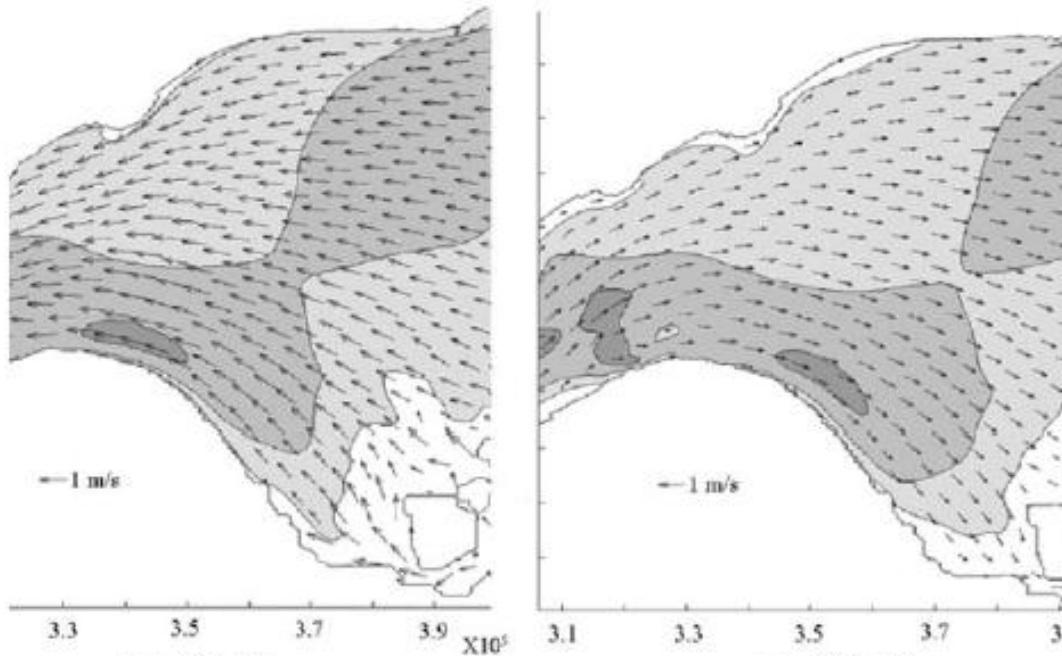


Figure 2.65 Mid ebb and mid flood velocity vectors and suspended sediment concentration after 30 year simulation (XI et al., 2009)

2.6 Previous Studies of Dingle Bay

Previous studies conducted in the area including stratigraphic analysis, sediment sampling, wave modelling and storm impact analysis both on Inch and Rossbeigh are detailed in this section.

2.6.1 Formation and Geological Studies

Several studies have focussed on establishing the time of formation and geological history of the barrier beaches and back barrier areas in Dingle Bay. These studies have ranged from stratigraphic analysis to luminescence dating.

Wintle et al. (1998) estimated the age of the sand deposition Inch using luminescence dating techniques. Five locations were sampled along the beach, figure 2.66, and at various heights on the dune ridge and fore dune, figure 2.67.

The youngest samples were found to be approximately 150 years old which would correlate to the night of the big wind (Shields et al. 1989) a major storm event in the 19th Century Ireland. The oldest sediments were found to be no greater than 600 years old suggesting that Inch formed in its present location occurred around this time.

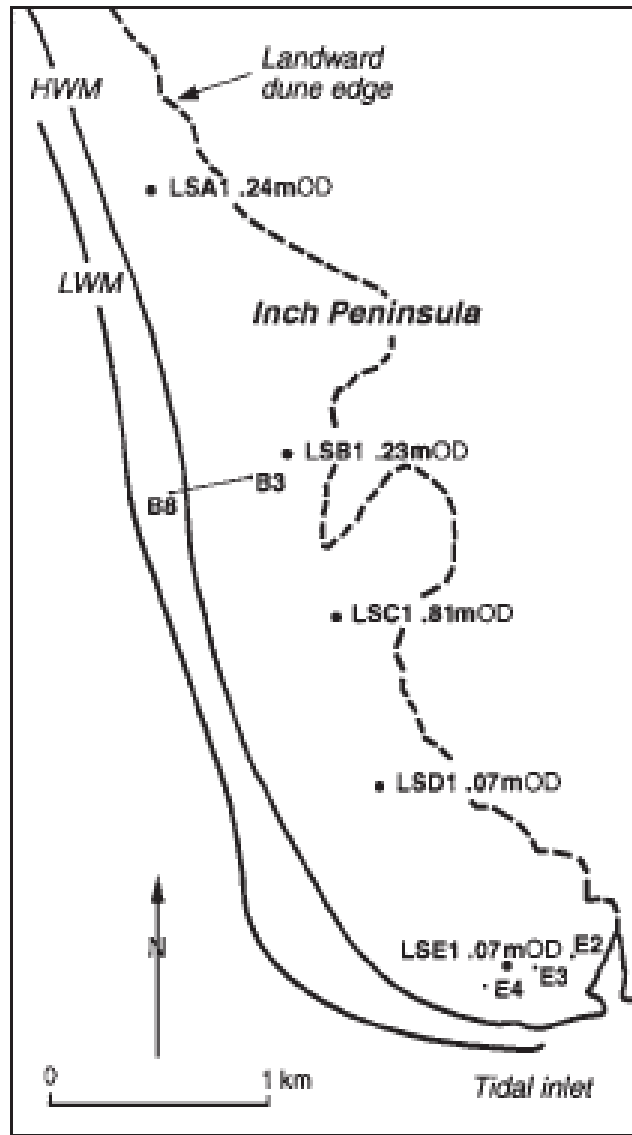


Figure 2.66 Location of samples used in Luminescence dating (Wintle et al., 1998)

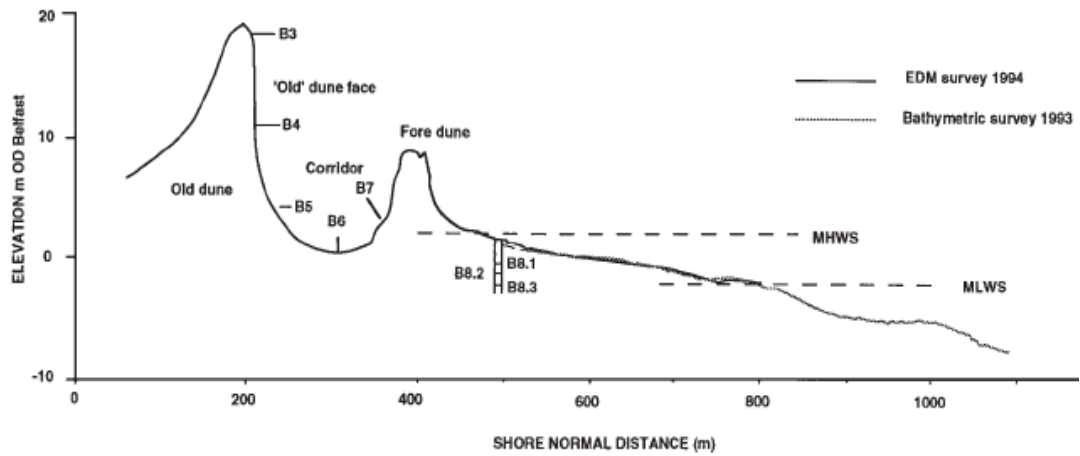


Figure 2.67 Cross-section of test locations on Inch (Wintle et al., 1998)

The sample location and corresponding calculated age is given in Table 2.1. The samples taken at the base of the Dune system in the north are the oldest suggesting that the Inch grew southward from this location on the coastline of the Dingle peninsula. The samples taken from the fore dunes are the youngest sediments. Samples taken from a core of the intertidal zone range from 200 to 500 years, this shows the beach face is relatively resilient to the forcing of large storms that have occurred over the last two centuries.

Table 2.1 Calculated ages of sediment samples on Inch (Wintle et al. , 1998)

Sample	Age (years)
A1	595 ± 52
B1a	147 ± 23
B1	352 ± 48
B2	151 ± 23
B3	208 ± 51
B4	227 ± 25
B5	368 ± 34
B6	332 ± 30
B7	325 ± 36
C1	138 ± 16
D1	146 ± 18
E1	501 ± 44
E2	357 ± 33
E3	520 ± 51
E4	266 ± 46
beachface	
B8/1	213 ± 25
B8/2	459 ± 52
B8/3	509 ± 56

The results at the southern end closest to Rossbeigh range from over 200 years to the formation period approximately 600 years ago. The newest sediments in this area are to the seaward front of the fore dunes while the older are on the leeward back barrier side. This area of Inch would have been considered the most sensitive to meteorological forcing appears to display similar resilience as the rest of the barrier beach dunes on Inch.

A geological study conducted on Rossbeigh beach and in Castlemaine harbour by Devoy et al. (2006) provides an insight into the formation and movement of the system throughout the Holocene (10,000 years BP – Present day). The stratigraphical analysis undertaken indicated that Rossbeigh may have breached just after 3000 cal year BP.

The effect of which was detectable throughout the estuary including the inner harbour eastward of Cromane point. The analysis suggests that the barrier re-established itself thereafter, as sediment deposition characteristics resumed to a pre 3000cal year BP state. The presence of a sand deposit layer on the salt marsh to the rear of Rossbeigh 800 years ago is considered a result of breaching. It is suggested that the barriers have retreated land ward due to presence of fresh water peats found on Rossbeigh.

Further study in the back barrier area was undertaken by Duffy & Devoy (1998) when they examined accretionary patterns in salt marshes, figure 2.68. The main techniques used were monthly sediment elevation measurements, sediment samples including 1.5 m monolith samples taken, tide gauge measurements. Erosion was found to increase to the east linked to growing fetch length within the harbour area. Elevation maximums were recorded in winter while minimums in summer are attributed to salt marsh shrinkage.

It was concluded that the tidal role is generally accretionary in nature but not as strong as experienced in other areas. Maximum erosion values were recorded at Ross Cullen, it is thought that wave forcing are much more significant, Reen point and Griffins were all identified as having negative accretionary relationships.

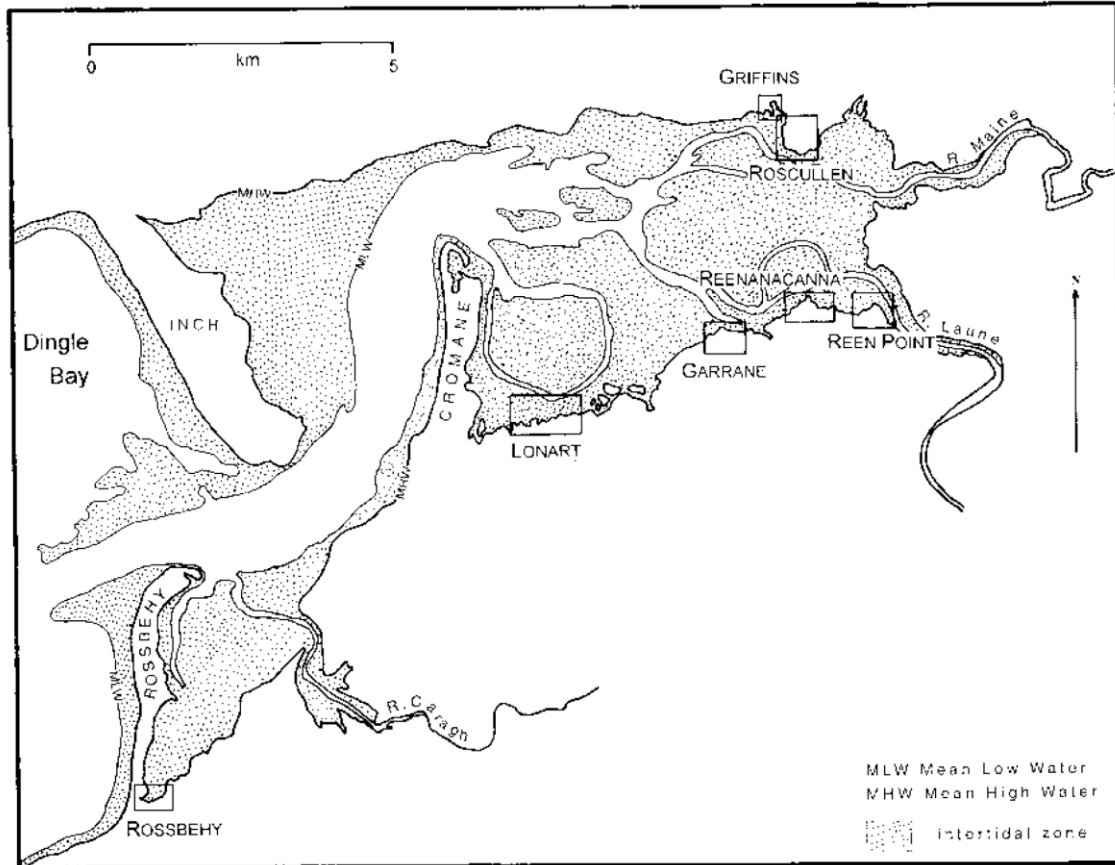


Figure 2.68 Salt marsh accretion rate measurement locations (Duffy & Devoy, 1998)

2.6.2 Wave Climate and Morphology

Two studies in particular focus on the wave climate and morphological drivers on the barrier beaches within Dingle Bay, Vial's (2008) study of storm impacts on Inch and Sala's (2010) study of morphodynamics on Rossbeigh. The former study was conducted on Inch over the winter of 2007 and includes wave data collection and analysis. The latter study focuses on Rossbeigh, post breaching, utilising historical mapping and topographical survey data from the end of winter 2008 to summer 2009. The data from both these studies is utilised in the present study and is detailed in the proceeding chapters.

Sala (2010) undertook a semi quantitative analysis of Rossbeigh. Following the guidelines of beach morphology classification outlined in Section 2.3.1, a Ω value of 6 and RTR value of 2.9 was calculated, concluding that Rossbeigh is at the boundary of barred dissipative and unbarred flat dissipative beach. Vial, (2008) concluded that Inch had similar hydrodynamic

characteristics, with sediment on the beaches of an average grain size of 235 μm .

Sala divided Rossbeigh beach into 5 sections; a proximal, 3 median and a distal end, figure 2.69. A breach in winter 2008/9 of 200 m occurred in median part 3, and between the years 2000 and 2010, 2 million m^3 of sand has been eroded.

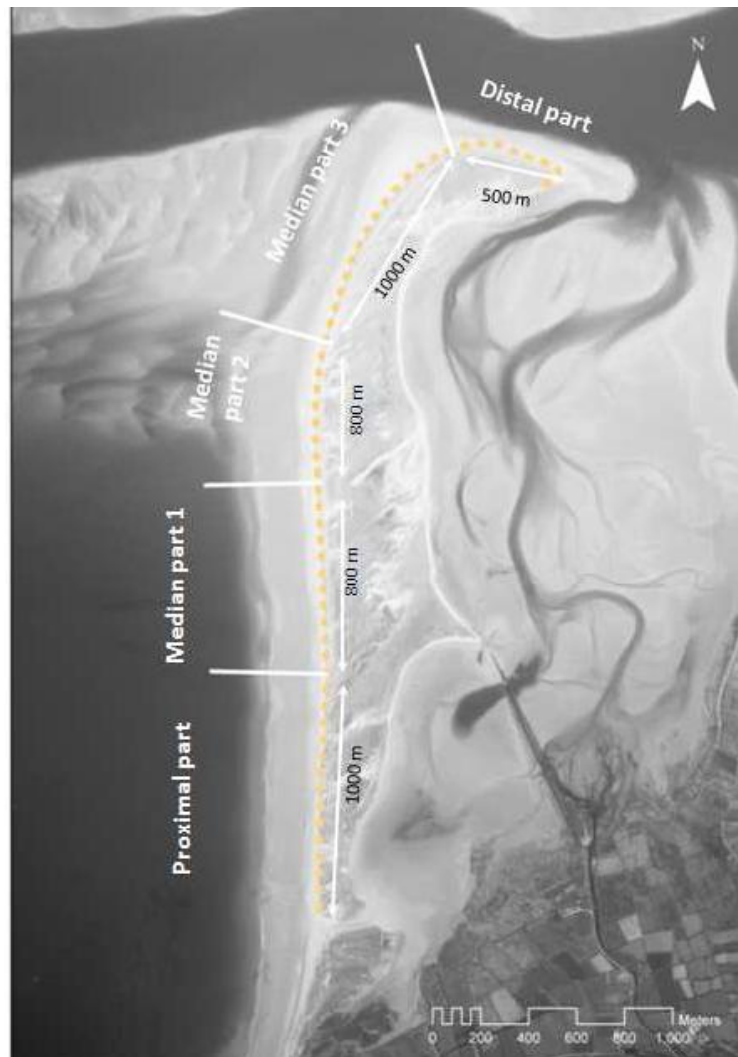


Figure 2.69 Division of Rosbeigh (Sala, 2010)

Vial (2008) undertook a tidal prediction analysis for Inner Dingle Bay. The main parameters are tabulated in Table 2.2. The Admiralty charts report peak tidal currents of 1.5 m/s (3 kn) within the tidal inlet, figure 2.70.

Vial (2008) undertook a historical analysis of extreme and average wave climate data examining statistics from the M3 offshore wave buoy. It was found that a calm wave climate exists for 70% of the time with $H_s < 3$ m and

4% of the time storm climate exists, the spring tidal range of 3.2 m and Hs of 2.8 with Tz of 7s in Dingle Bay.

Table 2.2 Tidal statistics for Inner Dingle Bay relative to Chart Datum (Vial 2008)

Highest Astronomical Tide	+4.36 m
Mean High Water Spring	+3.76 m
Mean High Water Neap	+3.15 m
Mean Sea Level (0m at Malin Head)	+2.30 m (Ordnance Datum)
Mean Sea Level	+2.15 m
Mean Low Water Neap	+ 1.17 m
Mean Low Water Spring	+ 0.58 m
Lowest Astronomical Tide	0 m

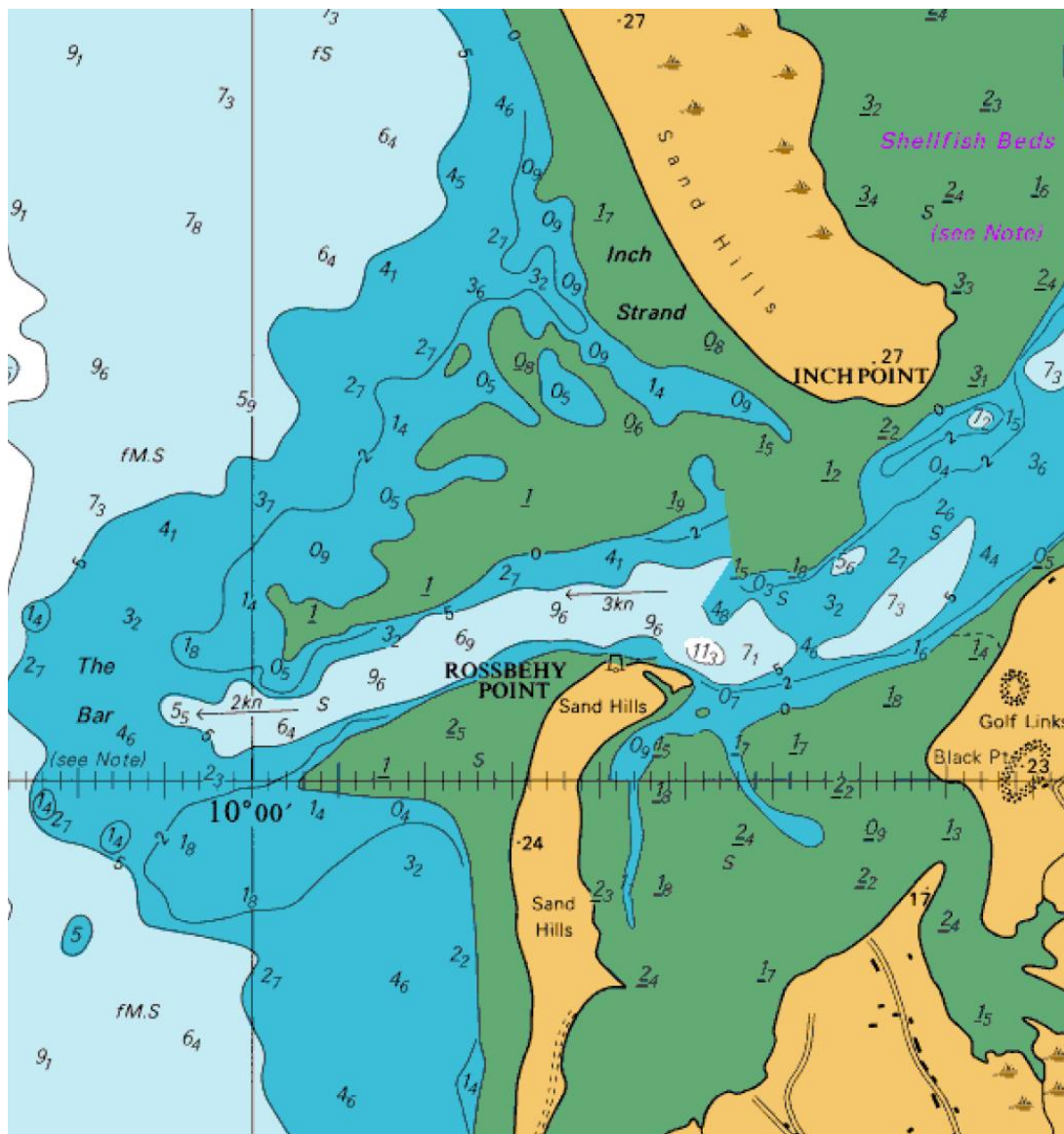


Figure 2.70 Currents in Dingle Bay (Admiralty, 2006)

The frequency of storms in Dingle Bay was analysed over a longer timescale by Sala (2010). WAM hindcast data from 1958 to 1997 was compiled, figure 2.71, with M3 Data from 2004 to 2009, the intervening years being unavailable in any format. A clear trend of increasing storm frequency is observed.

A wave gauge was placed 3 Km offshore of Inch in 11 m of depth as part of Vial's (2008) study, figure 2.72. Several storms were recorded over the deployment period. The largest of these was an event with a H_s of 13.4 m and associated period range between 12 s -14 s recorded offshore at the M3 buoy. Utilising a hindcast model it was calculated that this storm had a 1 in 20 year return period. The other storms were in the order of 4 to 5 m H_s and 12 to 13.7 s in period.

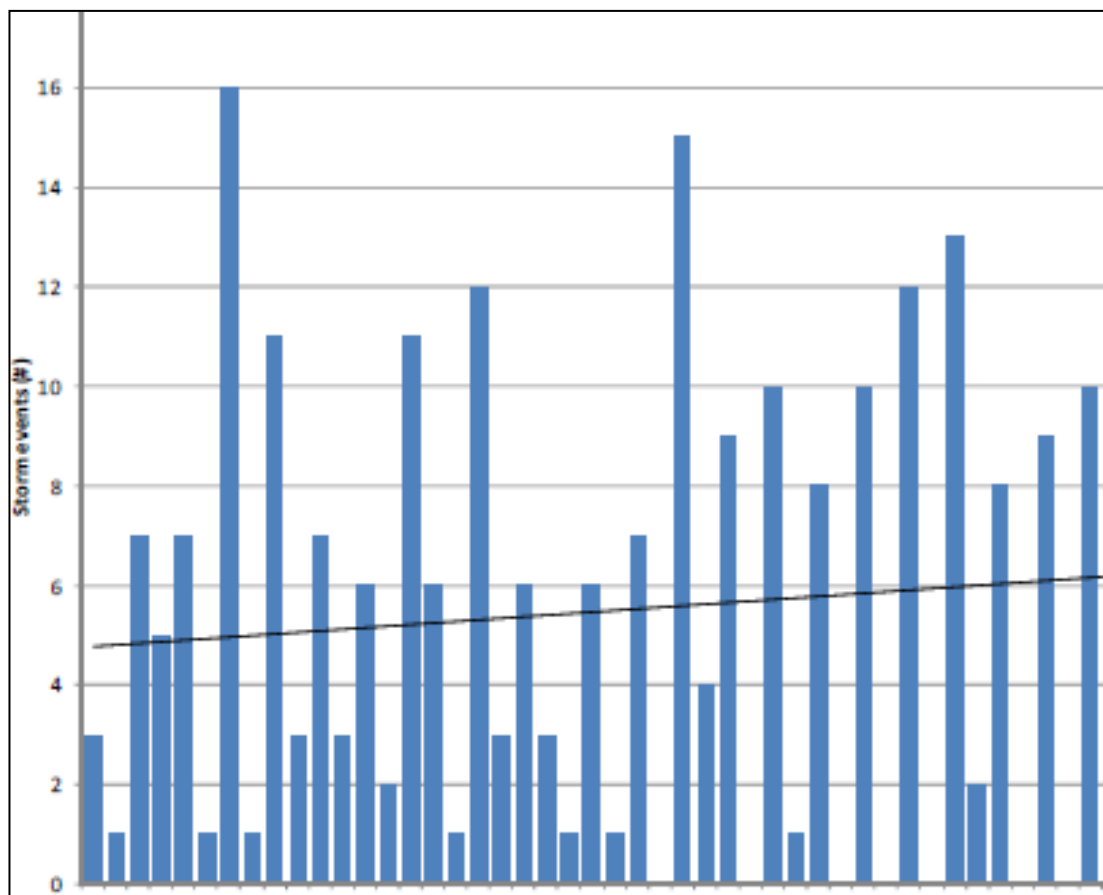


Figure 2.71 Seasonal storm events from 1958 to 1994 with increasing average frequency (black line) (Sala, 2010)

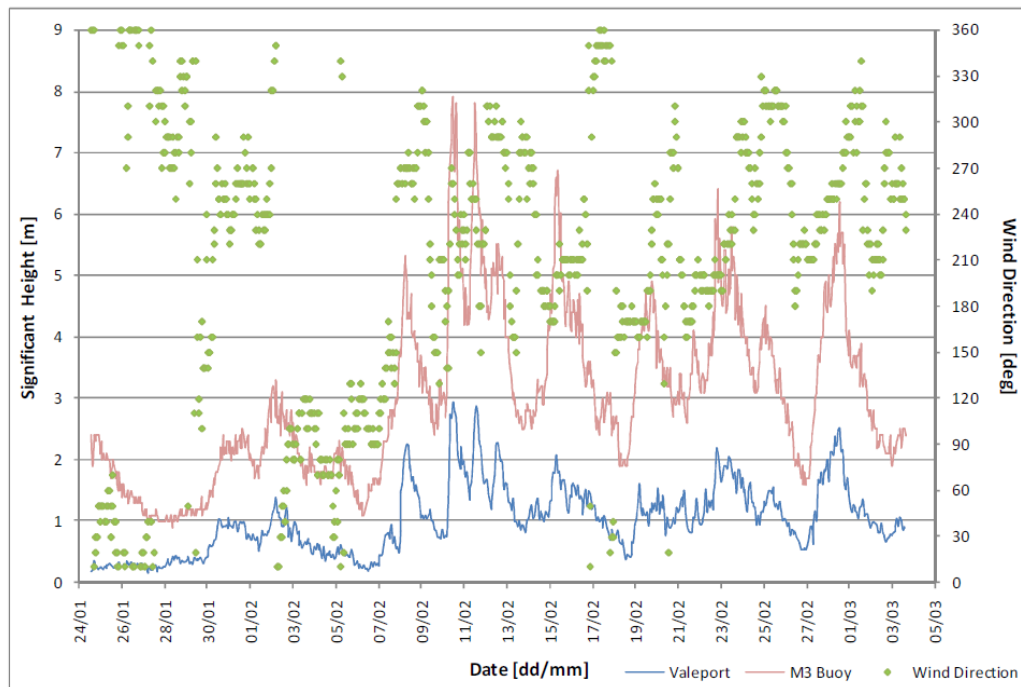


Figure 2.72 Wave gauge data compared to offshore wave buoy (Vial, 2008)

Sala (2010) conducted 3 surveys in the summer of 2009, winter 2009 and summer 2010. Digital elevation models (DEM) were created and features compared. Analysis found that slight infilling occurred at the breach and erosion rates reduced between 2009 and 2010. It was also estimated that 350,000 m³ of dune sediment was removed from Rossbeigh between June 2009 and July 2010. A fall in longshore sediment supply was suggested as possible cause of the breach. Finally, a conceptual model describing morphodynamic behaviour that lead to breaching was formulated. Two fulcrum points and 3 accretive zones were identified as critical components in this model, figure 2.73.

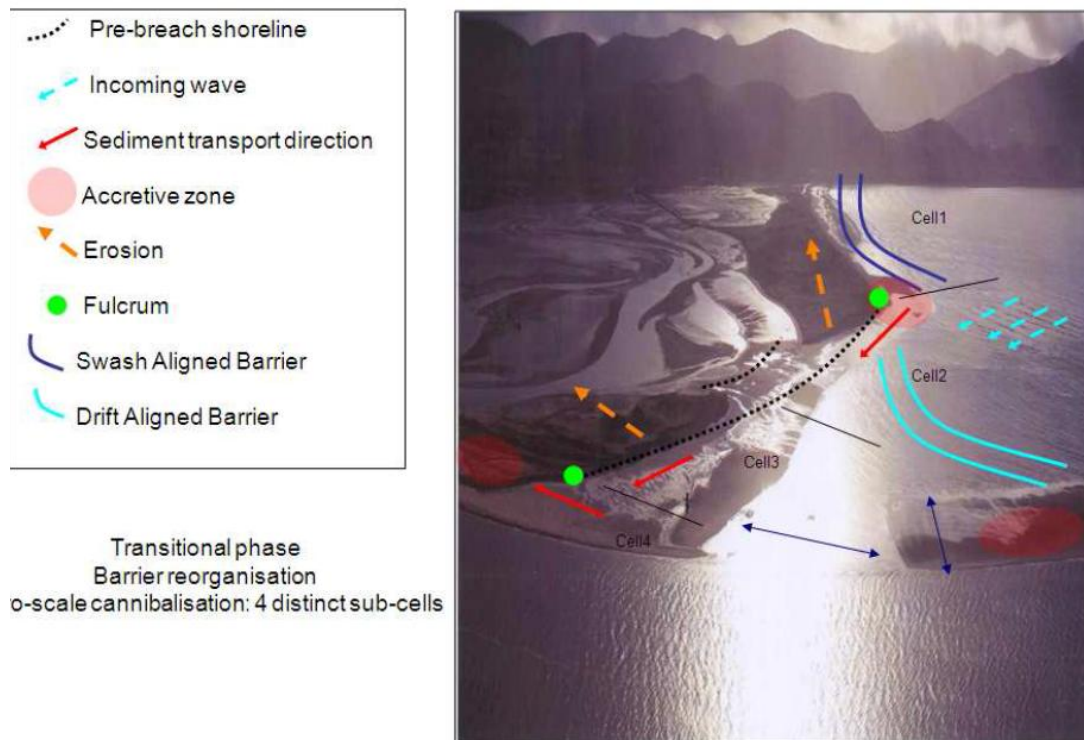


Figure 2.73 Conceptual model of breaching at Rossbeigh (Sala, 2010)

2.6.3 Wave and Storm Impact Modelling

Several studies of storm impacts and wave patterns have been undertaken in Dingle Bay. Orford et al. (1996) undertook wave modelling of Dingle Bay utilising the HISWA model. They examined potential triggers of mesoscale change on Inch Beach. The effect of a 90th percentile Hindcast storm (A 6.6 m high wave with 13.6 second period) was modelled without storm surge. The simulation showed that sediments on Inch were transported alongshore and then seaward. The ebb tidal delta was identified as a critical zone of wave refraction during storm conditions.

Cooper et al. (2004) undertook further storm simulations in Dingle Bay in an examination of storm surges along the west coast of Ireland. Again, using the HISWA model a variety of modal swell and storm wave conditions were run. The selection of storm conditions was made based on historical storms including the 90th percentile hindcast, figure 2.74, and wind waves associated with Hurricane Debbie, figure 2.75.

The general hypothesis of this paper states that large swell waves tend to dissipate offshore of Rossbeigh spit on the ebb tidal delta, not directly contributing significantly to dune erosion. During modal waves there is a concentration of orbital velocities on the Rossbeigh ebb tidal delta close to the present day breach. It was speculated that significant erosion takes place under locally generated shorter period wind waves under specific conditions occurring only twice at Rossbeigh in the previous 160 years. This research concludes that historic shoreline position analysis do not yield definitive conclusions regarding the impact of storms on erosion.

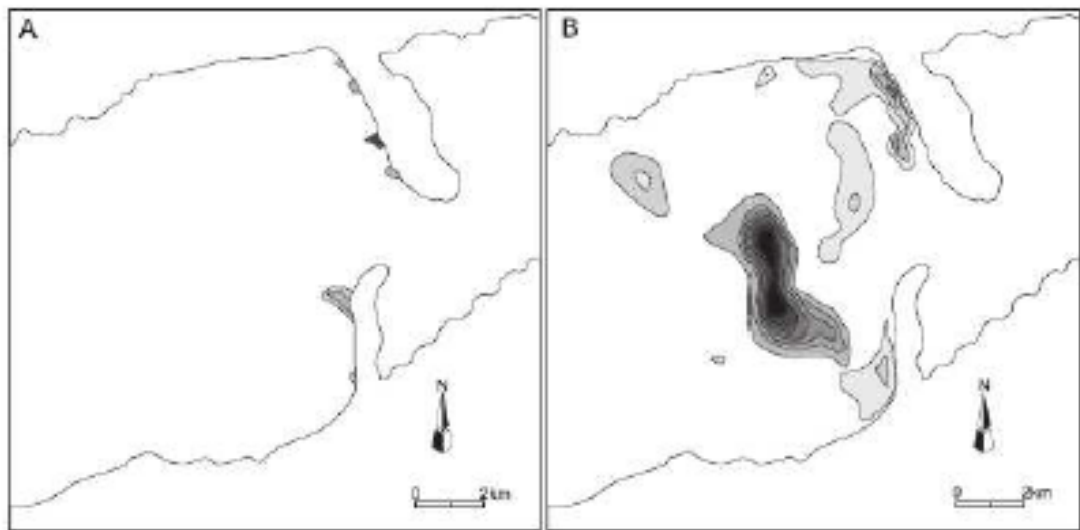


Figure 2.74 Distribution of Wave Energy under A) Modal swell and B) 90th Percentile storm (Cooper et al., 2011) - Darker shades indicating larger wave energy

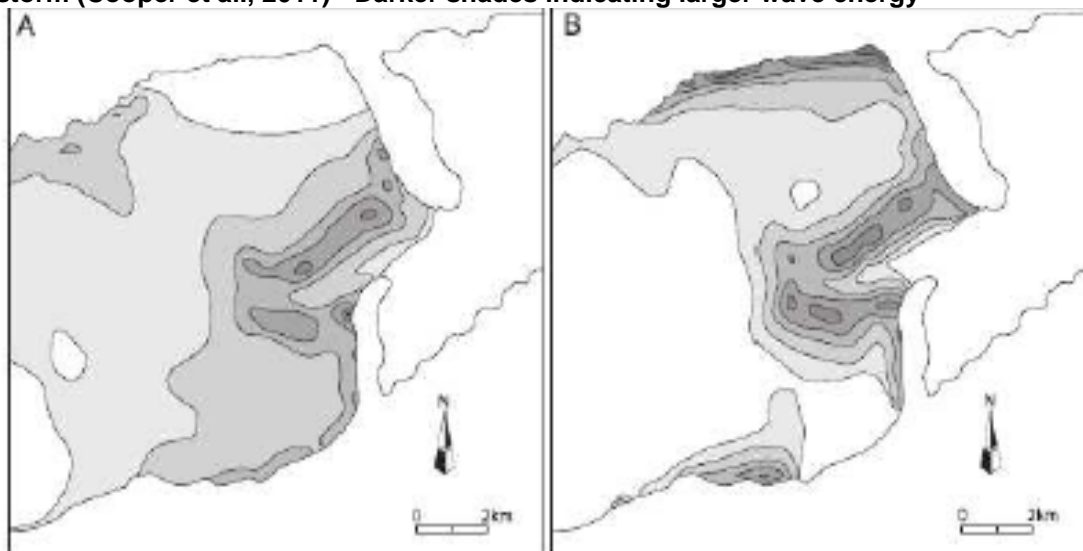


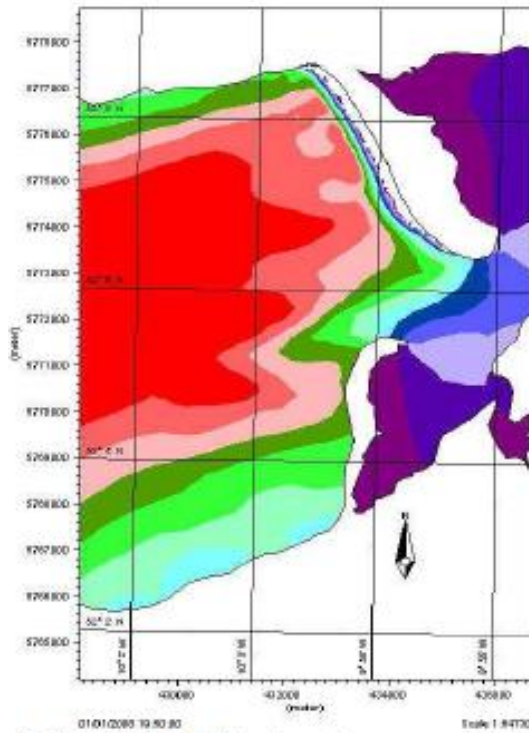
Figure 2.75 Wave orbital velocities of A) Modal Swell and B) Hurricane Debbie wind-generated waves (Cooper et al., 2011) - Darker shades indicating higher velocities

Vial (2008) simulated a 1 in 100 year storm in Dingle Bay using DHI Mike 21 SW spectral wave modelling software for three different stages of the tide, Mean Low Water, Mean Sea Level and Mean High Water Level. The results, figure 2.76, show that the significant wave height was greatest close to shore at high tide and that the ebb-tidal delta significantly reduces the wave heights.

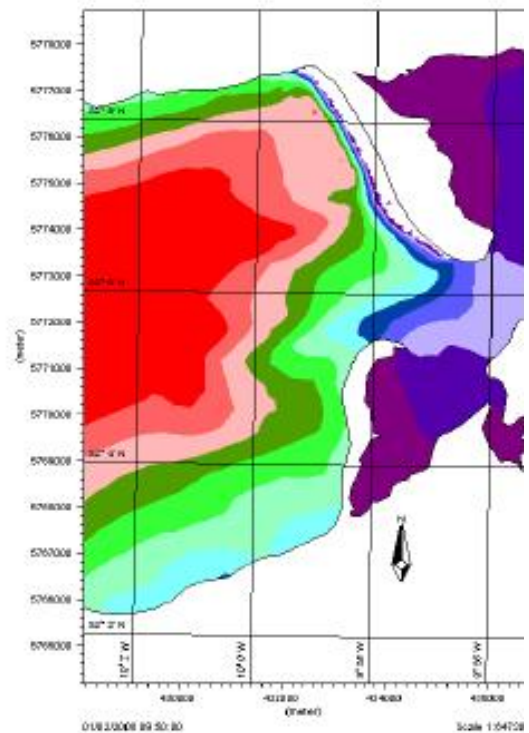
Sala (2010) refined Vial's model by updating nearshore bathymetry to represent 3 phases of evolution on Rossbeigh. The bathymetry was created by interpreting images of pre-breaching (2000), breaching (2006) and post-breaching (2009) phases.

The lack of near shore surveyed bathymetry restricts the analysis of simulation results to qualitative trends. Sala further refined the model by coupling tidal currents with wave simulations of H_s of 4 m and T_z of 8 s with direction of 270 °. The post breaching phase wave climate at high tide, figure 2.77, highlights the importance of the removal of the swash platform in front of the breach. A notable result from the modelling was the formation of a tidal inlet within the breach.

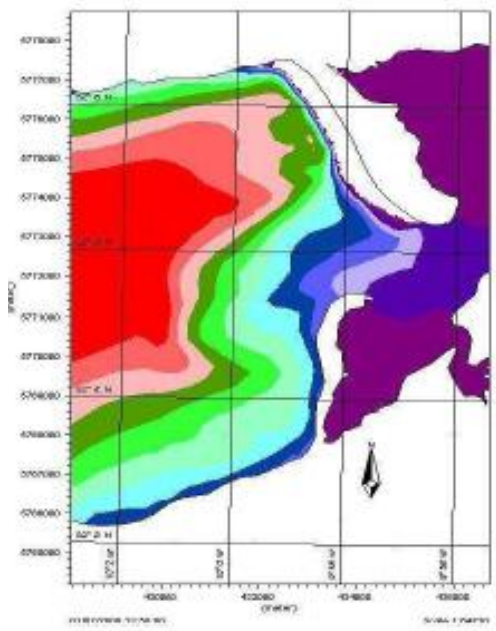
This newly formed inlet has simulated mid ebb, figure 2.78, and mid flood, figure 2.79, peak currents of over 1.1 m/s. However, no tidal current measurements were recorded to validate the simulations.



a) Mean High Water Level



b) Mean Sea Level



c) Mean Low Water Level



Figure 2.76 Significant wave height simulated for 1 in 100 year storm (Vial, 2008)

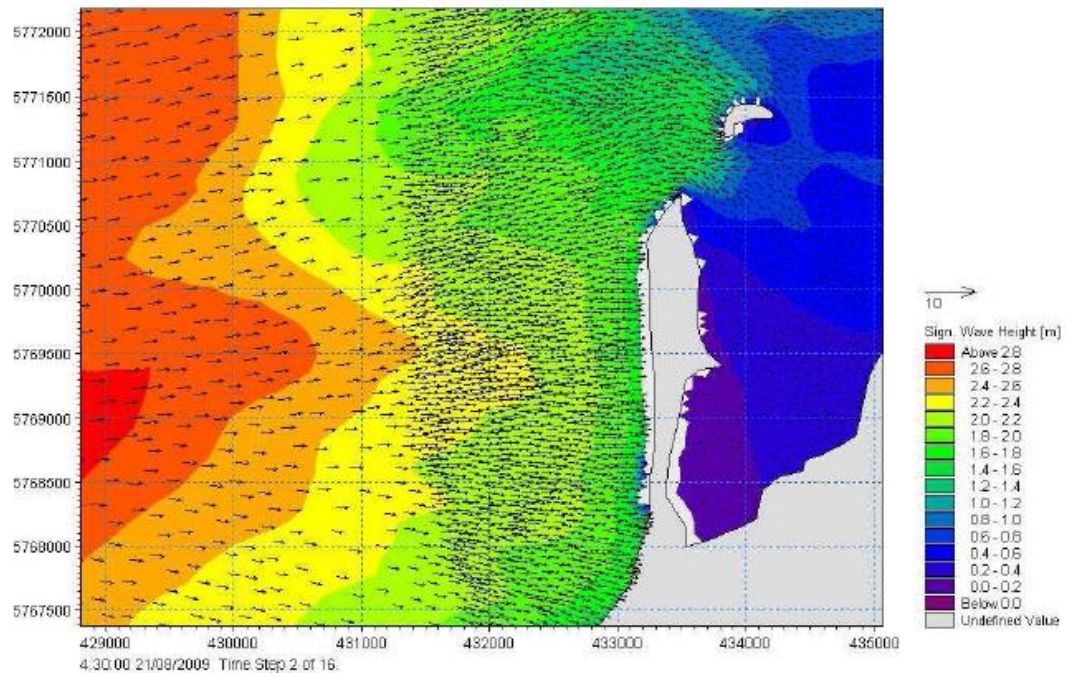


Figure 2.77 Hs at high tide post-breaching phase (Sala, 2010)

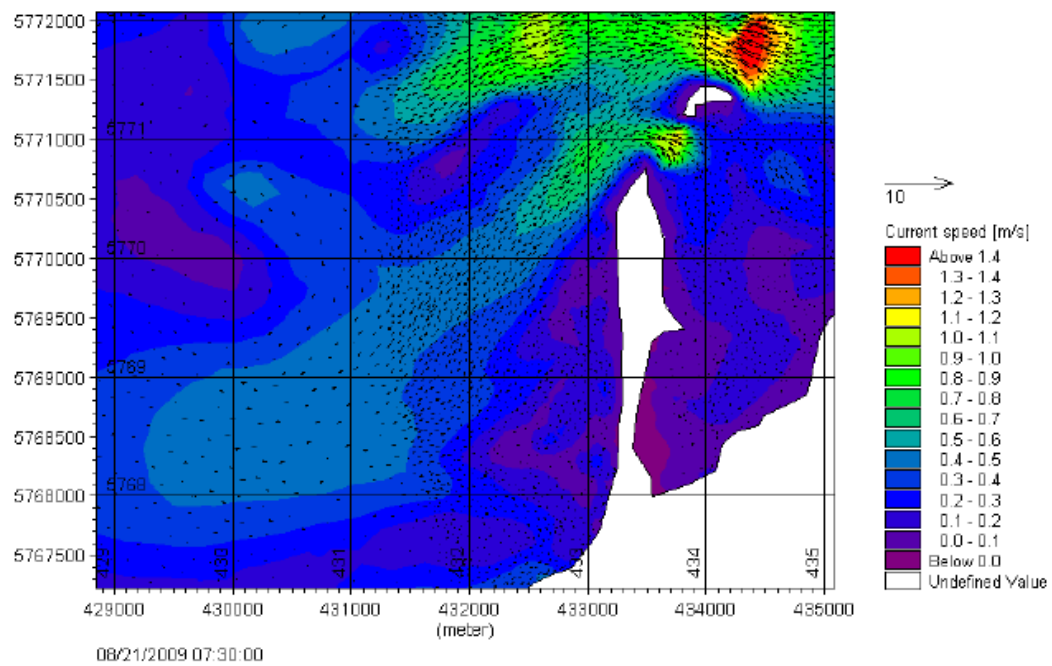


Figure 2.78 Mid ebb flows (Sala, 2010)

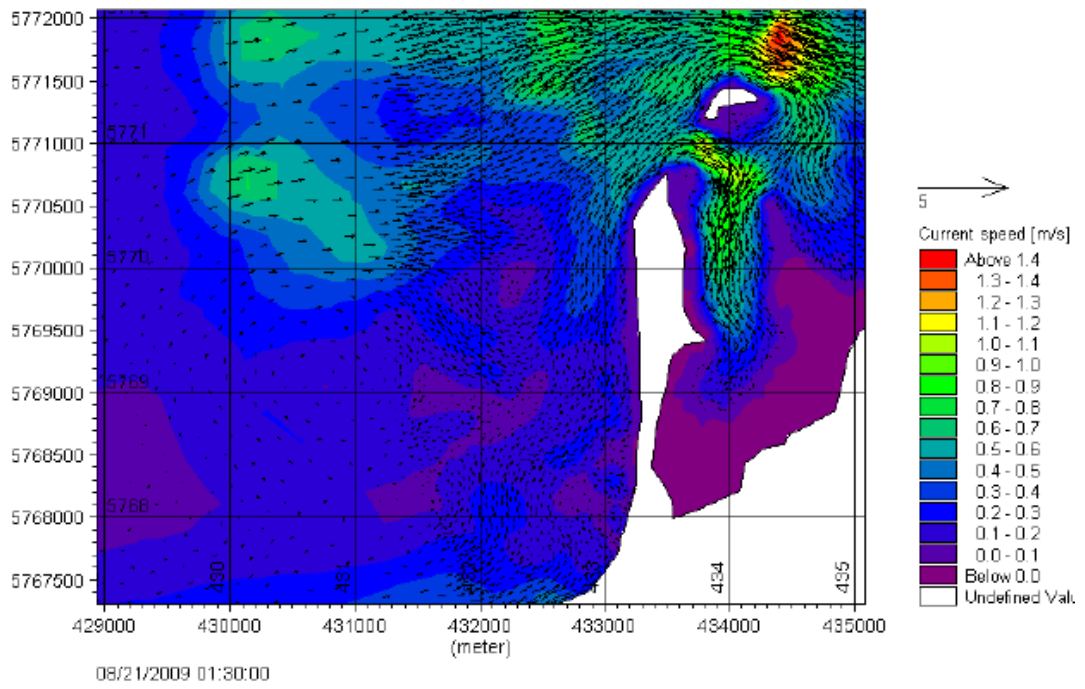


Figure 2.79 Mid flood flows (Sala, 2010)

2.7 Conclusions

In summary, there is a plethora of knowledge relating to barrier beach morphology. However, only a small percentage of research applies specifically to conditions similar to Rossbeigh and Dingle Bay. An introduction to concepts and technologies is presented to provide background for the experimental research undertaken for this research. A review of previous work conducted in Dingle Bay has yielded important background data relevant to the morphology of Dingle Bay.

It has been demonstrated from the examination of case studies that the accuracy of evolution prediction depends on the variety, quality and quantity of data sources. It has been shown that even with significant datasets, calculating the future morphology of a barrier coastal system is difficult. However, by recognising certain features of barrier beach morphology such as changing barrier alignment and tidal inlet channel migration, these studies have shown that conclusions on future evolution can be made.

The classification methodologies of coastal systems have been reviewed with particular attention being paid to the role of tidal inlets. The migration patterns and erosion trends of systems similar to Inner Dingle Bay were documented. Morphological mechanisms such as sediment by passing and cannibalisation are discussed.

Established and experimental coastal monitoring techniques were documented and evaluated. The theory underpinning experimental methodologies trialled as part of the present study including wave radar and grain size trend analysis were described in detail. Other techniques including aeolian transport and sediment dye testing methodologies were also trialled on Rossbeigh using the information and recommendations of previous research documented in this chapter. The selection of correct equipment such as sediment traps were identified based on previous assessments and field studies. Various morphodynamic numerical modelling software packages were detailed. Approaches to tidal inlet migration and

dune erosion prediction were examined and evaluated including long term and predictive techniques.

3 Coastal Evolution of Dingle Bay

3.1 Introduction

The initial investigation into the coastal evolution of Dingle Bay is presented in this chapter. The timescale ranges from the centennial to the inter-annual seasonal scale. The shoreline changes of both Inch and Rossbeigh over time were documented using various data forms including maps, satellite imagery, aerial photography and topographic surveying. Distinct morphological cycles were identified on both barrier beaches. The main focus was on Rossbeigh including recent changes leading to the breaching and morphology post breaching. The migration of an ebb tidal bar was examined and compared to shoreline change. Finally, the variation in sediment transport direction along Rossbeigh was analysed using common sediment transport formulae, the results give clear indications of a dual morphodynamic climate on Rossbeigh.

3.2 Long term evolution of Dingle Bay

Establishing the natural behaviour of the Dingle Bay coastal cell was the first step in distinguishing if recent erosion at Rossbeigh is part of, or a deviation from a natural morphological cycle. As coastal evolution occurs over varied timescales, robustness of analysis improves with longer dataset and greater temporal resolution. A basis for identifying causes and effects of breaching can also be inferred from such historical analysis if the data is of sufficient resolution and range.

The examination of historical Ordnance Survey maps, aerial photographs and recent satellite imagery of Dingle Bay using GIS software was undertaken to identify the evolution of the barrier beaches on a centennial scale. Each image was geo-referenced to analyse shoreline change over time. The earliest charts date from the 19th century, 1842, figure 3.1, and 1894, figure 3.2. There was a large gap in data until 1977 when the first aerial photograph, figure 3.3, of the area was taken. Despite these large data gaps it was possible to identify trends and characteristics of the morphological cycle.



Figure 3.1 Historical Map of Inch and Rossbeigh 1842 (OSI)



Figure 3.2 Historical Map of Inch and Rossbeigh 1884 (OSI)



Figure 3.3 Aerial Photograph of Rossbeigh 1977 (OSI)

Before analysis of the various maps could begin, consideration had to be given to the inherent error within the data sources, most notably the 1:10,560 scale historical maps. The High Water Mark (HWM) was used as a reference to the shoreline to discuss the changes on a centennial scale. An error of $\pm 10\text{m}$ has been attributed (Moore, 2000) to similar 19th century historical maps. This exceeds the limits for reliable quantitative analysis (Boak & Turner, 2005), therefore trends in the long term evolution were discussed on qualitative level only. The shoreline positions over time (1842 – 2000) were overlaid on a rectified aerial photograph from 2006 in figure 3.4.



Figure 3.4 Centennial Scale Shoreline Change

It was clear from figure 3.4 that Inch is a relatively stable barrier dune beach both in terms of orientation and size. The shoreline change is linear with no obvious deviations. The barrier has undergone several cycles of erosion and progradation since the initial survey of 1842. This was evident in the seaward position of the dunes in 1894. Subsequent erosion was visible in 1977 with the shoreline regressing further leeward than the 1842 survey. However, dune growth was visible between 1977 and the 2000 survey. Comparing the

2000 shoreline with the shoreline of the 2006 image, sections of the distal end of Inch have eroded slightly.

The evolution of Rossbeigh dune line appears to be independent of Inch. The barrier orientation width and position change significantly with time. The erosion patterns are non linear along the seaward shoreline. The 1842 shoreline was similar in shape to the pre breach dune of the mid 2000's with a narrow neck close to the distal edge of the dune. The 1894 and 1977 positions were similar with slight erosion on the back barrier side visible. It was unclear whether the position or shape of Rossbeigh changed in the 83 years between these two references.

The only visible difference between 1977 and 2000 shorelines was the shoreline erosion occurring in the area of Rossbeigh which is presently breached. The erosion has continued and increased between 2000 and 2006. Relative stability of the back barrier shoreline during this period confirms that the breaching was due to forcing from the western seaward side. Comparing the shape of Rossbeigh in 1842 profile and in the 2006, it was possible that different forcings may be responsible for the narrow necks. It is likely that the indentation in 1842 is created from the eastern estuary side suggesting river and tidal flow and water level increase as the driving erosive forces. However, with no mapping prior to 1842 available, this cannot be confirmed.

The present erosion cycle has caused an indentation that eventually led to breaching from the seaward side. The roll back of the Rossbeigh barrier between 1842 and 1894 was significant when contrasted with the seaward growth in Inch. It is unlikely that Rossbeigh and Inch have a direct morphodynamic relationship. Large growth in dune line on Inch between 1977 and 2000 coincides with a period of little change in Rossbeigh dune line. Comparing the 19th century profiles, the barriers were moving in opposite directions Inch's shoreline moved seawards while Rossbeigh moved landward (east). It could be speculated that Rossbeigh's loss of seaward position was inversely related to the progradation of Inch. However,

upon examination of the Rossbeigh shoreline shape it is clear that while the sediment was eroded from the seaward shoreline, the narrow neck was in-filled with a net growth of the barrier as a whole.

There is evidence of recurvature similar to those seen on Bartra (Section 2.3.2) throughout Rossbeigh, figure 3.5. This suggests that a breach may have occurred here previously. Identifying such events would increase the understanding of the underlying morphological cycles within Dingle Bay. A limiting factor in the analysis of the long-term morphology was the absence of positional data of the tidal inlet and associated ebb tidal deltas.

It is also possible that Rossbeigh undergoes a two phase evolution similar to Nauset barrier discussed earlier in Section 2.3.2. An inlet development phase prompted by breaching, followed by tide dominated sediment transport, updrift recurving and down drift instability all occurred post 2008 breach on Rossbeigh. Bar welding from offshore intertidal sand bar post inlet development may also be occurring. However, the tidal inlet channel appears geologically fixed in Dingle Bay with little migration occurring. A single stable inlet phase persisted in Rossbeigh for several decades although the dearth of historical records in comparison with Nauset makes it impossible to quantify the time period of the different phases.

In summary, the morphology of Inch can be characterised as dynamic on a decadal scale, but overall stable in position and shape while Rossbeigh undergoes long term stability followed by rapid shoreline change exhibited at least twice within the past 200 years.

3.3 Recent Evolution

The Barrier beach - Tidal inlet system is undergoing rapid dynamic changes, both hydrodynamically and morphologically. The availability of regular satellite imaging from the early 2000 onwards has facilitated the analysis of recent morphology in Dingle Bay at a greater temporal frequency. Annual and seasonal changes in erosion and deposition patterns can be observed from the imagery. Combined with regular topographic surveys which the HMRC initiated in 2009 post breaching, the influences of critical factors on Dingle Bay's future evolution were described.

The dune erosion trends pre and post breaching were examined using the dune vegetation line (DVL) as a reference. Key indicators of morphology such as the evolution of ebb tidal channel and delta over the last 10 years, beach profile and beach orientation change are also discussed

The extent of erosion occurring in recent years becomes apparent when the dune vegetation line of Rossbeigh was plotted over time, figure 3.5. The breaching event, occurring in 2008, has split the barrier beach into two distinct dune areas, a median section still attached to the coast line and a distal-island section which is disconnected from the main dune system between mid and high tide. The DVL's are overlaid on an aerial image from the year 2000. An estimated 2 million m³ of sediment has been removed since 2000. This removal of sediment has continued post-breaching with the median and island sections of the beach reducing in size year on year.

The breach measured a distance of over 900 m in 2013, spanning from the southern tip of the island distal section to the northern tip of the median dune. The erosion rate post-breaching on the median dune has been in the order of 50 m /m width of dune/ year. The island section is receding at approximately 30m /m width /year. This intense erosion has begun to alter the orientation of Rossbeigh's shoreline.

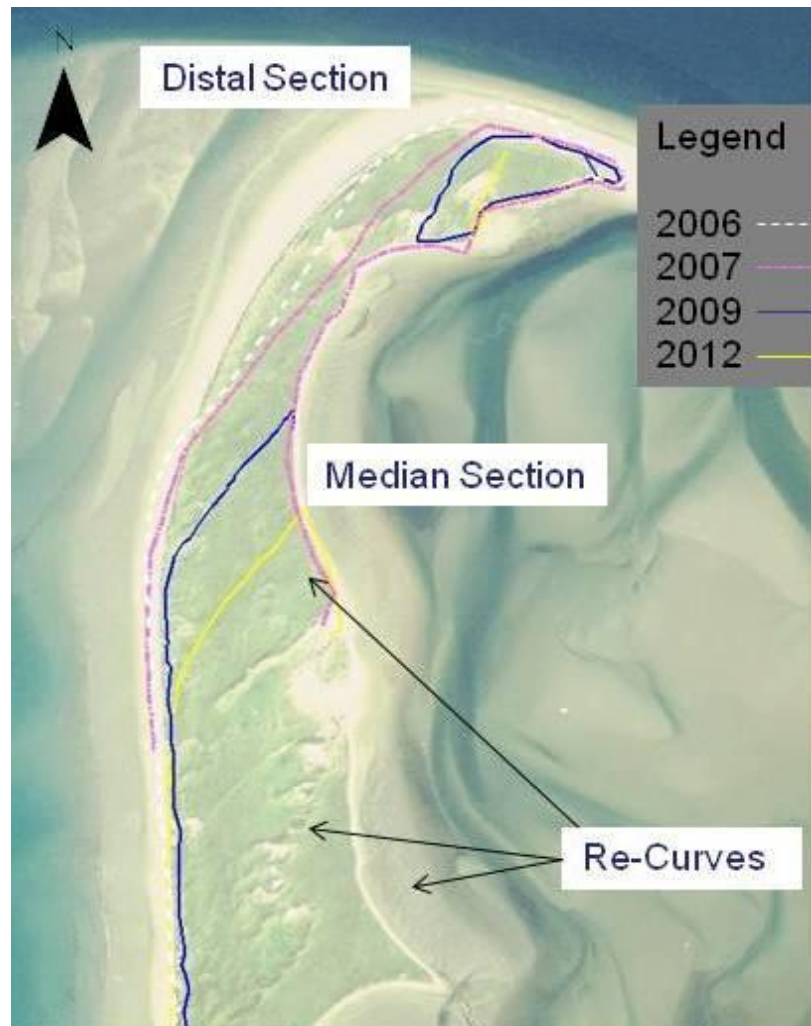


Figure 3.5 DVL variations since 2006 on Rossbeigh

In its current orientation, figure 3.6 (c), Rossbeigh can be divided into two distinct zones based on its alignment to the prevailing westerly incident wave direction. Starting at the southern end, the beach is swash aligned, with the shoreline running perpendicular to incident waves for 2.6 Km, the shoreline then turns at an angle to the incident wave direction and becomes drift aligned for approx 1.4 Km. There is a distinct hinge point between both zones denoted by the yellow line running normal to the shore.

Erosion and progradation alongshore in the swash zone is in a dynamic equilibrium. The drift zone, however, is undergoing rapid change. The hinge point also appears to be moving south resulting in the drift aligned zone growing at the expense of the relatively stable swash aligned zone.

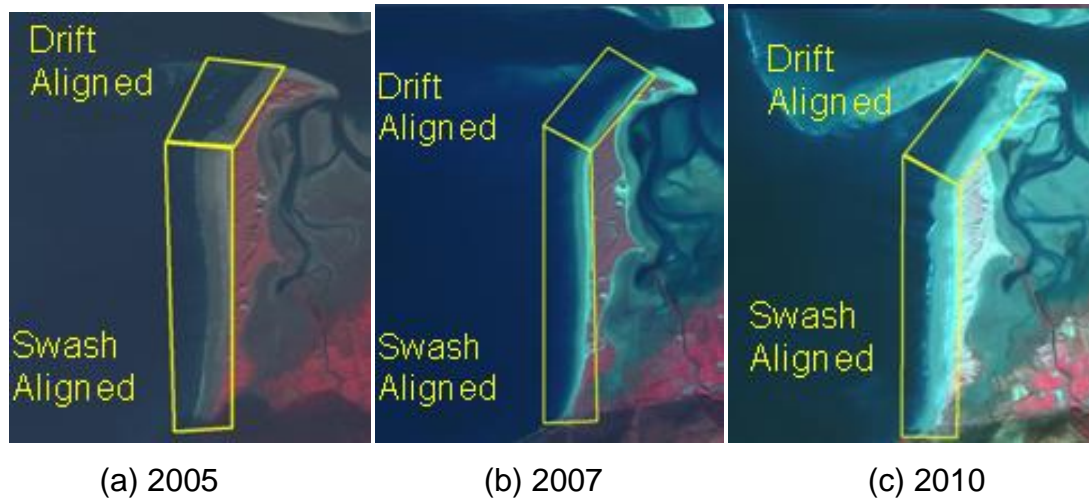


Figure 3.6 Evolution of beach orientation on Rossbeigh over a decade

Both macro and micro cannibalisation described by Orford et al. (1996) in Section 2.3.3 have occurred on Rossbeigh. In 2005, figure 3.6(a), the majority of the barrier was swash aligned and morphologically stable, now the barrier beach has begun transitioning to a drift aligned structure. This is the opposite of the gravel barrier beaches discussed in Section 2.3.3, which have changed from a stable drift aligned to unstable swash aligned.

During this macro cannibalisation phase in 2007, figure 3.6 (b), micro cannibalisation also occurred in the form of the breaching. As the swash aligned section continues to grow at the expense of the stable swash aligned section, macro cannibalisation can be deemed to be ongoing.

Whether or not micro cannibalisation will occur again is unclear. Alteration of the sediment supply pattern is the primary cause of this process. It is probable that the flux in ebb tidal bar size has altered the offshore-onshore sediment supply pattern, thus prompting the macro-cannibalisation.

The influence of offshore bars and ebb tidal delta has been identified by (O'Shea, 2011) , however, prior to this study, there has been no physical evidence produced to suggest that the bars affect the erosion. A data collection campaign undertaken to fill this knowledge gap is discussed in the Chapter 4.

3.4 Cross-sectional Analysis

The change in beach-dune profile on Rossbeigh from 2009 to 2012 gives an indication of the changes occurring post-breaching. Cross-sections were extracted from terrain modelling software 12D by triangulating topographic surveys. Four profile lines, figure 3.7, representing the 2009 hinge point, figure 3.8, the drift aligned dunes, figure 3.9, breach location figure 3.11 and the Island Section, figure 3.12 at approximately 6 month intervals from the summer 2009 to winter of 2012 where available.



Figure 3.7 Location of beach profiles

The migration of the hinge point is clearly illustrated in figure 3.10 by the continuous roll back of the dune face. This trend is slightly offset by the June 2010 profile which appears to signify seaward growth of the dune. This profile was actually representative of dune collapse. From 2011 to 2012 the erosion rate is regular and continuous at approximately 10m of dune eroded per survey interval.

The scale of the erosion in the drift aligned dunes is captured in figure 3.11. As with the hinge point there was no seasonal variation in trend with constant erosion between surveys occurring. The extent of the erosion accelerates after March 2011. This erosion continued and by May 2013 the Dunes were lowered to spring high tide levels allowing storm surge wash over.

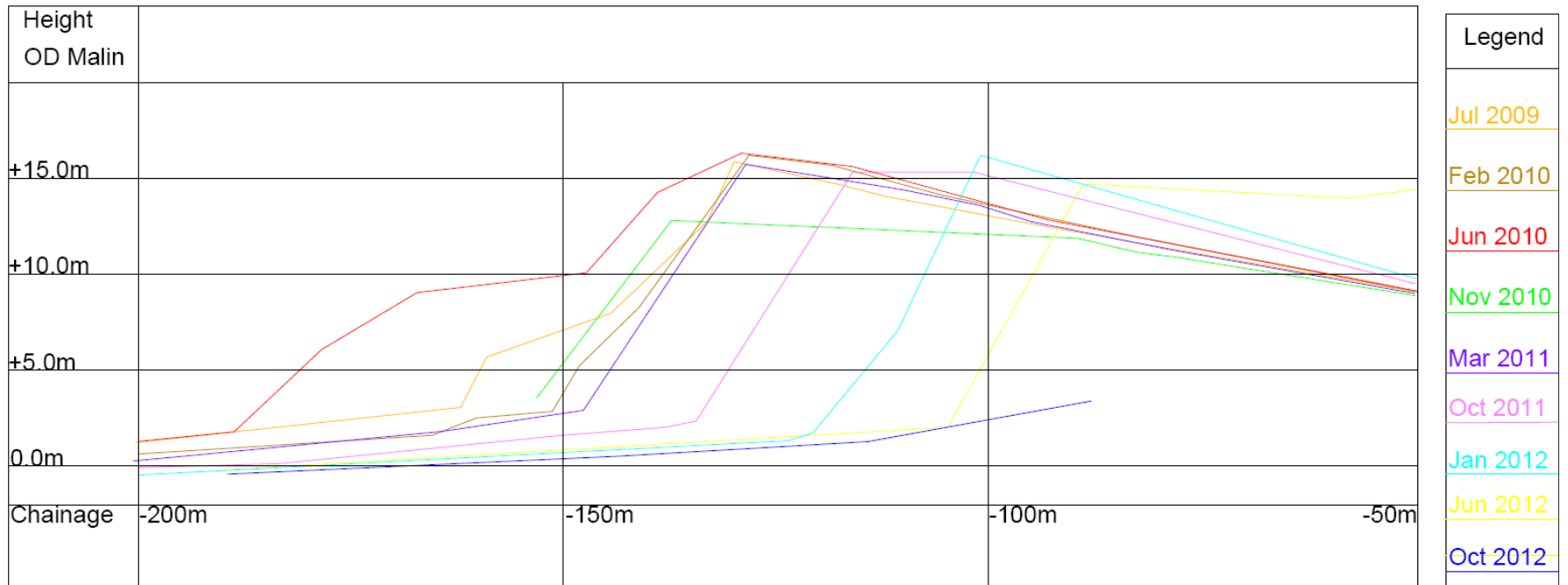


Figure 3.8 Profile analysis of Hinge point

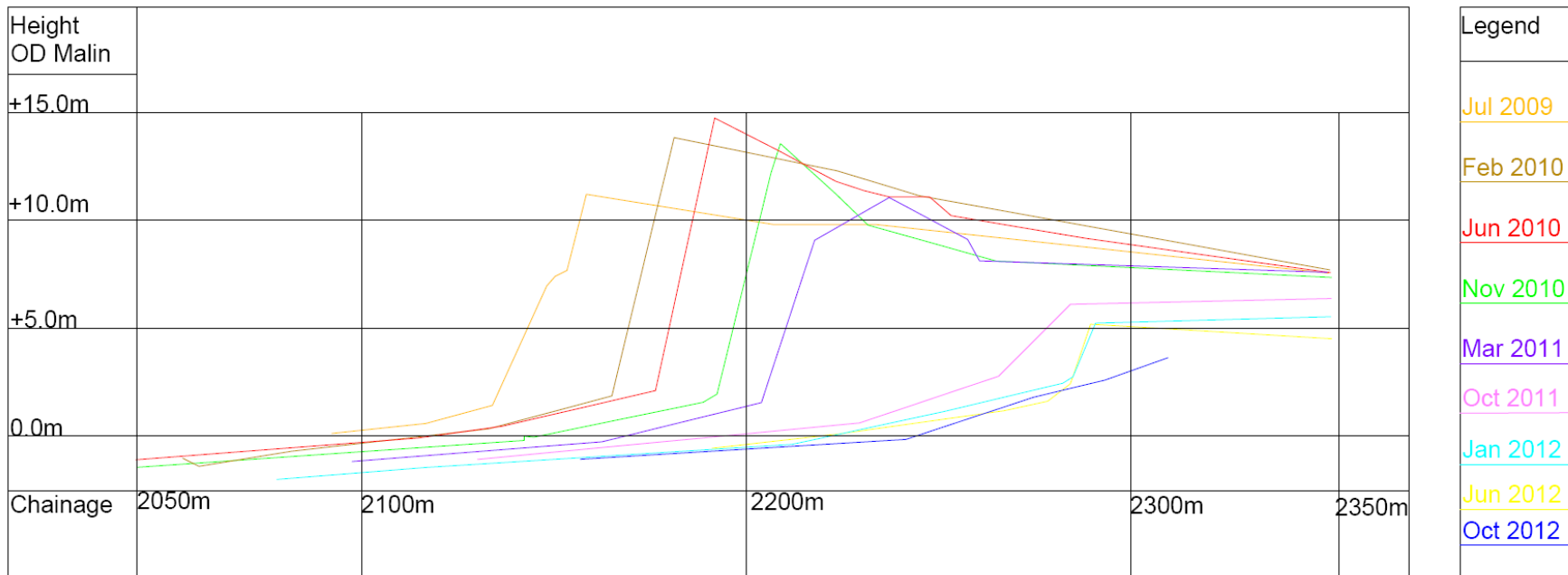


Figure 3.9 Profile analysis of Drift aligned Dunes

The evolution of the profiles in the breach location, figure 3.11 is more complex than the hinge point and drift aligned dunes. The lower part of the shore line displays a strong seasonal signal. The beach erodes and lowers over a winter cycle and accretes and rises after a summer season. Further up the beach in the supra tidal zone the activity is even more dynamic. The 2009 position in the breach showed a large depression on the shore face with the whole cross-section within the intertidal zone.

The growth of a gravel berm in the breached zone was visible from the summer of 2010 onwards. This berm migrated up the shoreline in successive seasons. The ridged berm reached a height of over 3 m OD Malin in March of 2011. Prior to berm formation this gravel was highly mobile during winter storms months notably on the southern end. However, in the summer of 2011 the northern edge of the ridge stabilised and vegetation has begun to grow, figure 3.10.



Figure 3.10 Vegetation in breach zone

The southern edge of the gravel berm closest to the median dune was previously attached to the median dune but with continued erosion, the gravel berm has re-organised to become a separate feature. It displays

resilience absent in the dune structure which as already mentioned is receding rapidly while the berm has maintained its position and has grown in height. The berm itself was formed by alongshore drift of gravel from the southern end of Rossbeigh. The gravel was transported from the southern shoreline of Dingle Bay via alongshore transport along Rossbeigh to the breach area. This alongshore transport of larger gravel occurs despite the predominantly swash dominated southern shoreline of the southern part of Rossbeigh.

The distal island section profile evolution, figure 3.12, showed the greatest change over the 3 year time period. The height of the dunes is reduced from 15m in February 2010 to less than 1m in May 2013. This change represents the complete removal of this section of dunes and is symptomatic of the extreme erosion occurring on the terminal end of Rossbeigh. It is clear that if this rate of erosion continues the entire Island section will be removed entirely.

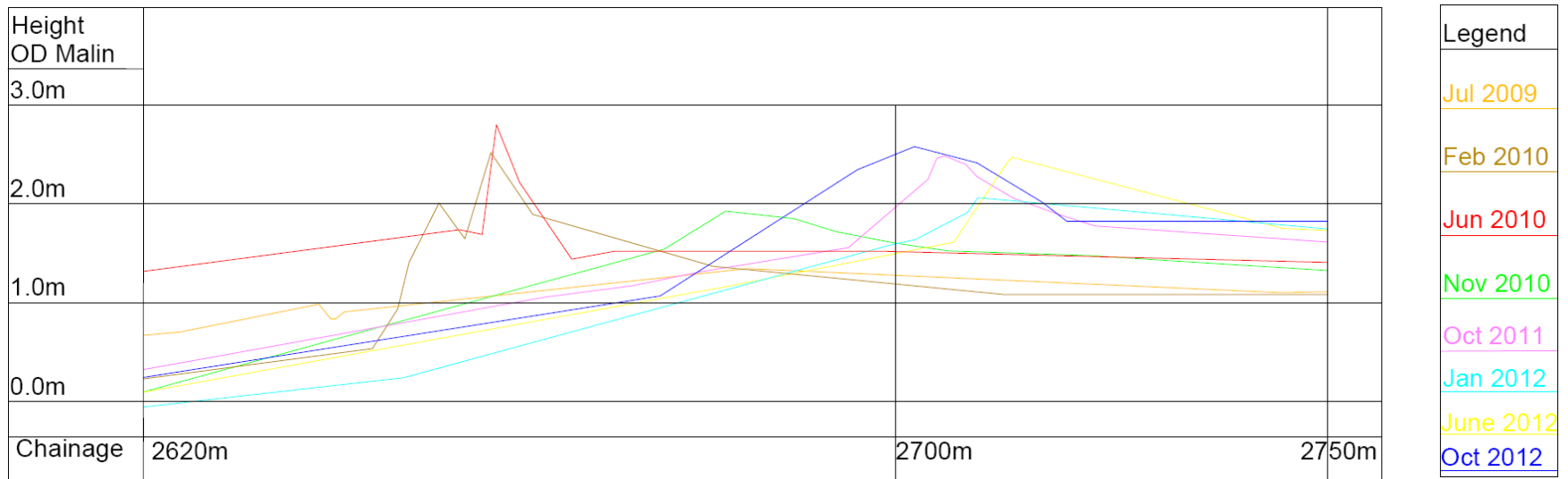


Figure 3.11 Profile analysis of Breach

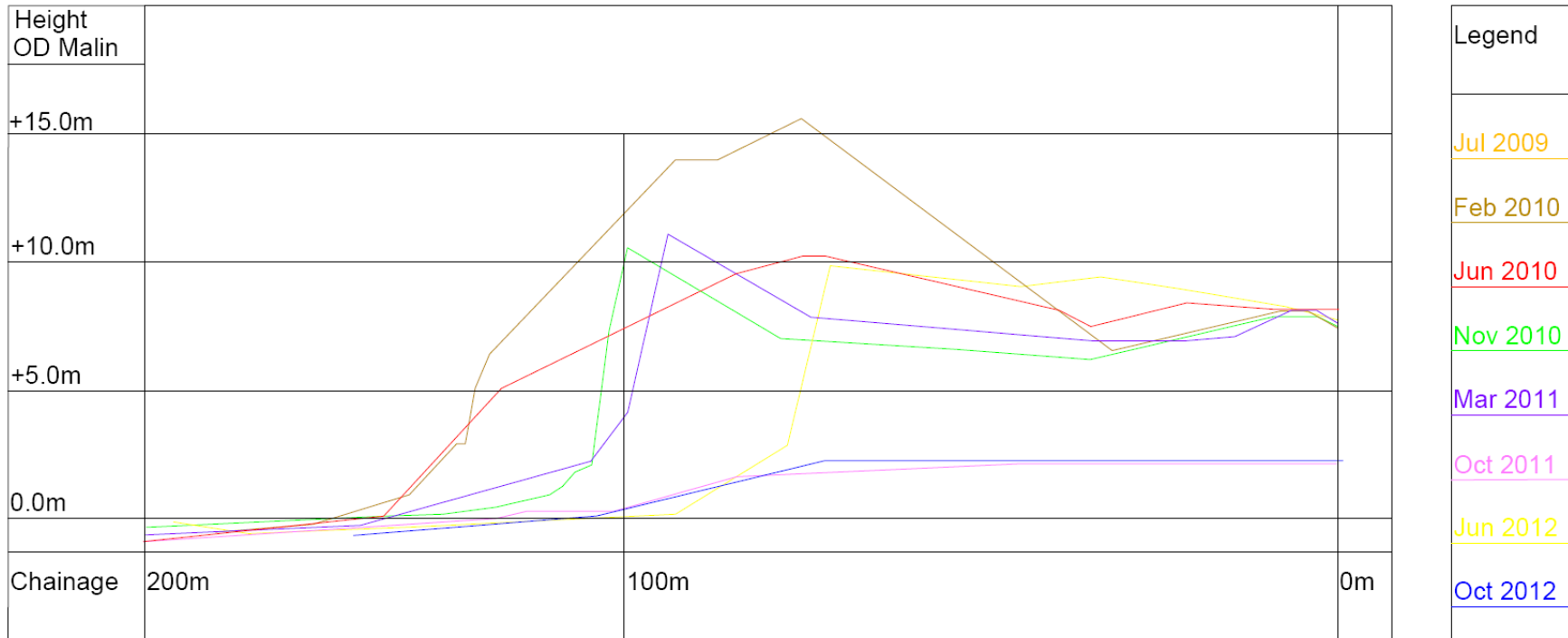


Figure 3.12 Profile analysis of Island

3.5 Tidal Inlet and ebb Tidal Bar Evolution

In a barrier beach inlet system, the main drivers of erosion and morphology are typically hydrodynamic. The quantitative monitoring of the hydrodynamics in Dingle Bay cannot be achieved retrospectively; post-breaching quantitative hydrodynamic data is discussed later. It is possible however; to qualitatively identify characteristics of hydrodynamic drivers from analysis of archived spatial data. This qualitative analysis focuses on the cross shore length of beach on Rossbeigh, the position and shape of the tidal inlet channel and ebb tidal bars.

The addition of satellite imagery provided imagery of the Bay on an annual basis from 2001 to the present. This enhanced both the long-term morphological analysis in the bay and the short term pre and post breaching analysis, compared to previous morphological studies on Dingle Bay.

The majority of the satellite images were obtained from the Spot satellite. All images used in the analysis were taken within 30 minutes of low tide. The images were added to GIS software and orthorectified to ensure accurate inter-comparison. The pixel size of images ranges from 10 m to 2.5 m.

The images, figure 3.13, from various sources chart the evolution of Rossbeigh beach, the tidal inlet and ebb tidal bars from 2000 to 2011. The images represent the post-winter stage of the seasonal morphological cycle at low tide.

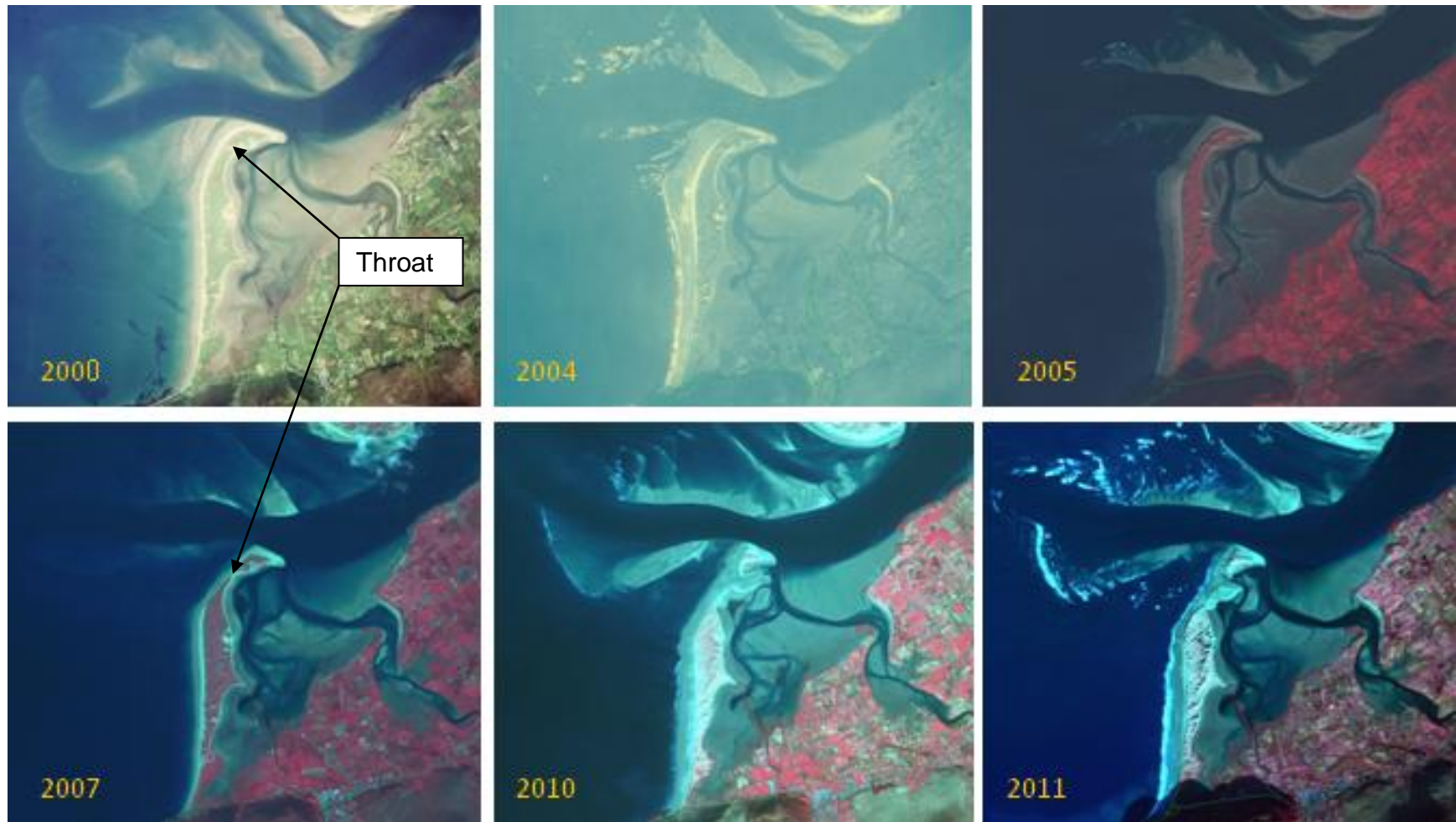


Figure 3.13 Decadal Evolution of Rossbeigh, ebb Tidal Bar and Inlet

Examining the images in chronological order it became evident that the morphology of the tidal inlet channel, ebb tidal bar and beach were all interdependent. In 2000 the tidal inlet was a distinct “S” curve meander with well developed ebb tidal bars on both sides; the cross shore beach length was large and joined to the ebb tidal delta. The dune system was also at healthy width with no risk of breaching evident.

As the inlet meanders it slowed and deposited sediment similar to the final stages of river sediment transport. This sediment fed the ebb tidal bars and through wave action was worked on to the beach. This provided natural dissipation protection, causing waves to break at a distance from the toe of the dunes, nullifying the wave’s erosive power. This explains the dunes relatively large throat thickness at this time.

In 2004 & 2005 the ebb tidal delta had eroded and tidal inlet has changed position. It flows in a straight westerly direction with little meandering. The removal of ebb tidal delta and shortening of the cross shore beach width has only marginally affected dune width by 2005.

However, with the tidal inlet channel flowing faster, deposition of sediment on the ebb tidal bars had ceased thus starving the beach of this sediment source. It was likely that deposition occurred further offshore. In Section 4.3 it was documented that large expanses of shallow sub tidal flats exist beyond the ebb tidal bar. These depositional areas extend north and into the path of the tidal inlet main channel. As these areas are not detected by satellite imagery analysis it was not possible to determine the exact extent of these sub tidal flats.

By 2007 the ebb tidal delta on both sides of the inlet channel had become severely eroded. This localised erosion is an example of micro-cannibalisation. This small area in the drift aligned zone was starved of sediment due to an interruption in the sediment supply on the macro scale but there was also a sink- source relationship developing due to a local increase in tidal current, shown in Section 4.2.3. The tidal inlet flowed

straight unconfined by ebb tidal bars, sediment was entrained for longer and transported further out into deeper areas Dingle Bay. The drift aligned beach area of Rossbeigh has also been significantly reduced in the cross shore direction. The dune system has undergone erosion to the point where breaching appears imminent. This erosion was the result of the removal of the protective dissipative beach and ebb tidal bar that fed it sediment. With water depth increasing in the intertidal zone and toe of the dunes larger waves are breaking at the dune toe.

Examining the final images, 2010 and 2011, the system evolution post-breaching was characterised by sedimentation of the back barrier channels, re-growth of the outer ebb tidal delta and erosion of the median and distal-island parts of Rossbeigh. The tidal inlet channel is currently in developing stages of S shaped meander reformation similar to 2000. The centre of the southern ebb tidal bar shows growth between 2010 and 2011 although a deep channel between Rossbeigh beach and ebb tidal bar remains.

High tidal currents, discussed in Section 4.3, in this area prevent the bar welding that allowed the swash bar present in 2000 to form. The role of swash plane sand migration in infilling breached dunes is a key consideration of barrier evolution. A comparison with the post breaching Bartra beach evolution, discussed in Section 2.3, could be made with the future evolution of Rossbeigh.

The recent evolution of the ebb tidal bar lying offshore of the breach area on Rossbeigh is documented in figure 3.14. This figure is only for qualitative analysis as the images used to produce the ebb tidal bar outline were taken at varying times within 30 mins of low water. Furthermore the elevation of the bar was not discernible in the imagery analysis.

To assess the vertical evolution of the bar, bathymetric surveying was required. This undertaking is discussed in detail in Section 4.3. It is evident that the bar has changed shape and location over the 5 year time frame. The bar, as noted already, has grown seaward and influenced the shape of the

tidal inlet from 2005 to 2010. The bar also appears to be growing/migrating in a drift shore normal plane towards the breach. This suggests that there is potential for bar welding to occur if current migration trends continue. Since 2010 the western/seaward boundary of the bar has receded shore-wards. This is most likely due to wave action reworking the deposited sand in the direction of the breached area on Rossbeigh.

The shoreward migration of the ebb tidal bar would have to overcome the dominant shore parallel current, in the shore parallel channel, Figure 3.15, to initiate breach repair on Rossbeigh, as occurred in Bartra (Section 2.3). In such a scenario the system would become wave dominant, with tidal currents reducing from present velocities. In terms of Fitzgerald's (2000) classification mentioned Section 2.3.5, the inlet doesn't fit into a distinct category. It displays characteristics of both model 3 (ebb-tidal delta breaching) and model 4 (outer channel shifting), further evidence of the complexity of this inlet barrier system.

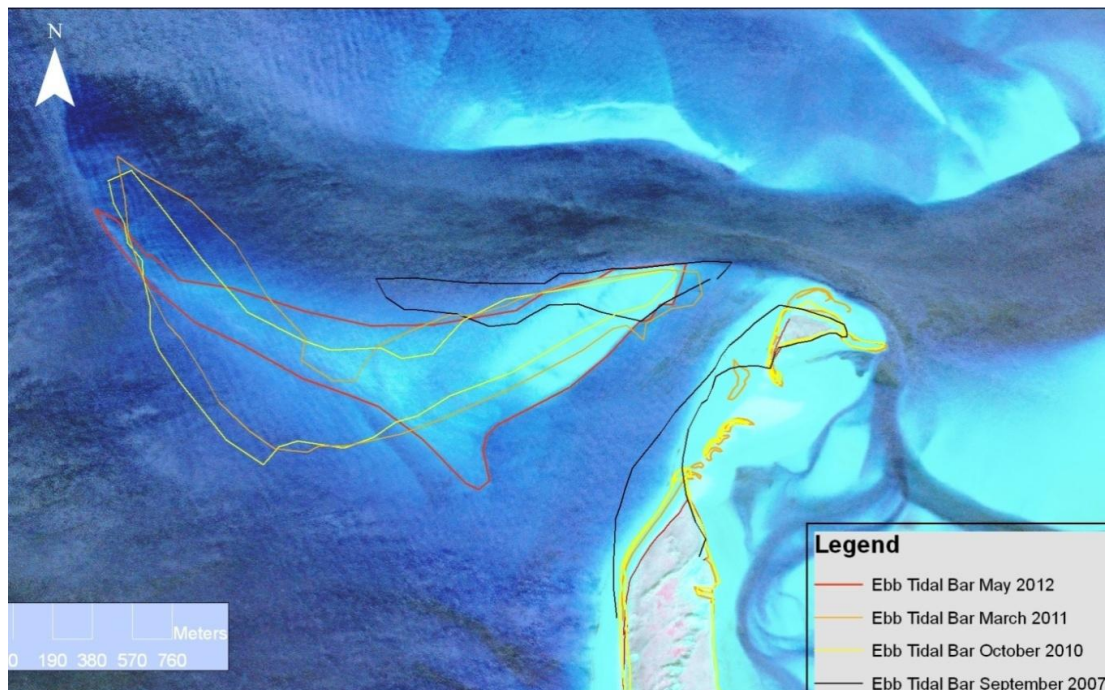


Figure 3.14 Ebb tidal bar evolution

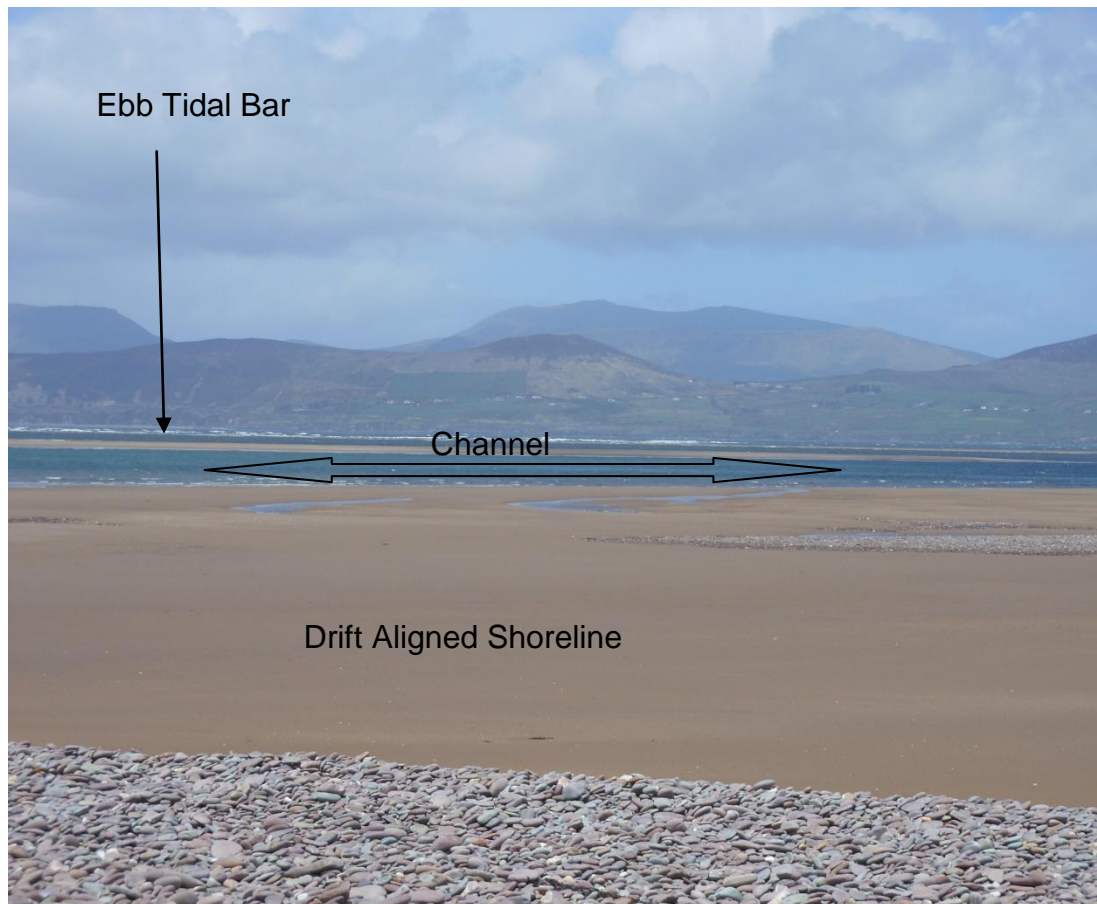


Figure 3.15 Channel between ebb tidal bar and drift aligned shore of Rossbeigh

3.6 Sediment Transport Analysis

An analysis of sediment transport formulae using storm data and shoreline change on Inch beach was undertaken as part of the FP7 Conscience project (ConScience, 2010). The cross-shore transport related dune recession rates on Inch were calculated using three methods, (Kriebel & Dean, 1985), (Hallermeier & Rhodes) and (van Rijn, 2009) described in Section 2.2.2.

Measured dune recession on Inch was then compared with three methods. The van Rijn formula showed good agreement between calculated and measured dune recession rates for the dataset period of 2007 and 2008. Similar analysis was carried out on the swash, drift and island sections of Rossbeigh using the van Rijn formula.

The island section was divided into two to accommodate the variation of dune height. Storm events were identified from wave data from 2009 to 2011 and recession rates were calculated. The calculated recession rates were then compared with recession rates measured from the surveyed DVL's. The results are tabulated in Table 3.1.

The results show that the van Rijn formula gave relatively good agreement with the dune recession measured in the swash aligned zone. It should be noted that a DVL survey for June'10 swash aligned was not undertaken. Despite this gap in the data the difference of calculated range and measured range was less than 1 m for the available dataset. The drift aligned median zone and island sections, however, show that the formula under predicted the recession rates.

The calculated rates, while inaccurate in magnitude, reflects the general trends in the recession rates measured for the most of the dataset. An unusual change in the measured recession during the last two periods of observation (February 2011-June 2011 & June 2011 to October 2011) was evident. The recession in the island lower section slows down while the

island high recession rate increased. This runs contrary to the calculated trend of higher recession rates in the lower section. The change can be explained by an observed gravel bank forming a protective barrier in front of the lower island section for this period of time.

The agreement of the van Rijn formula and measured recession rates on the swash aligned and previously on Inch indicates its suitability for stable barrier beaches. However, the formula when applied to a drift aligned beach under large tidal currents tended to under predict recession rates. The unsatisfactory results obtained from the van Rijn cross-shore formula to the drift aligned sections (Dunes and Island) indicate that the main mode of sediment transport was not cross-shore.

The annual alongshore transport rates were also calculated. Using three different methods, (Kamphuis, 1991), (Coastal Engineering Research, United, 1984) and (van Rijn, 1998) the alongshore transport was calculated for the swash, drift median and the island section of Rossbeigh for two years from 2009 – 2010 and 2010 - 2011. The calculated rates were then converted into effective dune recession rates using beach length and average dune height. This was compared with measured dune recession rates for validation. The results are shown in Table 3.2. The sign convention for the transport is negative northwards positive for southward transport.

Both Kamphuis and van Rijn methods showed some agreement with the recorded data, while the CERC formula over predicts transport for most locations. It is difficult to establish the most applicable formula to the swash aligned as the results are all within the range of recession. The significant result concerning the swash aligned zone was the direction of net alongshore sediment transport. For both years the sediment is transported away from the drift median section to the south. It should be noted though that the total sediment loads transported were relatively insignificant compared to the amount of sand moving annually in the drift and Island sections. The van Rijn formula was the best fit for the drift median section with Kamphuis under predicting according to recession rates.

There was a choice of best fit formulae for the island section as both van Rijn and Kamphius are in the same order of the measured recession range. Kamphius slightly under predicts the island high section, but the van Rijn over predicts the island low recession. It should be noted that these comparisons were based on dune recession rates and do not account for total sediment load but act only as a guide. It is more likely that the van Rijn was a better fit as it was the only formula to factor tidal current effects. This was apparent when looking at the total sediment transport results for the drift and island section.

Both CERC and Kamphius calculated total transport does not change and were based on the shore normal angle of the incident wave. The van Rijn formula takes into account the varying magnitude of tidal currents at each location. The most important metrics to be considered were the direction of total sediment load and its magnitude. These were the key factors when comparing sediment transport on the drift and swash aligned zones. Depending on the formula the difference in alongshore transport in the drift and island section is 1- 3 times the order of that calculated in the swash aligned zone. This highlights the significance of the reshaping of the shoreline from swash to drift and the encroachment of the latter into the former.

It was clear from the analysis of both alongshore and cross-shore transport that the sediment transport regimes differ greatly on swash and drift aligned zones. The good agreement of swash aligned measurements with the van Rijn cross-shore transport formula indicates that the main mode of sediment transport is cross-shore in the swash zone. This was further evidenced by the relatively low total sediment load transported by alongshore processes when compared to the other sections. The drift aligned sections were well described by the alongshore transport formulae. The total sediment loads were large but close to the range of calculated recession. The formulae show net sediment transport was in a northerly direction towards the tidal inlet.

Table 3.1. Cross-shore Dune Recession Analysis (Van Rijn)

Period	Location	Calculated Dune Recession (m)	Measured Dune Recession(m)
July '09-Feb'10	Swash	2.2-3.3	0-4
July '09-Feb'10	Drift	12.5-18.77	37-70
July '09-Feb'10	Island Low	16.1-24.2	26-30
July '09-Feb'10	Island High	2.5-3.9	0-22
Feb'10-June10	Swash	0.65-1.0	N/A
Feb'10-June10	Drift	3.6-5.5	0-11
Feb'10-June10	Island Low	4.7 -7.1	10-22
Feb'10-June10	Island High	0.7-1.1	0-7
June '10 –Nov'10	Swash	1 -1.5	N/A
June '10 –Nov'10	Drift	5.8-8.7	19-35
June '10 –Nov'10	Island Low	7.5-11.3	21-22
June '10 –Nov'10	Island High	1.2-1.8	10-21
Nov'10-Feb'11	Swash	0.9 -1.44	0-0.5
Nov'10-Feb'11	Drift	5.6-8.4	26-29
Nov'10-Feb'11	Island Low	7.3-11	12-16
Nov'10-Feb'11	Island High	1.1 -1.66	7-8
Feb'11- June'11	Swash	0.7-1.1	0
Feb'11- June'11	Drift	4.25-6.30	0-8
Feb'11- June'11	Island Low	5.4-8.14	0
Feb'11- June'11	Island High	0.8-1.29	0-7
June'11-Oct'11	Swash	0.5 - 1.06	0-0.5

Period	Location	Calculated Dune Recession (m)	Measured Dune Recession(m)
June'11-Oct'11	Drift	3.9-5.9	10-33
June'11-Oct'11	Island Low	5-7.6	0.5-7.5
June'11-Oct'11	Island High	0.8-1.2	10-16

Table 3.2. Annual Alongshore Transport

Year	Location	Total Sediment Transport Load			Effective recession rates from alongshore transport (Load/length*avg dune height)			Measured Dune Recession Approx(m)
		van Rijn (m ³)	CERC (m ³)	Kamphius(m ³)	van Rijn (m)	CERC (m)	Kamphius (m)	
'09-'10	Swash	816	26,835	2,674	0.02	0.66	0.07	0-4
'10-'11	Swash	7,125	66,141	6,310	0.2	1.6	0.2	0-1
'09-'10	Drift	-145,250	-1,227,941	-44,590	73	614	18	45-80
'10-'11	Drift	-206,969	-1,559,507	-58,158	82	623	23	30-70
'09-'10	Island High	-172,984	-1,227,941	-44,590	31	223	8	10-44
	Island Low				138	982	36	36-100
'10-'11	Island High	-246,028	-1,559,507	-58,1578	44	283	10.5	17-36
	Island Low				196	1247	46	20-50

3.7 Conclusions

The results of the shoreline analysis, topographic surveys and sediment transport calculations in this chapter influenced the scope and direction of the quantitative aspect of this research. The aims of Chapters 4 and 6 were identified within this chapter. The scale, location and type of hydrodynamic, sedimentological and bathymetric field work were influenced by the conclusions reached as outlined below;

- The morphological cycles of both Inch and Rossbeigh have been established using shoreline analysis.
- Inch beach has been identified as potentially having a stable 30 year cross-shore cycle while Rossbeigh was found to be more dynamic and flexible with breaching occurring in the past.
- The morphological climate on Rossbeigh has been erosive since at least the year 2000. The breaching was a result of systematic erosion rather than single storm event driven, although such storms were contributory and accelerated the breaching process.
- There was evidence of two morphological climates on Rossbeigh distinguished by shoreline orientation. This was supported by the existence of two separate sediment transport regimes on the beach. A cross-shore dominated regime in the swash aligned zone was identified by the agreement of recorded dune erosion and transport formulae, while an alongshore dominated sediment transport regime is evident on the drift aligned zone of Rossbeigh.
- The evolution of the ebb tidal bar and tidal inlet were linked to the erosion processes ongoing in the drift aligned zone of Rossbeigh. As the bar grows landward the shore line recedes and the tidal channel begins to develop a meander.

These conclusions were predominantly trend based and qualitative. To quantify such morphological trends, field data and numerical modelling were required. The collection of this physical data is discussed the Chapter 4, while the numerical modelling undertaken for this research project is detailed in Chapter 6.

4 Wind, Wave and Hydrodynamic Monitoring

4.1 Introduction

This Chapter presents the results of the field data collected in Dingle Bay as part of this research. The aim of this Chapter was to examine the validity of the conclusions reached in Chapter 3 utilising collected field data and enhance the understanding of the morphodynamics of Inner Dingle Bay.

The various monitoring strategies conducted in Inner Dingle Bay were documented within this chapter. The monitoring includes;

- bathymetric surveying
- wave data collection
- tidal current recording
- wind data measurement
- aeolian transport measurement
- sediment sampling
- sediment dye study

Significant results were observed with the wave and tidal current monitoring, while some aeolian provided useful data. This work provides quantitative values on the qualitative trends observed in Chapter 3. The GSTA undertaken as part of the field work has yielded a trend case that has not been identified in case studies previously. It is potentially the first documented and validated trend case of its type.

A conceptual model was developed based on the field data describing the morphology of the beach. A knowledge gap in the hydrodynamic field data monitoring was identified and forms the hypothesis for the Ocean radar trial detailed in Chapter 5.

4.2 Field Data Collection

A data collection campaign was undertaken in the summer of 2011. The focus of the campaign was on gathering wave and tidal data, collection methodologies for sediment transport and aeolian transport are also documented. The main aim was to gather data that quantitatively describes the processes influencing morphology of Rossbeigh Beach and specifically the breached area. The wave conditions during the recording period predominantly represent low energy sea states. Even so, the data collected provide insights into the patterns of both tidal and wave forcing. As the erosion patterns were occurring irrespective of storms and breaching occurred after a relatively low energy storm, the offshore conditions were not as critical as other morphology studies where evolution is primarily storm driven.

4.2.1 Wave Data

The wave data collection consisted of utilising two Valeport bottom mounted pressure sensors, described in Section 2.4.1. The gauges sampled pressure over a period of time or 'burst'. The recording interval details are shown in figure 4.1. A summary of the wave activity during these bursts was then calculated.

The screenshot displays the 'Setup Screen' for a Valeport Wave Gauge. The interface is divided into several sections:

- Sampling Setup:** Rate, Hz (2); Tide Burst Duration, seconds (20); Interval, minutes (44); Wave Burst Duration, samples (4096); Interval, minutes (44); Wave Sampling Mode (ON); Trigger Level (0).
- Save and Output Settings:** SAVE: Tide Burst Summary (checked), Raw Wave Burst Data (checked), Non-Dir. Wave Summary (checked), Dir. Wave Summary (unchecked), Wave Freq. Spectrum (unchecked), Wave Dir. Spectrum (unchecked), Freq. / Dir. Summary (unchecked), Cross and Auto Spectra (unchecked). OUTPUT: Tide Burst Summary (unchecked), Raw Wave Burst Data (unchecked), Non-Dir. Wave Summary (unchecked), Dir. Wave Summary (unchecked), Wave Freq. Spectrum (unchecked), Wave Dir. Spectrum (unchecked), Freq. / Dir. Summary (unchecked), Cross and Auto Spectra (unchecked).
- Wave Burst Parameters:** Pressure (checked), Current (checked), Compass (checked), Temperature (checked), Conductivity (unchecked), Turbidity (unchecked), Windspeed (unchecked), Wind Direction (unchecked), Air Pressure (unchecked).
- Clock Settings:** Instrument Time (29/07/2011 14:42:32), Set Time button, Delay Start (NO).
- EM Sampling:** ON.
- Battery Type:** Alkaline.
- No. of Cells:** 32.
- Memory Life:** Memory will last 32 days.
- Battery Life:** Batteries will last 10 days.

An 'Apply' button with a green checkmark is visible at the bottom center of the screen.

Figure 4.1 Burst details of Valeport Wave Gauge

One instrument was placed offshore in approximately 15 m of water at a distance of 4.5 Km offshore of Rossbeigh. The wave conditions were recorded for a 30 day period. The second Valeport pressure sensor, figure 4.2, was placed in 5 locations alongshore of Rossbeigh beach at approx 1 m below mean low water line for a spring- neap cycle at each location, figure 4.3. To prevent burying of the onshore wave gauge due to scouring and sedimentation, a custom stainless steel raft was designed. This raft also enabled the quick deployment and movement of the onshore wave gauge along the intertidal zone of Rossbeigh.

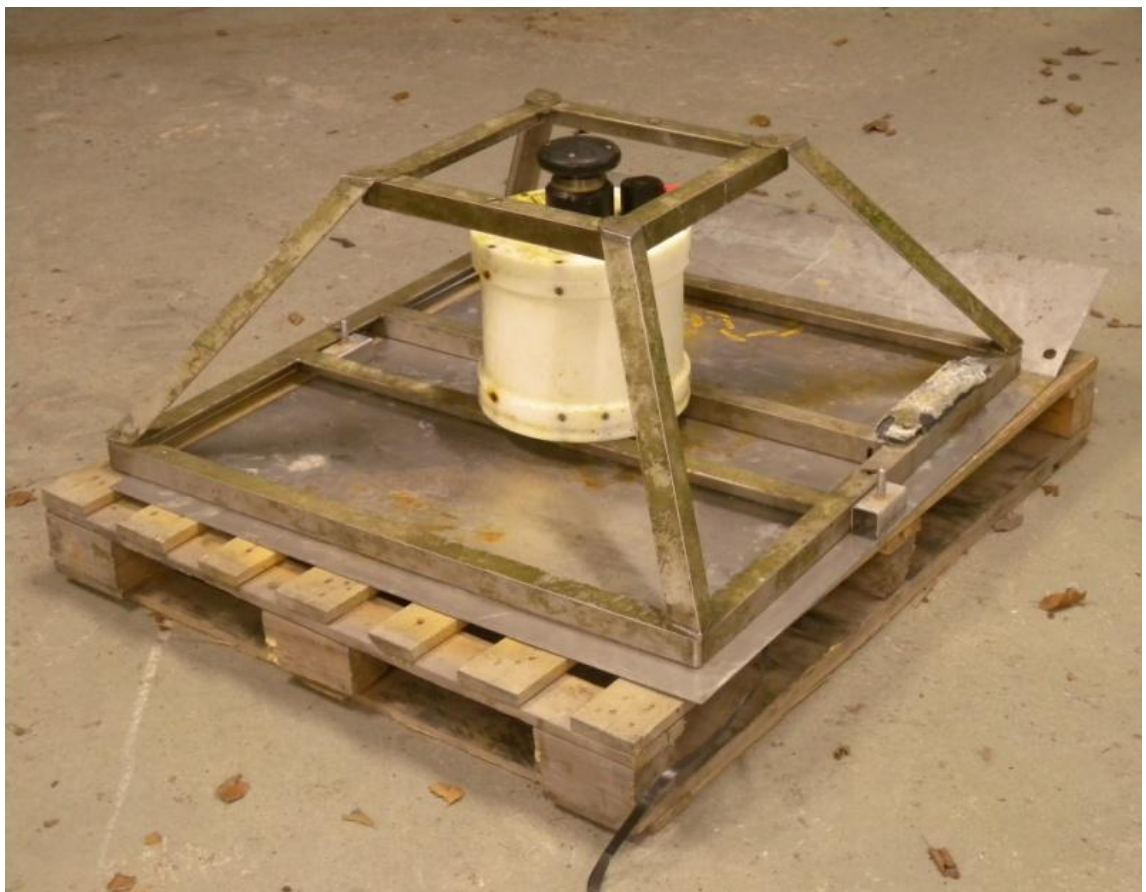


Figure 4.2 Onshore Valeport Wave Gauge on custom steel raft

The recording locations are shown in figure 4.3. The locations were chosen to capture the variation, if any, in the hydrodynamics of the two morphological zones on Rossbeigh beach, swash aligned and drift aligned. A location in front of the island was also considered for deployment. However, this was abandoned due to the risk of losing the instrument in the strong tidal currents surrounding the island section of Rossbeigh.

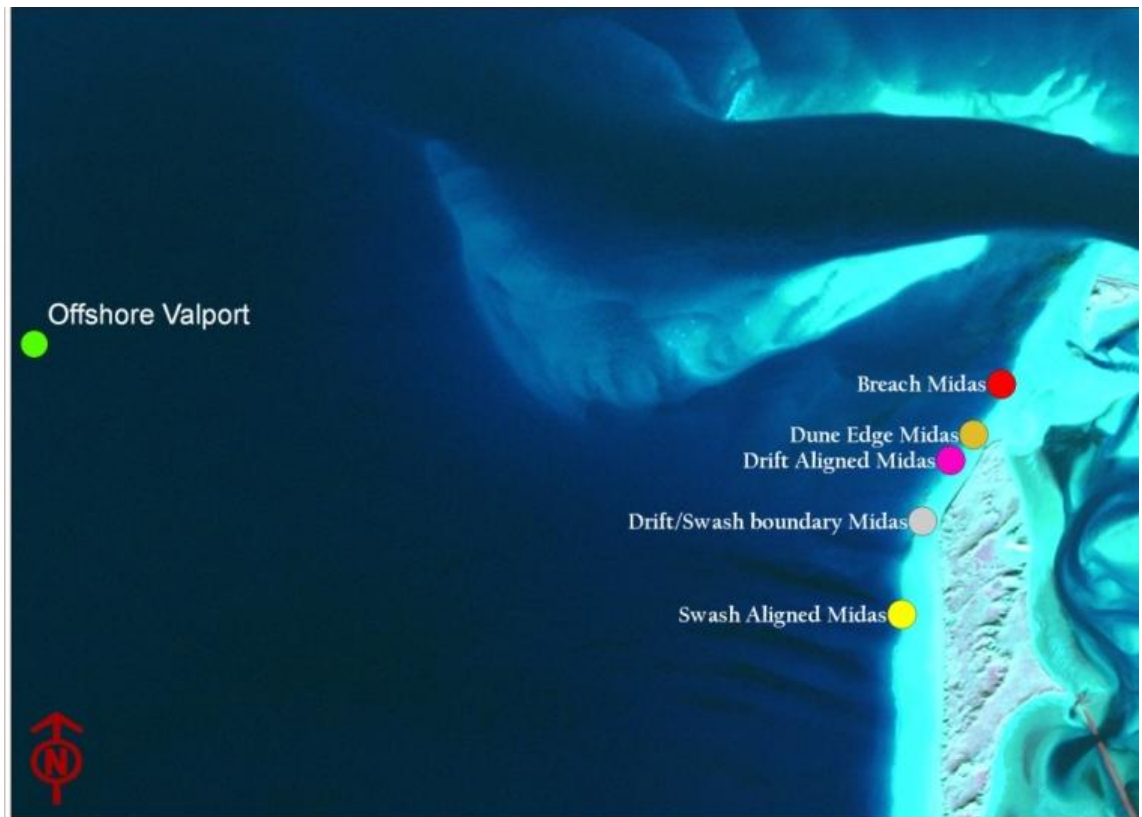


Figure 4.3 Wave Gauge Locations

The summary statistics of the offshore Valeport gauge were binned in a scatter diagram, figure 4.4. It was evident from this that the wave climate is mild with the over 90% of wave conditions having an H_s of less than 1m. The peak period T_p was predominantly between 7 to 10 s suggesting most of the wave energy was swell dominated.

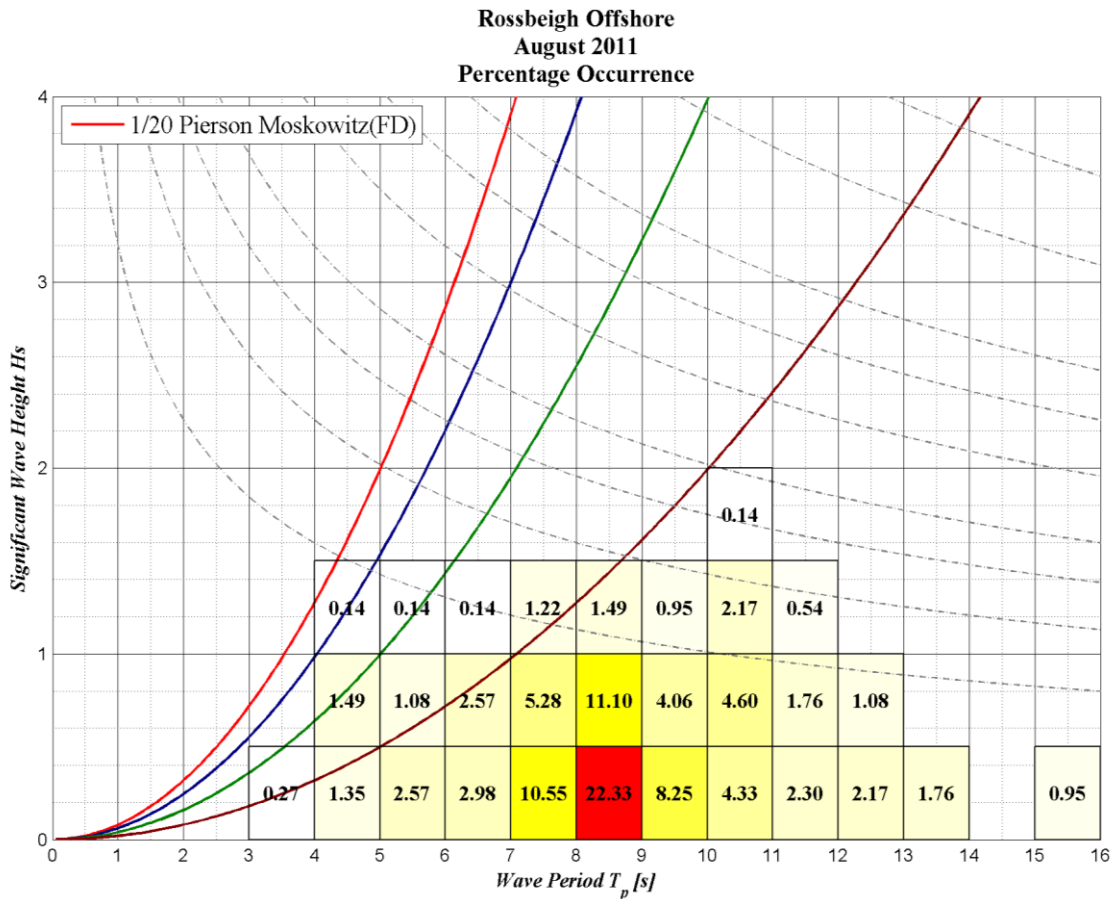


Figure 4.4 Scatter plot of Wave data recorded offshore of Rossbeigh in August 2011

Initial analysis of the onshore and offshore wave data yielded pertinent results. In all 5 locations along the beach the H_s varied with tidal height with the maximum H_s occurring at high tide. This was shown clearly in Figure 4.5 to 4.9, where the offshore wave height does not show a relationship with tidal height but the onshore recorded wave height clearly peaks with high tide. This was an important factor when considering erosion and morphology of the beach. The results confirm that erosion from wave forcing on Rossbeigh beach was at its greatest at high tide.

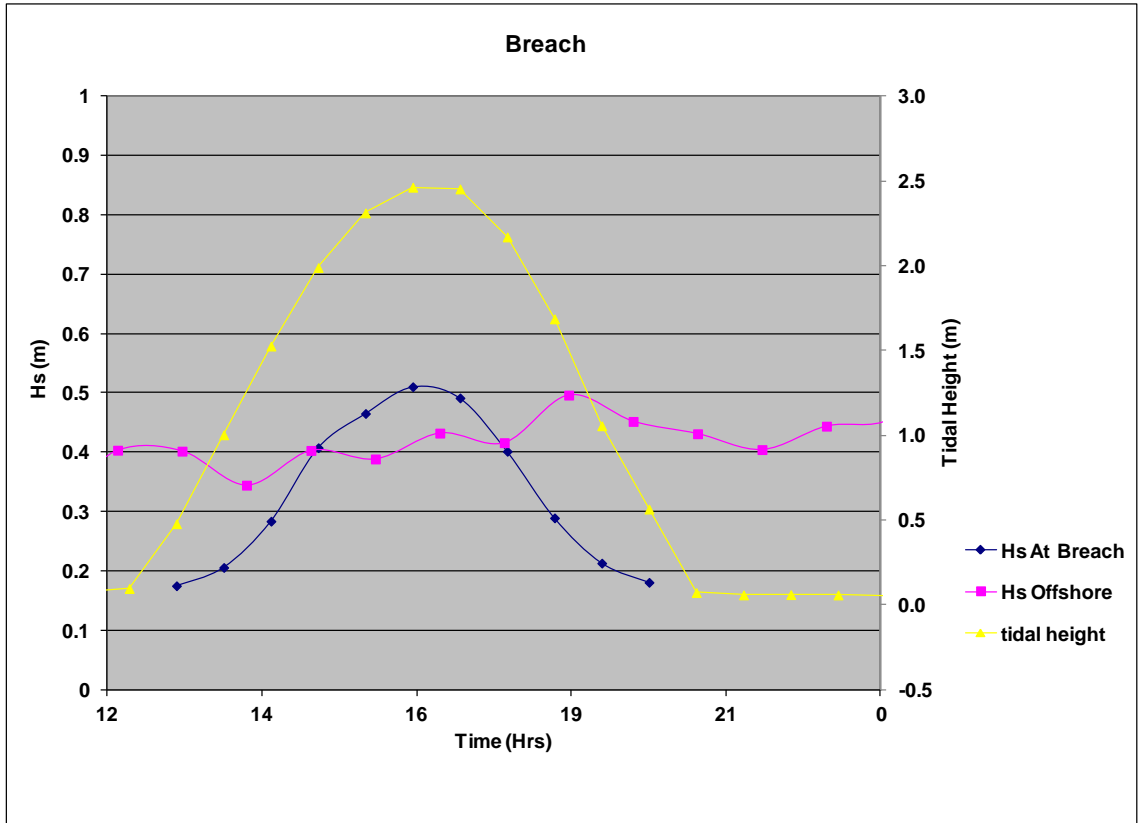


Figure 4.5 Hs plot at breach location

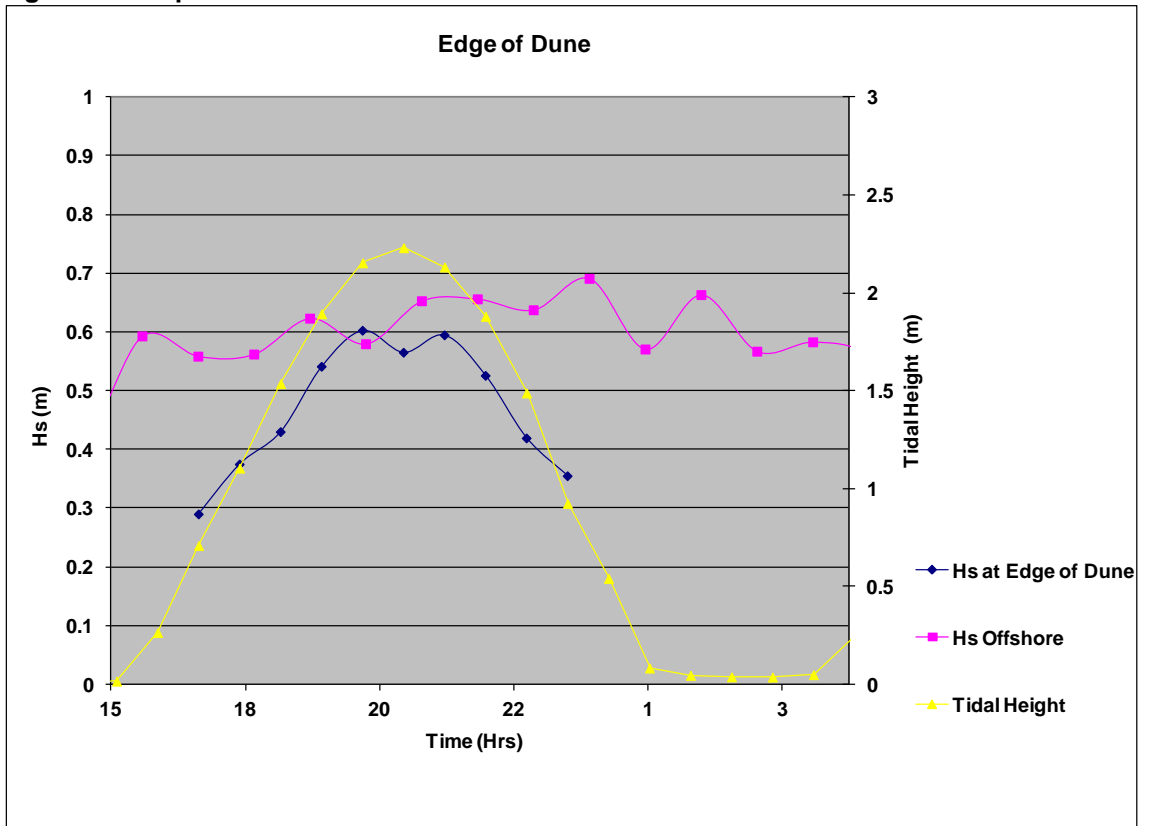


Figure 4.6 Hs plot at Edge of Dune location

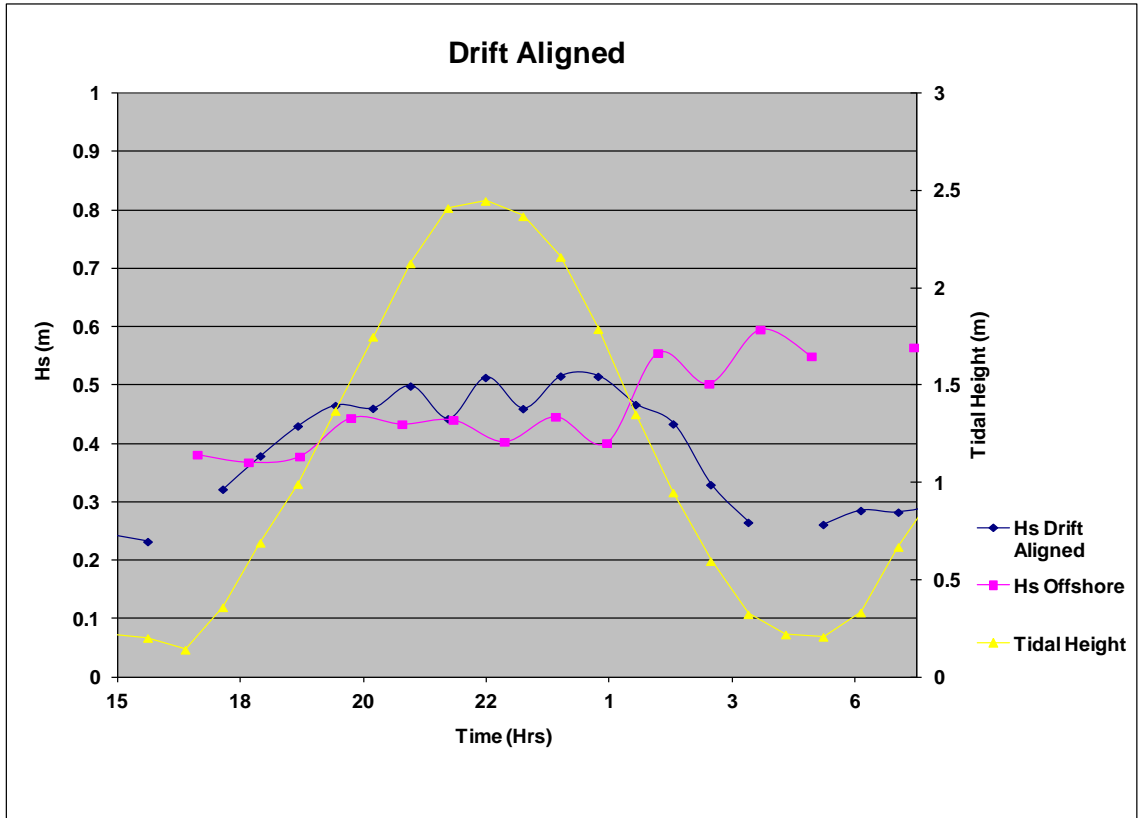


Figure 4.7 Hs plot at Drift aligned shoreline location

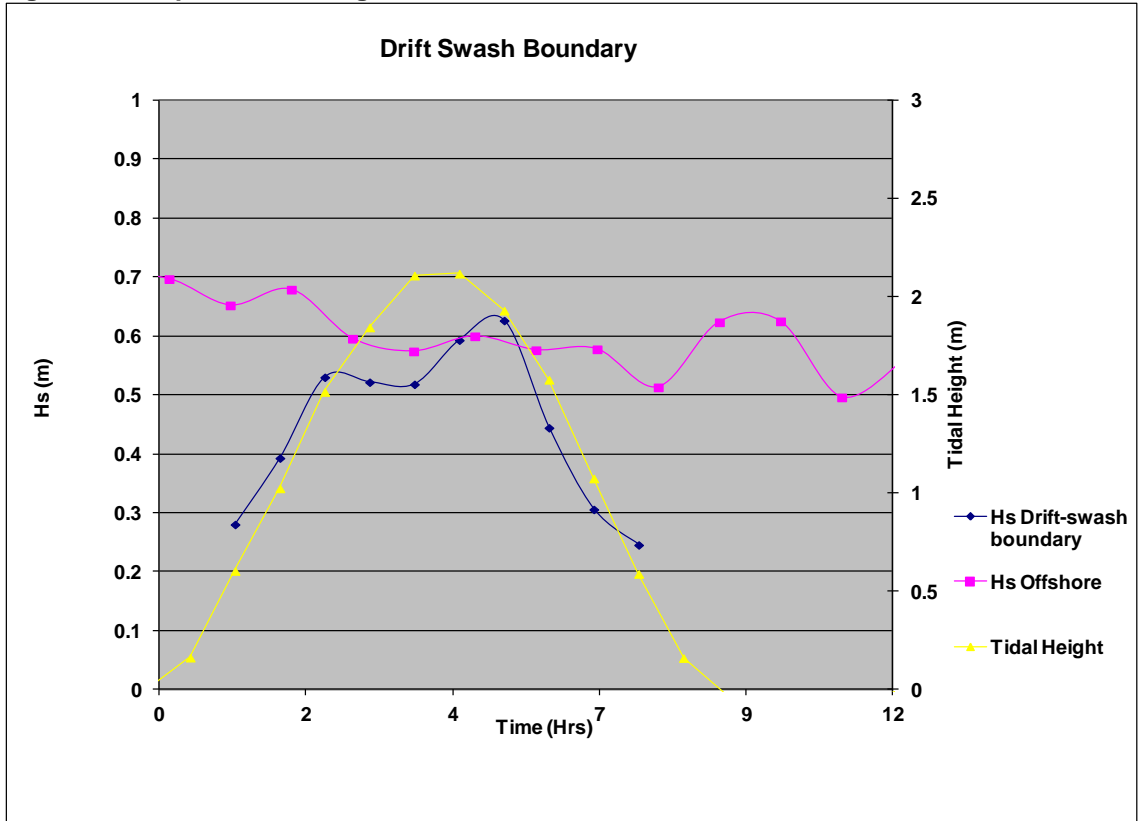


Figure 4.8 Hs plot at Drift/Swash Boundary

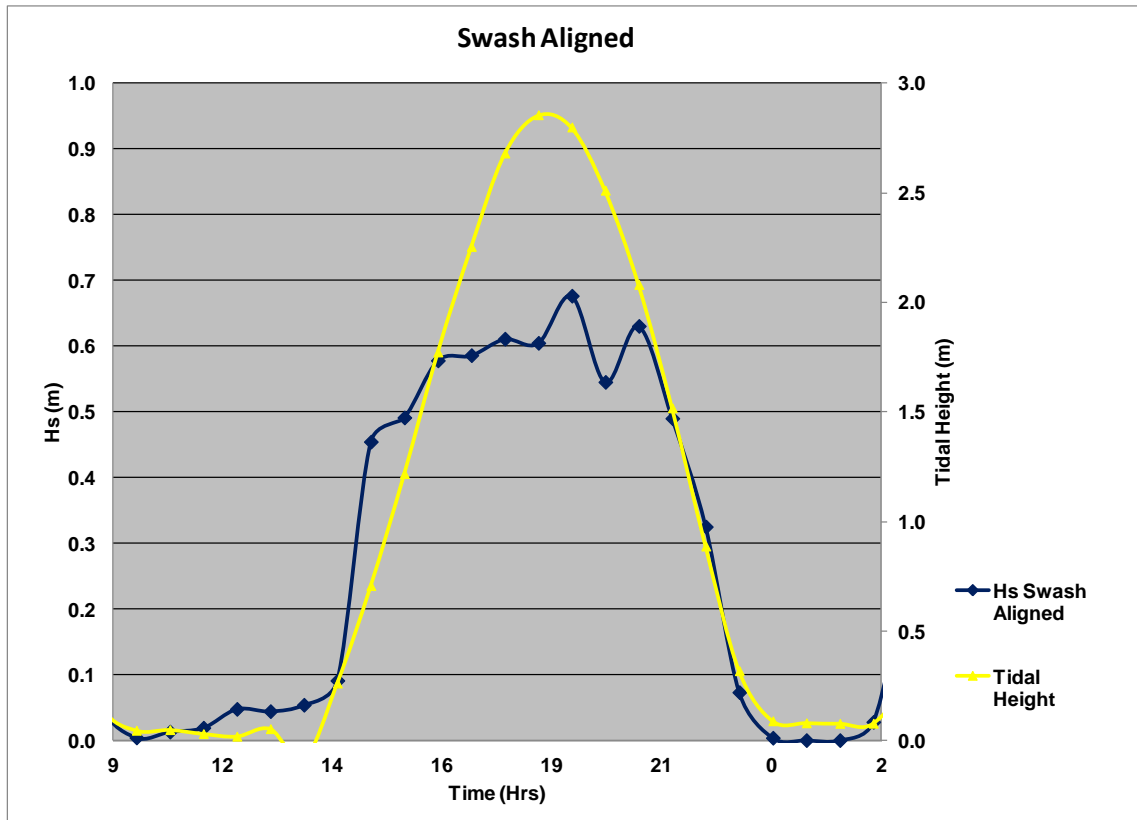
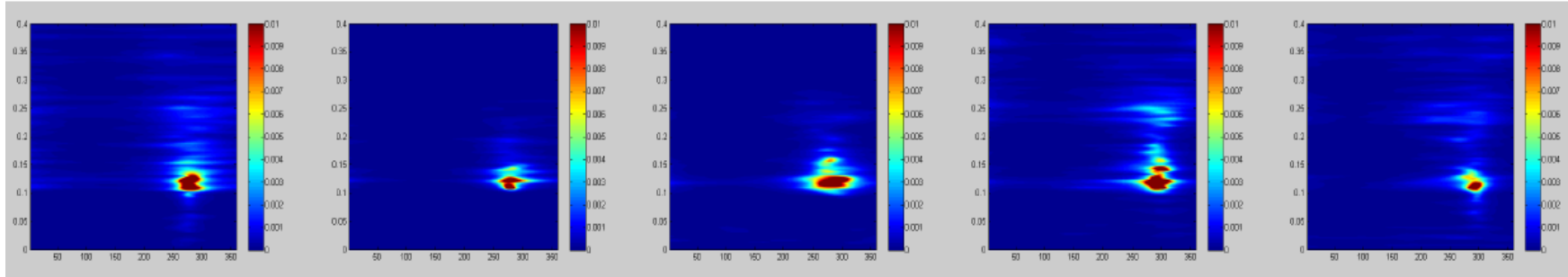


Figure 4.9 Hs plot in Swash aligned zone

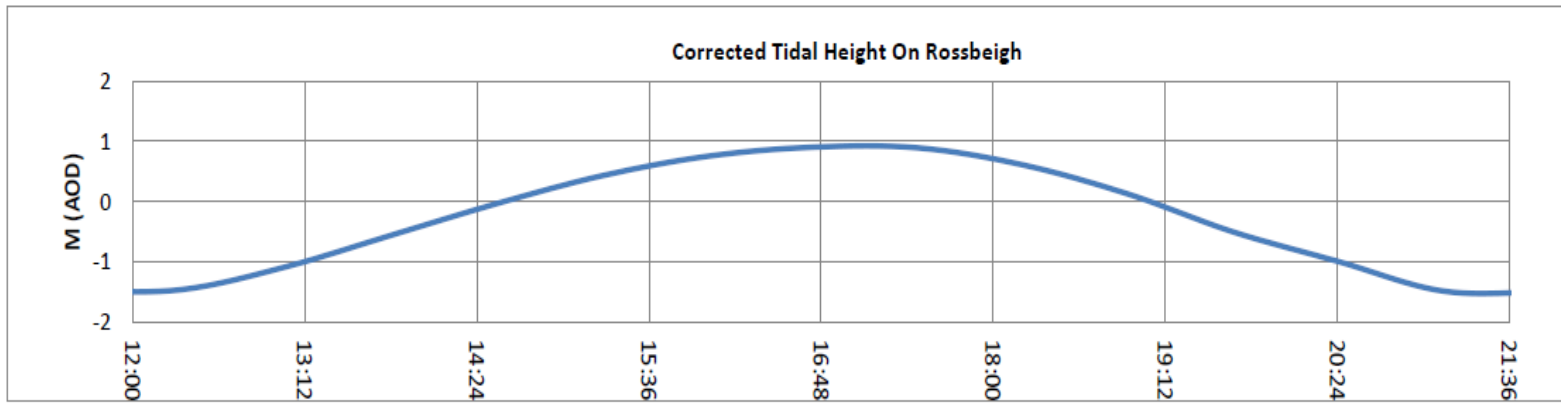
The variation in incident wave directionality along Rossbeigh over the tidal cycle was significant finding during the data collection campaign. Figure 4.10 shows spectral energy plots with frequency on the y and direction on the x axis. Both the swash and drift aligned zones are represented over a tidal cycle. The spectral energy intensity was represented in a colour scale, varying from blue(low) to red(high). The plots were derived at specific times of the tidal cycle; at low, mid flood, high, mid ebb, low.

The figure shows that the drift aligned shore was subject to two distinct wave forcings acting at different times of the tidal cycle. During the lower part of the tidal cycle, below 0.0 m OD Malin, the incident wave energy had a peak direction of approximately 250°. As the tide rises above 0.0 m OD Malin, a second wave forcing appeared from approx 315° and began to dominate from 0.5 m OD Malin until high tide. At high tide, the drift aligned zone was dominated by the north westerly wave front. When the tide receded the North westerly wave forcing reduces in energy and eventually disappeared at approximately 0.0 m OD Malin with the 250° wave front remained.

Swash Aligned



Corrected Tidal Height On Rossbeigh



Drift Aligned

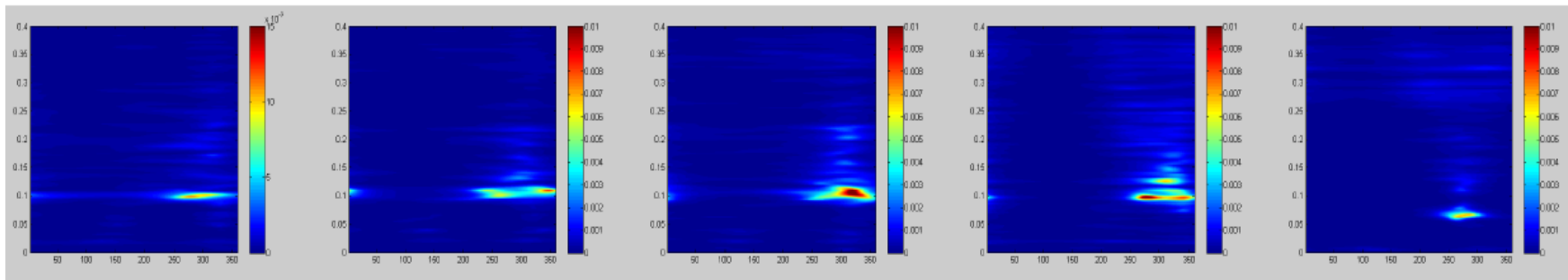


Figure 4.10 Wave Direction variations over tidal cycle on Swash and Drift Aligned Zones

The swash aligned incident wave direction was narrow banded centred at 270° throughout the tidal cycle and corresponds to the offshore wave direction. There was no evidence of other wave directions acting on this location. These variations in wave direction on the drift aligned shore can be explained by the size, shape and position of the ebb tidal bar.

At low tide, the ebb tidal bar caused the waves to funnel towards the breach location and slightly altered the direction, figure 4.11 A). Thus giving the incident wave direction of 250° when the wave direction is 270° offshore and 270° incident on the swash aligned section of Rossbeigh.

As the tide rose to over 0.0m OD Malin, the ebb tidal bar influence on wave direction increased. The wave front then moved over this bar but at a different speed to the waves in the deeper water each side; this caused the wave to refract, thus providing the new wave forcing from 315°, yellow arrows, figure 4.11 B).

The change of wave direction at high tide in the drift aligned zone explains the changing orientation of the shoreline in this zone. The dunes in the drift aligned zone were shaped by the wave action at high tide, which was now incident from a north westerly direction.

It remains unclear what the wave direction at high tide in this zone was prior to the breaching event. However, it is likely that much less, if any of this area of shoreline was subject to a wave forcing at high tide from an angle much greater than 270°, given the orientation of the dune line pre-breaching. Considering this, it is apparent that the influence of ebb tidal bar, which emerged post breaching, on wave direction at high tide is driving the increase in erosion in the drift aligned zone.

Wave Direction at Lower Tide Height

Wave Direction at High Tide

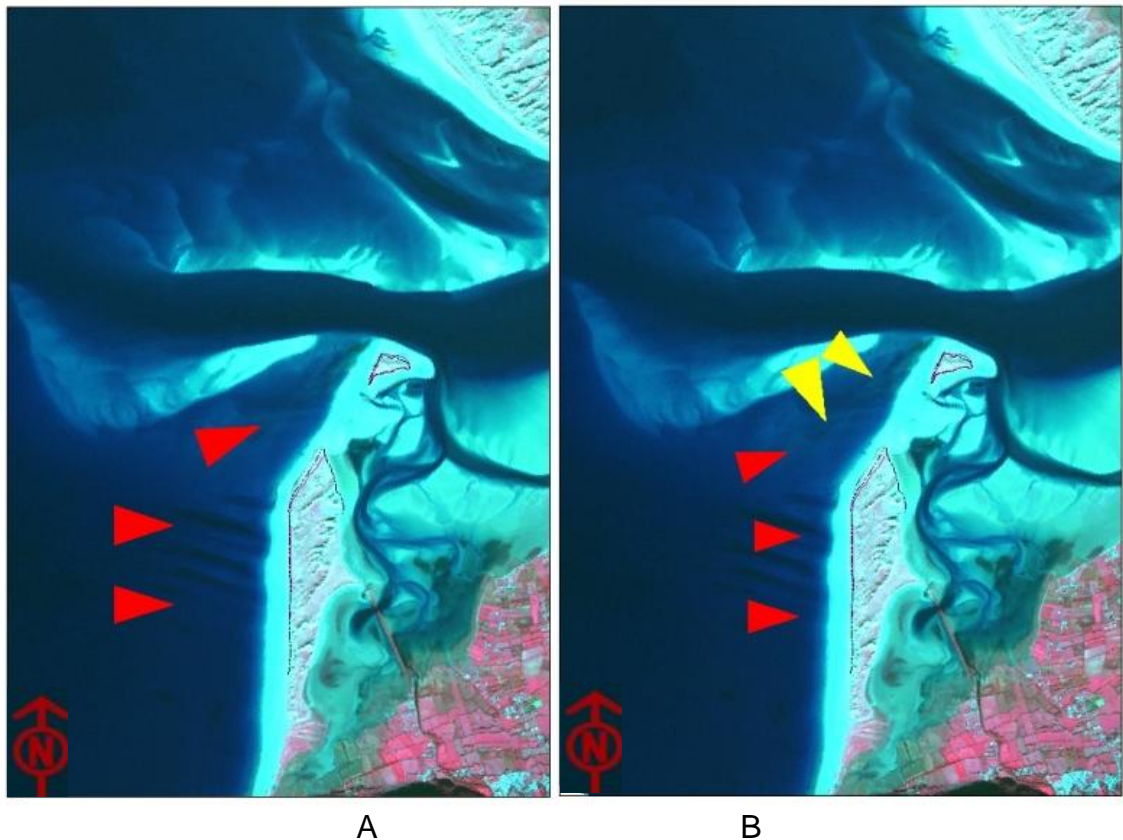


Figure 4.11 Wave direction at A) lower and B) higher tides incident on Rossbeigh

Wave Gauge Monitoring for HF Ocean radar Validation

As part of the HF Ocean Radar trial, Chapter 5, wave gauge monitoring was undertaken to validate the work. The results of this monitoring are presented below. It should be noted that no morphodynamic analysis was undertaken with this data set. It was examined for validation purposes only.

A wave gauge was deployed in Dingle Bay for a 4 week period during the wave radar trial. The gauge was located in at co ordinates 52° 03' 50" N, 10° 01' 40" W, figure 4.12. This location was selected to ensure there was overlap of the beams from both north and south transmitting stations of the radar stations, Section 5.2.

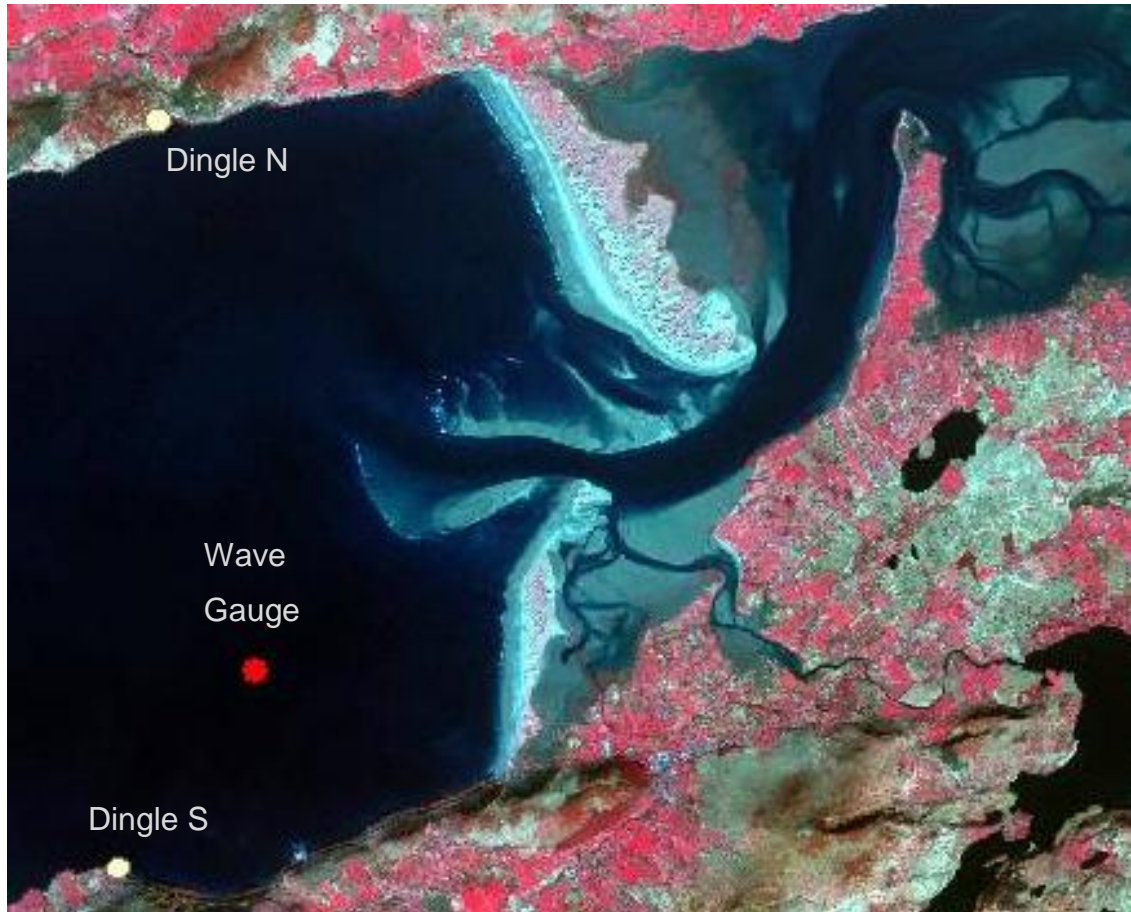


Figure 4.12 Wave gauge location during wave radar trial

The significant wave height in Dingle Bay, figure 4.13, shows that there was a varied range of conditions during the wave radar trial. There were several storm events with wave heights of over 1.5 m. A large event on the 21st of November had a maximum H_s of 2.6m. There were also periods of calm weather when the H_s was below 0.5 m and a minimum H_s of 0.2 m on the 30th October, the 6th of November and on the 16th of November. The wave direction recorded at this location, figure 4.14, ranged from between 225° and 320°. The mean wave direction was 268°.

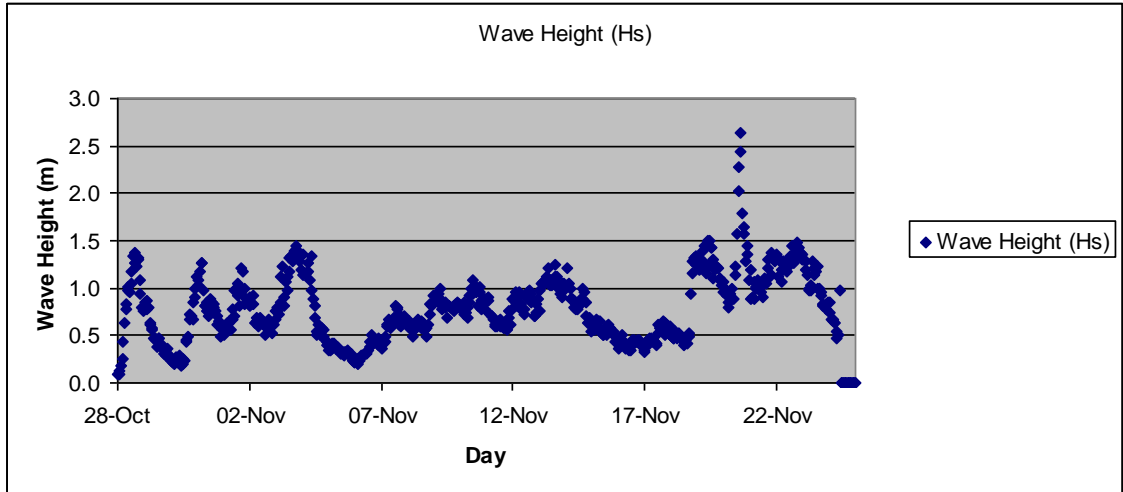


Figure 4.13 Measured significant wave height (Valeport)

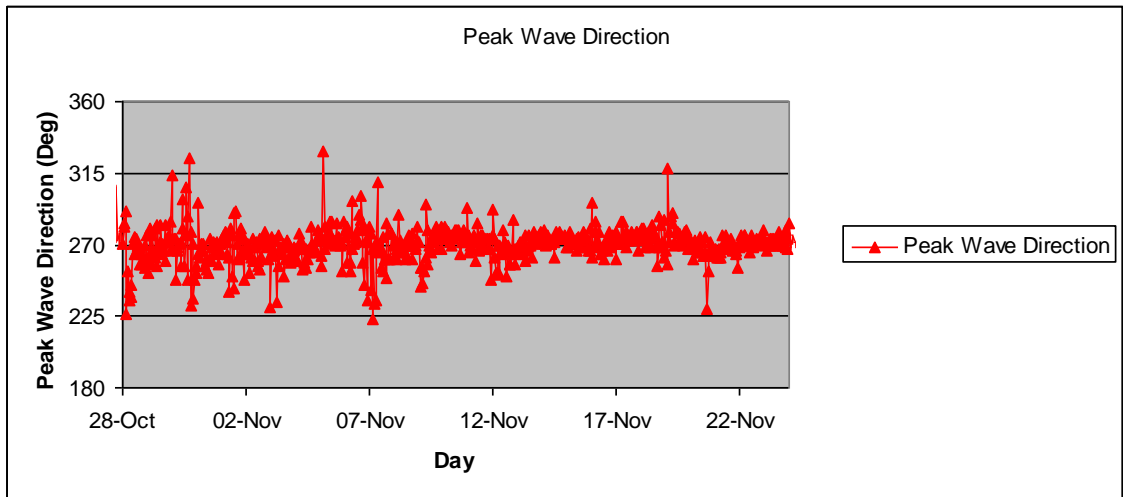


Figure 4.14 Measured peak wave direction (Valeport)

As noted in Section 2.4.1, the Valeport wave gauge records current speed, figure 4.15, and current direction, figure 4.16, 100 mm above its pressure sensor. This gave tidal current measurements approximately 1 m from the sea bed. The gauge also provided a continuous vertical distance measurement from the sea bed to the water surface, providing a water level recording, figure 4.17.

The maximum current velocity recorded during the monitoring period was 0.185 m/s on the 20th of November, which corresponds to the middle of the spring neap cycle. There was also a sustained period where max currents are above 0.1 m/s on the 16th November which corresponds to the spring ebb and flood tides. The mean current direction, figure 4.16, showed no clear directional trends this was attributed to the low magnitude of tidal current velocity recorded.

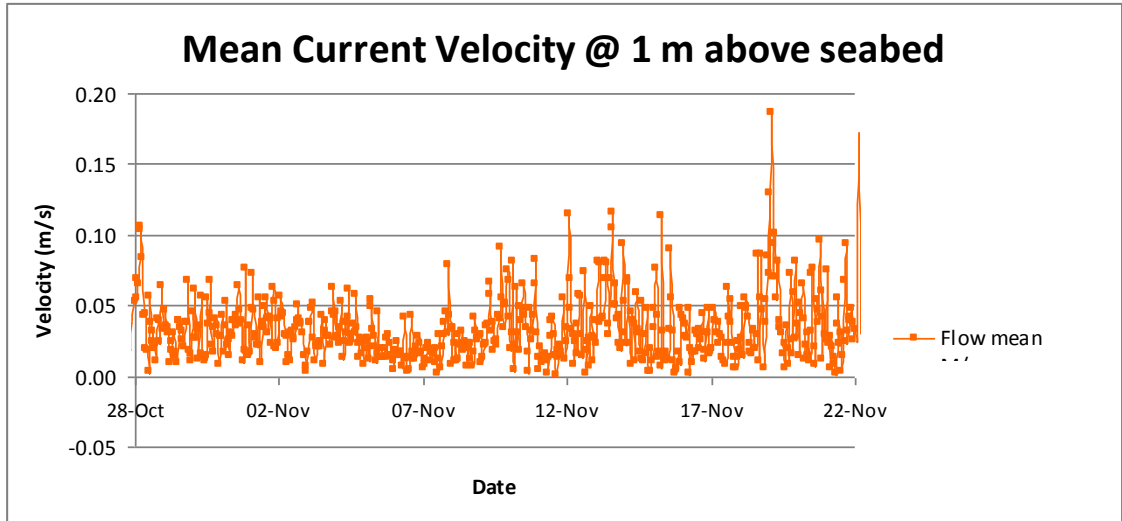


Figure 4.15 Measured mean current magnitude at instrument (Valeport)

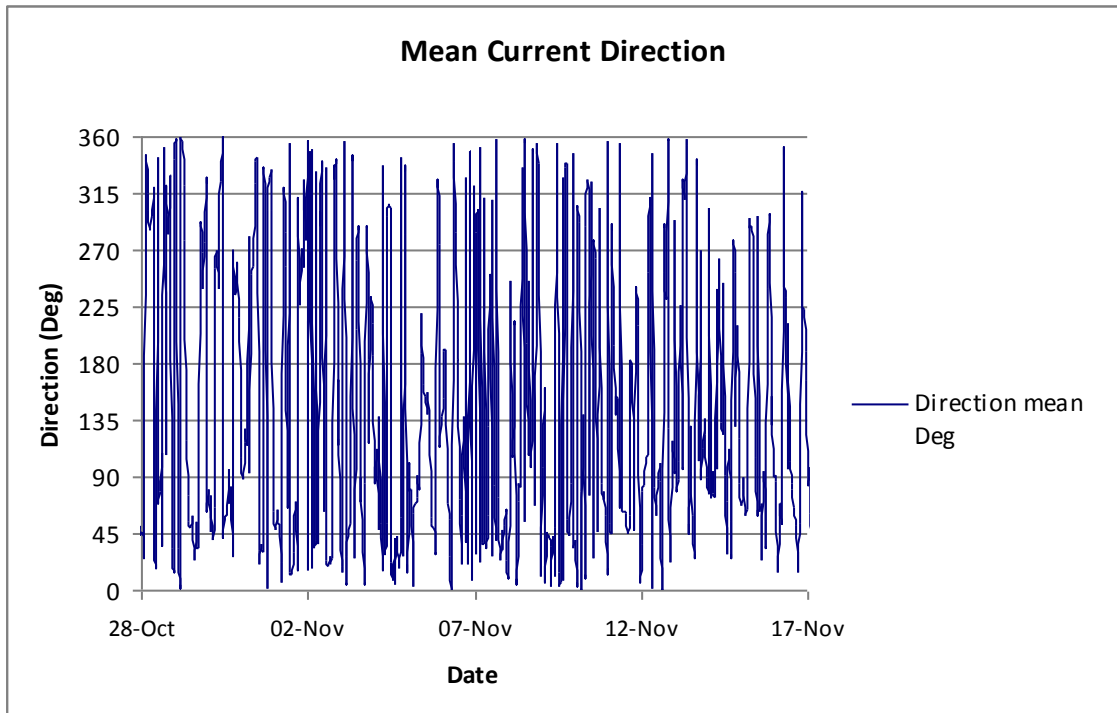


Figure 4.16 Measured mean current direction at instrument (Valeport)

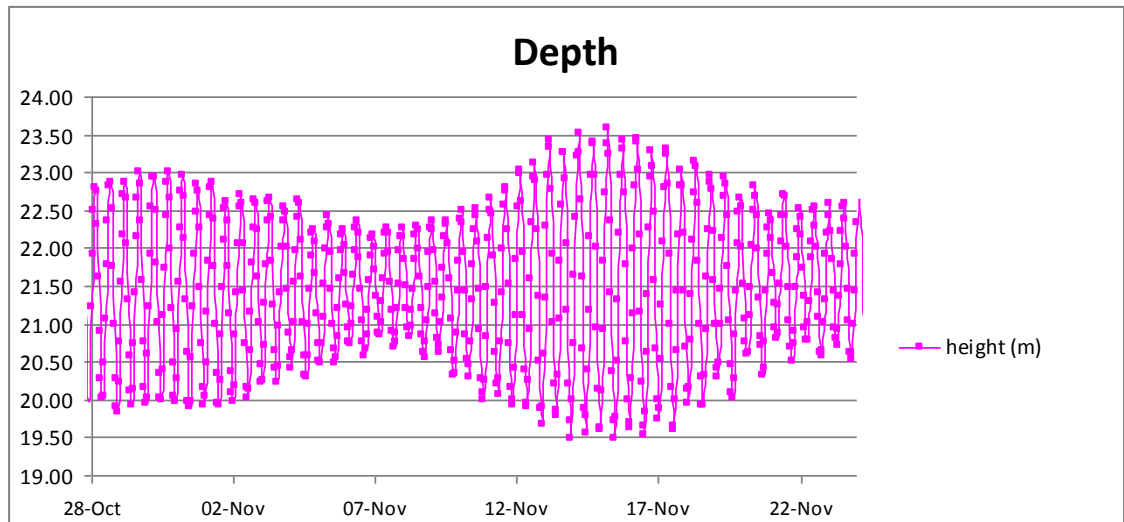


Figure 4.17 Measured depth of water at instrument (Valeport)

4.2.2 Tidal Current Data

The tidal current data collection programme included the same recording locations as the wave data collection but was also extended further north encompassing the island and breached areas of Rossbeigh, Figure 4.18. The instruments used were an Aanderra RCM8 solid state encapsulated recording current meter and a Valeport electromagnetic current meter, detailed in Section 2.4.1. Both recorded tidal velocity and direction at height of 1.0 m above seabed. It is notable that a tidal current meter was placed further northwest of the last point but the current was exceptionally strong and the device was undermined and swept away.

Tidal Current Data Collection Points

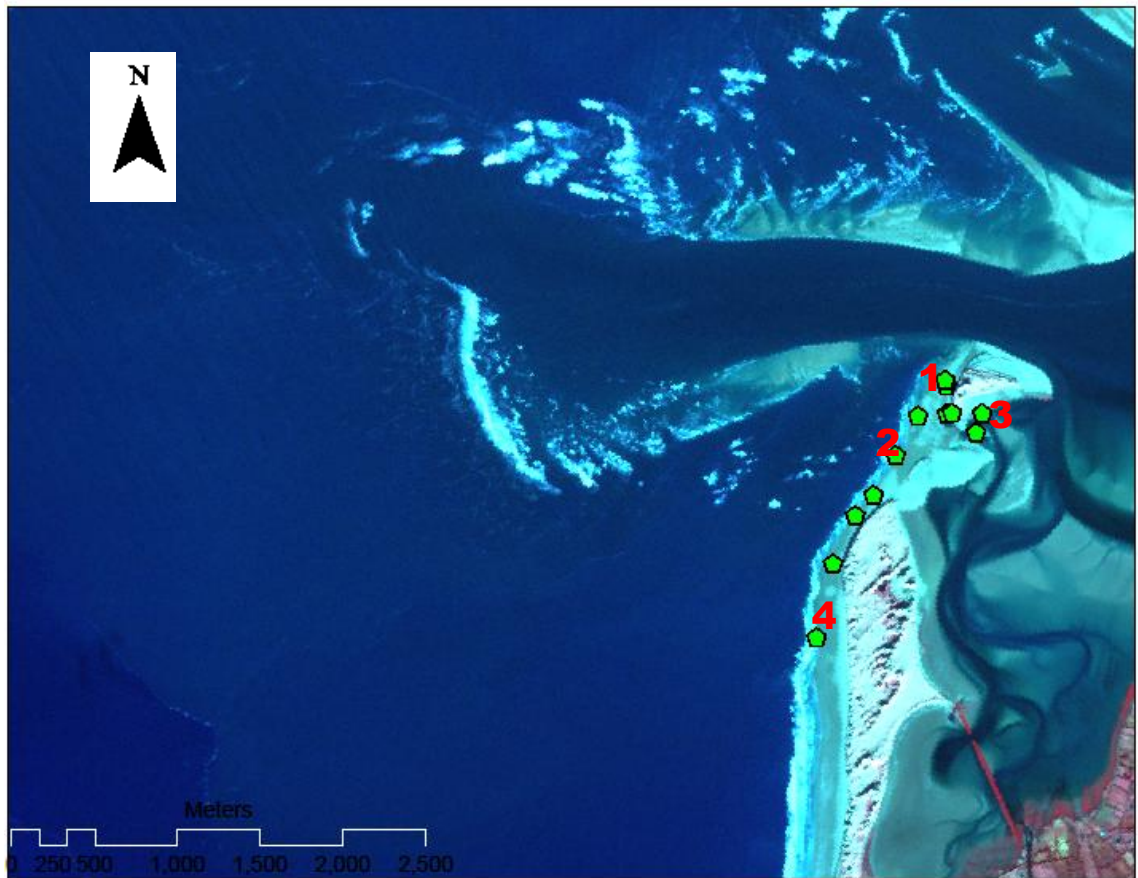


Figure 4.18 Tidal current data collection points

The measurement results revealed that the magnitude of current velocity varied greatly between drift aligned zone and swash aligned zone of Rossbeigh, at mid flood figure 4.19 A) and mid ebb figure 4.19 B). The largest magnitude current of 0.9 m/s, was recorded at mid flood, location 1, seaward of the Island, figure 4.20. The magnitude of the flow is twice that of the flow in the breach zone and channel between the ebb tidal bar and drift shore, 0.4-0.3 m/s, figures 4.21 and 4.22.

The direction of mid flood currents also varied alongshore. Shore normal currents recorded at the swash aligned zone of insignificant magnitude, figure 4.23, contrast with large shore parallel currents recorded in the drift aligned zone.

In the breached area, currents were directed at an angle to the shoreline. Significantly, north of the breach and adjacent to the island, the current turned

shore parallel. There was also some evidence of local turning to the south east and south west of the island.

The tidal current regime at mid ebb, figure 4.19 B), was less energetic than at mid flood. The largest ebb current of 0.6 m/s was recorded in the channel by the island, Location 2, figure 4.21. The ebb current seaward of the Island, Location 1, was also significant at 0.3 m/s, figure 4.20.

Directionally, the ebb currents were shore normal with the exception of ebb currents at the south west end of the island and the rear of the island. These currents were of a shore parallel or channel parallel orientation.

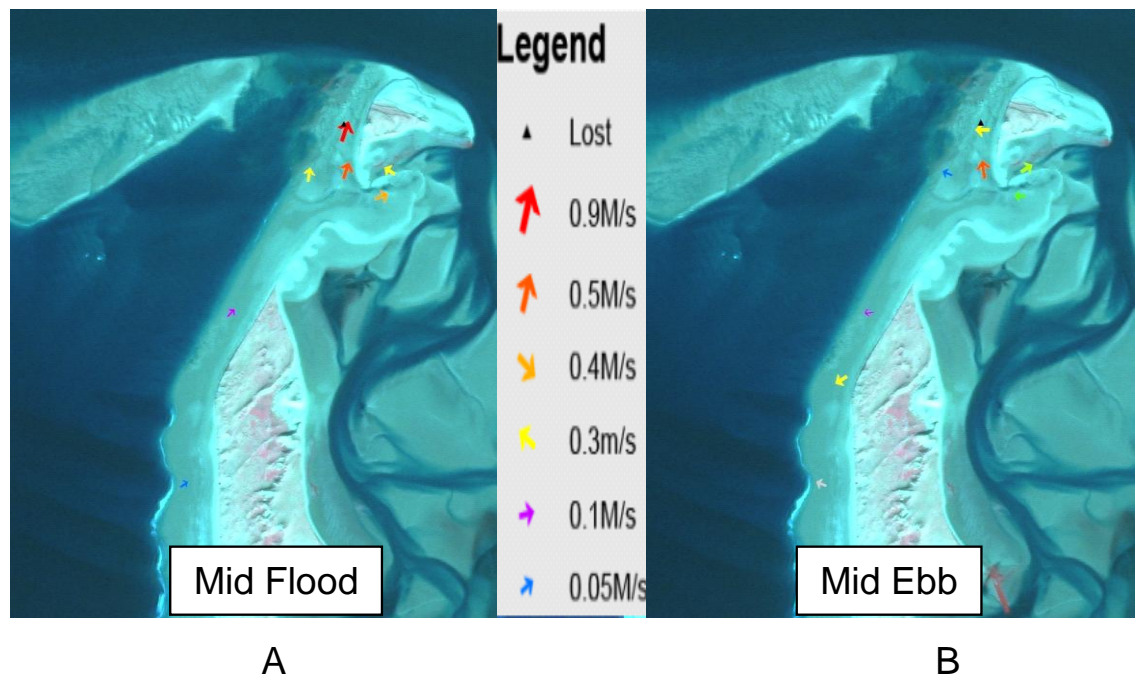


Figure 4.19 Tidal current velocity at A)mid flood and B) mid ebb

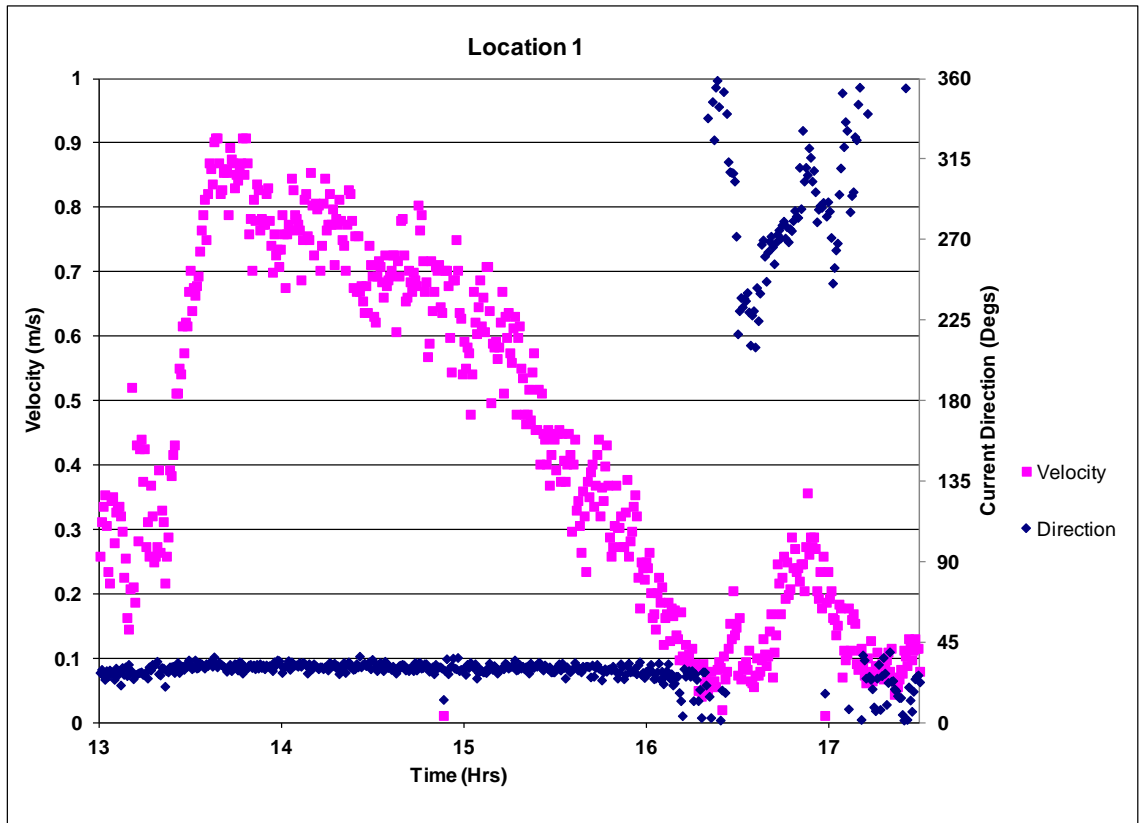


Figure 4.20 Time series of tidal current recording at Location 1 (RCM8 measurement)

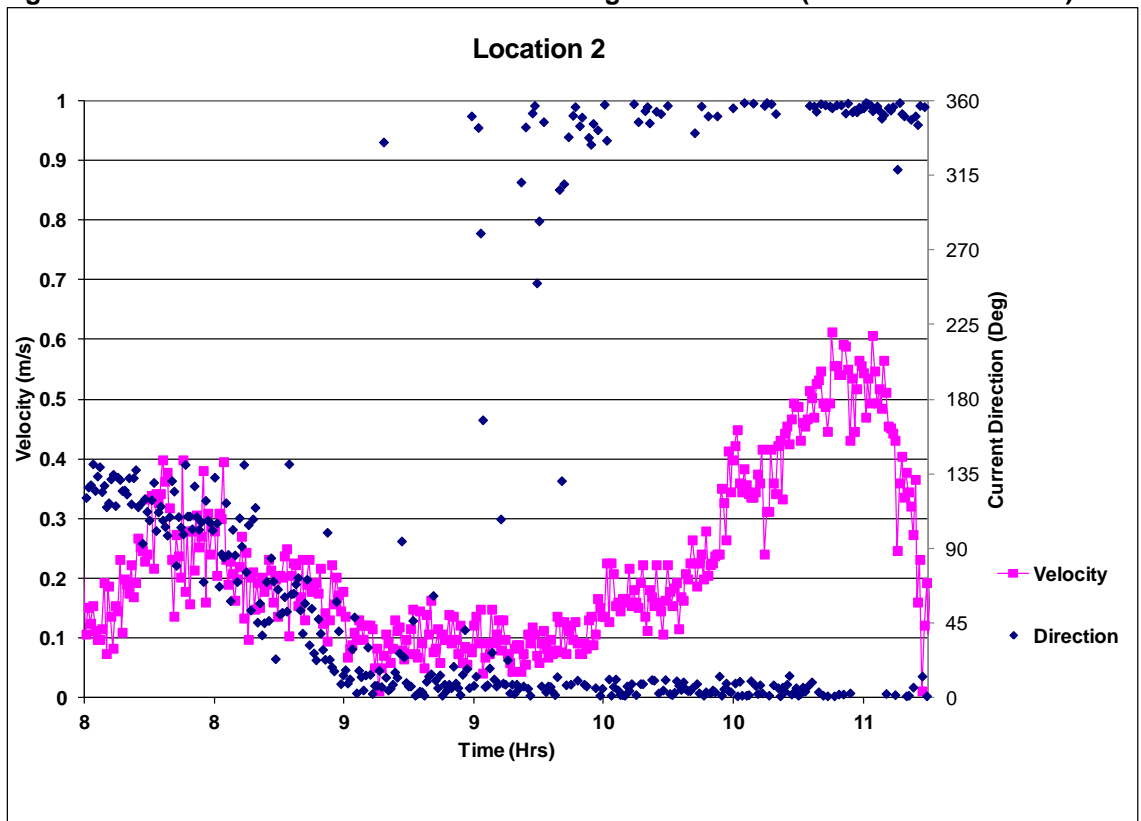


Figure 4.21 Time series of tidal current recording at Location 2 (RCM8 measurement)

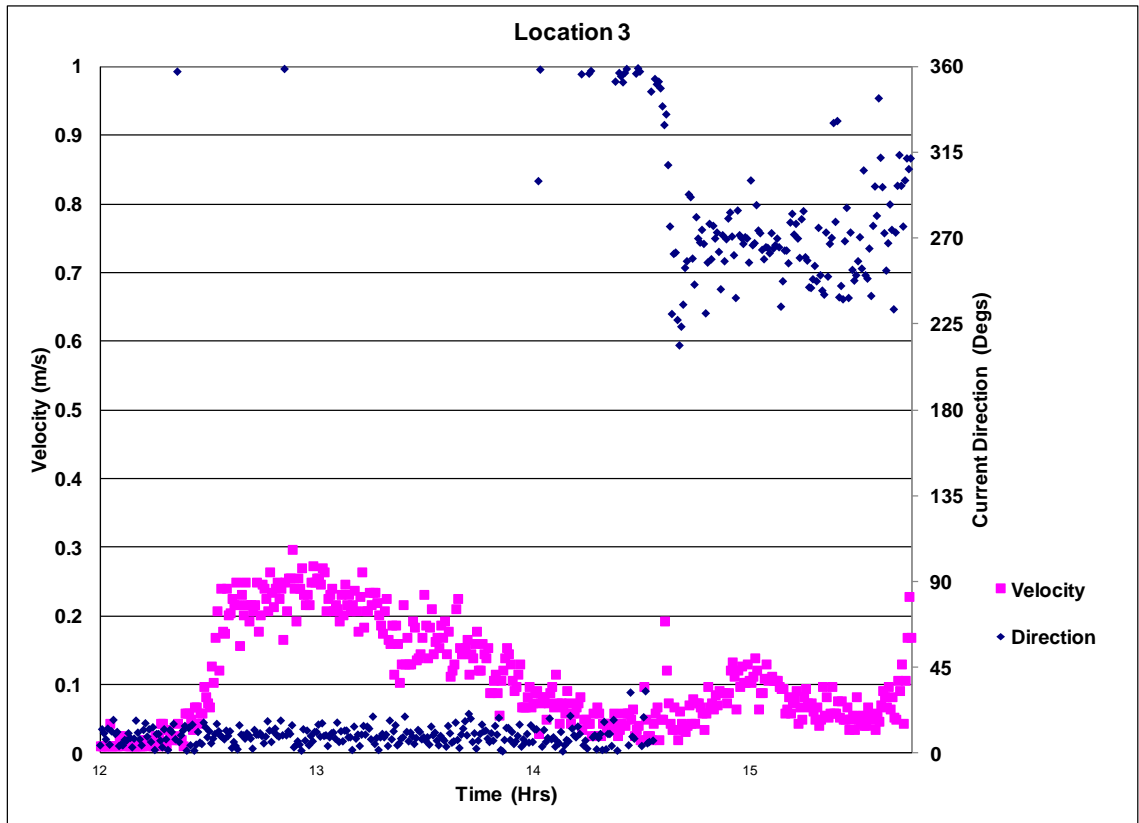


Figure 4.22 Time series of tidal current recording at Location 3 (RCM8 measurement)

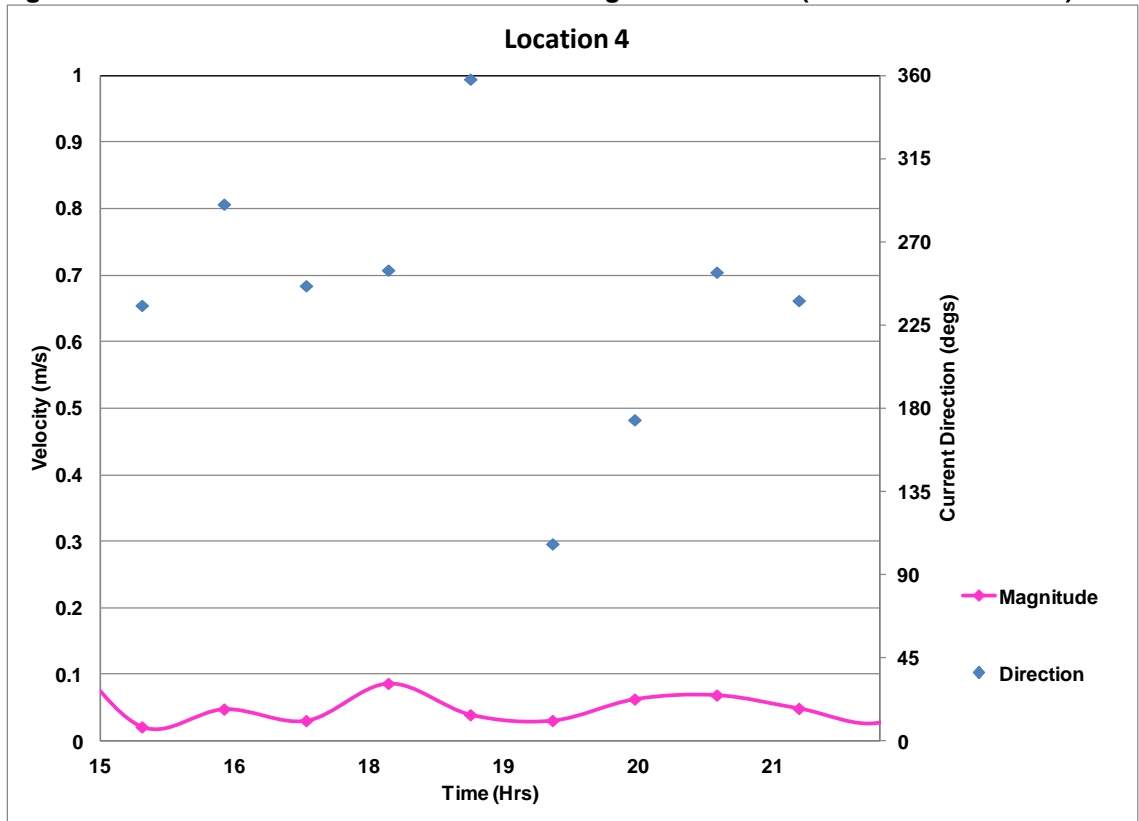


Figure 4.23 Time series of tidal current recording at Location 4 (Valeport measurement)

The role that tidal currents play in the erosion patterns becomes apparent when considering the magnitude and direction of the flood currents recorded. The direction of this current allows sediment to be carried into the main tidal inlet and redistributed away from Rossbeigh. The ebb tidal currents moved in a shore normal direction, also transporting sediment offshore and not replenishing the sediment removed on the flood tide. This sequence of processes indicates that significant sediment was removed from the beach at the distal end of Rossbeigh.

4.2.3 Morphological Analysis of Hydrodynamic Field Data

The identification of several trends in the hydrodynamic data collection campaign has enabled the formulation of a morphodynamic conceptual model. This model describes the morphodynamic drivers acting on Rossbeigh beach over a tidal cycle. Erosion patterns including the expansion of the drift aligned zone and migration of the hinge point are explained in this model. The influence and growth of the ebb tidal bar was also discussed.

Stage 1 of the model is at low tide or below 0.0 m OD Malin, figure 4.24(A). At this point the incident wave direction is acting shore perpendicular in the swash aligned zone and undergoes a slight deviation as the waves are funnelled towards the drift aligned zone. This funnelling and alteration of wave direction is caused by the presence of the ebb tidal bar which is exposed at low tide. It causes the incident wave front to constrict, diffract and refract. This forces the wave front to travel at an angle to the shoreline increasing the alongshore transport in this zone (drift aligned).

The second stage, figure 4.24(B) is initiated as the tide rises to 0.5m OD Malin, and the flood tidal current velocity increases. Funnelling of the wave continues to occur, due to diffraction and refraction. The shape of the channel between the ebb tidal bar and drift aligned shore line causes a constriction close to the island leading to a further increase in along shore sediment transport. This sediment is moved shore parallel by the strong tidal current into the main channel of the tidal inlet. The variation in tidal current velocity is caused by the channel width differential between the southern end of the drift aligned zone where the channel

between bar and shore is relatively wide and the constriction by the island where velocities are twice as high. This differential in velocity affects the sediment budget in this zone leading to high erosion rates and breaching of the dunes.

The third stage, figure 4.24(C) occurs above 0.5m OD Malin when the waves can pass over the ebb tidal bar. Tidal currents do not play a significant part at this stage of the morphodynamic cycle. The waves refract and change direction as they pass over the ebb tidal bar. The waves reach the shore line at an angle thus shaping the dune line and beach to that angle as the waves are most erosive at high tide. The recent (since 2008) increase in size of the ebb tidal bar both vertical and horizontal, is driving the increase in drift aligned shoreline and hence the migration of the hinge point.

The fourth stage, Figure 4.24(D), occurs as the tide drops below 0.5m OD Malin and the ebb tidal currents increase. These currents move the eroded dune material further down the shoreline and into the channel between the ebb tidal bar and drift aligned shoreline. This material is then transported alongshore into the main channel which in turn moves the sediment offshore and deposits onto the ebb tidal bars in the next cycle. As this cycle continues the ebb tidal bar grows and the drift aligned zone expands.

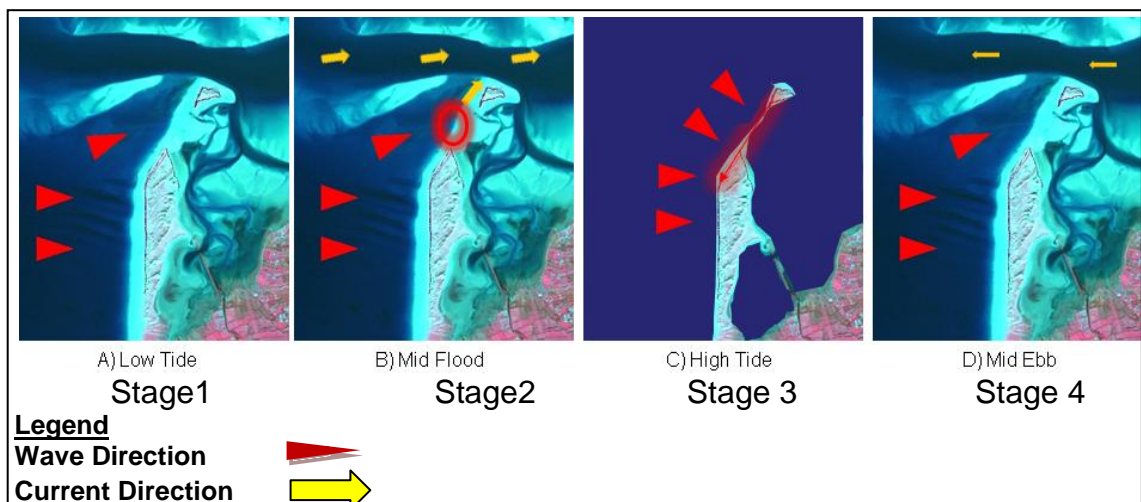


Figure 4.24 4 Stage Morphodynamic Conceptual Model of Rossbeigh

4.2.4 Sediment Dye Test

A limited sediment transport dye test was undertaken during the field monitoring campaign to confirm the direction and magnitude of sediment transport in the drift aligned zone. A 100 mm deep by 1 m² area of dyed sand, figure 4.25, was placed in a mid- tide location at the centre of the drift aligned zone. Methodology similar to Bertin et al. (2007) was implemented.

The weather conditions were mild with mean H_s of 0.25 m. The area was then sampled on a grid figure 4.26, after 1 and 2 tidal cycles. A 100 m alongshore by 50 m cross shore grid was sampled at 1 m intervals. Outlying points along the beach were also sampled to account for larger than expected sediment movement. The cores were then transported to the lab for analysis.



Figure 4.25 Dyed sand injection point

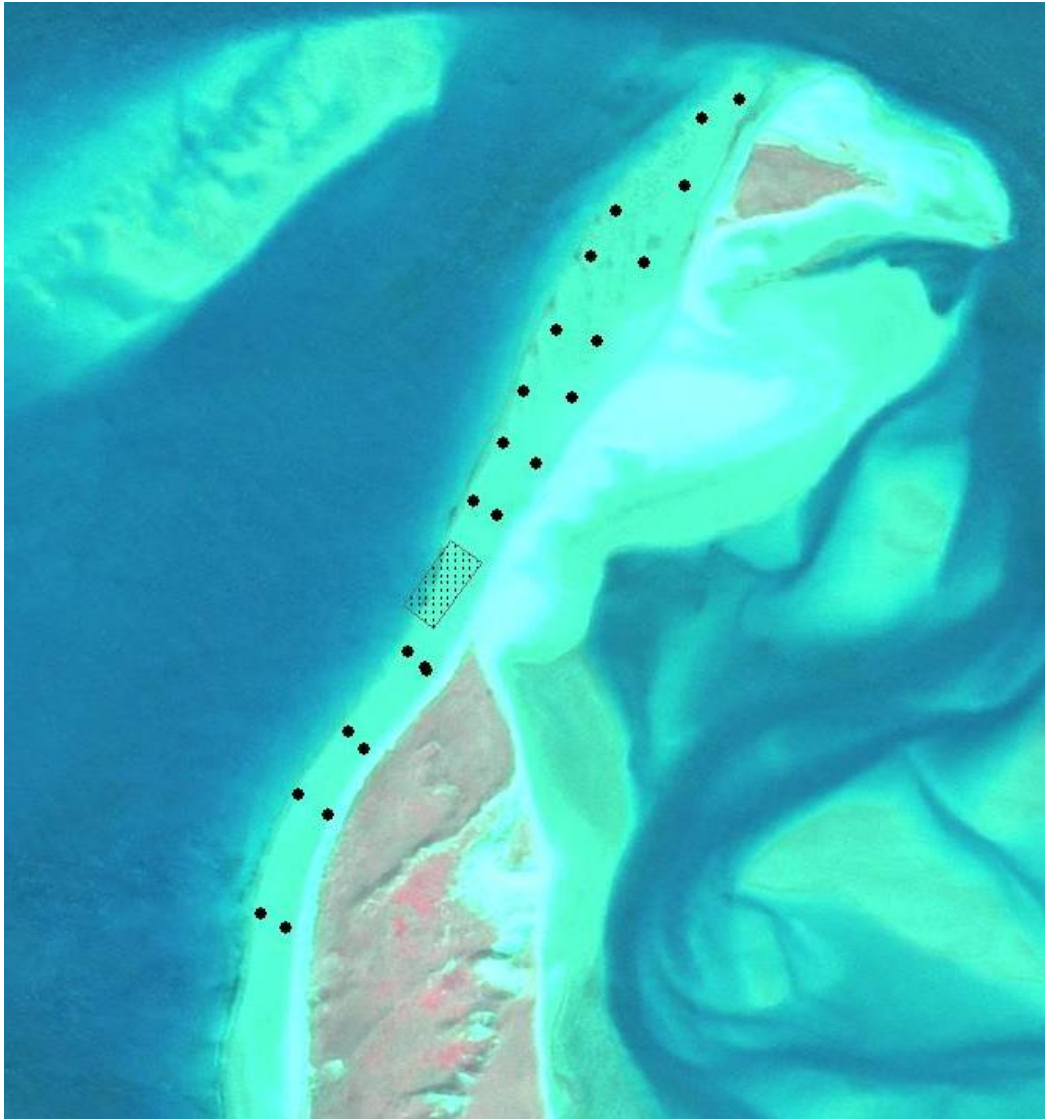


Figure 4.26 Dyed sediment sample grid with outliers along beach

Each core was separated into 3 sections representing surface middle and bottom of the core. The sections were then spread on a plate and exposed to ultra violet light in a dark room. There was no trace of the Rhodamine dyed sand remaining at source point or in either direction of the grid or even as far as the furthest outlier sample point. This illustrates the unsuitability of dye tests in such an active area. It also shows that even in mild onshore condition $H_s < 1$ m the depth of disturbance was greater than the 100 mm depth of the core.

4.2.5 Sediment Fencing

Sediment fencing was trialled in two locations within the breached area during the 2011 data collection campaign. The purpose of the fencing was to trap

windblown sediment in the breach area in an effort to stabilise it and quantify the potential for aeolian regeneration of the breached area.

Tenax II PVC fencing was used during this experiment. This high density polyethylene porous fencing causes the wind speed to decrease as it passes through and hence sediment is dropped. The fences were attached to 100mm square timber posts which were driven in 2.5 meters. The location of each fence is shown in figure 4.27. Fence 1 was situated adjacent to the terminus of the main dune structure while Fence 2 was situated in the middle of the breached area.

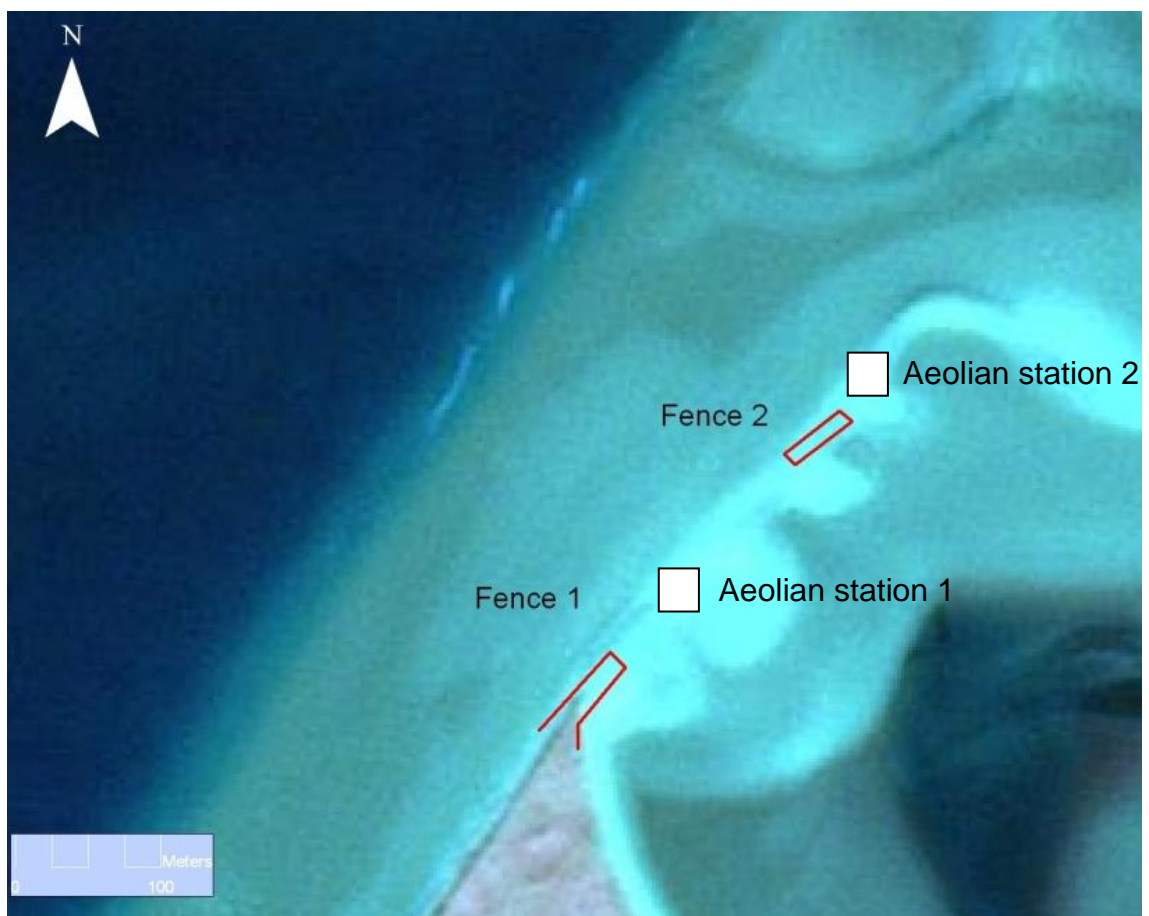


Figure 4.27 Location of sediment fencing and aeolian measuring stations

The Fence 1 location proved to be unsuccessful as the proximity of median dune reduced aeolian sediment supply. This area was also subject to extensive erosion and from September 2011 onwards the timber posts began to be undermined from wave action. The fencing was completely removed by erosion

by January 2012. At the Fence 2 location, figure 4.28, the sediment build up was progressive.

Over a 4 week period, the sand had built up to a 0.5 m high ridge at the centre of the fencing. In September 2011 tidal inflow and wave action broke several sections of the fencing although the majority of posts remained intact and accretion continued. This location has now been covered by alongshore driven gravel and is approximately 1 m higher than before the fencing was installed. While most of the fencing is now removed the posts have remained in situ.



Figure 4.28 Sediment fencing in Location 2

This trial showed that sediment fencing may have limited applicability in healing the breached area of Rossbeigh. The fencing proved ineffectual in preventing the wave driven reshaping of the beach close to the distal dune (Fence 1). However, in the centre of the breach, Fence 2 location, the fencing has aided in the development of an embryo gravel bank. Erosion has reduced significantly in this area since the breaching event in 2008.

The effectiveness of the sediment fencing as an erosion prevention strategy is limited while erosion rates remain high. This trial has shown that a sediment fencing strategy is unsuitable for installation in active erosive zones including the island, the southern part of the drift zone and drift/swash boundary. There is, however, merit in extending the fencing on the embryo gravel bank where erosion rates have stagnated and dune vegetation has been re-established.

4.2.6 Aeolian Sediment Transport Measurement

Aeolian sediment transport measurement was undertaken in the drift aligned zone of Rossbeigh, to assess the regeneration potential of aeolian transport. Two stations which consisted of sediment traps, as described in Section 2.4.2, and wind measurement instruments were installed. Sediment and wind measurements were collected for a 6 week period in the summer of 2011.

The aeolian measuring stations were placed adjacent to the sediment fence locations, figure 4.27. These stations consisted of one Guelph trap, Nickling et al. (1995), a sediment profiler, Goosens et al. (2000), figure 4.29, and a wind speed and direction recorder, figure 4.30 which recorded wind speed and direction. The surface moisture content was recorded in the windward direction for 100 m in front of the aeolian measure stations.



Figure 4.29 MWAC sediment profiles (Goosens et al., 2000)

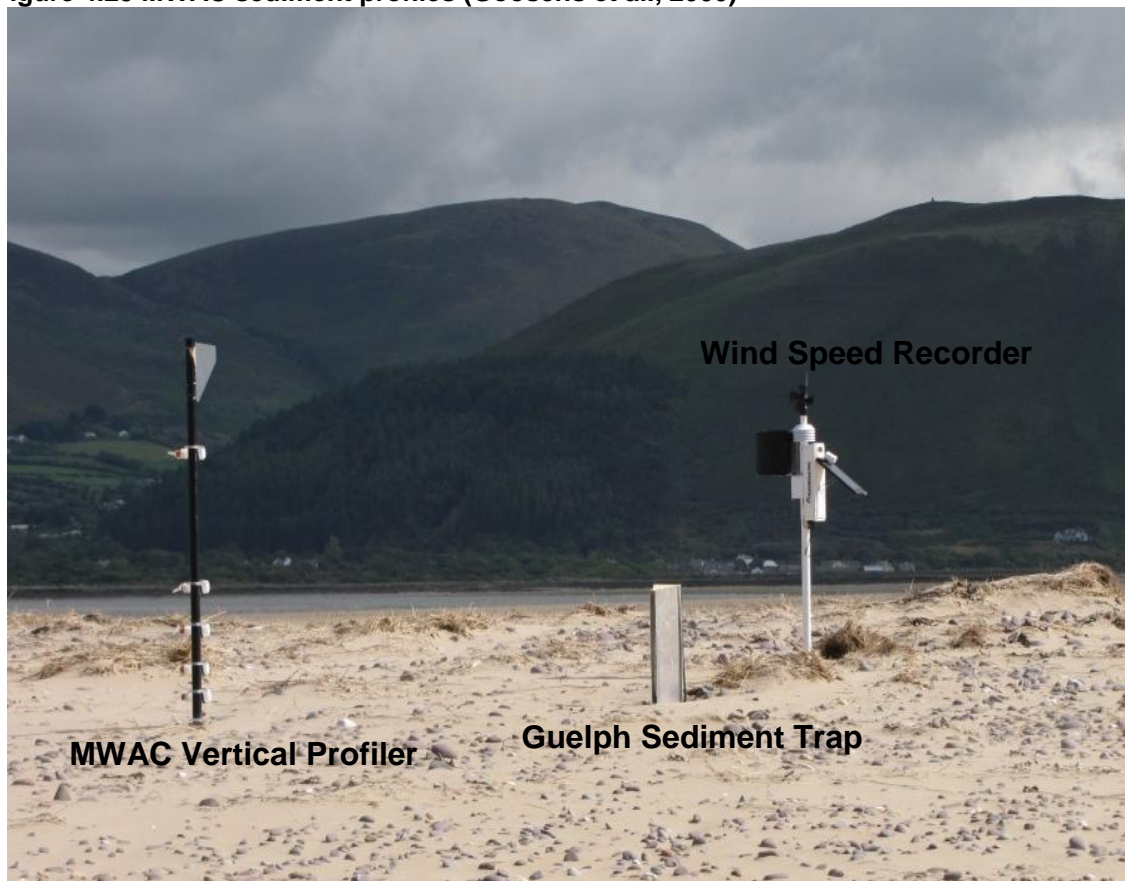


Figure 4.30 Aeolian recording equipment at Station 2

The results of the aeolian transport are presented in Table 4.1. The Guelph trap results showed that the largest sediment was transported during north westerly

and south westerly winds. There was a significant difference in sediment collected between Station 1 and Station 2. Station 2 generally collected more sediment as was expected due to its more exposed location. It was noteworthy that the maximum amount collected does not correspond with the largest average wind speed. This was due to weather conditions at the time of the maximum wind speed. Specifically it was due to moisture content of the sand being too high to be mobilised by the wind. The results show that the average weight of sediment passing the traps was 20.1 grams/hour for Station 1 and 67.75 grams/hour for Station 2.

Table 4.1 Guelph trap results

Avg Wind m/s	Direction	Guelph Trap @ Station 1	Guelph Trap @ Station 2
		g/hr	g/hr
7.6	SSE	0	0
7.8	SSW	117.9	0
8.3	SW	12.2	633.3
6.0	SW	103.2	229.6
4.9	SW	2.6	4.8
6.6	SW	48	48
14.3	SW	20.6	40.8
5.0	SW	0.5	0.5
5.0	W	9.3	7
7.1	WNW	11.3	3.2
16.0	NW	3.4	22.7
6.1	NW	10	14
8.0	N	0	11.1
7.0	NNE/NNW	37.1	40
5.9	NNE	23.8	28.6
2.2	NE	0.7	0.5
Average		20.14	67.75

The vertical profile of aeolian sediment transport is presented in Table 4.2. It gives a clear indication that the majority of the sediment transported by the wind at both locations was by saltation. The amount of sediment captured in the vertical profile from 150 mm and on the beach surface was negligible.

Table 4.2 Typical MWAC results on Rossbeigh

Avg Wind m/s	Wind Direction	Duration Hrs	Condition	Location of MWAC Bottles above surface				
				50 mm	100 mm	150 mm	200 mm	250 mm
7.8	SSW	2.8	sunny	1g	0.3g	0.15g	0.05g	0g
6.6	SW	5	overcast	0.1g	0.05g	0g	0g	0g
4.9	SW	11.5	light breeze	3.5g	0.1g	0g	0g	0g
7	NNE/NNW	7	overcast	1.4g	0.05g	0g	0g	0g

The measured rates in these tables can be used to give an indication of the rate and form of potential regeneration of the breached area through aeolian transport. It was clear that both beach surface moisture content and fetch length are important factors to consider when attempting such a calculation. This is further discussed in Chapter 7 when regeneration timescales are estimated.

4.3 Bathymetry

Knowledge of the bathymetry is critical to understanding the morphology of a coastal cell. When bathymetry is monitored over a period of time, clear conclusions can be made on the nature of sediment transport in the cells by observing how the seabed changes. Bathymetry is also an essential input for hydrodynamic modelling. However, seabed surveying in the coastal zone can be difficult. Breaking waves and strong currents can affect the quality of the survey data. When the study area includes a dynamic tidal inlet and several offshore bars as is the case with Dingle Bay, these difficulties were compounded. One solution was to survey the bed level using remote sensing techniques. Several remote sensing methods of undertaking bathymetric surveys exist. Satellite imaging has been used to good effect (Stumpf et al. , 2003). Surface penetrating LiDAR has also been used (Irish et al. , 1998). One of the restrictions with such remote sensing technology is the effect of turbidity on shallow coastal areas or highly dynamic coastal areas such as Rossbeigh.

4.3.1 Previous Bathymetric Surveys in Dingle Bay

The first evidence of a bathymetric survey undertaken in Dingle Bay was an Admiralty Chart from the 1850's. Prior to the present study the only other recorded survey undertaken since then was in 2009. A multi-beam deep water (Depth>10 m) survey was commissioned by the Marine Institute/Infomar, figure 4.31. This survey provided comprehensive cover of outer Dingle Bay. The shallow limit of this survey borders the depth contour of maximum closure depth of the barrier beach system. This is the offshore limit of sediment transport based on average maximum wave conditions.

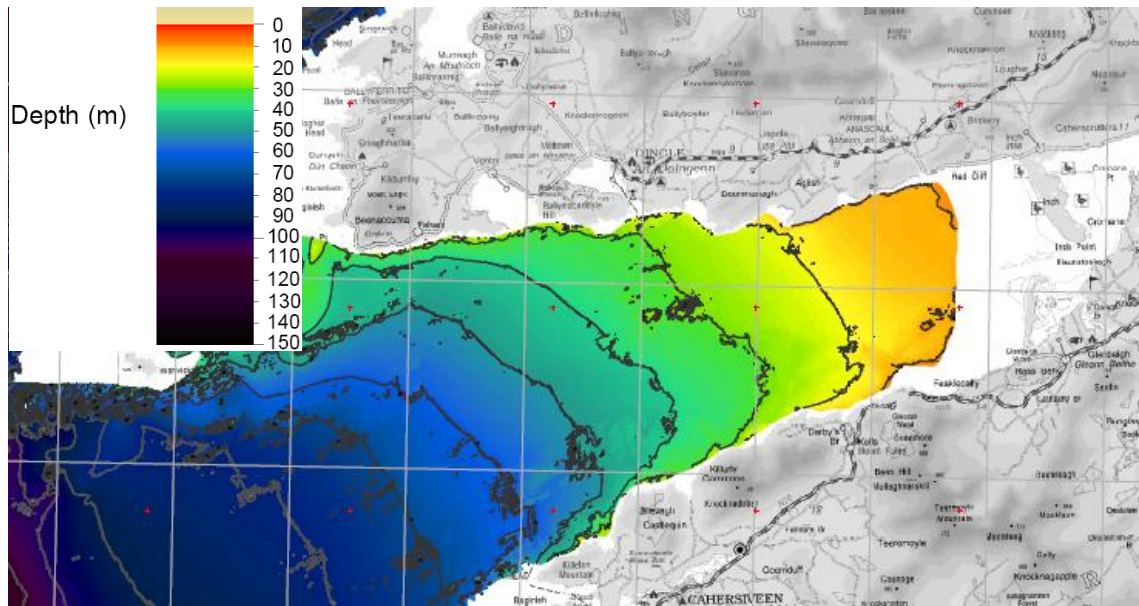


Figure 4.31 Outer Dingle Bay Bathymetry (Courtesy of Infomar)

In an effort to complete the mapping of Inner Dingle Bay, the Marine Institute attempted a LiDAR survey. This proved unsuccessful due to the turbidity levels in the bay. The HMRC commissioned a multi-beam survey inside the limits of the original 2009 survey. This was undertaken in August 2011 with limited success, figure 4.32. The inflatable rib based survey craft had a limiting depth of 1 m. It was unable to survey over the ebb tidal bars and inner surf zone of Rossbeigh and Inch, due to shallow depths, large currents and wave action. This is the critical area in terms of morphological change. Due to the failure of the rib based craft to undertake a complete survey of the inner bay, other methods were investigated. However, this survey has proven useful when compared to later surveys in which migrating bars are detected.



Figure 4.32 Survey of Rossbeigh and Inlet August 2011

4.3.2 Design of PWC Surveyor

The personal water craft (PWC) has recently emerged as a suitable surf zone survey craft. The low draught and high power to weight ratio allow it to access shallow areas such as sand banks, traditional survey craft do not have this ability. The US Geological Society (USGS) has used PWC's for surf zone coastal profiling for over a decade. A design utilising RTK GPS and a single beam echo sounder interfaced with a survey planner on a rugged laptop has been the preferred method (MacMahan, 2001). Delft University of Technology have also developed a bathymetric profiler utilising a PWC/Echo sounder system (S T J van Son, 2010).

As part of this study a PWC surveyor, figure 4.33, was commissioned to undertake bathymetric surveys in the coastal zone of Inner Dingle Bay based on the aforementioned designs. The system is based on integrating existing survey software and hardware with new PWC craft and echo sounder. The echo sounder is an OHMEX Sonarmite single beam echo sounder that interfaces directly with the HMRC's Leica RTK-GPS via Bluetooth.

The Echo sounder transducer and GPS antenna are connected to the stern of the craft via a custom made survey transom. Both devices transmit to the PC logger via Bluetooth which is located in the VDU (Visual display unit) of the PWC. The VDU also houses a navigational GPS for survey tracking. The GPS antenna and transducer are co-located on the same vertical axis to reduce moment errors due to the movement of the craft. The depths and position of the antenna are logged every 1 Hz or greater depending on survey requirements. The offset between antenna and transducer was also measured prior to survey.



Figure 4.33 PWC Survey Craft

4.3.3 Error analysis of PWC Survey Craft

Awareness of the error range of survey is vital when the surveys are being used for volume calculations. There are several suggested acceptable error limits. The critical factors are speed of the craft and hull motion due to rough seas. After several speed trials a speed limit of 10 Km/h was found to be the upper limit before echo sounder accuracy was compromised. The error due to wave action on the craft is minimised by restricting surveys to conditions of less than 0.5 m wave height.

To calculate the error limits, the source of the errors must firstly be identified. The three significant sources of error in the PWC survey system, are the RTK GPS error, the Echo sounder error and the error produced by platform motion. The GPS error is in the order of 10 mm in the horizontal and 25 mm in the vertical.

The Echo sounder can lose accuracy due to erroneous bottom reflections and also air bubble caused by the propulsion system. There is an inbuilt quality assurance check for this. This is displayed as a number from 0 to 128 depending on the quality of the return beam. The other error associated with the echo sounder is the calculated speed of sound in saltwater. Once this is accounted for by onsite salinity and temperature measurement, there is expected to be minimal error with the echo sounder output. The largest expected source of error, however, is that produced by platform motion.

The error from the roll and pitch of the PWC due to waves produces two main errors. The tilting platform causes an offset between the GPS antenna and the echo sounder which results in a shortening of the vertical distance between the two and an error in horizontal positioning. This can be reduced by keeping distance between echo sounder and GPS antenna to a minimum (500 mm in this case). The roll or pitch of the hull also changes the depth the echo sounder reads.

TU Delft (2006) suggests an angle of 6° for calm seas and 12° for rougher seas ($H_s > 1$ m). To evaluate the possible maximum horizontal and vertical errors due to platform motion and maximum depth of 5m and a pitch angle of 6° was used with the standard formulae (MacMahan, 2001) for the PWC surveys. This gives the following errors:

Vertical Error

$$V_{GPS} = M_{arm} - M_{arm}/\cos(\text{pitch}) = 500 - 500/0.997 = -1.5 \text{ mm}$$

$$V_{echo} = h_{water}/\cos(\text{pitch}) - h_{water} = 5000/0.995 - 5000 = 15 \text{ mm}$$

$$\text{Total } E_{vertical} = V_{echo} + V_{GPS} = 15 - 2.5 = 13.5 \text{ mm}$$

Horizontal Error

$$H_{\text{GPS}} = M_{\text{arm}} \sin(\text{pitch}) = 35\text{mm}$$

$$E_{\text{cho}} = h_{\text{water}} \sin(\text{pitch}) = 349\text{mm}$$

$$\text{Total } E_{\text{horizontal}} = H_{\text{echo}} - H_{\text{GPS}} = 314\text{mm}$$

Where:

V_{GPS} = Vertical error from GPS

M_{arm} = Moment of rod between antenna and echo sounder transponder

V_{echo} = Vertical error from echo sounder

H_{water} = Max operational water depth

E_{vertical} = Total vertical error for survey craft

H_{GPS} = Horizontal error from GPS

H_{echo} = Horizontal error from echo sounder

$E_{\text{horizontal}}$ = Total horizontal error for survey craft

However, it should be noted that the 5 m depth reflects only a small percentage of the survey area. The majority of the points collected were in less than 3 m depth, this reduces the vertical error further. Such errors were negligible considering the scale of the changes in depth recorded between 2011 and 2013, discussed later in Section 4.3.7. The morphological changes in the horizontal were in the order of tens of meters. The calculated maximum error of 314mm was an acceptable margin when identifying morphological trends on plan.

4.3.4 Bathymetry Survey of March 2013

A survey of the near shore zone (water depth < 5 m) of Rossbeigh, the ebb tidal bar and the tidal inlet was undertaken in March 2013, figure 4.34, utilising the PWC survey craft described. The survey provides the first bathymetric information of the ebb tidal bar, previously unachievable by traditional survey methods. The drift aligned and swash aligned near shore zones were also profiled.



Figure 4.34 Bathymetry Survey of Rossbeigh March 2013

4.3.5 Bathymetry Survey of September 2013

A second survey was undertaken on the 22nd of September 2013. This survey followed similar lines to that of the March 2013 survey discussed. This survey encountered higher elevation peaks in the ebb tidal bar along the Eastern shore ward edge. The channel between ebb tidal bar and shore has deepened. The survey took place over a tidal cycle and the change in wave direction noted earlier due to the ebb tidal bar was observed in reality.

It is also notable that during this survey intense wave activity in an otherwise calm bay was observed west of the ebb tidal bar approx. 1.5 Km offshore of Rossbeigh. It is likely that this was caused by the rapid transition from relatively deep water (10 m) to the beginning of the ebb tidal bar (<2 m).

4.3.6 Morphodynamic analysis of near shore Bathymetric Surveys

The 2011 bathymetric survey with incomplete ebb tidal bar data and both the spring and autumn 2013 PWC surveys were analysed. While the time period between the three surveys was not equal, important trends can be identified by comparing them. The duration of almost 18 months between the first and second near shore survey was representative of one summer and two winter periods, while comparison between the second and third surveys represents one summer period in terms of morphology.

The comparison of the surveys was achieved by creating a digital elevation model (DEM) of each survey and utilising the triangulation method. The survey data was converted into a triangulated Irregular network (TIN) consisting of a set of triangles in 12D by 12D Solutions, a terrain modelling software. The vertex of the triangle has a z value interpolated from the survey data. It was possible to set a maximum triangulation length to restrict the size of the network to best fit the survey data. This nulling method was used to null any triangle with a side of length greater than a user specified length. This was useful when processing incomplete surveys such as the 2011 bathymetry survey or surveys where the length between points varies significantly, such as the swash aligned profiles of the 2013 survey.

Once created the TINs of each survey were compared. The -2 m contour is plotted in figure 4.35. Changes in height between TIN's in areas where they overlap are shown in figure 4.36, for August 2011 and March 2013 comparison and for the March 2013 and September 2013 comparison. The change of depth was colour coded with green signifying a growth and brown signifying erosion or deepening. These plots give a very clear indication of the morphodynamic activity occurring over the time periods.

The analysis shows that there was a clear migration trend apparent in the ebb tidal bar moving eastwards towards the drift aligned shoreline. This was offset by a deepening of the channel between bar and drift aligned shoreline. There was also evidence of infilling at the "neck" of the channel to the north entering the main tidal inlet channel, figure 4.37. The bar also appeared to have

expanded to the south during this time period. This finding was in agreement with the conceptual model documented earlier and also the satellite imagery analysis in Section 3.5.

Analysis of the second survey period provides further evidence of infilling at the neck of the channel. It should be noted that this was representative of a summer period which is usually associated with beach growth and expansion. Converse to this, the main body of the ebb tidal bar appears to have eroded and reduced in elevation. The reduction in ebb tidal bar height in the centre of the bar is explained by the expansion of the bar shore wards and the growth of a sand bar to the south of the main ebb tidal bar. The survey also shows significant beach erosion on both drift and swash aligned shorelines. This again illustrates that the morphology occurring on Rossbeigh and specifically the erosion is not driven by seasonal variations in meteorological conditions.

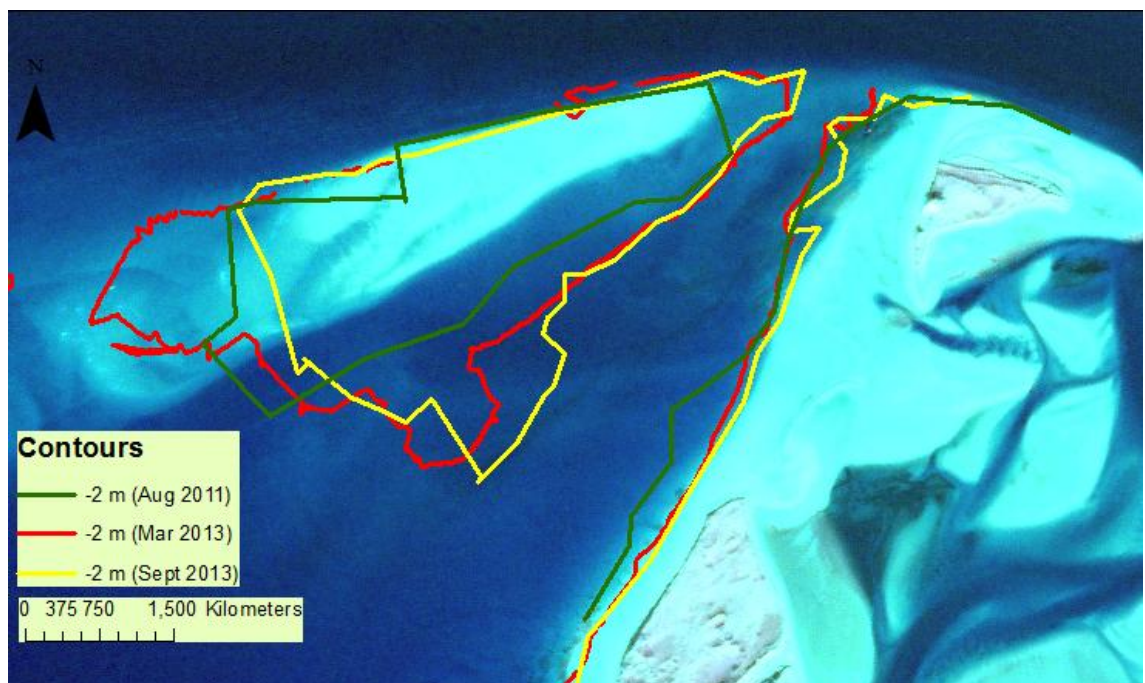
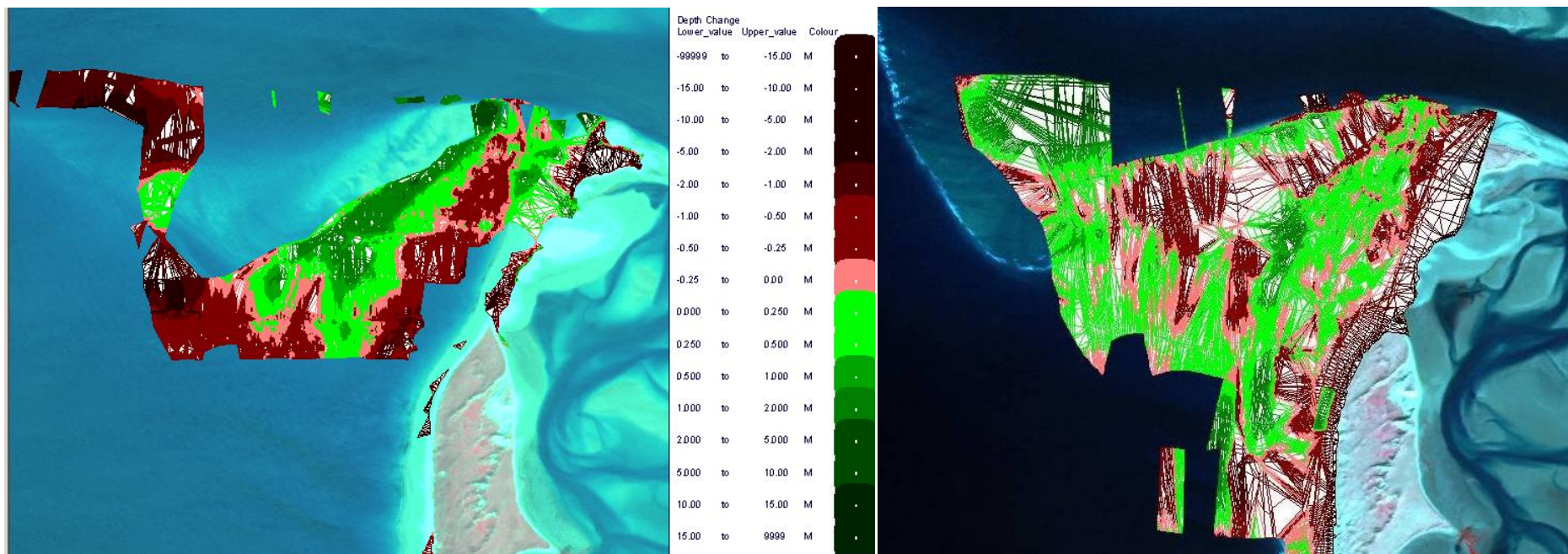


Figure 4.35 Contour of ebb tidal bar and drift aligned shoreline from successive bathymetric surveys



A

B

Figure 4.36 Change in Bathymetry between A) August 2011 and March 2013 and B) March 2013 and September 2013



Figure 4.37 Trends identified from bathymetry survey analysis

The channel between ebb tidal bar and drift aligned shoreline appears to undergo extensive change. Long section profiles with all three near shore surveys were plotted. Three sections were plotted with starting chainages at the shore running towards the bar, figure 4.38. The long sections were chosen where the three surveys had the greatest density of real data overlap.

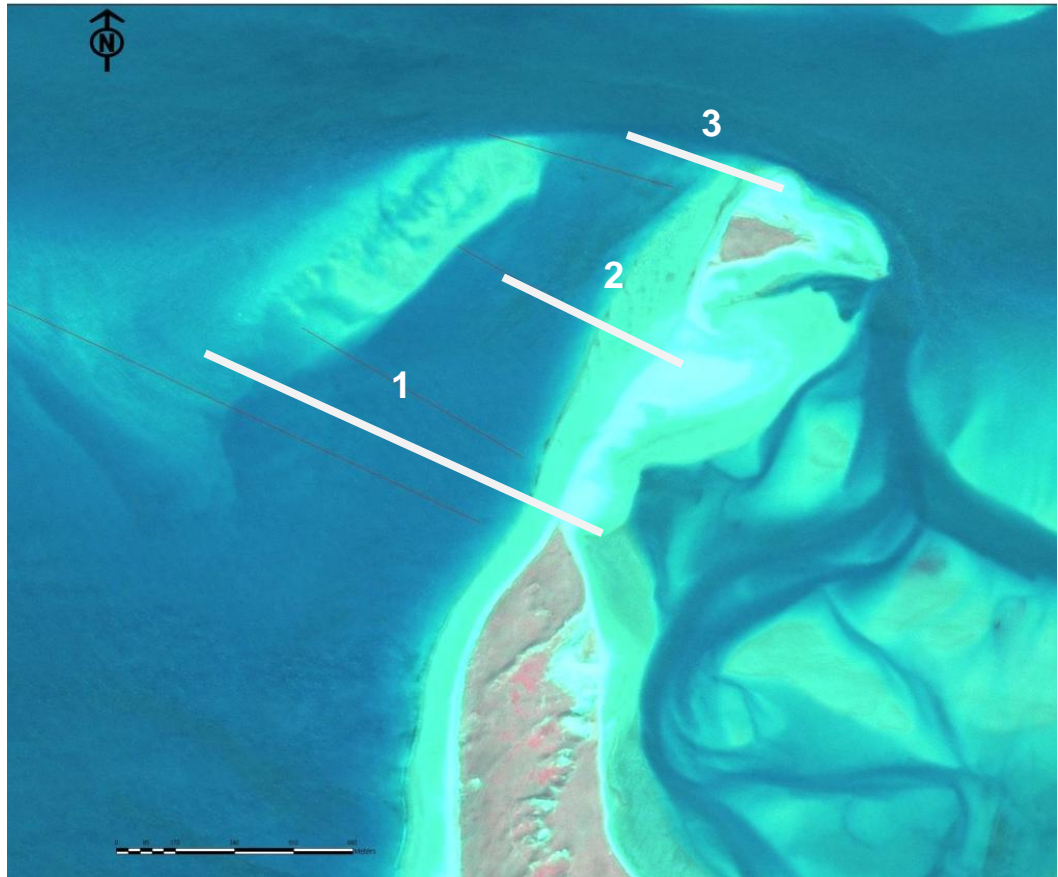


Figure 4.38 Plan of Survey long sections

The bathymetry at the entrance of southern extent of the channel, figure 4.39 shows that the bar has migrated and grown almost 0.8 m at chainage 400 m. The channel has also deepened significantly in this period with a 0.9 m difference between August 2011 and September 2013. A similar trend was apparent in the middle of the channel, figure 4.40 with changes less dramatic. The channel has deepened by 0.5-0.6 m close to the shoreline but moving closer to the ebb tidal bar the elevations were progressively higher in 2013 than in 2011.

At the neck of the channel, figure 4.41, the channel has not changed significantly over the two year survey period. At chainage 100 m there was approx 0.1 m between initial and final survey and similarly at chainage 200 m. The migration of the bar and growth of seabed at chainage 300 in the 2013 surveys was significant (over 1.5 m of an increase). Interestingly the majority of this depth change (1.3 m) happened between the 2011 and March 2013 survey which represents two winter and one summer period.

There was a slight growth (0.15 m) between March and September 2013. This would be expected to be larger if Rossbeigh had a regular summer/winter

morphodynamic system, given the extent of depth change between the previous 18 months. It is clear that at the neck there was a depositional trend occurring that was uncharacteristic of the channel in general which is narrowing and deepening.

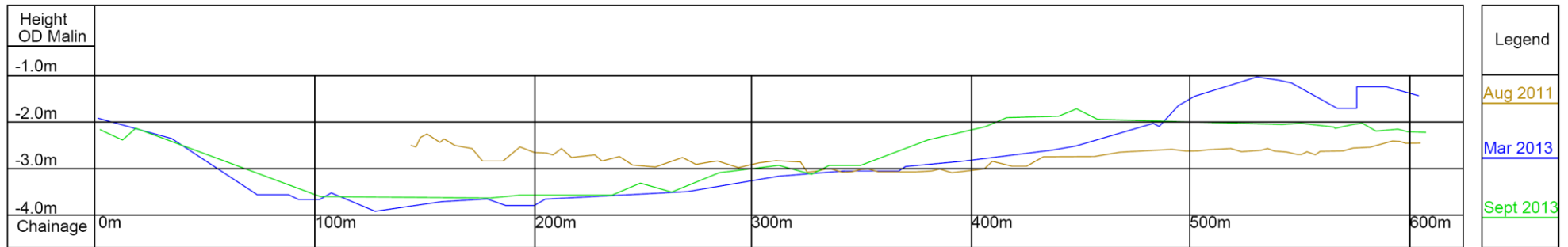


Figure 4.39 Long Section Profile at Southern Channel Entrance (Profile 1)

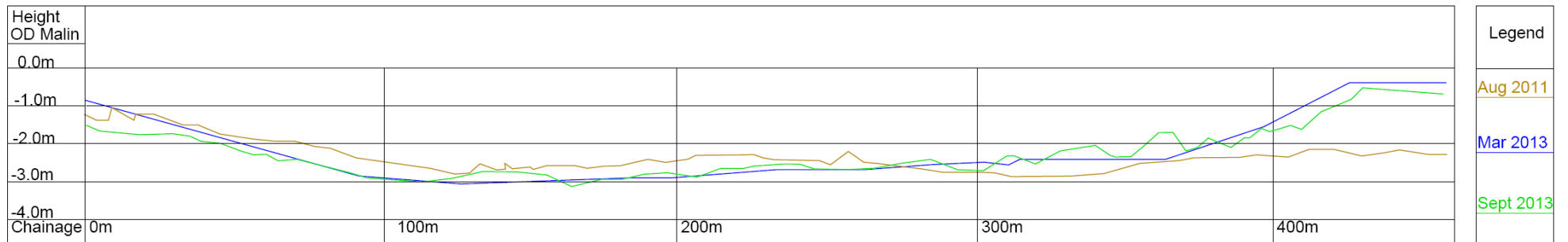


Figure 4.40 Long Profile in Channel (Profile 2)

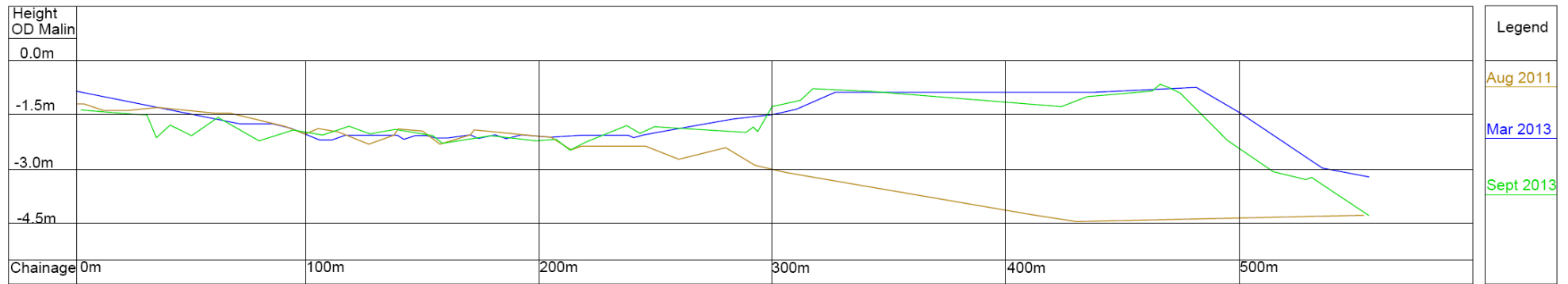


Figure 4.41 Long Profile in Northern end of Channel (Profile 3)

In an effort to quantify the change in volume in the channel, an area of 740,000 m², figure 4.42, was examined in greater detail. The change in volume of this polygon between successive surveys was calculated and presented in Table 4.3. There was net erosion of over 75,000 m³ between August 2011 and March 2013 in the polygon area of the channel. This figure masks the fact that over 63,000 m³ of sediment was transported into the area during this period. The erosion in the channel, however, exceeds this, but it is clear that there was both significant erosion and deposition occurring in the polygon region, with erosion in the channel dominating the bar migration driven accretion.

The period between March 2013 and September 2013 similar to the previous survey period shows both erosion and depositional trends. However, during this period the trends were reversed with deposition dominant over erosion. There was a net gain of sediment of almost 60,000m³ during this summer period. The actual amount of deposition was over 120,000m³ but this was offset by 60,000m³ of erosion.

It is clear from both volumetric and profile analysis that the ebb tidal bar is migrating towards the drift aligned shoreline. The sediment deposited offshore by the tidal inlet is being forced shoreward over the bar and into the shore parallel channel by wave action. As the channel is slowly narrowing it is being deepened by tidal currents to maintain its cross sectional area, as described by Escoffier (1940) in Section 2.3.5.

It also appears that this rate of migration has increased from 2011 to 2013. The surveys show that the channel is deepening and narrowing is most locations from the southern channel entrance with the exception of the neck of the channel. The neck of the channel did not experience major channel deepening over the survey time period and remains relatively shallow compared to the rest of the channel. Considering that the bar migration is continuing to accelerate, it is likely that if bar welding of the ebb tidal bar to the drift aligned shore is to occur it will initiate at the neck of the channel. This is discussed further in Section 7.3.

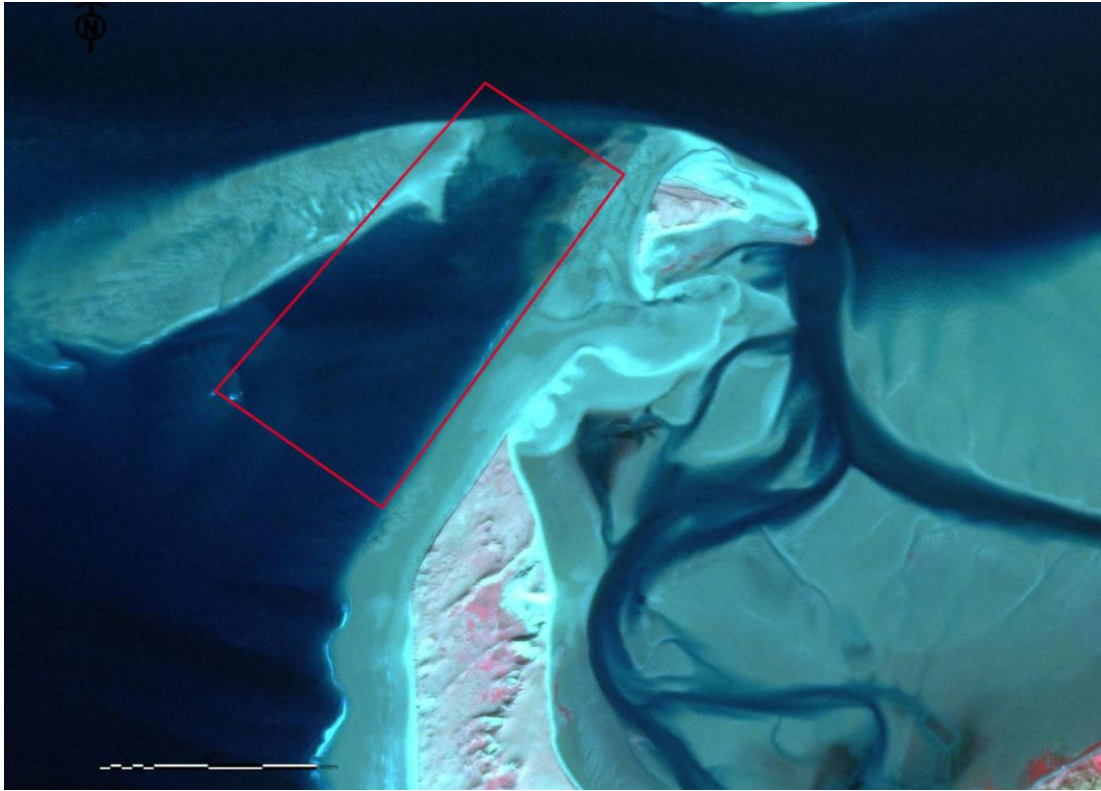


Figure 4.42 Plan of shore parallel channel area calculation polygon

Table 4.3. Volumetric difference between surveys within polygon

Survey Period	Total cut m ³	Total fill m ³	Total balance m ³
August 2011 to March 2013	-138595	63243	-75352
March 2013 to September 2013	-60212	120106	59894

4.4 Sediment Trend Analysis

The practice of determining sediment transport pathways through grain size trend analysis (GSTA) has been discussed in Section 2.4.2. As part of this study on coastal morphology, the GSTA method was applied. The main aims of undertaking GSTA on Rossbeigh were:

- 1) Establishing tangible sediment pathways to provide another insight into the morphology of Rossbeigh.
- 2) Provide a case study into the accuracy and applicability of the GSTA method in inlet- ebb tidal bar scenario.

Considering the other forms of analysis undertaken as part of the overall morphology study, results from GSTA on this site could be critically analysed and validated. Such case studies are in short supply as noted in Section 24.2.

4.4.2 Sediment sampling

The study site was subject to this analysis to ascertain the suitability of such methods in calculating sediment transport pathways. The intertidal locations are suitable for such analysis given the sediment transport activity inherent in regular water level variation. Sixty samples were taken altogether, 18 on the ebb tidal bar and 42 along Rossbeigh beach. The sampling locations can be seen in figure 4.43.

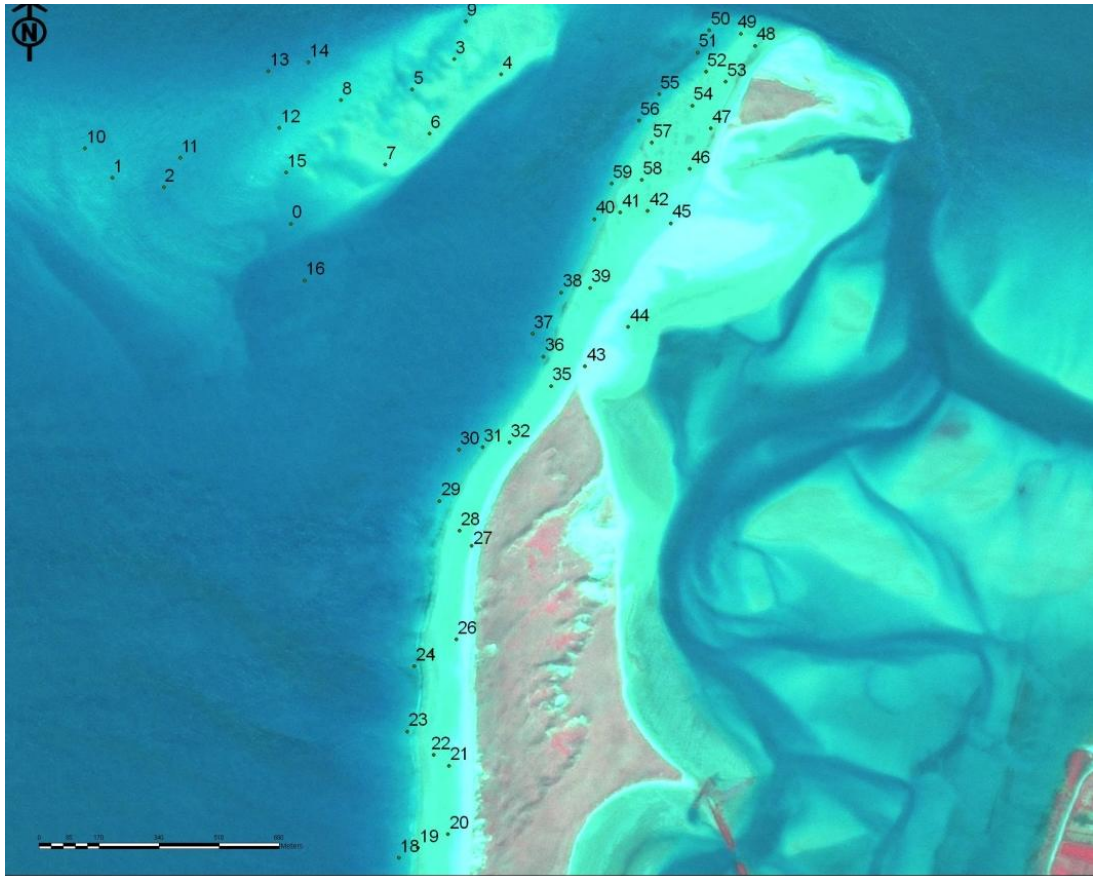


Figure 4.43 Sediment sample locations

The sampling took place in April 2013 with wave conditions being between 0.25 m and 0.50 m H_s in the previous week. The tidal range was 3.2 m. To ascertain correct sampling methodology, in particular depth of samples to be taken, consideration had to be given to the prevailing hydrodynamics that control sediment transport. The depth of disturbance based on recent wave conditions prior to sampling is calculated; from this the sample depth was set. The depth of disturbance was attained from Saini et al's (2009) formula of (19):-

$$Z_m = 0.22 H_b \quad (19)$$

Where

Z_m = Depth of Disturbance

H_b = Breaking wave height

Defining a time period for the recent wave activity, in turn defines the time period related to the represented sediment pathway analysis. It is important to differentiate between recent and older sediment sorting patterns as confusion between the two is easily achieved through incorrect sample depth.

In the highly dynamic climate of Dingle Bay dye testing results, Section 4.24, showed sample depths of 100 mm were removed even in mild wave conditions on the drift aligned zone. This is more related to tidal current driven sediment transport which was not factored into established depth of disturbance formulae, such as Saini et al's (2009) and others. The samples taken for GSTA were at 110 mm deep.

4.4.3 Sediment sieving analysis

Sediment samples were left to dry for one week. The samples were checked for shell and other erroneous elements before being processed for sieving. The sieving was undertaken by a Malvern Mastersizer Laser Diffractometer. The Malvern uses laser diffraction to measure the size of particles. A laser beam is passed through a sample and the intensity of light scattered was measured. This was then analysed to calculate the size of the particles that created the scattering pattern.

Five sub samples from each sample location were placed in the Laser diffractometer and an average sediment distribution for each location was calculated. Statistical analysis on the sample distributions was then undertaken. This involves calculating the three parameters necessary for GSTA; Mean grain size, Sorting and, Skewness. A specific program called Gradistat as detailed in Section 2.4.2 was utilised to calculate the statistics for each sample location. The results of this are shown in Table 4.4.

Table 4.4 Sediment Sample Statistics

Location	Easting	Northing	Mean (mm)	Sorting	Skewness
0	464191	594426	287.4	83.32	0.765
1	463685	594556	268.8	76.84	0.737
2	463831	594530	278.7	81.11	0.772
3	464653	594893	226	64.72	0.752

Location	Easting	Northing	Mean (mm)	Sorting	Skewness
4	464787	594851	255	66.16	0.686
5	464535	594807	250.1	64.78	0.683
6	464583	594682	268.2	76.36	0.74
7	464458	594593	257.8	66.54	0.691
8	464333	594777	255.3	66.07	0.678
9	464686	595001	231.8	59.3	0.672
10	463607	594640	261.6	74.25	0.725
11	463877	594614	240.7	64.43	0.692
12	464158	594699	250.5	67.31	0.706
13	464127	594860	220.1	56.84	0.682
14	464240	594885	220.9	57.21	0.691
15	464177	594571	257.1	65.81	0.663
16	464230	594265	267.7	84.38	0.818
17	464484.6	592379.5	245.7	140.1	4.089
18	464496.9	592623.3	244.2	137.4	4.161
19	464551.4	592652.2	237.3	91.11	1.997
20	464636.1	592690	209.8	60.44	0.735
21	464638.2	592885.3	240.4	83.99	0.899
22	464596	592915.8	250	98	1.064
23	464520.1	592982.3	225	77.58	0.88
24	464540.8	593167.8	257.4	101.6	1.496
25	464589.6	593205.3	273.7	125.7	2.064
26	464659.6	593243.8	215	61.31	0.73
27	464703.3	593510.7	247.4	77.34	0.77
28	464668.2	593553.9	258.6	88.73	0.889
29	464612.2	593637.6	262.9	95.84	0.937
30	464666.8	593782.7	250.5	94.53	1.528
31	464734.2	593791.2	261.7	87.22	0.865
32	464809.7	593804.1	220.4	68.25	0.754
33	464578.3	592351.6	297.3	149.6	1.571
34	464630.9	592321.4	225.6	71.59	0.807
35	464928.4	593964.5	249	78.85	0.783
36	464906.4	594048.3	256.2	80.28	0.778
37	464875.5	594113.2	269.2	104.3	1.164
38	464957.2	594230.4	293.8	120.4	1.262
39	465038.2	594243.7	250.9	78.58	0.779
40	465050.7	594439.2	239.9	75.78	0.811
41	465124.4	594457.5	254.3	81.5	0.825
42	465201.9	594462.5	252.4	86.2	0.884
43	465024.3	594020.2	251.7	80.2	0.787
44	465146.6	594132.2	246.9	69.97	0.71
45	465266.6	594427.5	253	72.25	0.732
46	465320.9	594581.3	279.3	98.01	0.841
47	465380.5	594697.2	246	70.69	0.733

Location	Easting	Northing	Mean (mm)	Sorting	Skewness
48	465505.6	594932	267.7	85.07	0.794
49	465465.9	594966.4	278.8	116.8	2.887
50	465376.7	594976.2	238.7	71.84	0.778
51	465343.1	594912.4	265.1	98.38	1.261
52	465367	594857.7	291.9	121.4	1.138
53	465423	594829.4	248.3	77.99	0.786
54	465328.4	594761.7	280.5	100.8	0.925
55	465234.4	594793.4	278.8	131	2.79
56	465177.4	594719.7	264.8	123.9	2.601
57	465213.4	594656.9	271.9	87.49	0.836
58	465184.5	594550	293.5	97.13	0.864
59	465099.8	594539.7	232.9	78.49	0.879

The sediment statistics summarised by region are presented in Table 4.5. All three locations have similar averages except for the ebb tidal bar Skewness. It is apparent that the swash aligned and the drift aligned zone share similar sorting statistics.

Table 4.5 Summary stats by location

D _{mean} (mm)				
Location	Total	Bar	Swash	Drift
Max	297	287	274	297
Min	210	220	210	220
Avg	255	252	243	260
Sorting				
Location	Total	Bar	Swash	Drift
Max	150	140	137	150
Min	57	57	60	68
Avg	88	73	92	92
Skewness				
Location	Total	Bar	Swash	Drift
Max	4.16	4.09	4.16	2.89
Min	0.66	0.66	0.73	0.71
Avg	1.1	0.9	1.39	1.11

4.4.4 Grain Size Trend Analysis Results

Establishing a characteristic distance (D_{cr}) is the first step in GSTA. This theory is detailed in Chapter 2. The D_{cr} calculated for the Rossbeigh site was 1050 m, Utilising the guidelines of Poizot (2008). There are 12 different cases for GSTA, these relate to the various permutations of the three

parameters, Mean Grain Size, Sorting and Skewness. All twelve permutations were tested using the Sedtrend Gis tool discussed in Section 2.4.2.

The Finer Poorer and more positively skewed (FP+) trend case gave the most realistic plot of sediment transport trend when compared with sediment transport calculation, bathymetry surveys, hydrodynamic monitoring and morphological modelling (detailed in Section 6.4).

The results of this case are shown in figure 4.44 along with 3 other test cases, FB-, FP- and FB+. The FB+ case figure 4.46 showed the least correlation with other methods with very small vector magnitudes and negligible variation in direction. The FB-, figure 4.45 and FP-, figure 4.47, both displayed some agreement with the sediment transport trends observed/calculated.

However, the strongest correlation in terms of trends and vector magnitude was the FP+ case. The trend vectors of the FP+ case showed strong onshore pathways on the ebb tidal delta. This was in agreement with the results of both tidal current monitoring and bathymetry detailed earlier in the Chapter. The direction of the pathways was also significant, as it follows the pattern of the high tide wave direction identified earlier. The majority of the vector arrows on the bar are in agreement with the drift aligned shore normal wave that occurs at high tide. As the bar is only covered and influenced by waves and tidal current at the upper stages of the tide, this reinforces both the validity of the trend analysis and also the influence of a dual directional wave climate at high tide in Rossbeigh drift aligned zone.

The results of the pathway analysis onshore at the drift aligned section of Rossbeigh were also pertinent. The trends show a strong offshore trend at both the island dune line and the distal edge. This was in agreement with the erosion trends shown on surveys in Chapter 3. Further south along the shore in the drift aligned zone the trend vectors are running shore parallel or slightly angled to the shore. This conforms to the theory that the drift aligned

zone sediment transport is dominated by shore parallel currents, documented by sediment formula comparison in Section 3.6.

In the Swash aligned zone the trends show vectors running perpendicular to the shoreline both offshore and onshore. These trends were in agreement with the cross shore transport calculations in Section 3.6. This result gives confidence to the theory that the sediment transport in the swash aligned zone is predominantly cross shore.

There were also previously undocumented trends observed, for example, at the very edge of the island section a sediment pathway trend is running south in direction contrast to the general trends. This can occur through localised wave effects on the transport pathways. It may also have been caused by edge effects of the computation grid. It was also possibly a real trend as the bathymetry survey analysis shows this area to be morphological distinct. The neck of the channel does not erode like the entrance or middle section of the channel. There was very little change in bed level over the survey periods. There is a possibility that this trend vector identifies a sediment pathway previously not described. This is discussed in further detail in Section 7.3.2 and compared with numerical modelling results that display similar trends.

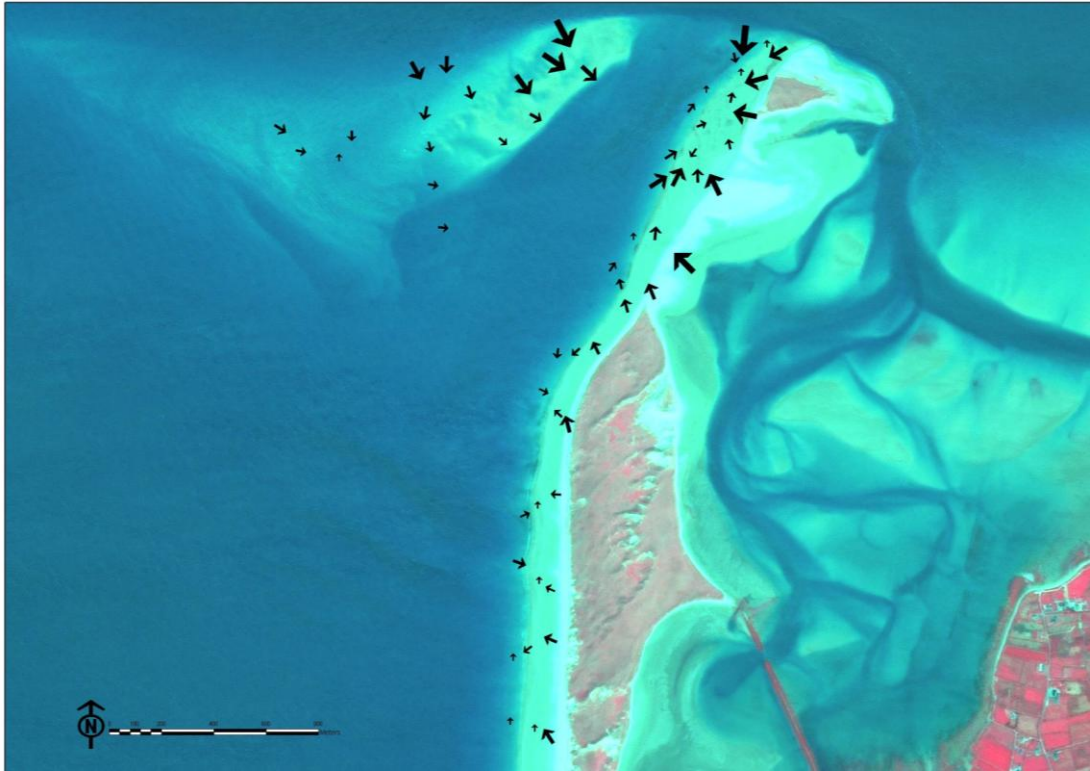


Figure 4.44 FP+ trend

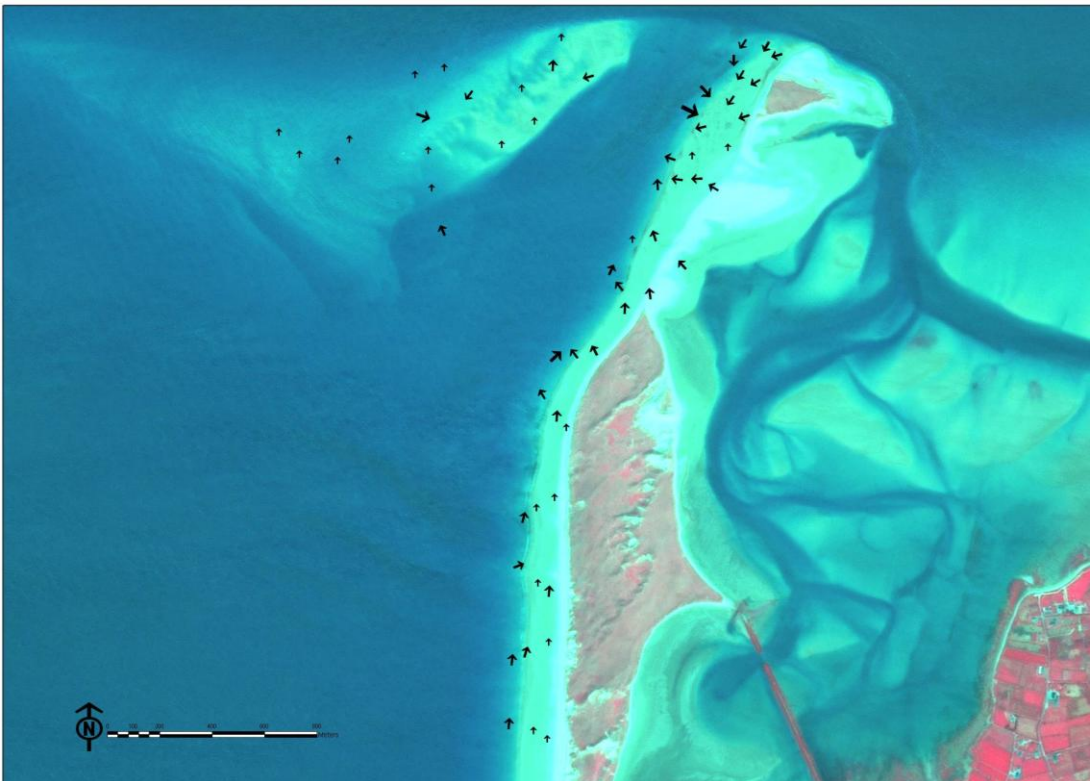


Figure 4.45 FB- trend

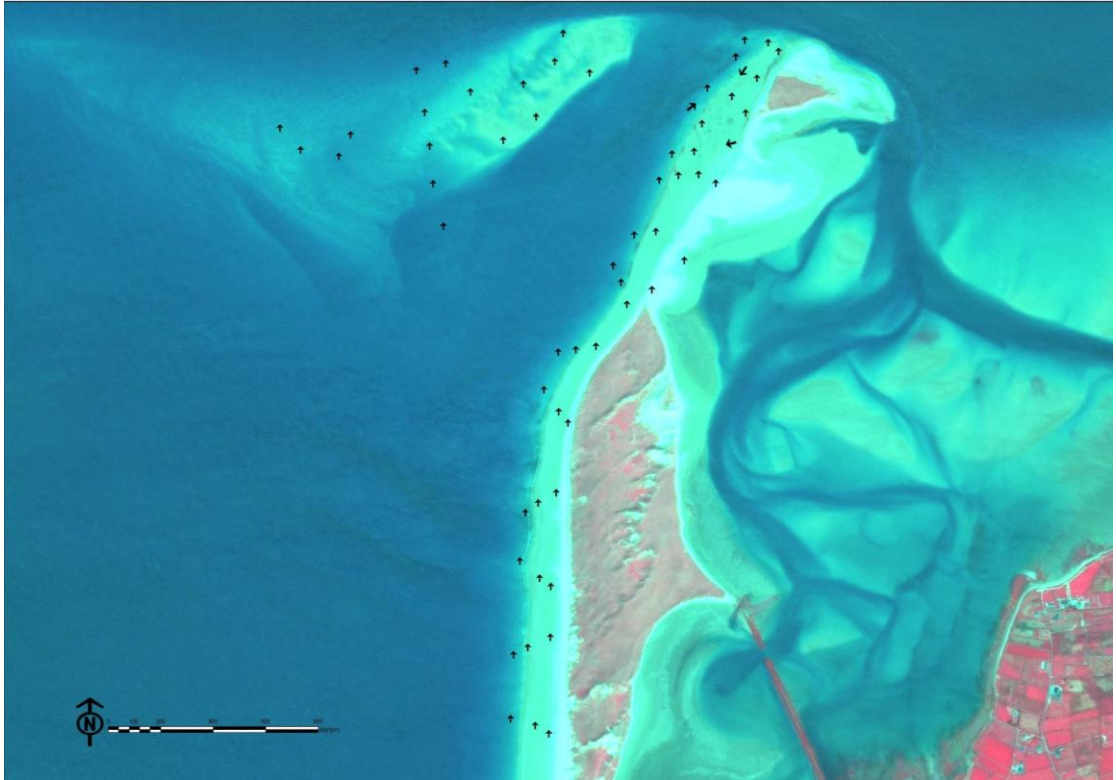


Figure 4.46 FB+ trend

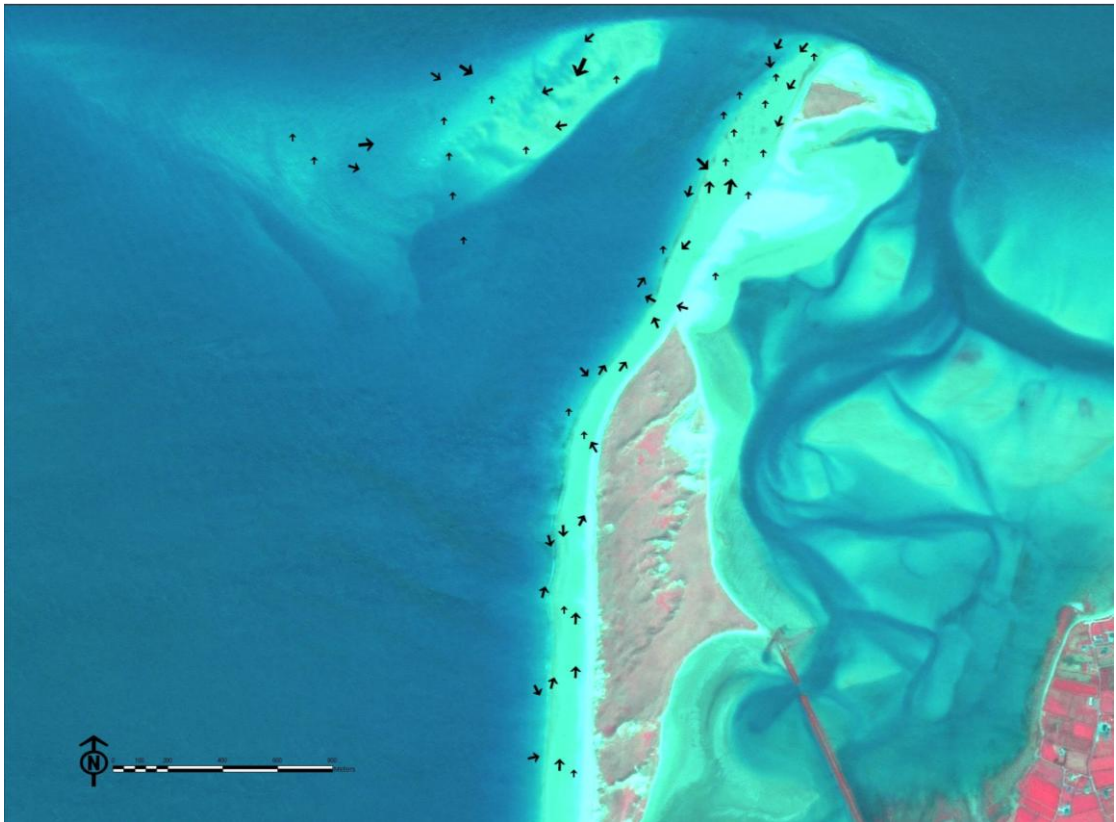


Figure 4.47 FP- trend

As discussed in Section 2.4.2, the most common trends on beaches similar to Rossbeigh are CB+ and FB-. Only several other cases have been validated including one case of FB+. However, until the present study there has been no FP- shown to be the dominant trend case. This was the first documented and validated case of FP- in a case study.

The finer and poorer combination trend case is rare. In the drift aligned zone it could be attributed to the intermittent dominance of wave and tidal forcings on sediment transport during the tidal cycle as identified in Section 4.3.7. However, for the trend case to be accurately sediment pathways on the Swash aligned is unusual.

4.5 Conclusions

The analysis of the field work presented in this Chapter has provided significant conclusions relevant to both the understanding of the current morphology but also to the future of the dune beach system. The data collected from this field work is used for further analysis discussed in later Chapters. The bathymetry data is used in the numerical modelling Chapter 6 and as a basis for error analysis of the radar post processing (Chapter 5). The wave data collected is utilised in the modelling Chapter 6 as validation. The aeolian data collected is used in Chapter 8 to inform the morphological timeline of Rossbeigh.

The main Chapter conclusions are as follows;

- The identification of a variation in wave climate on Rossbeigh beach from wave data collected on-site was a significant finding. The directional variation on the drift aligned shore aids in the explanation of the increasing drift aligned zone and the migration of the hinge point. Combined with the analysis of the tidal current field work a conceptual model was created. This model describes the current morphological cycles acting on Rossbeigh.
- The trends and conclusions on the morphology of Inner Dingle Bay presented are based on the analysis of point recording locations for both tidal and wave data collected. To improve the robustness of this method, data collection over a greater area and higher spatial resolution is preferred. HF Ocean radar was identified as one such technology that could enhance the coverage and resolution data collection on this project. The trialling of this technology is described in detail in Chapter 5.
- The sediment fencing experiment and aeolian transport field data recording have provided quantitative data as well as qualitative trends. The experiment concluded that in certain areas of the Drift aligned zone there is a large potential for dune regeneration provided that the fetch is long enough and the embryo dunes are above the high tide and storm surge level. It was also found the SW and NW directional

winds provided the most sediment. These trends and data will form the basis of an analysis of the potential for regeneration of the eroded dunes in Chapter 7.

- The bathymetric surveys combined with volumetric and morphodynamic analysis provided clear conclusions on the migration of the ebb tidal bar. The shoreward migration of the ebb tidal bar along with changing bathymetry of the channel between bar and drift aligned shore adds further detail to the conceptual model developed.
- The analysis of the results of the Grain Size Trend Analysis indicated broad agreement for the trends observed in both the bathymetry and hydrodynamic data analysis. The emergence of the FP+ case as the most applicable is noteworthy in itself, as this is rare in field studies and difficult to explain from a sediment transport driver viewpoint. The finer and positively skewed in the direction of transport was easily explained due to wave action and current sorting the grains but the poorer sorting metric is unexpected.

5 Dingle Bay Ocean Radar Trial

5.1 Introduction

The following chapter documents the trial of an ocean radar monitoring system in Dingle Bay. The aim of the trial was to record wave and surface current data in Dingle Bay over a large spatial area on a low temporal scale to identify hydrodynamic patterns that drive the morphology of the bay. This knowledge gap was identified in the previous chapter as being critical to the understanding of the sediment transport patterns in the bay.

This trial was the first application of the ocean radar technology over a large bandwidth (3 MHz) in a dynamic tidal inlet/barrier beach system. The radar system had never been implemented in a setting of dynamic currents, breaking waves and shallow bars such as Dingle Bay. Considering this, the trial was also an evaluation of the technology in highly dynamic coastal systems at a previously untested high resolution.

The technology and theory underpinning wave radar was discussed in detail in Section 2.4.1, but the specific system configuration and site geography was presented in this chapter. The initial results from the radar trial were analysed and errors associated with the results identified. An error analysis methodology formulated to fix these erroneous results along with data post processing techniques was also presented in this chapter.

Conclusions of the trial and the suitability of HF Ocean radar technology to Dingle Bay as a monitoring tool were discussed.

5.2 Dingle Bay Radar Setup

To achieve comprehensive coverage of the inner bay and also measure directionality of the wave and current fields, two radar stations were required. The locations in figure 5.1, were chosen based on distance from the barrier beaches, coverage and site suitability. The northern site was mains connected and the southern site was powered by a generator and battery system.

The southern site, Cork-S-Tx, figure 5.2 consisted of 12 receive (RX) antennas and 4 transmit (TX) antennas as there was adequate space for decoupling of the signals. The northern site, Cork-N-Tx, figure 5.3, was more restricted spatially and only 2 transmit antennas were used with 12 receive antennas. The stations were 10.8 Km apart. The distance of the southern site to Rossbeigh was 6.7 Km and the distance of the Northern site to Rossbeigh was 7.8 Km.

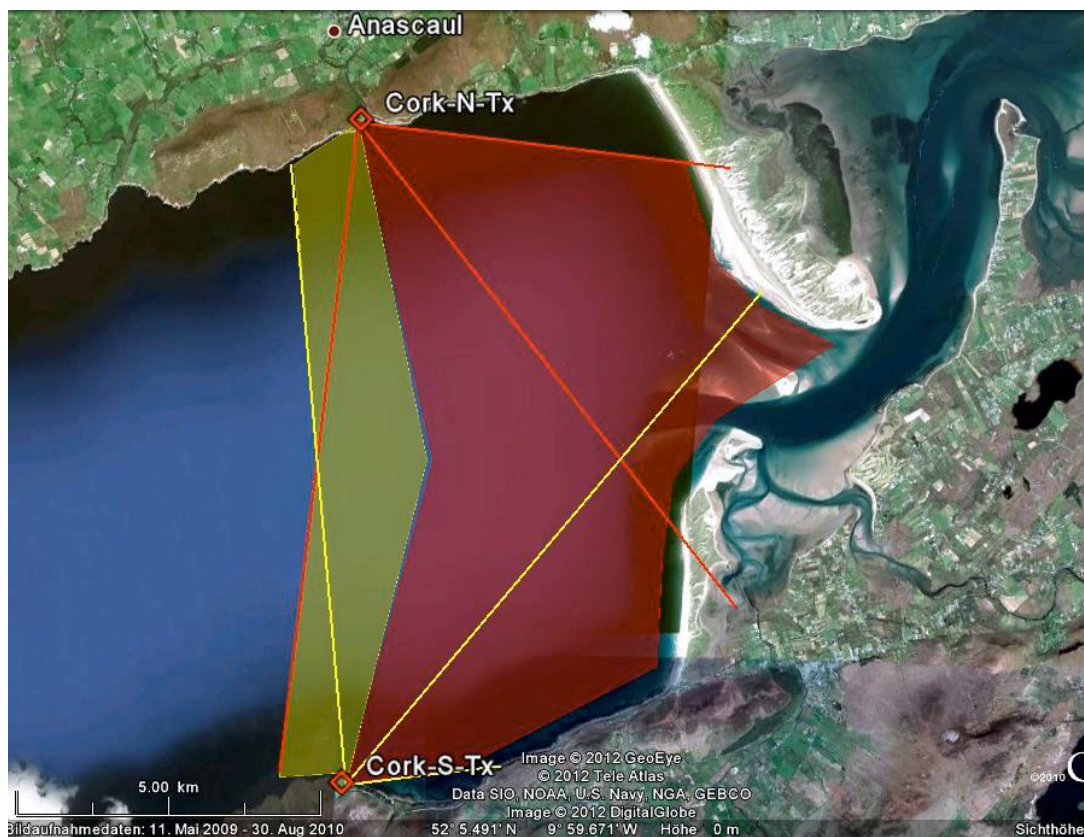


Figure 5.1 Station locations

An application to the statutory body responsible for wireless transmission, COMREG was required to transmit the radar signal. During the application process, the Department of Defence had initial reservations over the operating frequency and prompted a move from the 25 MHz range to the 30 MHz range. After several revisions Comreg approved an operating bandwidth of 6 MHz from 30 MHz to 36 MHz

This was one of the largest band widths used to date in WERA HF Ocean radar monitoring projects. During the course of the commissioning of the project, the onsite computer processors had issues with processing backscatter from 6 MHz of bandwidth. It was decided to use only 3 MHz of the available bandwidth to reduce the amount of data collection.

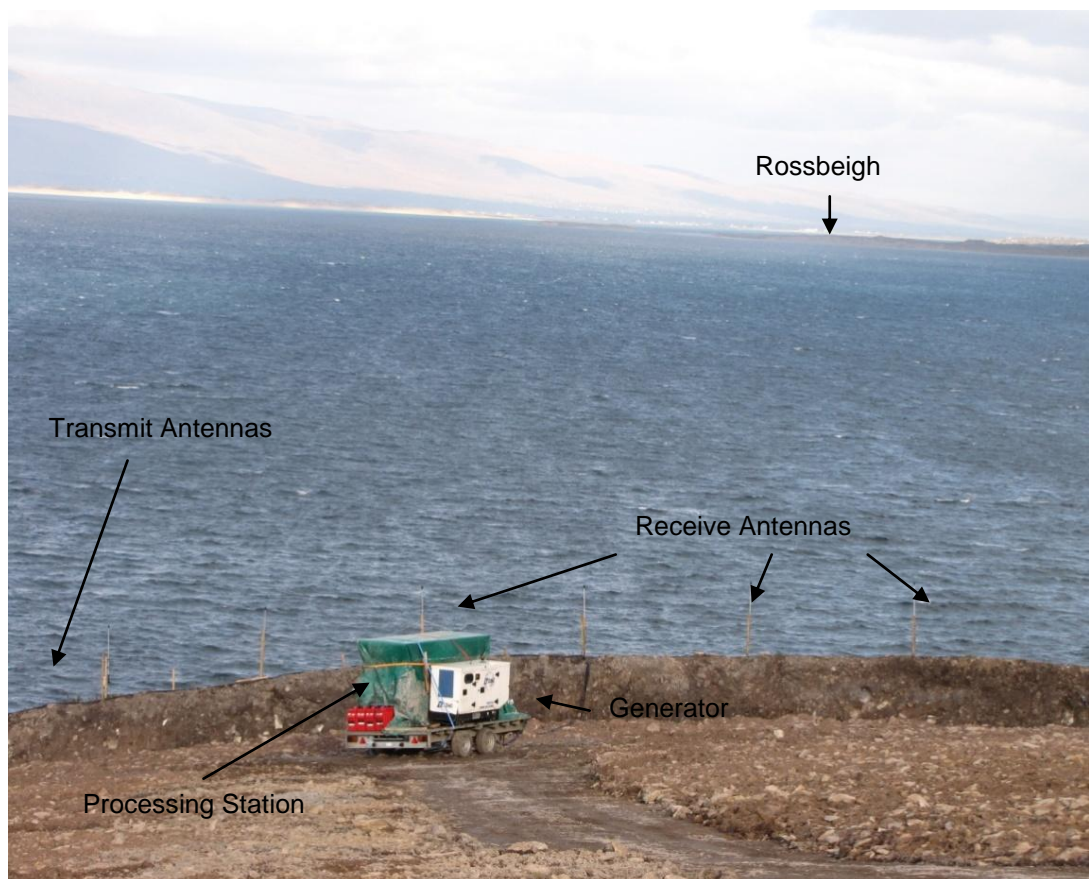


Figure 5.2 South site radar setup looking towards Rossbeigh



Figure 5.3 North Site radar station setup looking toward Inch

Developing a solution to power the radar equipment was the next stage of the trial. Once permission from the site owners was granted on the northern site, the WERA station was powered from electricity mains of a holiday home adjacent to the installation site. The only issue with the source was that it was subject to intermittent power cuts. This had the potential to damage the equipment and result in the loss of recorded data. A solution based on consultation with the WERA was formulated. An uninterruptable power supply (UPS) that would allow the system to shut down safely in case of power cut was purchased through Helzel. This enabled the UPS to be calibrated with the WERA system before shipment to Ireland.

The southern site was more difficult to power. The site was 1 Km from power source so it was deemed unsuitable for mains connection. After several designs it was decided that a generator backed battery system using a grid

management system already owned by the HMRC would be the best solution in terms of reliability, cost and convenience.

The initial plan was to purchase a 2.2kw generator to match the max output of the grid management system. This would run the WERA radar system and charge the batteries. The generator would be running for approx 12 hours a day to charge batteries. This design necessitated daily fuel fills at a high consumption and long generator run times. This was deemed unsatisfactory and an option of hiring a larger generator was explored. It was established that renting a larger generator would cost the same amount as buying the original one. The original design utilised a single grid management but the HMRC has 3 such devices. Charging the batteries in three phase using the 3 grid managers and the 3 phase 15 kW generator was investigated

Upon undertaking a cost benefit analysis the revised 3 phase rental generator plan was cheaper in total cost to run, had large storage and only needed 2 hrs run time a day to charge the battery system. The added benefit of remote switch on meant that man hours spent at the site were also reduced.

5.3 Wave Radar Results

Although the radar system was installed in the first week of October 2012 and commissioned on the 7th of October, the first surface current map was produced on the 23rd of October. This delay was due to calibration and on site processing faults. Once operational, the WERA radar systems recorded data until the 17th of November, when the trial licence expired. Within this time frame, there were several periods of non-operation due to problems with the in-situ data processing computers stalling. The most significant gap in result as a result is 4 days between the 11th November and 14th November inclusive.

5.3.1 Validation of Results

As discussed in Section 4.2.1, a Valeport wave gauge was deployed in Dingle Bay during the HF ocean radar trial. The tidal current velocities and wave heights recorded by this instrument are compared to surface currents and significant wave heights measured by the Wera HF ocean radar system.

The Valeport bottom mounted sensor also houses an electromagnetic current recorder as noted in Section 2.4.1. This sensor records the current velocity at an elevation of 1 m above the seabed. The results from this sensor are extrapolated up to the sea surface utilising the $1/7^{\text{th}}$ power law as discussed by De Chant et al. (2005). The extrapolated velocities were compared with a time series of surface current velocities extracted from the Wera HF Ocean radar results from the same location, figure 5.4.

There was a significant difference in tidal current velocity magnitude between the recorded Valeport and radar measured values. The Valeport gauge records a peak velocity of 0.1 m/s while the Wera HF Ocean radar measured the same peak in velocity as 0.7 m/s for the given dataset. The radar derived current velocity time series displayed many peaks and troughs when compared with the smooth variation of the Valeport recorded current velocity.

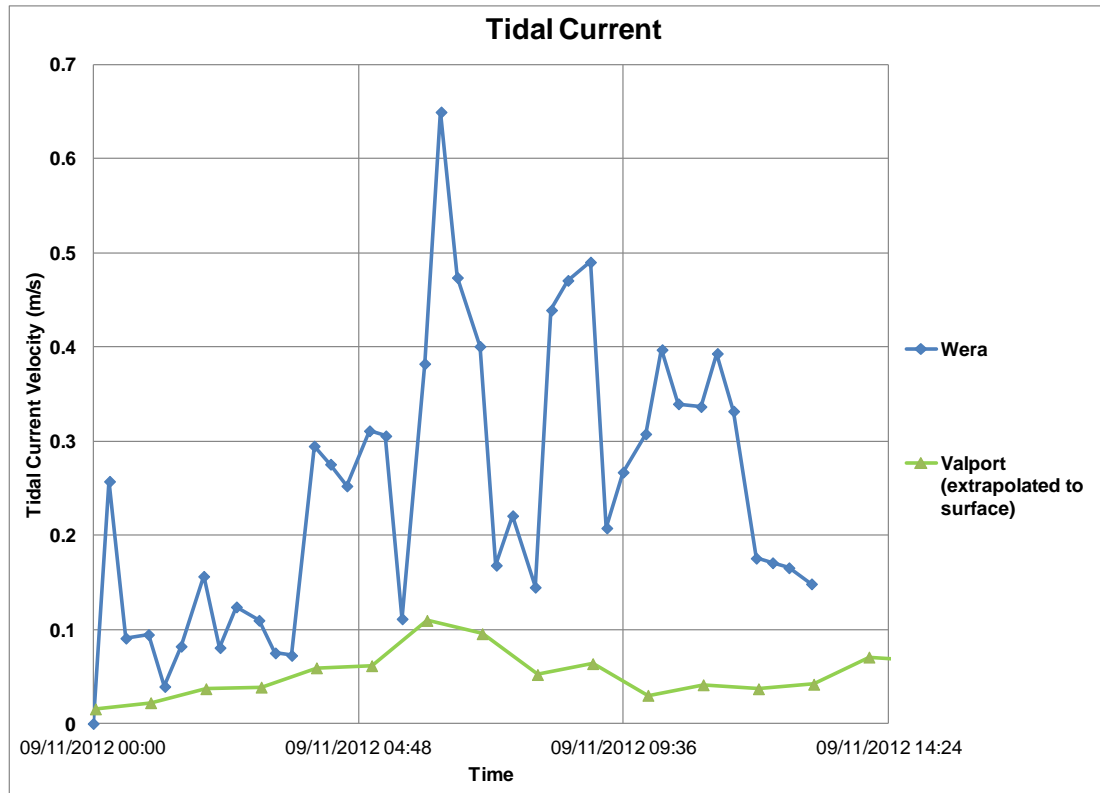


Figure 5.4 Comparison of recorded and WERA measured tidal current

This disparity in surface current time series measurement was also reflected in the HF Ocean radar surface current plot mapping detailed in Section 5.3.2. This indicates that the problem with the radar results was not restricted to the location of the Valeport wave gauge. Erroneous current patterns were widespread across the measurement grid.

Considering the failure to validate the HF Ocean radar surface currents with recorded data, the accuracy of the entire Radar derived data set was unreliable. Without validation of the HF surface current measurements, it was not possible to identify spatial variations in current patterns. Therefore the desired detailed morphodynamic analysis could not be undertaken with confidence. However, despite the unreliability of the dataset, some interesting features are identified from the radar derived surface current maps; these are discussed in Section 5.3.2.

As discussed in Section 2.4.1, analysis of the second order Bragg energy can yield wave energy statistics. The significant wave height and direction

can be deduced if the energy spectrum is not distorted. The range of wave direction data can be detected depends on the area covered by the intersection of beams from both stations and this range is typically half that of the surface current 1st order Bragg energy.

Similar to the surface current validation results, the radar derived wave statistics were poorly correlated with the recorded wave data from the Valeport wave gauge. The H_s , calculated from the Wera HF ocean radar was compared to Valeport measured wave heights, figure 5.5. The radar derived H_s was consistently larger than the H_s recorded at the Valeport. The radar wave height time series also displayed greater peaks and troughs, similar to the radar derived surface current time series.

The largest H_s measured in the radar dataset was 4.2 m while the corresponding value of the recorded Valeport H_s was only 1.35 m. There were also several instances in the data set when radar derived H_s and Valeport recorded H_s were equal. However, the inconsistencies over the entire time of the dataset between the results were too large to assign any confidence in the radar wave height results.

Similar to the surface currents, despite the lack of confidence in the results, some trends in wave patterns in Inner Dingle Bay were observed in the Wera HF ocean radar results. These trends were discussed in Section 5.3.3.

The source of the error noted in the validation of the radar results is discussed further in the Section 5.4.1. The development of a radar data post processing technique to correct the radar derived results was documented in Section 5.4.2. The results of this technique applied to the Inner Dingle Bay radar dataset were presented in Section 5.5.

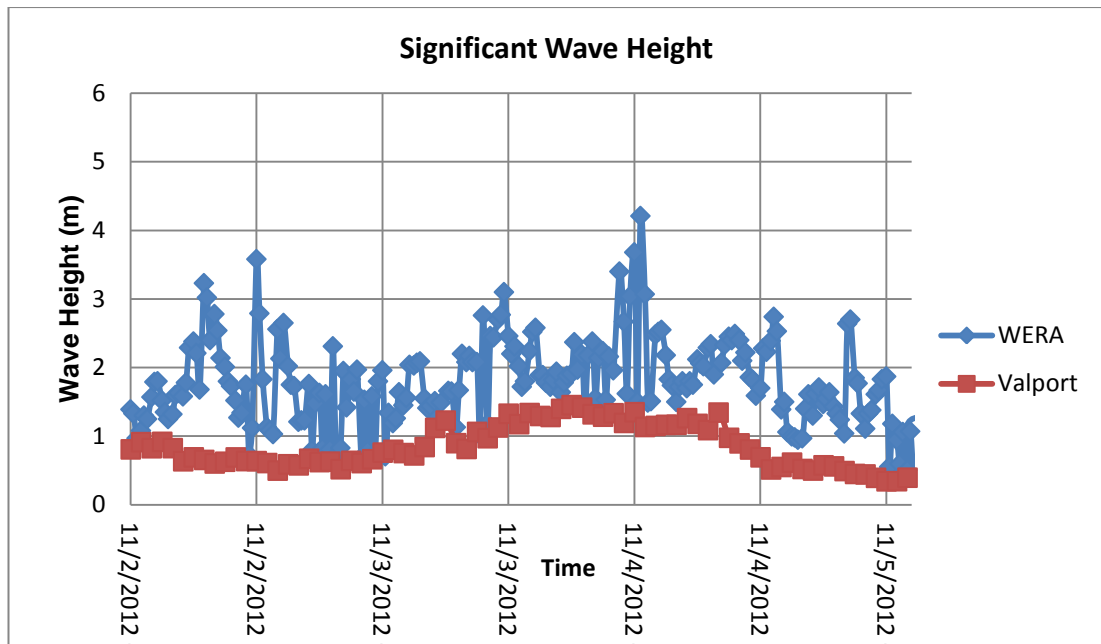


Figure 5.5 Comparison of recorded and WERA measured Hs

5.3.2 Surface Current Mapping

A large percentage of results were erroneous and the analysis of the errors is dealt with in Section 5.5. The results presented in this section represent the best cases in terms of data quality and coverage of the 5 weeks of recorded data.

The current vector maps for a spring tide and neap tide were examined. The processed surface currents were presented in cells on a rectangular grid, figure 5.6. The grid origin was located close to the northern station and extends 120 cells south beyond the southern station and 110 cells to the east covering both barrier beaches and parts of the estuary behind. Each grid cell represents an area of 100 m². The plots also contain directional vector arrows and colour grading to signify velocity magnitude. The direction vectors were averages of 5 cells. The velocity magnitude colour grading was plotted for every grid cell.

Plots of surface currents were presented over a spring tide at mid flood, figure 5.7, to the following low tide figure 5.10, including high tide, figure 5.8, and mid ebb, figure 5.9. This time period coincided with a calm wave climate

in Dingle Bay. The wave height was approximately 0.2 m for the duration of the tidal cycle presented.

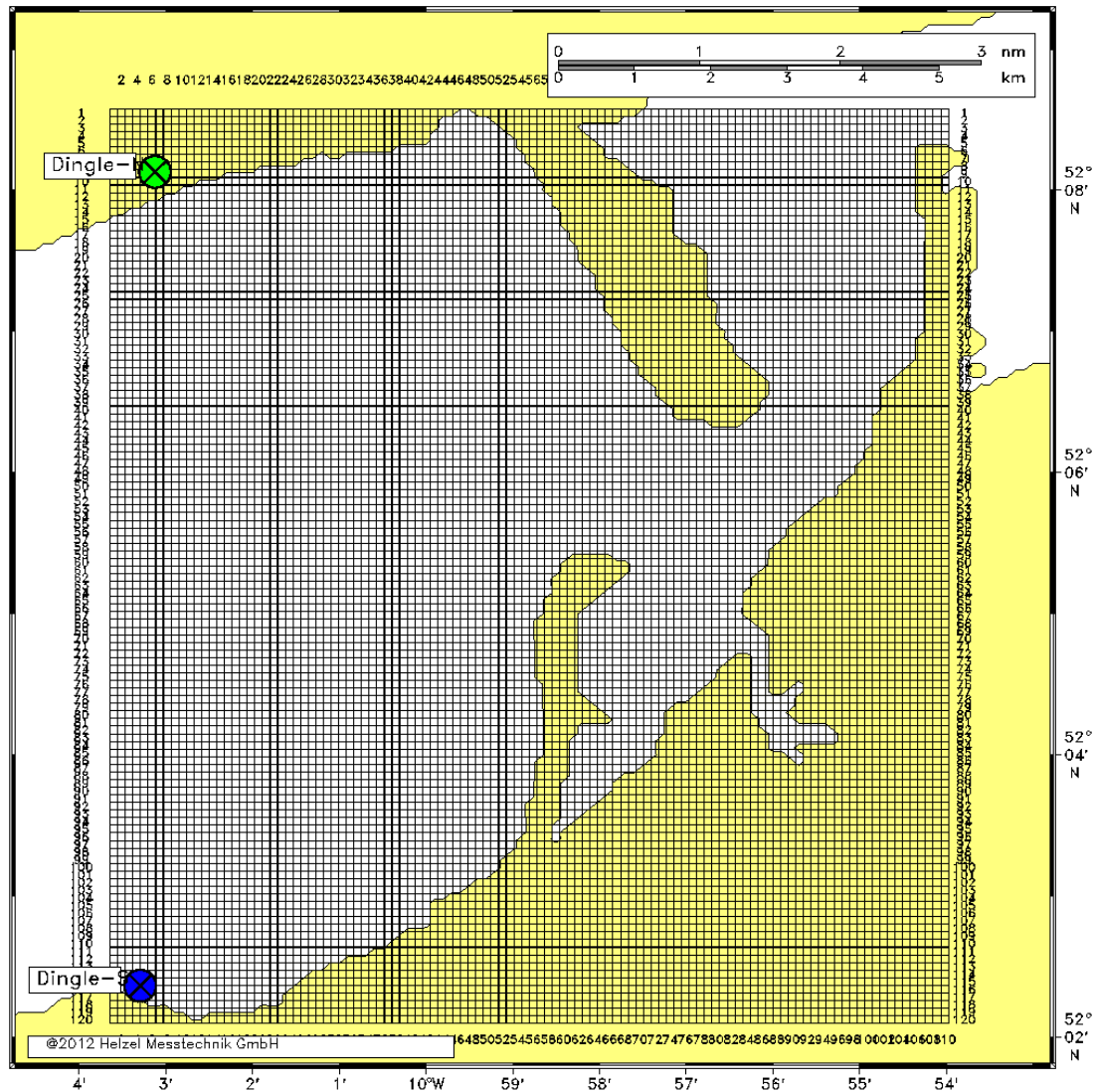


Figure 5.6 Data cell grid of Combined Radar results

The high velocities in the tidal inlet channel in the centre of the bay were not reproduced as expected. Although large velocities of approximately 1.3 m/s were observed at the approximate seaward boundary of the tidal inlet, a distinct channel is not identifiable, compared to numerical modelling plots in Section 6.4. The radar systems recorded very low velocities (>0.3 m/s) in the middle of the inlet channel in where the barrier termini of Inch and Rossbeigh are closest. High velocity currents would be expected that this location during mid tide.

Strong currents of 1.3 m/s at the northern tip of the distal section of Rossbeigh were recorded, while the direction of along shore current in the channel between ebb tidal delta and drift aligned shore as reported in Section 4.3.2 was reproduced by the radar results. The dynamic nature of surface currents at mid tide on the ebb tidal delta was captured. Speeds of up to 1.1 m/s were recorded flowing over the bar in a progressively drift aligned shore normal direction.

The shore parallel currents measured on Inch became progressively stronger in a southerly direction towards the beach distal end. A maximum current of 0.9 m/s was recorded at the end of the swash aligned end of Inch thereafter the current reduces as the shoreline adopts a slightly drift aligned orientation.

One of the primary features that suggested the measurements were unreliable was the strong band patterns visible in the plots. Radial bands of higher current velocities emanated from each station. These bands were present throughout the dataset and distort the plots in critical areas of morphodynamic interest such as the tidal inlet and ebb tidal bars. A distinct band of higher surface current, presumed to be erroneous emanates radially from the North station and bisects the ebb tidal bar. A solution methodology to remove this error is discussed further in Section 5.5.

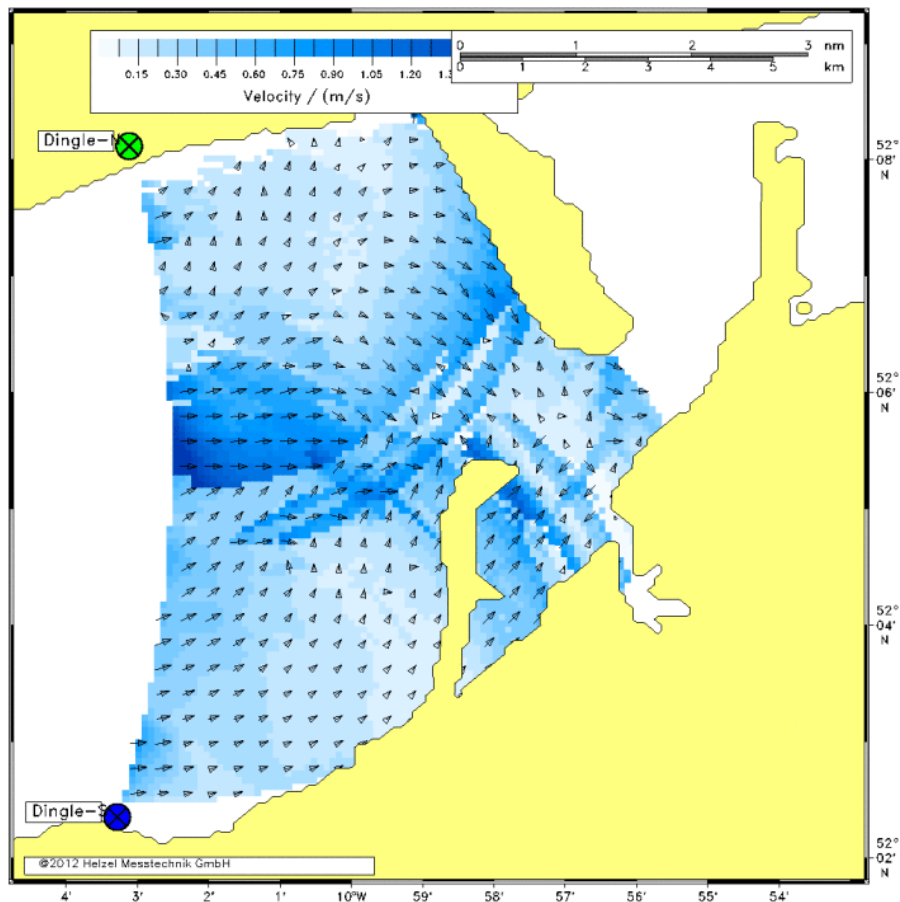


Figure 5.7 Surface currents at Spring tide mid flood

The surface current patterns on a calm, low wave energy spring high tide are presented in figure 5.8. As expected, the velocity levels were very low relative to velocities recorded at mid flood. It is apparent from these plots that little surface current circulation occurred at high tide when wave energy was low. In this low energy sea state the presence of the radial band error was more pronounced with several bands of residual energy visible from the northern station.

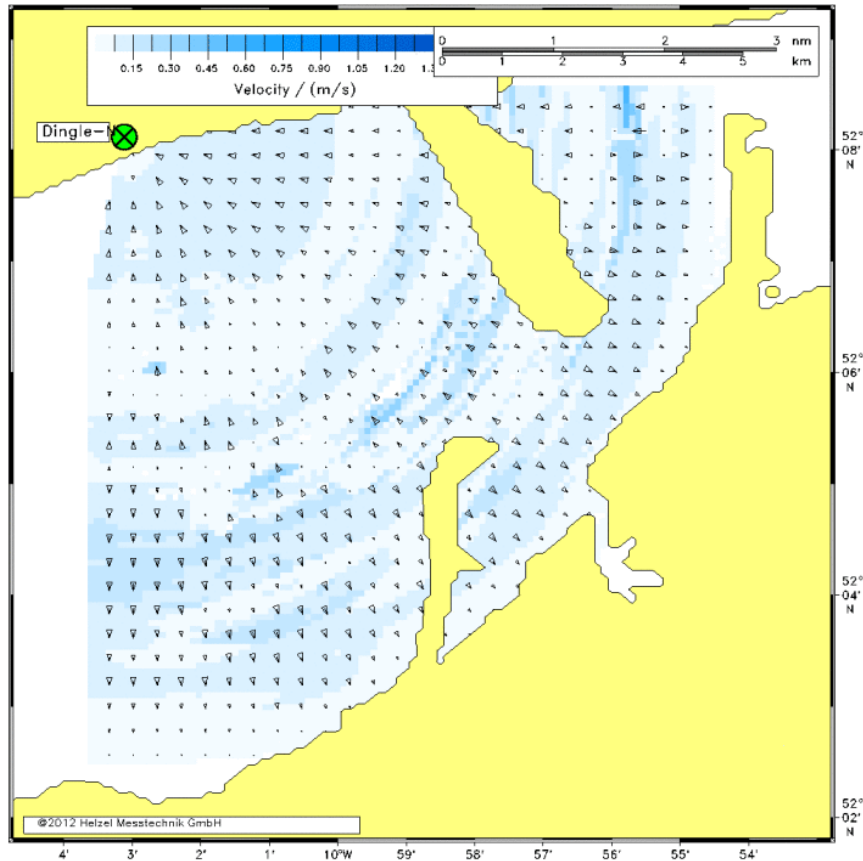


Figure 5.8 Surface currents at Spring high tide with low wave energy sea state

The surface current plot of the spring mid ebb, figure 5.9, was similar in pattern to the mid flood with the directions reversed. High velocity flows were visible in both the inlet channel and the seaward interface of the ebb tidal bar. Velocities were larger than the flood peak velocities with maximum flow over ebb tidal bar and inlet channel approximately 1.4 m/s.

The surface currents measured in the region between Inch and Rossbeigh were not what would be logically expected or as observed in the field. The mid ebb plot suggests that the current flowing from the estuary between the two barriers is zero. However, further eastwards, large velocities were recorded as expected where the inlet channel is constricted by Inch and Cromane. This suggests that there was a gap in coverage of the radar stations during mid ebb. Coverage in this area was sporadic throughout the ocean radar trial. The most likely cause was interference by the Island dunes at the distal end of Rossbeigh with the South station backscatter.

This intermittency of coverage combined with the continuous presence of erroneous error bands severely reduces the confidence in the results of the radar.

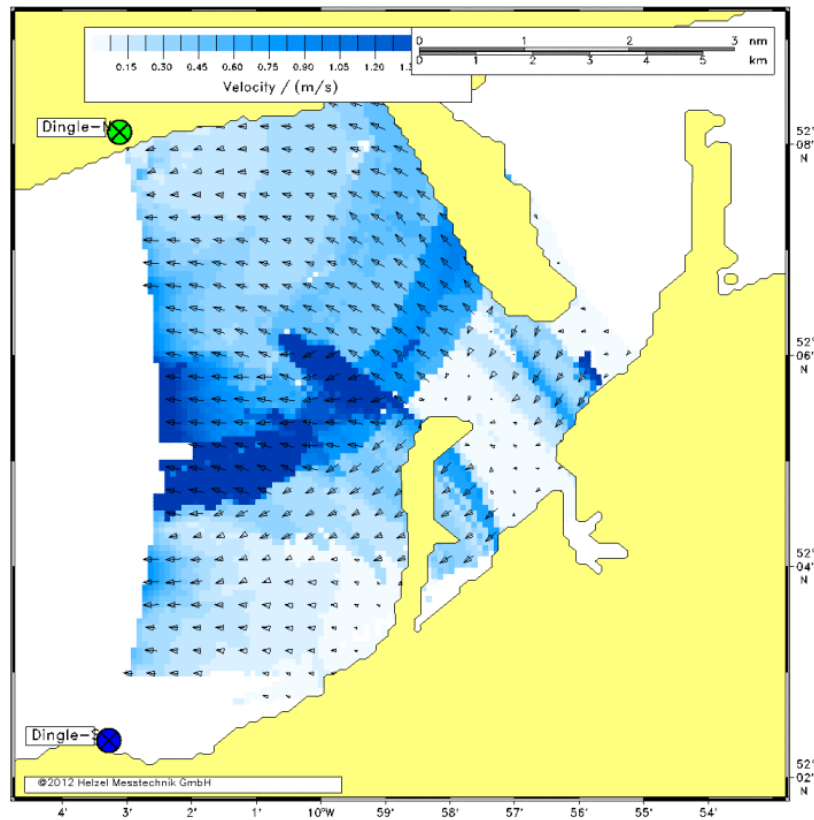


Figure 5.9 Surface currents Spring tide mid ebb

The spring low tide plot figure 5.10, revealed some interesting characteristics. The zero velocity areas recorded in front of Rossbeigh drift aligned shore, was possibly due to the influence of the ebb tidal bar. The zero velocity area closely matches the outline of the intertidal plan of the ebb tidal bar, figure 3.14. An area of large velocity recorded at the sea ward end of this zero flow area was most likely to be caused by breaking wave driven currents. Even though wave conditions were mild at this time, wave breaking has been observed during bathymetry surveys in this location during calm periods. It was most likely caused by waves breaking over sub tidal sand bars seaward of the ebb tidal delta.

There were also visible signs of error in this plot. The radial banding evident at other stages of the tide was again present. Subtle bands from both north and south stations were visible, particularly in the area of the tidal inlet

channel between Inch and Rossbeigh. The constant presence throughout the tidal signal suggests that the banding error was not tidally linked. It appears to be a systematic error.

While the surface current results are presented for just one semidiurnal tidal cycle. The features described here including errors were repeated throughout the radar dataset.

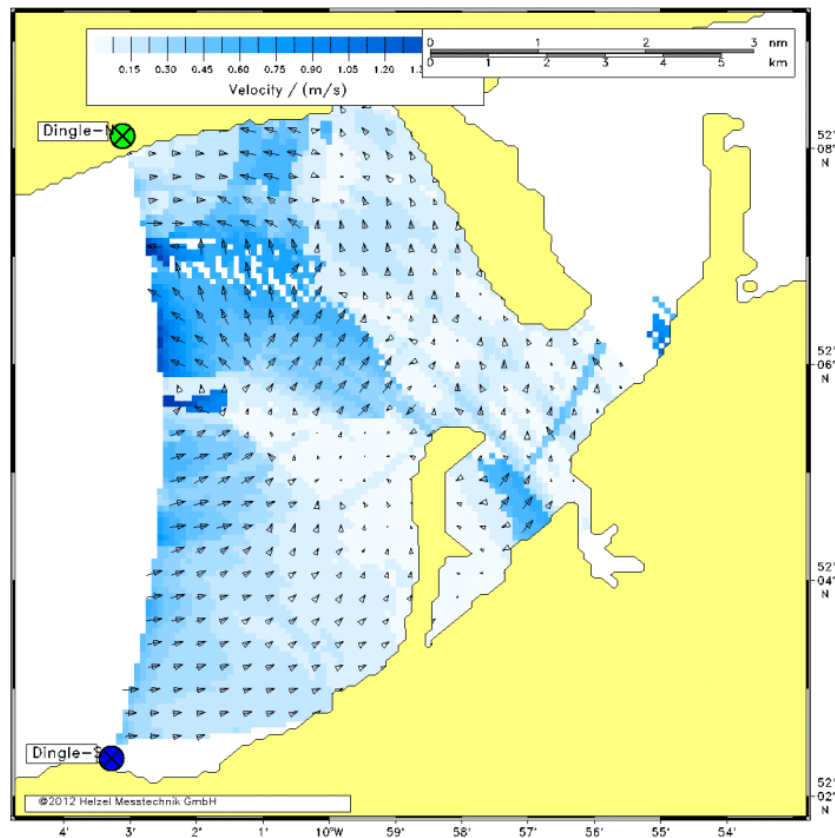


Figure 5.10 Surface currents at spring low tide

5.3.3 Wave Height Mapping

The wave height and direction were examined for a low energy ($H_s < 0.2$ m) and high energy ($H_s > 1.5$ m) event at low and high tide. As these plots were derived from the same data as the surface current plots, the same errors were evident. The wave height at low tide during a period of low wave height is plotted on figure 5.11. The banding error emanating from the northern station dominates this plot. The scale of wave height was over exaggerated in the areas of expected high wave energy.

The wave radar results did identify the outline of the ebb tidal bar in front of Rossbeigh. The shape of the bar was represented by low with a surrounding high energy border.

Large wave heights were also recorded seaward of the tidal inlet termination and in the tidal inlet channel north of Rossbeigh. The directional vectors were scattered in the area seaward of the offshore ebb tidal bar suggesting a large amount of turbulence associated with breaking waves.

There were erroneous directions in the north of the plot showing waves moving in a northerly direction, which was an unlikely scenario. The waves should be moving in a westerly direction. The presence of strong radial band of energy that emanated from the northern station highlights the errors previously mentioned. The plot incorrectly indicates that large wave heights existed behind Inch. Given the sheltered location this was not a valid result from this location.

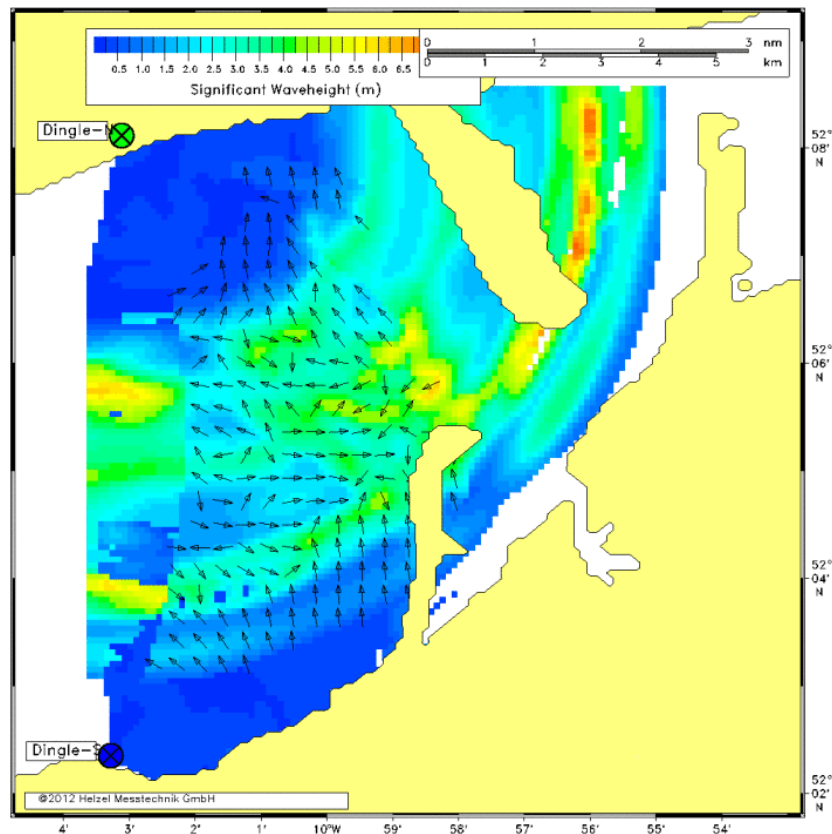


Figure 5.11 Mild wave climate at low tide

The outline of the ebb tidal bar offshore of Rossbeigh was not identifiable during the high tide plot during this mild period, figure 5.12. This was expected, as the low tide outline was likely due to waves breaking around the bar. The directionality at high tide shows less erroneous trends than at low tide. The turning of waves moving over the ebb tidal delta discussed in Section 4.3.6 was replicated in this plot close to Rossbeigh drift aligned shoreline. The radial banding error emanating from the north station is very widespread in this plot also.

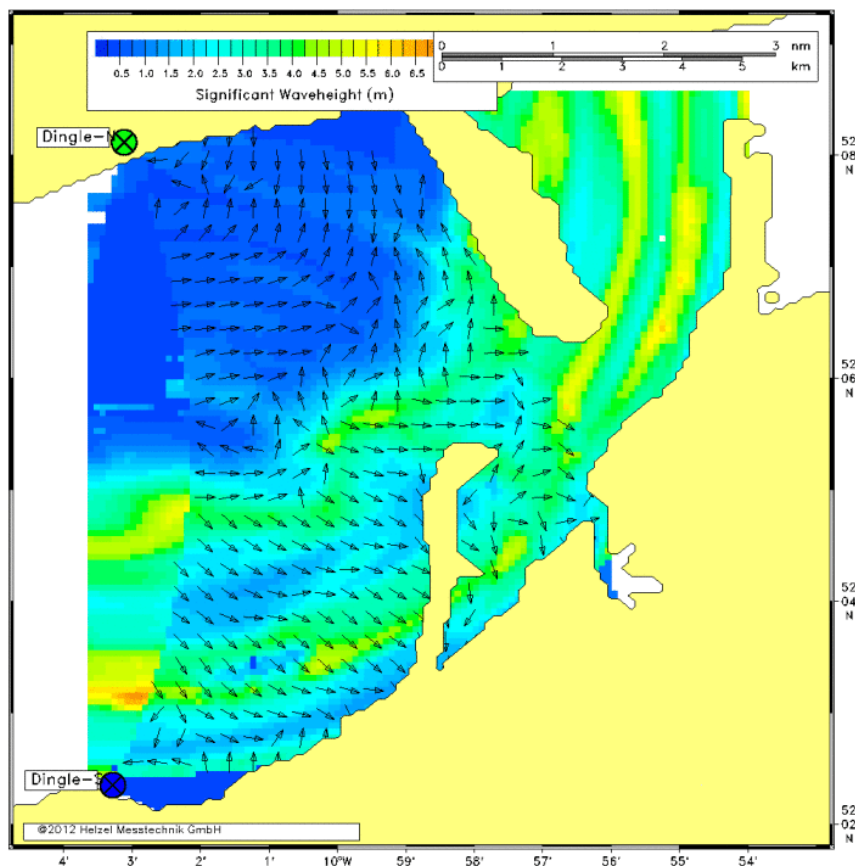


Figure 5.12 Mild wave climate at high tide

The radar recorded wave heights and directions during a storm at low tide, figure 5.13 were unrealistically large and widespread. The directional vector patterns display orbital characteristics. Large radial bands of wave energy were visible across the plot. These features re-affirm the erroneous nature of the radar derived plots.

At high tide during the same storm event, figure 5.14, the banding error reduced. A clear outline of the ebb tidal bar offshore of Rossbeigh is visible

in this plot. However, the wave directional vectors did not agree with wave directions recorded at high tide in this location. The radar results recorded no turning of waves at high tide as reported in Section 4.2.1. The scale of wave height recorded by the radar was double the recorded magnitude.

The wave plots were similarly error ridden as the surface current plots. Unfortunately, the quantitative results expected from the wave radar plots were not achieved. As the radar derived wave statistics were dependent on the same raw data as the surface current calculations, the error analysis in Section 5.4 is relevant. The reasons why the wave radar failed to produce consistent reliable data is discussed in Section 5.7.

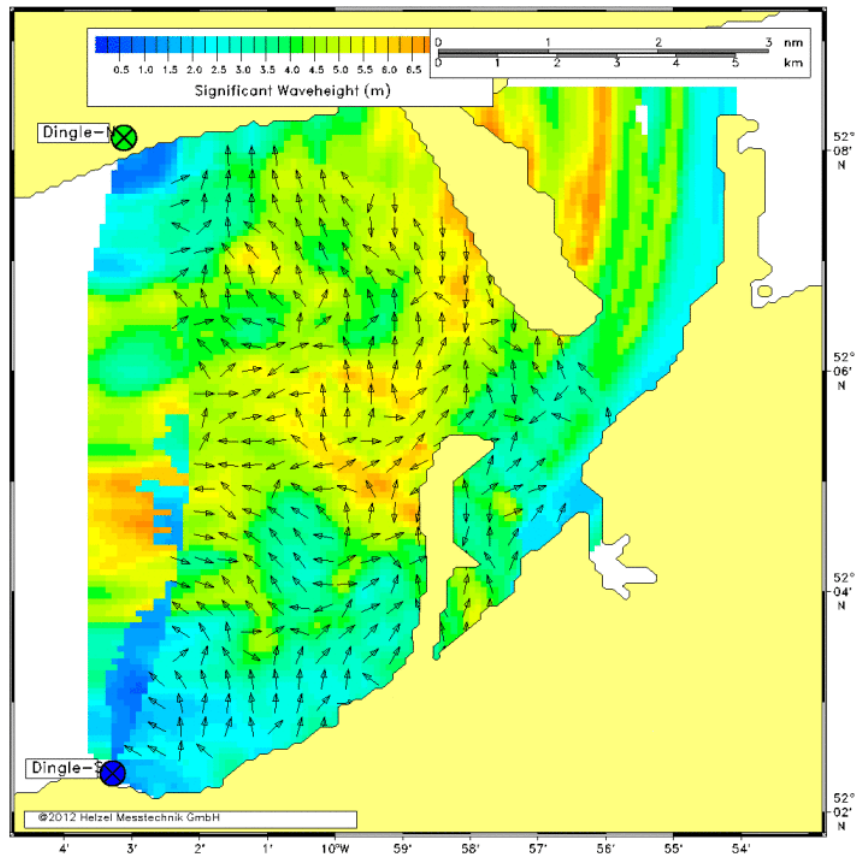


Figure 5.13 Large wave climate at low tide

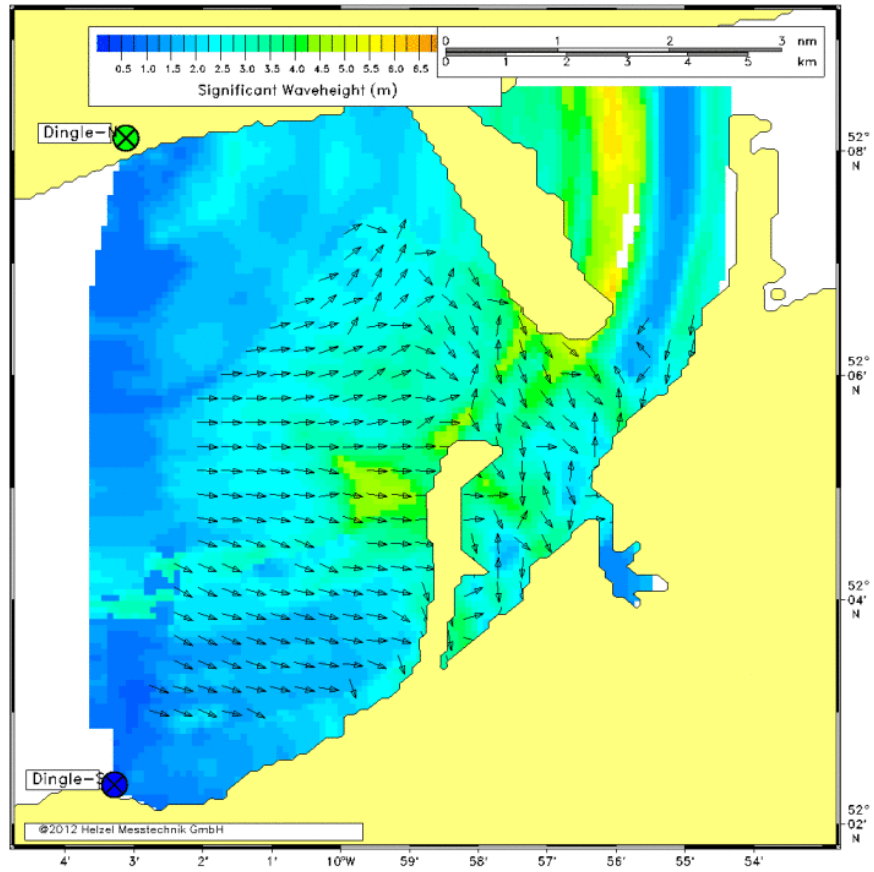


Figure 5.14 Large wave climate at high tide

5.4 Error analysis

It was evident from the analysis presented in Section 5.3 that the majority of radar results were predominantly erroneous or contain significant errors. This rendered any conclusions on the morphodynamics derived from the data unreliable. In an attempt to enhance the quality of the plots, a second stage of data post processing analysis was developed. The aim of this analysis was to identify the source of the erroneous results and rectify the associated errors in the radar results plots.

A new method of error analysis was developed in co-operation with Professor Mal Heron of Cooke University who is an expert in the field of HF Ocean radar.

5.4.1 Error Identification

The first step in developing a solution was identifying the main causes of the erroneous data. In particular, identifying the source of the banding error visible in most wave and current plots. This identification process involved examining the raw surface current radar data from the Dingle Bay radar trial and comparing the results to numerical modelling results.

A hydrodynamic model of Inner Dingle Bay was developed using DHI Mike 21 HD & SW, as discussed in Section 2.5.2, to simulate surface currents. The set up and validation of this model is presented in Section 6.2. A version of this model was run over the same time period as the wave radar trial. The model was driven by offshore weather buoy data and predicted tidal heights. It was validated by the Valeport measurements presented in Section 6.3. Tidal current vectors with magnitude and direction were produced and plotted for similar times as the radar outputs. Maps of the significant wave height and wave direction were also plotted.

The dataset of simulated tidal currents were compared to a radar surface current plot of the same time, figure 5.15. This plot was used as a reference to identify locations in Dingle Bay where the radar surface current contrasted significantly with the simulated tidal current velocity vectors. The raw data

from the grid cells relating to these locations was then analysed to identify the source of erroneous velocity vectors.

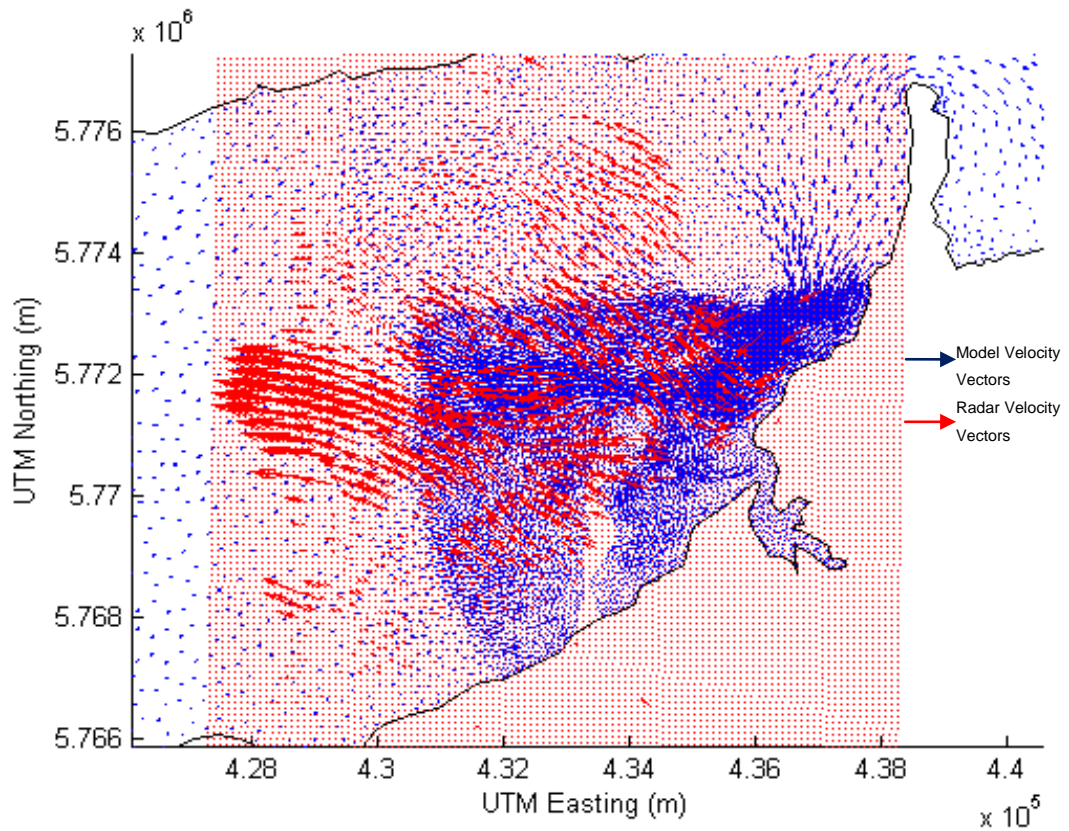


Figure 5.15 Radar derived surface current velocity vectors overlaid on simulated velocity vectors

The raw Doppler frequency shift spectrum files from each station were examined at several of the locations where erroneous results were identified. The Doppler frequency plots, figure 5.16 and figure 5.18, represent the backscattered Doppler energy plotted against frequency for individual radial cells. However, the shape of these plots were significantly different to the typical Doppler frequency plot from a HF ocean radar station, as seen in figure 2.36, Section 2.4.1. These plots represent two significant errors identified in the raw data.

The first error, figure 5.16, was the uneven broadening of the right Doppler peak compared to the left. This error was common in the southern station data files. The left and right Doppler peaks seen in this figure at ± 0.58 Hz should be relatively equal in terms of energy and frequency spread, but the

left hand peak is much larger. This was likely due to additional energy being included in the creation of these plots.

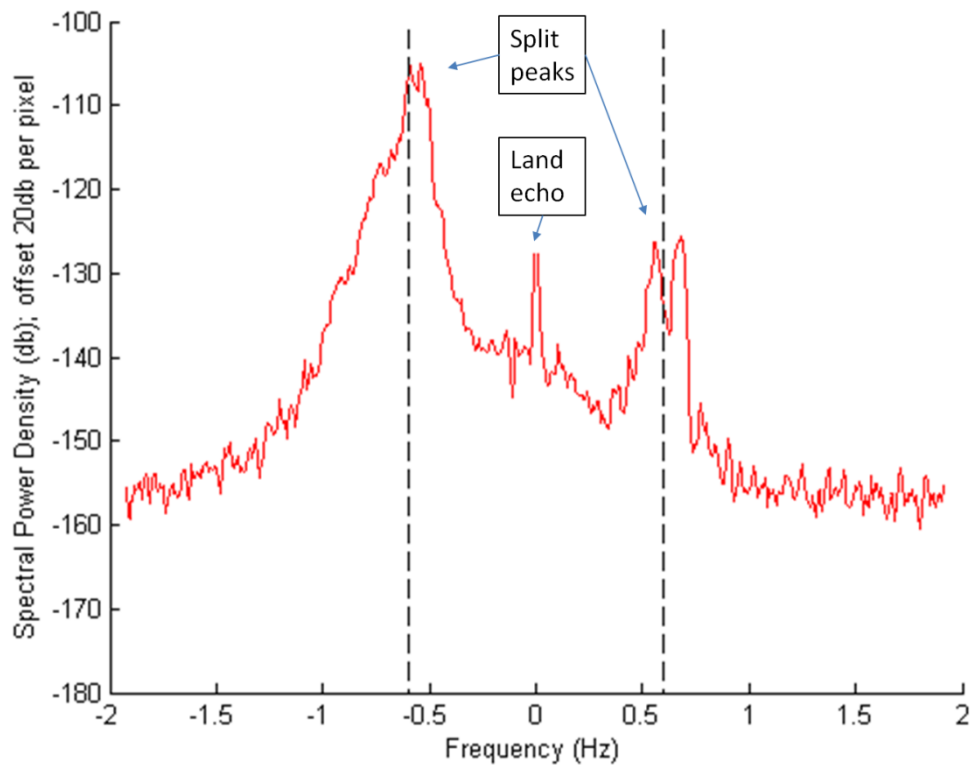


Figure 5.16 Uneven Doppler shift

The source of the error, Doppler peak broadening, was identified as additional energy from side lobes being included in the analysis process. The spectral energy of each grid cell from each station was computed from the main beam of radar and also from side lobe energy, as shown as the dashed red line, figure 5.17. In normal ocean radar circumstances this is legitimate as there is no major impact on results by including side lobe energy due to the homogeneity of the open ocean currents. However, in a semi enclosed bay with protruding land forms and high shear currents the inclusion of method can significantly impact the spectral energy signature of the grid cell.

For example, in figure 5.17 the main beam, black dashed lines, covers an area of large current, but the 1st side lobe, the red dashed line, covers an area of zero velocity. The Doppler energy for the cell, black rectangle, was

calculated from spectral energy measured from both main beam and side lobes, thus giving erroneous spectral energy signatures.

9

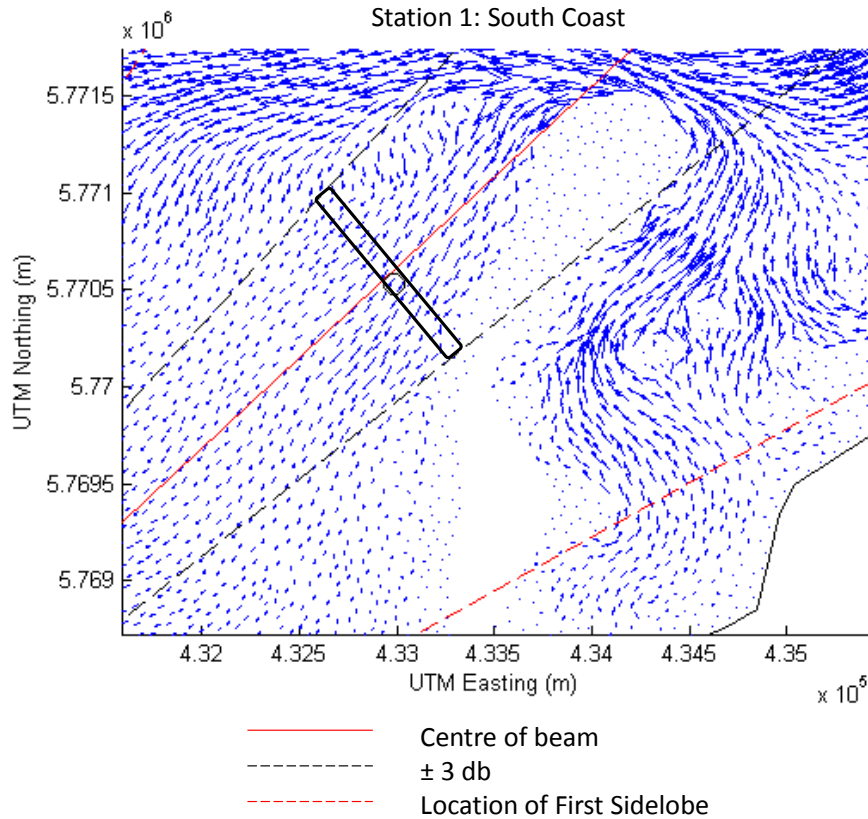


Figure 5.17 Side lobe impact on grid cell data

The second error identified by comparing simulated and radar derived surface currents was the presence of excess land echo. This was seen as a distinct spike in the spectral energy plot, figure 5.18, at 0 Hz. The presence of land echoes is not unusual in Doppler energy plots, but standard software processing undertaken should differentiate it from real “sea echoes” like the Doppler peaks.

However, the strength and interference pattern associated with the land echo visible in the Dingle Bay Doppler energy plots appeared to be interfering with the standard analysis algorithms. This problem was visible at both stations but was predominantly related to the Doppler plots in the northern station.

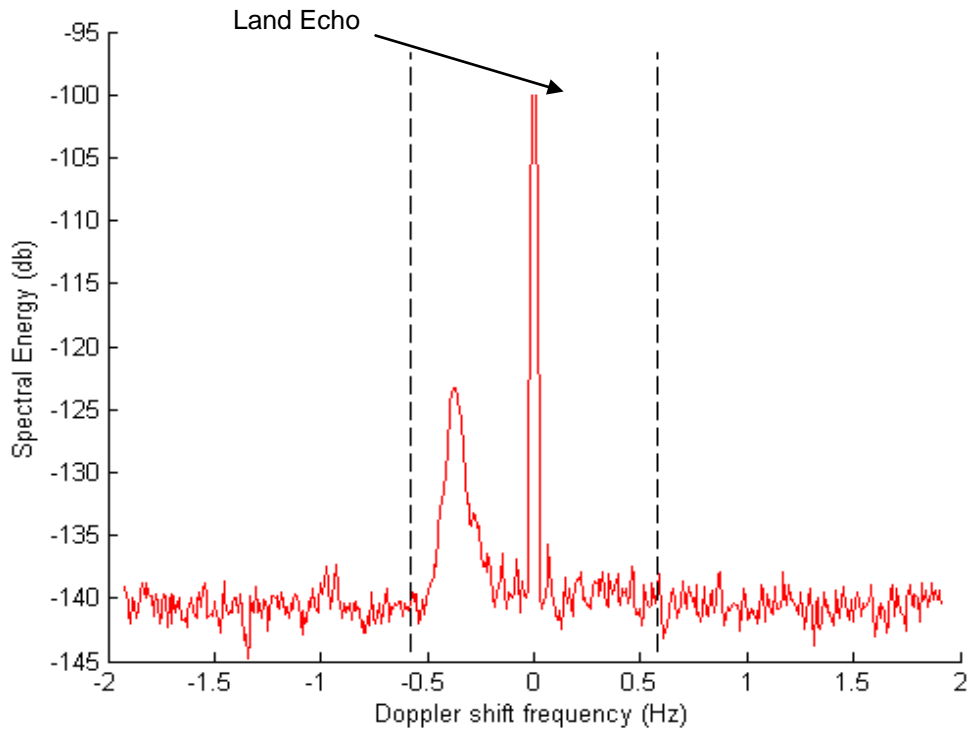


Figure 5.18 Land echo interference

Professor Heron developed a method to identify the two sources of error across the entire wave radar grid. The Transect method flags grid cells with Doppler energy spectrum plots that display characteristics of the two error sources outlined. The Transect method is described in detail in Section 5.4.2.

5.4.2 Transect method

This analysis was based on examining the entire spectral energy signature recorded at Dingle Bay from each station at a particular time, figure 5.19. Sweeping through the data, from east to west and in increasing azimuth steps, erroneous energy plots are flagged. The flagged cells were then eliminated and the surface current plots were regenerated.

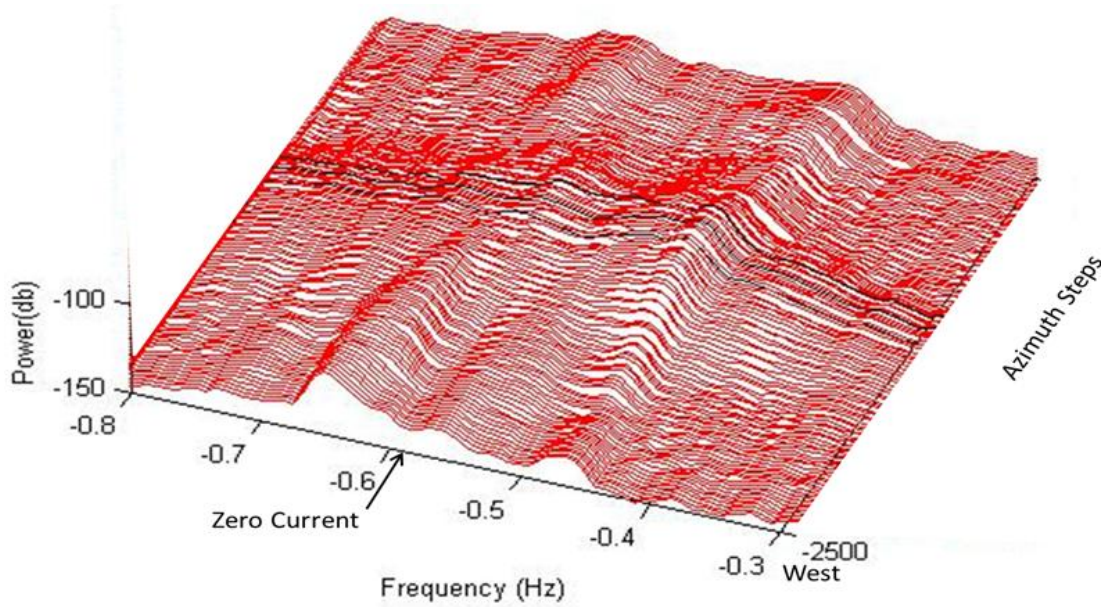


Figure 5.19 Transect of entire grid

The presence of the error related to the side lobe energy in the spectrum was identified by using a limiting condition. The main beam power was predominantly greater than -0 db and side lobe energy was below -13 db, as seen in figure 5.20. Therefore by only considering power above -10 db, the side lobe influence on cells could be eliminated.

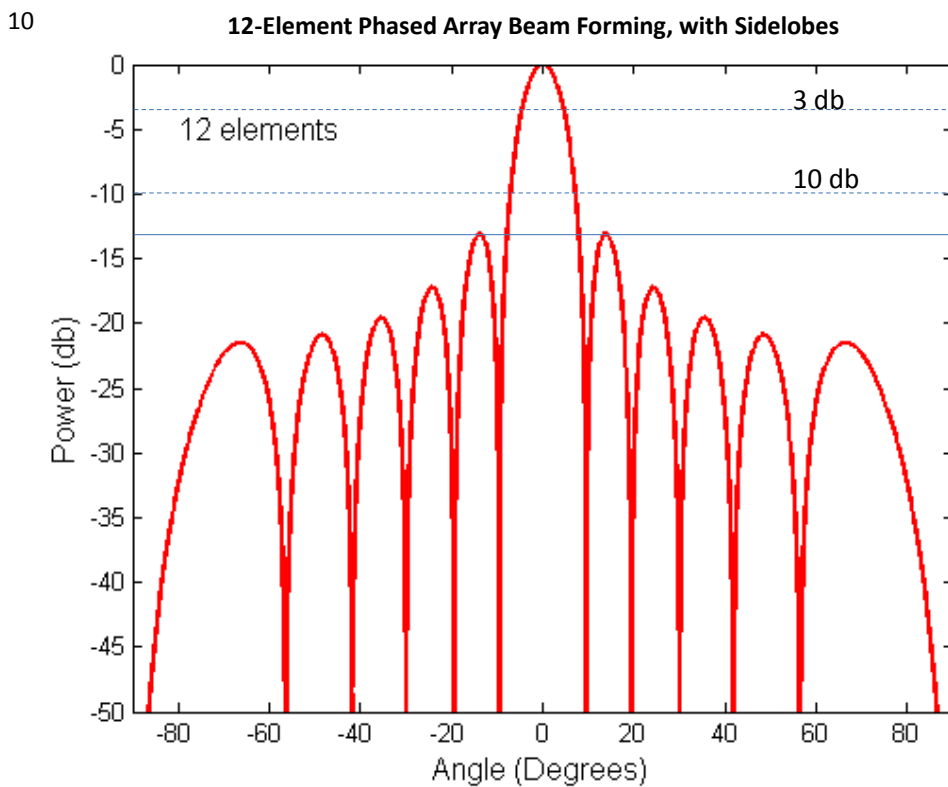


Figure 5.20 Side lobe energy contribution

Similarly, a flag was written to detect the large land echo spectral plots, figure 5.18. If the energy plots fulfilled either the side lobe error condition or land echo condition, they were flagged, as demonstrated by the blue and black dots in figure 5.21. This resulted in an average reduction in the plots by 5,000 points in a grid of 13,200 points. The surface current plots were then regenerated using the reduced flagged grid with erroneous cells excluded. The regenerated results are discussed in the next section.

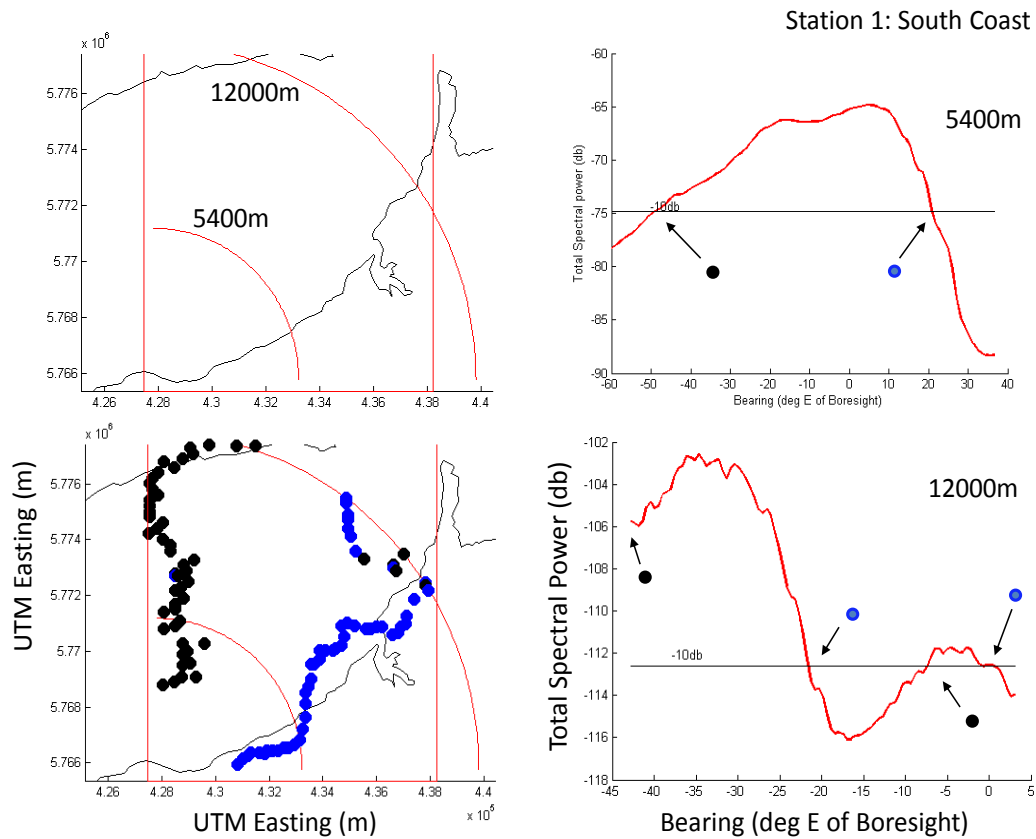


Figure 5.21 Transect flagging method

5.5 Error Analysis Results

To assess the effectiveness of the error analysis procedure described above, the tidal current plots at high tide, mid ebb, mid flood and low tide, figures 5.22- 5.25, were presented in both original form and after undergoing the error analysis. The first obvious result of the error analysis was the removal of the majority of the data east of the barrier dunes. Large currents regularly featured in this area in the original analysis.

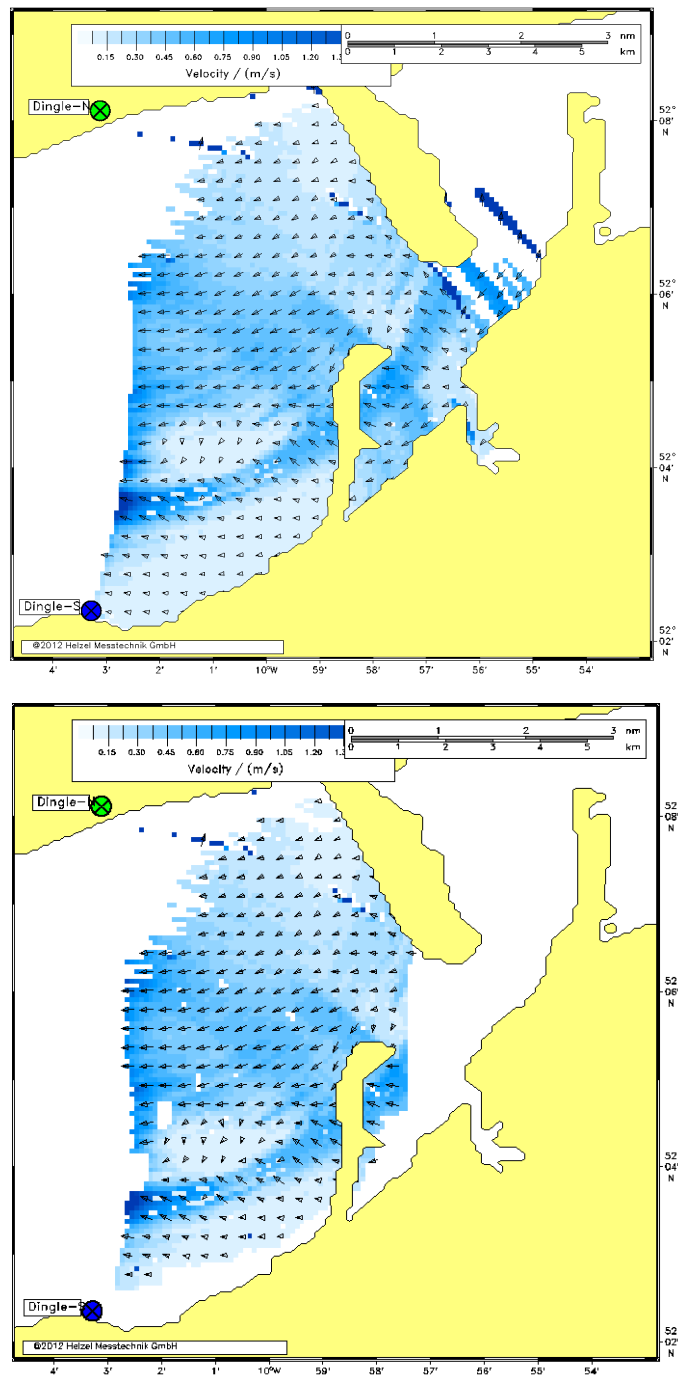


Figure 5.22 High Tide tidal current plot original (upper) and reprocessed (lower)

The error analysis flagging method, however, failed to remove the banding error completely. The erroneous patterns reported in the original analysis were again present in the reprocessed plots. The strong band of energy emanating from the northern station was particularly visible at mid ebb, figure 5.23 and mid flood, figure 5.24. This coincides with higher velocities in the bay.

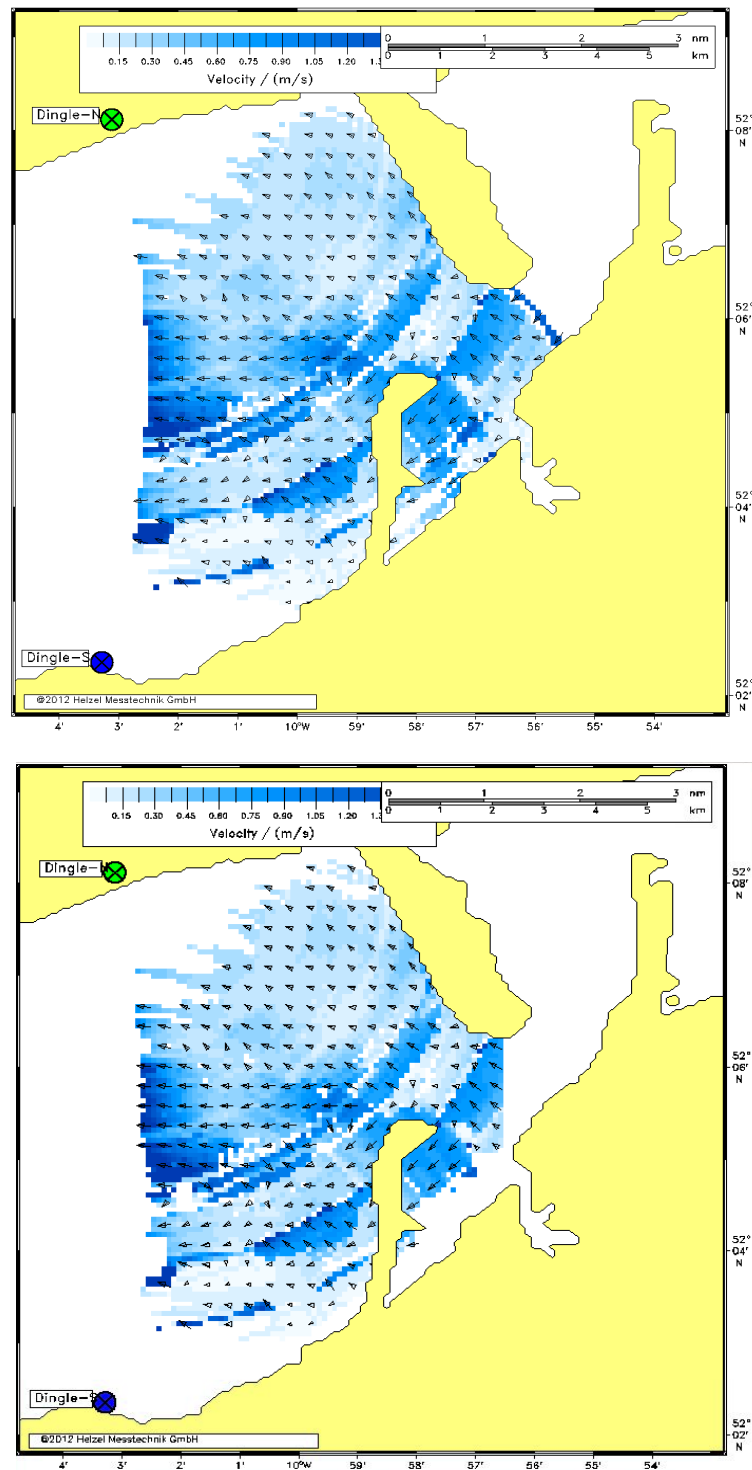


Figure 5.23 Mid ebb tidal current plot original (upper) and reprocessed (lower)

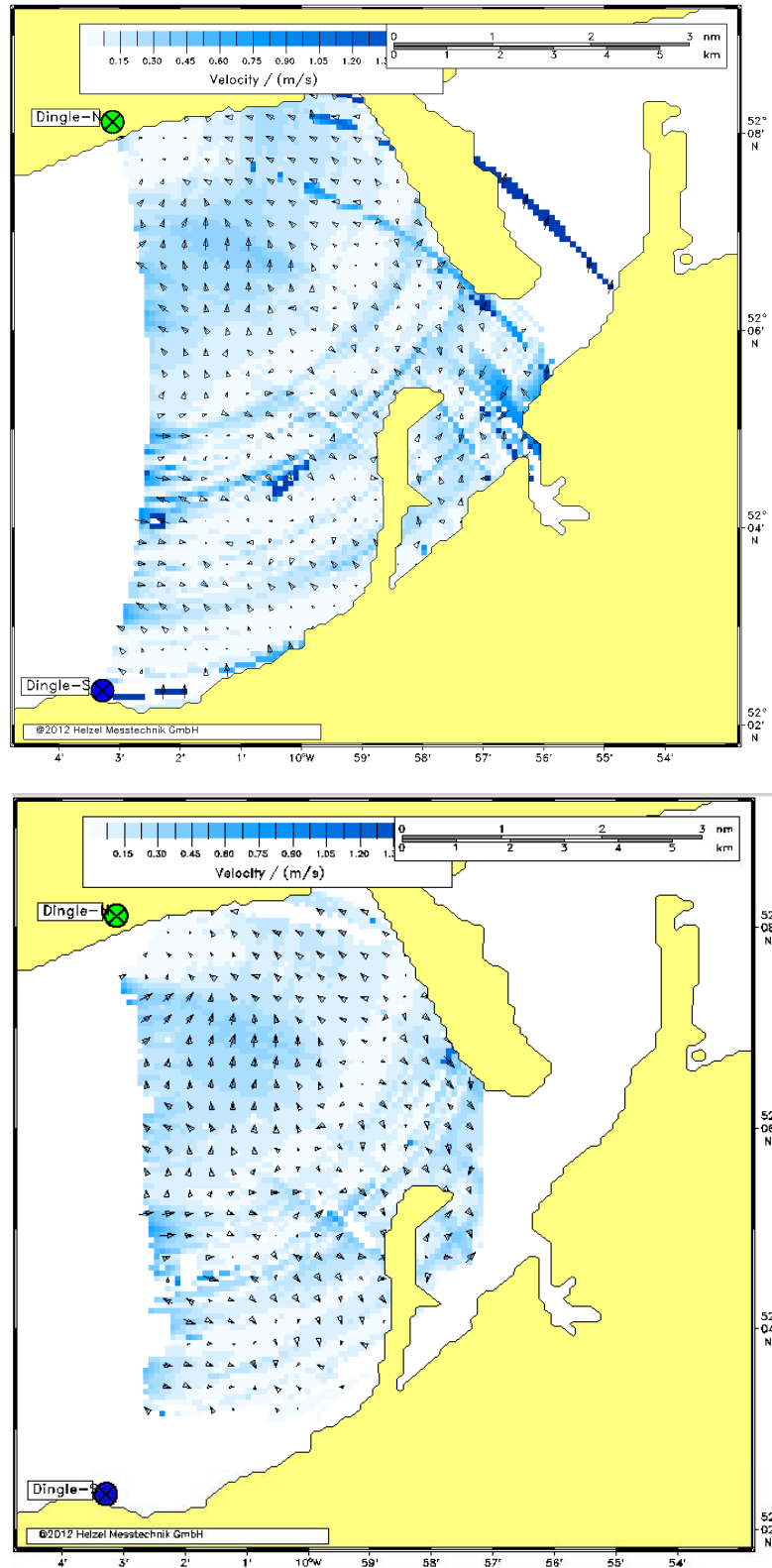


Figure 5.24 Low tide tidal current plot original (upper) and processed (lower)

The re-analysis of the predominantly static sea states, high tide, figure 5.22 and low tide, figure 5.25, have improved with the majority of the strong banding signal reduced. There remained traces of the northern station error through these plots as well.

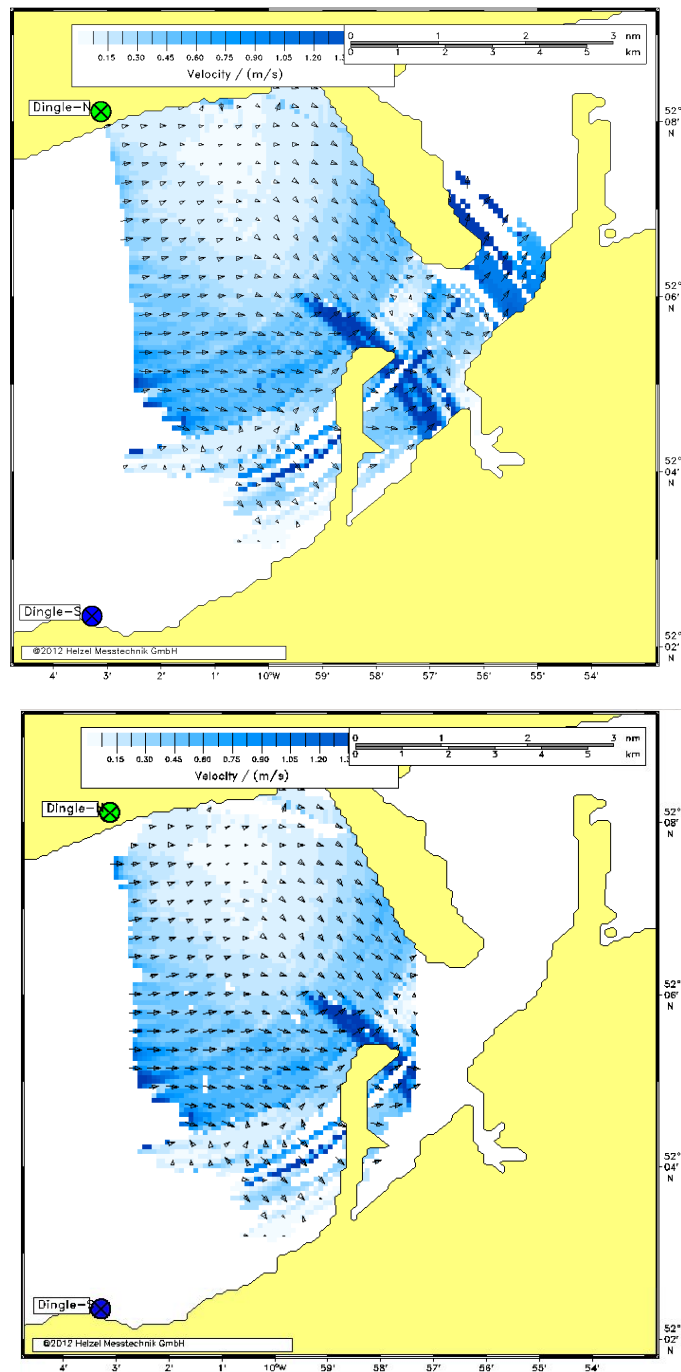


Figure 5.25 Mid flood tidal current plot original (upper) and reprocessed (lower)

It is apparent that this methodology has improved the radar derived surface current plots, but was not in itself a definitive solution for the entire dataset. The error analysis flagging method undertaken should be considered a step to acquiring a dataset with minimal erroneous results. Currently, work by Memorial University Newfoundland is being undertaken on another method of spatial filtering that may yield further refinements to the Dingle Bay dataset.

5.6 Critique of HF ocean radar

The Dingle Bay radar trial failed to produce a reliable dataset from which morphodynamic analysis of the bay could be undertaken. The deployment has raised issues that have not been addressed in ocean radar monitoring previously.

As the Dingle Bay radar trial, utilised the largest bandwidth to date in a Wera radar installation, difficulties in data processing were expected. The high spatial resolution produced very large datasets. However, the scale of erroneous results was unprecedented. After initial analysis, it appears the source of error was related to ocean radar data processing methods unsuitability to capturing the complex hydrodynamics of Dingle Bay.

The failure of standard HF ocean radar processing algorithms to accurately calculate surface current and wave statistics is a major finding. The errors could be due to large variation in surface currents over a small area. Typically ocean radar data is validated in open ocean settings with larger grid resolutions of 1 Km or more. The presence of a tidal current channel of high velocity in close proximity to breaking wave generated surface currents, potentially flowing in opposite directions to each other were too complex for ocean radar to describe in terms of current radials.

Interference of intertidal ebb tidal bars were another possible source of error. The reflection of energy from these bars located in the centre of Dingle Bay potentially contributed to the highly erratic radar plots at low tide. It is notable that several grid cells corresponding to the location of ebb tidal bars were flagged as erroneous in the error analysis documented in Section 5.4.2.

The source of the banding error that remains in the results after the error analysis post processing remains unknown. Given that it was stronger in the northern site it is plausible that the error was related to inconsistencies in the station set up. However, it should also be noted that the error analysis did remove certain bands of erroneous data emanating from the northern station.

Further analysis of this dataset may remove all of the banding errors in both the surface current and wave height plots.

As well as the work being undertaken by Memorial University New Foundland, the Dingle Bay radar dataset is being assessed by ocean radar researchers in Cooke University in an effort to refine the transect method of error reduction further, (Heron et al. , 2013).

5.7 Conclusions

The wave radar WERA system was trialled with limited success in Dingle Bay. The main aim of the trial was to produce plots of wave and currents in the bay, to aid in the identification of morphological pattern. A secondary aim was to assess the technology's suitability in a highly dynamic bay at a spatial resolution higher than typical ocean radar systems. The analysis failed to yield salient results that give insight to the coastal processes in the bay. Ultimately the quality and reliability of this technology remains at an experimental stage when applied to the coastal zone.

One key highlight of this work was the contribution of this dataset to the development of a new analysis method for coastal radars. The dataset has been used to develop the "Transect methodology" for coastal radars, and is also being used to formulate further refinement methodologies, which will be applied to other coastal radar systems.

The results of HF Ocean radar trial in Dingle Bay, was also a clear indication of the limitations of the ocean radar systems being applied to dynamic coastal settings. The standard algorithms and processing methods used in ocean applications failed to describe dynamic environments at a high resolution.

In terms of coastal processes outputs, features identified by other monitoring methods were visible intermittently in radar derived plots. The unreliability of the data, however, prevents any quantitative conclusions on Dingle Bay's morphology. The features visible in certain plots is summarised below:-

- The large currents in the tidal inlet channel in the vicinity of Rossbeigh's northern tip were recorded by the radar system. The speed of these currents was in the same order of previously recorded data.

- Strong shore parallel currents were recorded in the drift aligned zone at spring tide during mid-flood agreeing with previous conceptual model developed in Section 4.2.3.
- Currents, most likely due to wave breaking, seawards of the ebb tidal bar were identified. This area was identified as being highly dynamic zone during near shore bathymetric surveys.
- The outline of the ebb tidal bar was observed to affect the wave pattern produced at high tide. During larger ($H_s > 1.5$ m) storm events the wave height increased on the bar significantly compared to the surrounding areas.
- The turning of the waves at high tide incident on the drift aligned shoreline, a key feature of recent morphology identified in Section 4.2.1, was repeated in lower wave conditions in certain plots of the radar wave output but not in larger storm conditions.

6 Morphodynamic Modelling

6.1 Introduction

This chapter describes the numerical modelling undertaken as part of this research. While modelling has been referenced in other chapters including ocean radar analysis in Section 5.4.1, this chapter is focused on discussing the morphodynamic output of the modelling. The data collected to build such models has already been documented in Section 4.2 and Section 4.3.

The modelling undertaken for this thesis can be divided into three parts:-

- Wave and tidal coupled modelling that has contributed to the results of previous chapters.
- Morphodynamic modelling based on real data sets as collected and documented in Section 4.3
- Finally the scenario modelling based on the interpretation of results from the first two modelling sections.

The numerical modelling software (DHI Mike 21) used in this study was described in detail previously in Section 2.5.2. The model set up including inputs and parameters is presented along with the model validation using hydrodynamic field data and bathymetry.

The results of the grain size trend analysis in Section 4.4 are compared to sediment transport modelling results. Conclusions on the long term evolution of Inner Dingle Bay made from the numerical modelling are also discussed.

6.2 Numerical Model Set up

6.2.1 Model Domain and Boundary Conditions

The model domain, figure 6.1 covered Dingle Bay extending from Castlemaine Harbour in the east to the open ocean beyond the mouth of Dingle Bay in the west. The bathymetry used was a combination of deep water survey data, the inner Dingle Bay survey of 2011 and the near shore survey of 2013 as discussed in Chapter 3.

As mentioned in Section 2.5.2, the model domain was represented on an unstructured mesh. The mesh cell density was varied, based on the complexity of the bathymetry, with density increasing moving from open ocean in the west to Castlemaine Harbour beyond Rossbeigh in the east. The Dingle Bay model domain had three distinct levels of mesh density, an outer bay mesh, an intermediate density mesh in the middle of the bay and a high density mesh covering the area around the tidal inlet channel and Rossbeigh. By reducing the density of the mesh in the deeper areas of the domain where bathymetry was more homogenous, the amount of calculation nodes was reduced and hence computation time of the model.

The wave and tidal input data were applied at the offshore model boundary, figure 6.1. This model boundary encompassed the entrance to Dingle Bay in an arc shape. It was designed to ensure every possible wave direction incident in Dingle Bay could be simulated. A time series of water level elevation was applied at this boundary to simulate the tidal forcings in the bay. Likewise a time series of offshore wave data was applied at the offshore boundary to generate wave forcings incident in the bay.

A land boundary of the domain was also required to be defined. This process involved several iterations due to instabilities in the model at locations of sharp change in bathymetry/topography. Areas of the coastline on the northern shore of Dingle Bay were particularly susceptible to convergence errors. Reducing the severity of change in the land boundary and increasing

the mesh density at these locations enabled the formulation of a stable model domain.

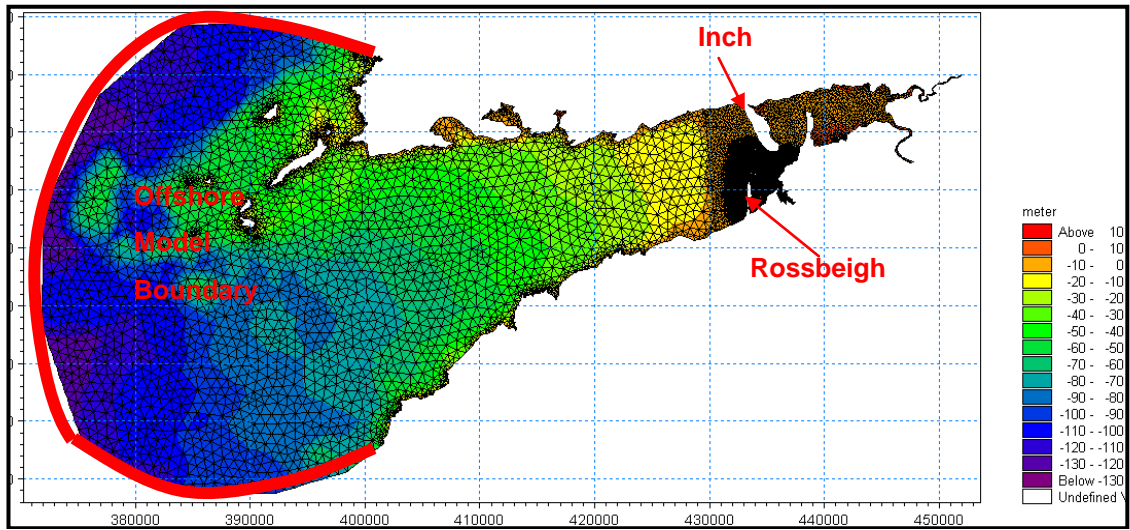


Figure 6.1 Model Domain

6.3 Model validation

Validation of hydrodynamics and wave modules was necessary before morphodynamic modelling of Dingle Bay can be undertaken. The coupled HD and SW models were run with several parameters changed including bed roughness and diffraction coefficients and wave spreading before model results reproduced recorded data records. The following table, Table 6.1, details the final values of the critical model parameters.

In HD model the Bed resistance was the parameter that was varied to achieve validation. The Manning coefficient was varied from 35 m⁻³/s to 25 m⁻³/s before a value of 32 m⁻³/s provided tidal current velocities comparable to recorded values.

The SW model parameters varied were related to wave forcing, specifically the wave spreading value. Early versions of the SW model of Dingle Bay, failed to model the spreading of offshore wave energy from northerly directions into the bay. To improve this, the Directional spreading index was varied. The Directional spreading index, n is given by (20);

$$D(\theta) = \beta \cos^n(\theta) \tag{20}$$

Where $D(\theta)$ = directional distribution function

The wave spreading index, Table 6.2, was decreased until inshore wave heights agreed with recorded values for all wave directions in the offshore boundary.

Table 6.1 Final model parameter values

Module	Parameter	Value
HD	Eddy Viscosity - Smagorinsky	0.28
	Bed Resistance (Manning)	32 m ⁻³ /s
ST	porosity	0.4
	grain size	0.25
	Bank erosion slope failure	30 Deg angle of repose
SW	Spectral	Fully spectral
	Time	Interstationary
	Spectral discretisation	25 frequencies, min of 0.055hz
	Directional discretisation	16 over 360 Deg rose
	Wave breaking	Gamma of 0.8 Alpha 1
	White capping	4.5 - constant
	Directional Spreading Index	4

Table 6.2 Directional spreading index (DHI Software, 2007)

Directional spreading index	Directional standard deviation (deg)
1	39.15
2	32.52
3	28.36
4	25.45
5	23.28
6	21.58
7	20.20
8	19.05
9	18.08
10	17.24
11	16.52
12	15.87
13	15.30
14	14.78
15	14.31
16	13.88
17	13.49
18	13.13
19	12.80
20	12.49

6.3.1 Tidal height and current validation

The water surface elevation was validated against the recorded height at the offshore Valeport location described in Section 4.2.1. The simulated water levels correlate well with the recorded water surface elevations, figure 6.2. Tidal velocity was more difficult to validate as a long term dataset of tidal currents does not exist. The modelled tidal current velocity on the drift

aligned zone of Rossbeigh beach, figure 6.3 was compared with recorded current velocity measured during the field monitoring campaign as described in Section 4.2.2.

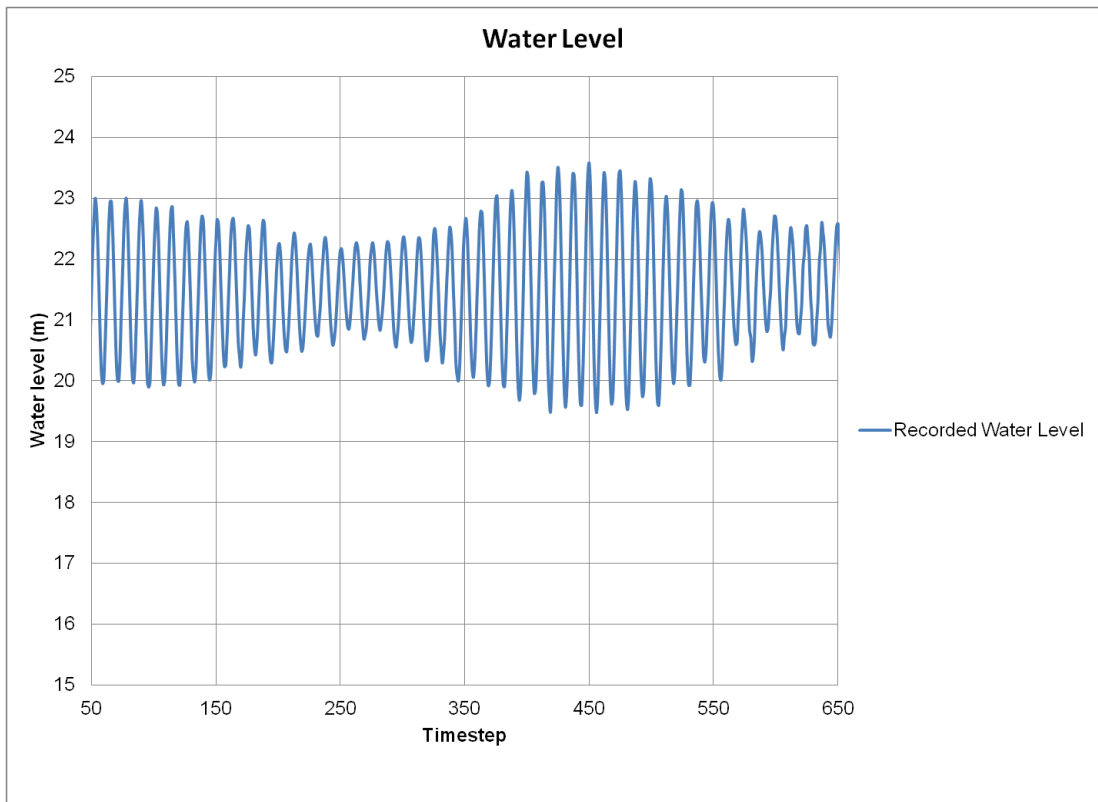


Figure 6.2 Recorded and simulated tidal current velocity in drift aligned zone

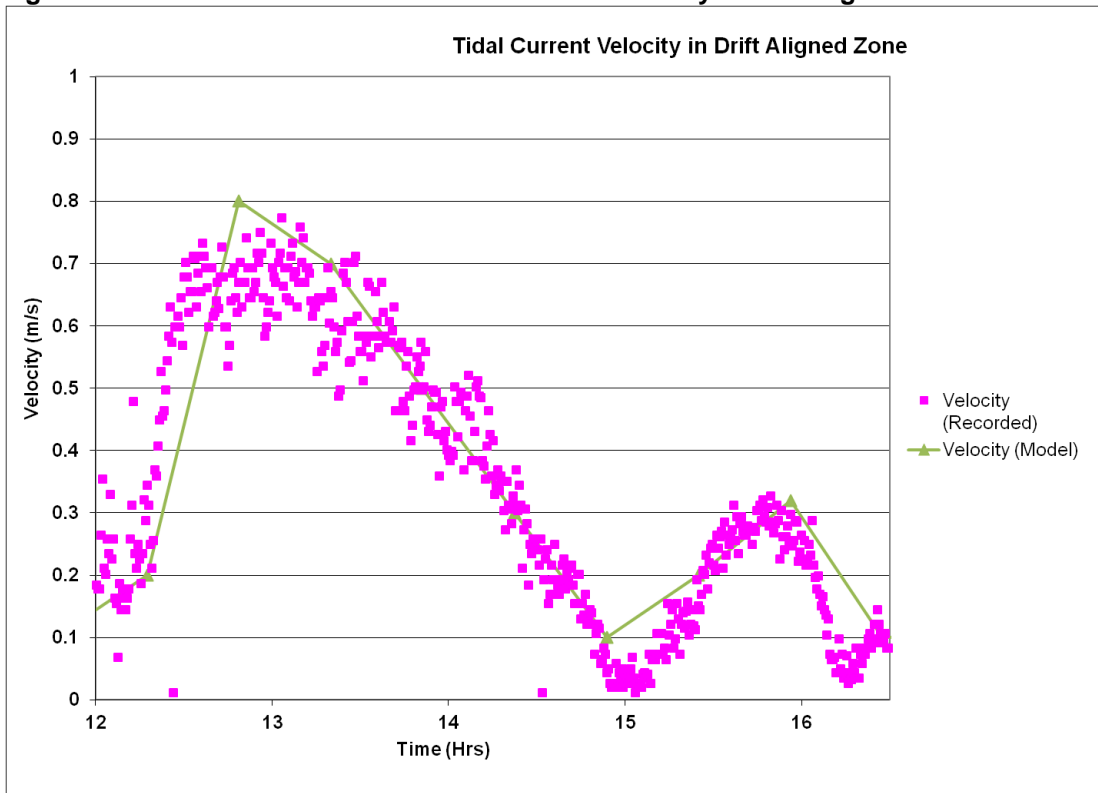


Figure 6.3 Recorded and simulated tidal current velocity in drift aligned zone

The recorded peak flood velocity of 0.8 m/s correlated well with the simulated velocities. The recorded secondary peak ebb velocity 0.3 m/s in the diurnal tidal cycle also agreed with the simulated results.

6.3.2 Wave height and Wave Period validation

The wave height and wave period was validated against a month of Valeport data collected in 2011 and detailed in Section 4.2.1. The modelled wave period T_z shows good agreement with the period recorded at the Valeport location, figure 6.4. The recorded wave period displays less variability than the modelled period and has slightly larger peaks and greater minimum values.

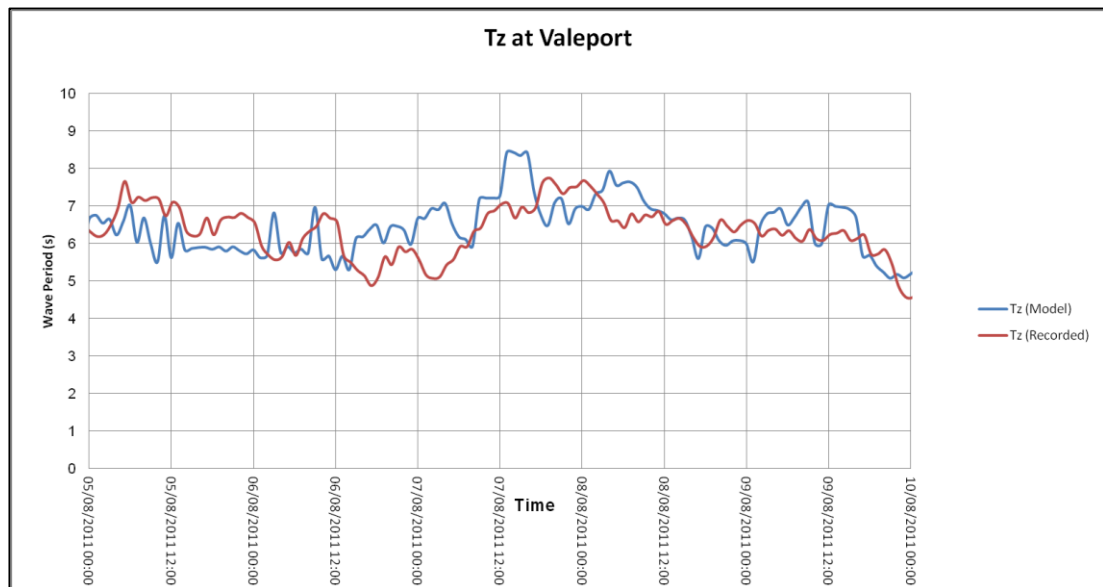


Figure 6.4 Modelled Vs Recorded T_z in Dingle Bay

The significant wave height, H_s also showed good correlation, figure 6.5. During the model calibration process it was difficult to achieve agreement between modelled and recorded wave heights. The solution arrived at was increasing the wave spreading coefficient of the input wave data. This enabled a greater range of swell direction to enter the narrow bay.

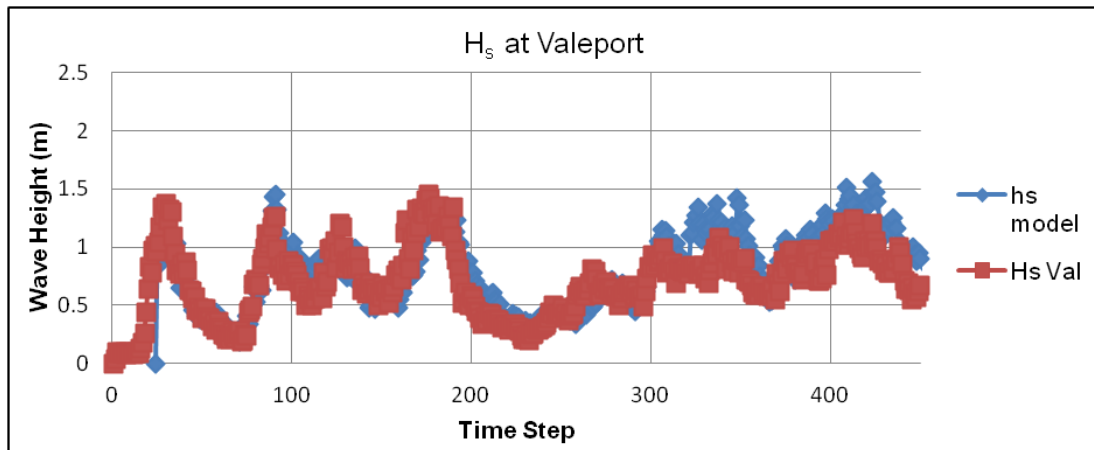


Figure 6.5 Modelled vs recorded Hs in Dingle Bay

6.3.3 Sediment Transport and Morphology

To determine the accuracy of sediment transport and sediment transport modelling, a simulation of 6 months equivalent duration was run. The bed level volume changes were compared with the results of volume changes in bathymetric surveys over a 6 month period, from March 2013 to September 2013. The wave data time series of 1 month duration was used in the model. This data was representative of a mild climate and detailed in Section 4.2.1.

A morphological scale factor was applied to account for the acceleration of bed-level changes during updates at each hydrodynamic timestep. This method reduced computational run time. A morphological acceleration factor (Morfac) of 6 is applied to the model, simulating morphological changes that occurred over approximately 6 months utilising only 1 month of wave data. This form of schematisation was discussed earlier in Section 2.5.3.

The channel location, figure 6.6, was selected for comparison because it has the highest density of recorded data points in the domain. Table 6.3 details the amount of sediment removed from the channel by using cut and fill volumes extracted from TINs of the start and end bathymetry, this methodology was described in Section 4.3.6.

The volume results from the model are similar to the surveyed volume changes. The cut volumes were within 15% of the survey while the fill

volumes were within 5% of each other. The model over estimates the erosion rate but underestimates the fill rates slightly.

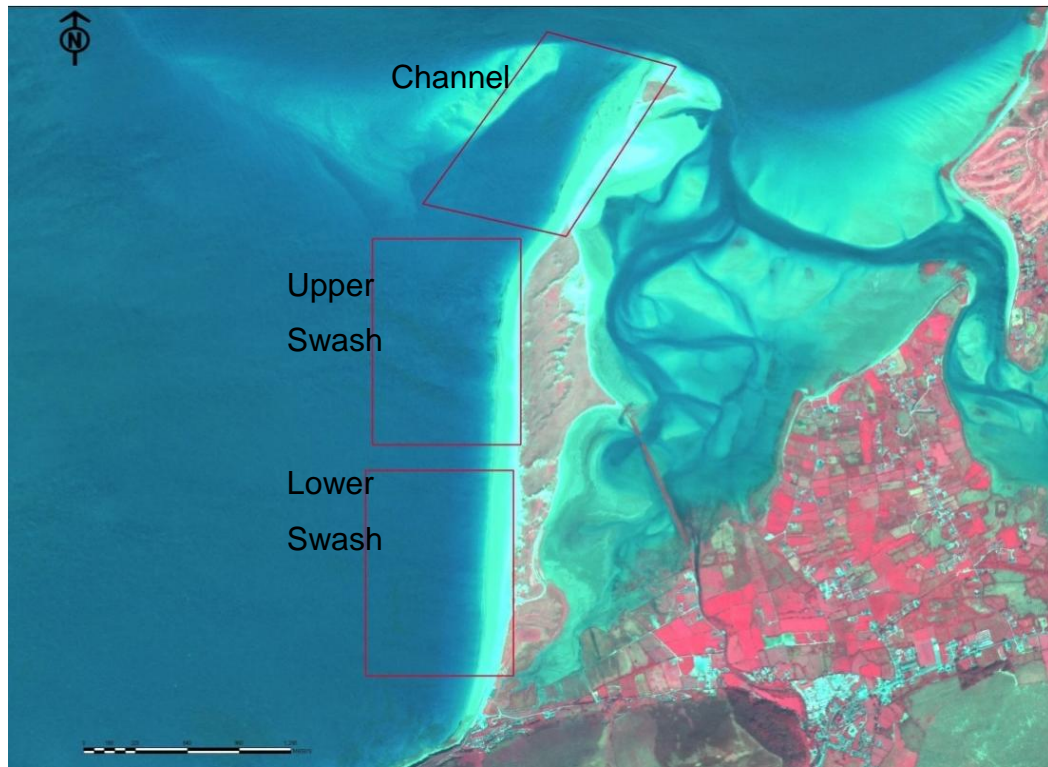


Figure 6.6 Volume comparison locations

Table 6.3 Volume comparison of morphodynamic simulations

Location	Cut (m ³)	Fill (m ³)	Balance (m ³)
Channel	Survey		
	-60212	120106	59894
	Model		
	-69210	114697	45487

6.4 Morphodynamic Modelling Approach

With the validation of the fully coupled wave, hydrodynamic and sediment transport model in the previous section, the morphodynamics of Dingle Bay were examined in detail. The approach taken was to divide the modelling into 3 stages. Stage 1 represents the first two years of evolution beyond the March 2013 survey. The evolution was modelled with a dataset representative of 2 years. Each year simulation took 7 weeks real time to complete.

To reduce computation time and increase time scale of evolution, an experimental approach to long term morphodynamic modelling was taken for Stages 2 and 3. This approach was based on the interpretation of evolutionary trends instead of running year on year simulations. The initial bathymetry for Stages 2 and 3 were altered to represent bathymetry after longer term change. The model was then run for a year and trends observed. The simulation timeline is presented in Table 6.4 for all stages of the morphodynamic modelling.

Table 6.4 Morphodynamic simulation stage timeline

Stage	Representative Start Year	Representative End Year	Simulation Length
Stage 1	2013	2015	2 Years
Stage 2	2025	2026	1 Year
Stage 3	2034	2036	2 Years

This form of schematisation has not been documented previously, although various examples of applying schematised wave and tidal approaches was discussed in Section 2.5.3. The combination of a process based modelling approach with evolutionary trends to predict the long term evolution was a novel approach to long term morphodynamic modelling.

It should be noted that this approach to long term modelling makes an assumption that influences the conclusions made, particularly in the Stage 2 and Stage 3 models. This assumption is that the general trends observed in the field and predicted in the short term modelling will persist during the later stages of the long term morphodynamic modelling. It is considered a

reasonable assumption as it is based on all the available data influencing morphodynamic evolution.

6.5 Morphodynamic Modelling – Stage 1

6.5.1 Stage 1 Approach

The first stage of the morphodynamic modelling was to examine the trends in the near future. The first two years of evolution beyond the 2013 survey was simulated and discussed in this section.

The morphological timescale of each simulation was representative of one year. This was achieved by concatenating a month of summer wave data, already discussed in Section 6.3.3 with a month of wave data collected during the winter season as part of the Ocean radar validation. Both wave datasets were documented in Section 4.2.1. The model was run over a 2 month long tidal cycle with a morphodynamic scale factor of 6. This gives each model run a morphological timescale of 1 year.

The bathymetry at the end of each year long simulation was used as the input bathymetry for the next run. To gain an understanding of the morphodynamics in Dingle Bay, the simulation was run twice giving morphodynamic results for the end of year one (2014) and year two (2015). The changes in bathymetry, wave climate, tidal current regime and sediment transport patterns were examined.

6.5.2 Stage 1 Results

Examining the changes in bathymetry from model start up, figure 6.7 to the end of the first year of simulation, figure 6.8, and to the end of the second year, figure 6.9, clear trends on Rossbeigh were evident. The ebb tidal bar was beginning to merge with the beach of the Island section after year 1 and after year 2 a small section of the channel had become shallower. Erosion was also evident as the drift aligned section and Island reduce dramatically in size over this 2 year period. A section along the drift aligned beach south of the original breach undergoes severe erosion this appears to be leading to the emergence of a new inlet.

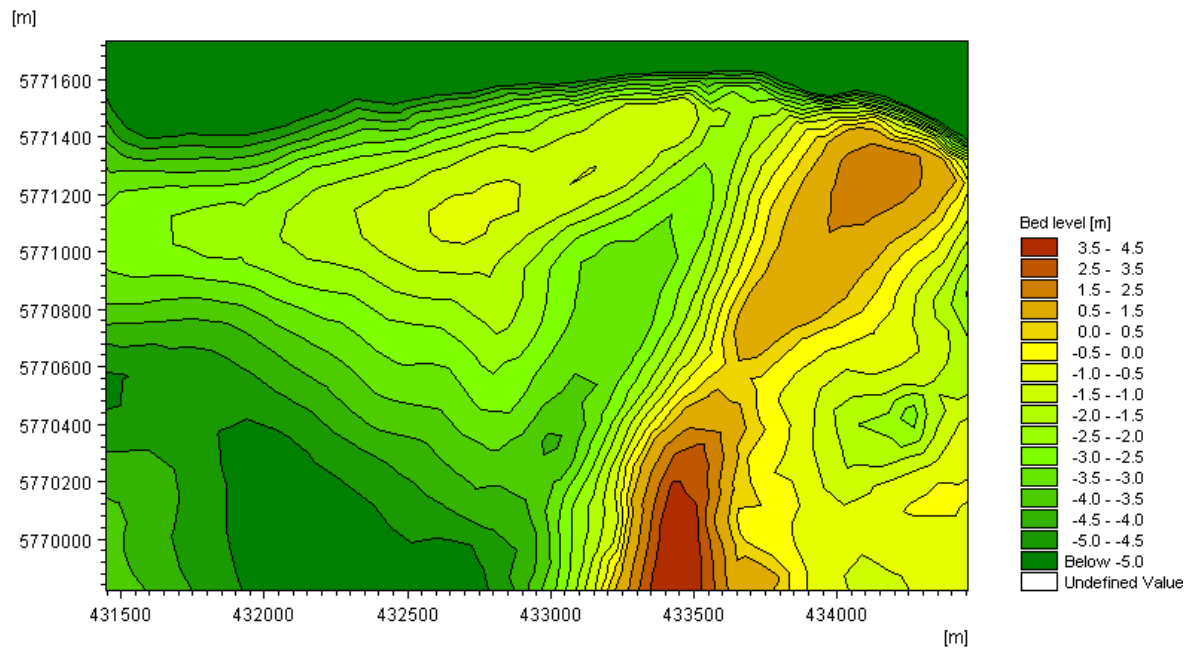


Figure 6.7 Initial Bathymetry of drift aligned section Stage 1 (2013)

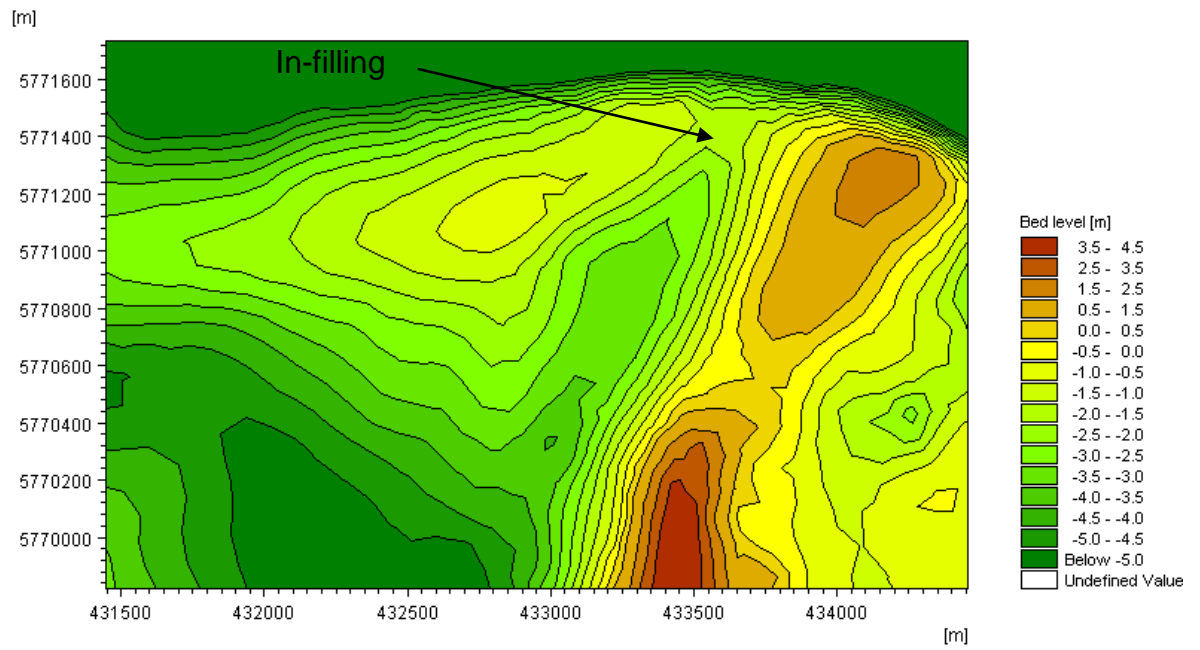


Figure 6.8 Bathymetry at end of Year 1 Stage 1 (2014)

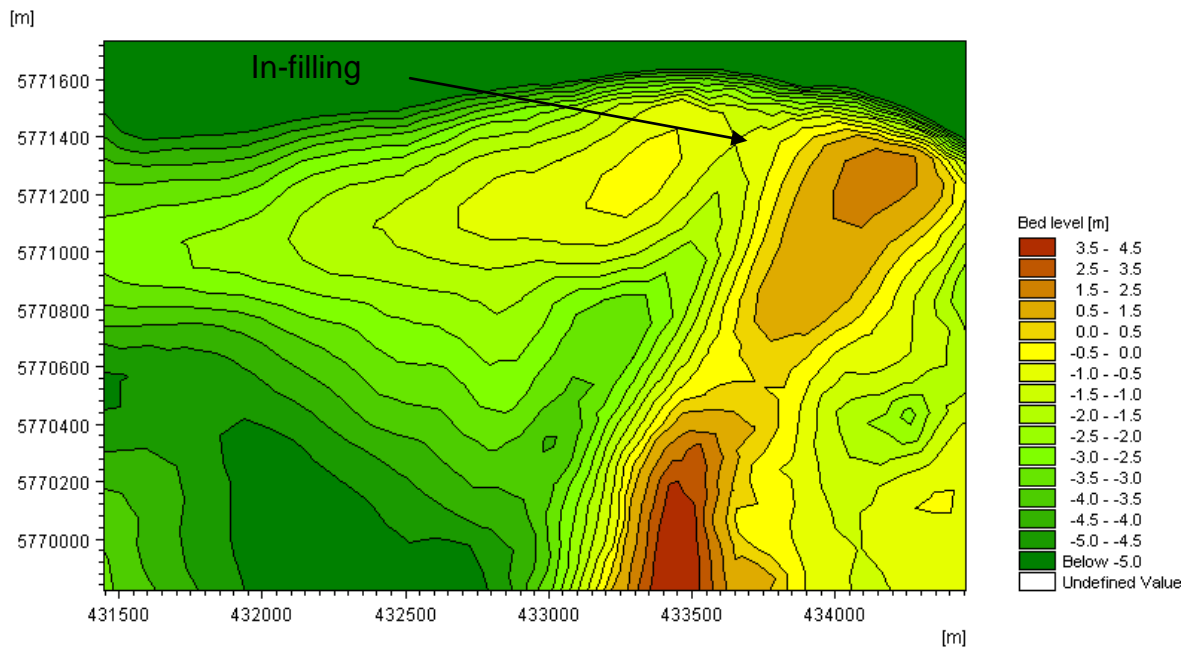


Figure 6.9 Bathymetry at end of Year 2 Stage 1(2015)

Significant wave height at high tide during a storm period was plotted for year 1(2014), figure 6.10, and year 2 (2015), figure 6.11. The white polygons represent the beach of Rossbeigh at high tide with the polygon in the centre left of the images representing the Island section and the larger representing the drift aligned dunes. The wave height appears to have increased slightly for the same storm period from year 1 to year 2 in the area north of the distal dune section. This was as a result of the increased erosion at this location and deepening of the inlet discussed previously. Reduction and splitting of the island section in a storm at high tide at the end of year 2 was also noteworthy

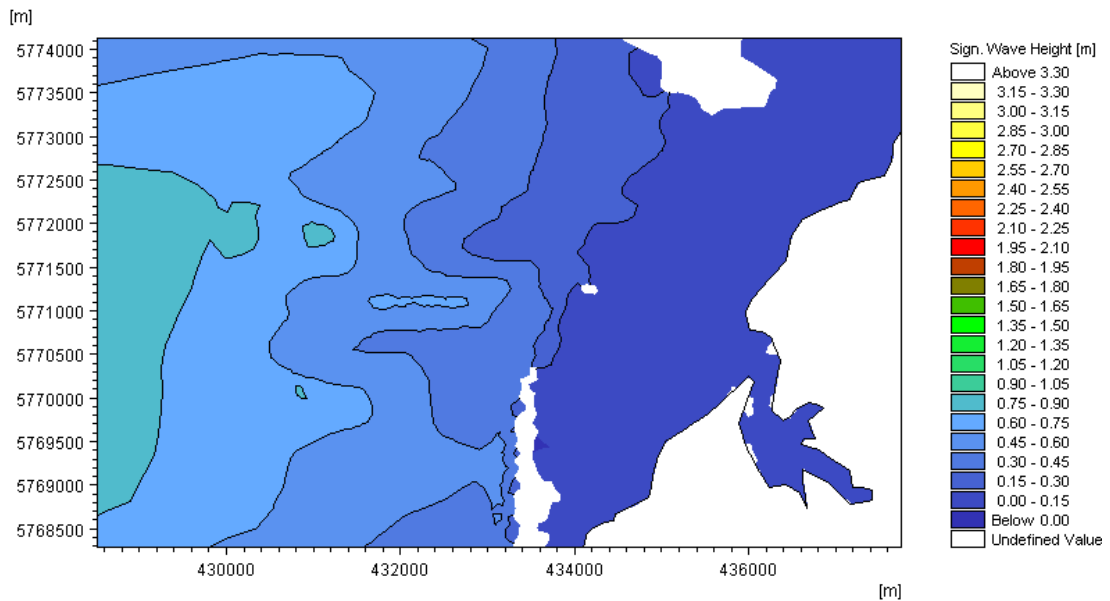


Figure 6.10 Significant wave height in drift aligned zone in Year 1 Stage 1 (2014)

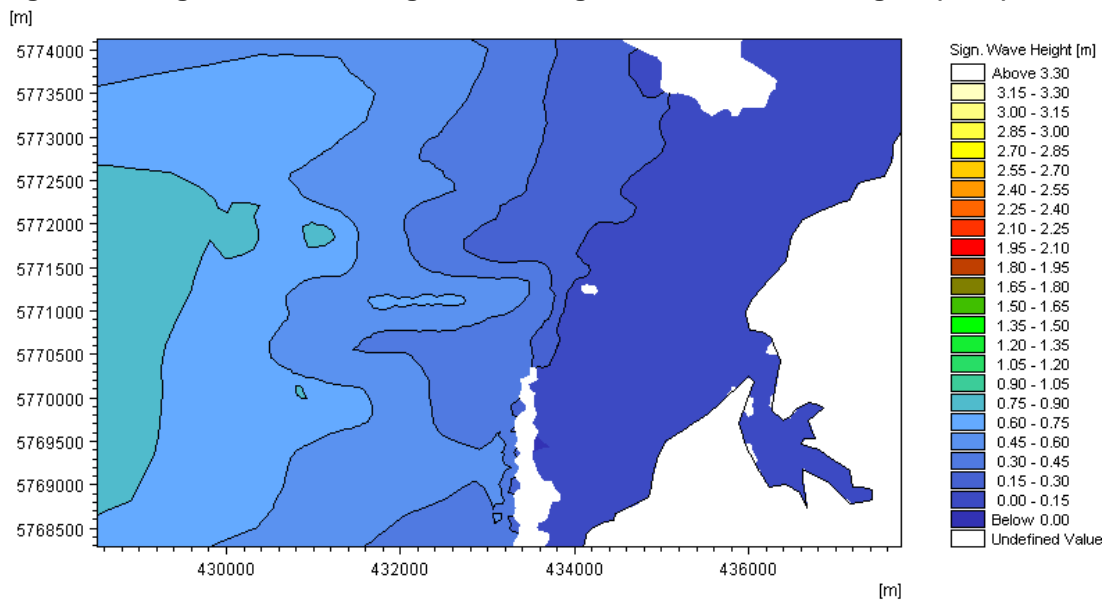


Figure 6.11 Significant Height at high tide in drift aligned zone in Year 2 Stage 1 (2015)

The mean wave direction for the same storm period was plotted for year 1, figure 6.12, and year 2, figure 6.13. It is significant to note that the difference in wave direction at high tide between drift and swash aligned zones was reproduced in the model. This was previously documented in Section 4.2.3 as being a cause of the growth in drift aligned zone at the expense of swash aligned. It is also significant that the ebb tidal bar was shown to have an effect on wave direction.

The mean wave direction in the swash aligned zone was in the 250°-275° sector while the ebb tidal bar and the drift aligned shore experienced wave

action from the 275°-300° sector. There was a significant change in the mean wave direction between year 1 and year 2 at the entrance to the channel between the ebb tidal bar and the drift aligned shoreline. In year 1 a large area of the channel entrance shows wave direction in the 275°-300° sector but in year 2 this changes to the 250°-275° sector

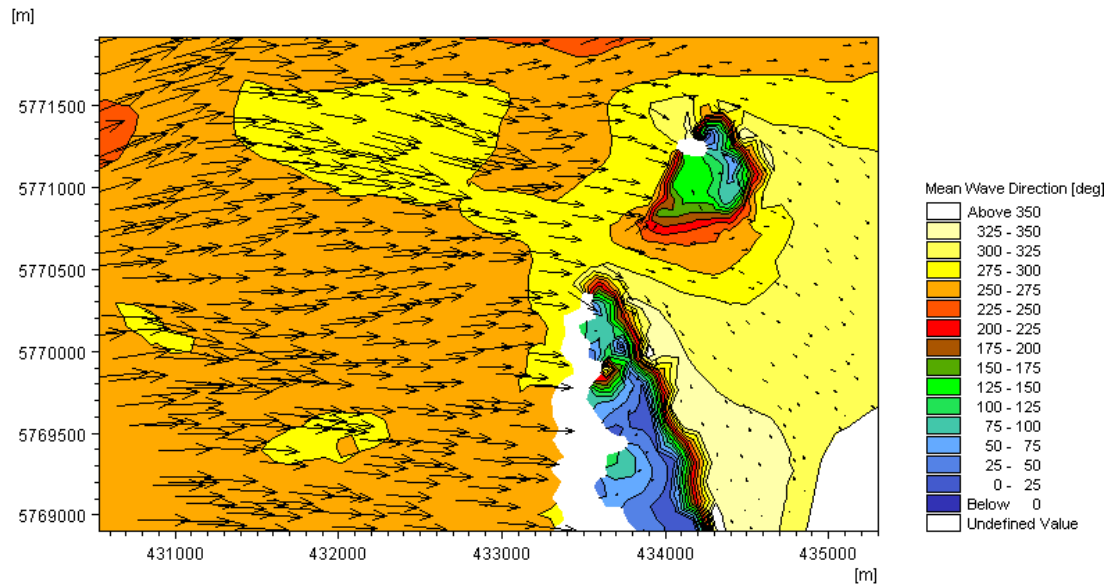


Figure 6.12 Mean wave direction in drift aligned zone in Year 1 Stage 1(2014)

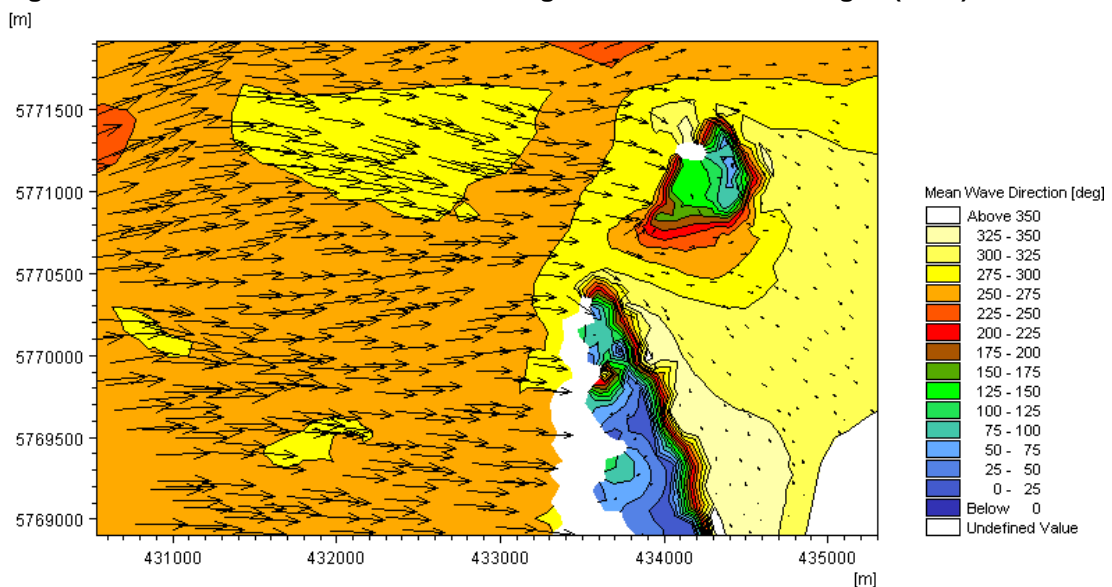


Figure 6.13 Mean wave Direction at high tide in drift aligned zone in Year 2 Stage 1(2015)

The tidal current regime at both mid flood, figure 6.14 and figure 6.15, and mid ebb, figure 6.16 and figure 6.17, showed little variation between the years 1 and 2 of the simulation. The flood currents had a peak of over 0.8m/s at the tip of island with strong currents also visible in the newly formed inlet

north of the distal section. The increase in magnitude and shore parallel direction of these currents in the drift aligned section were contrasted with the smaller currents in the swash aligned section. The current accelerated at the narrow part of the channel between the ebb tidal bar and drift aligned shoreline which exited into the main tidal inlet.

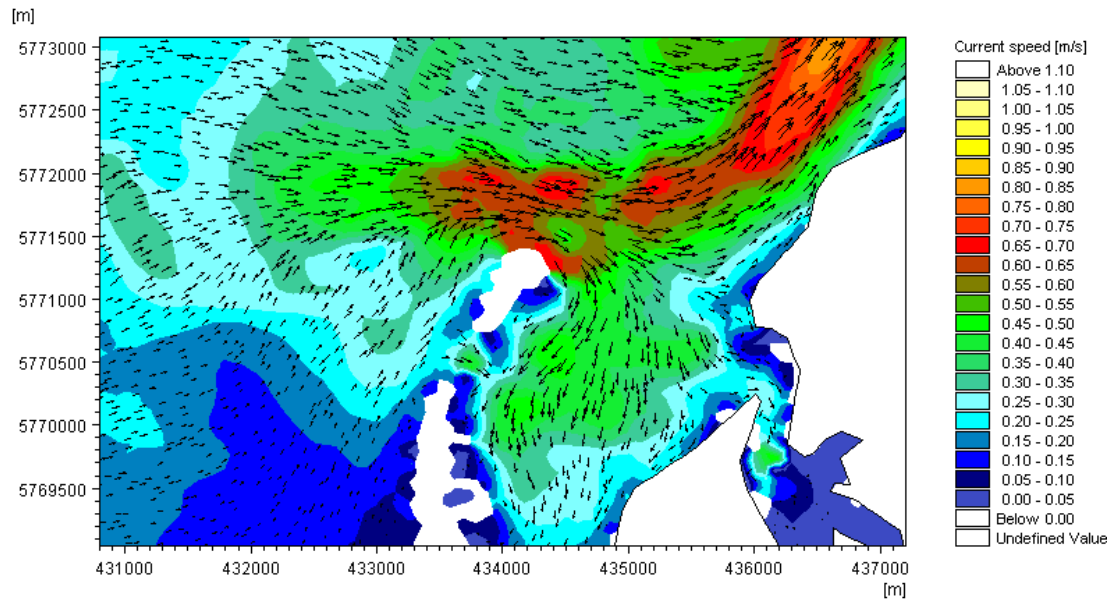


Figure 6.14 Mid flood drift aligned zone in Year 1 Stage 1(2014)

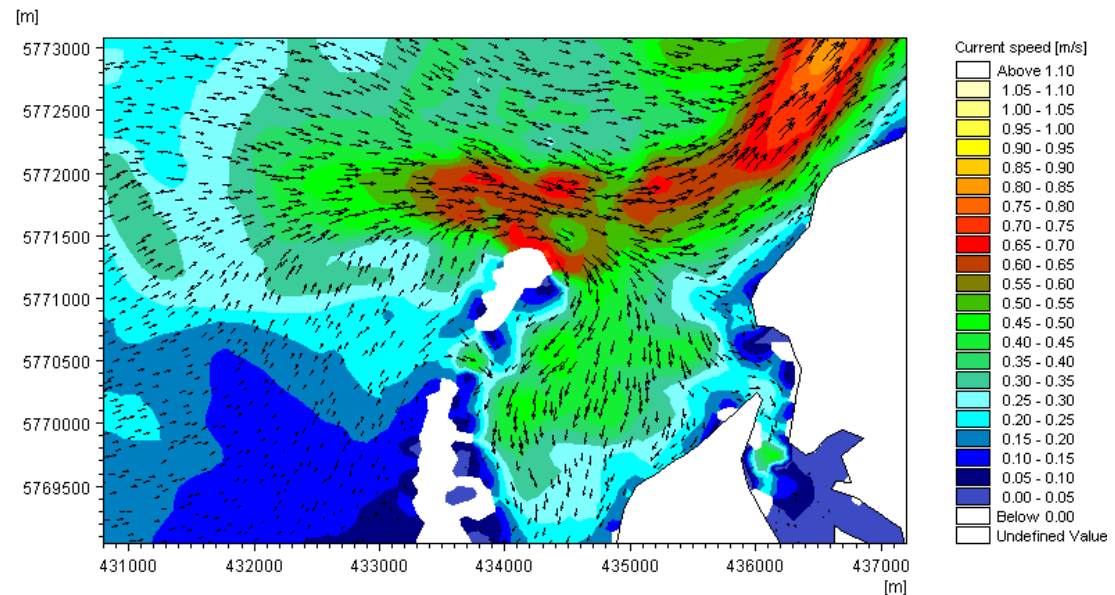


Figure 6.15 Mid flood drift aligned zone in Year 2 Stage 1(2015)

At mid ebb in both year 1, figure 6.16, and year 2, figure 6.17, sections of the main tidal inlet current turned south onto the bar. The observed pattern of the currents reinforces the theory developed in Chapter's 3 and 4 that the ebb tidal bar is nourished by the main tidal inlet.

Once passed the constriction caused by the northern tip Rossbeigh in the inlet channel, the ebb current slowed down. The current jet then fanned out in several directions with a significant flows observed over the ebb tidal delta.

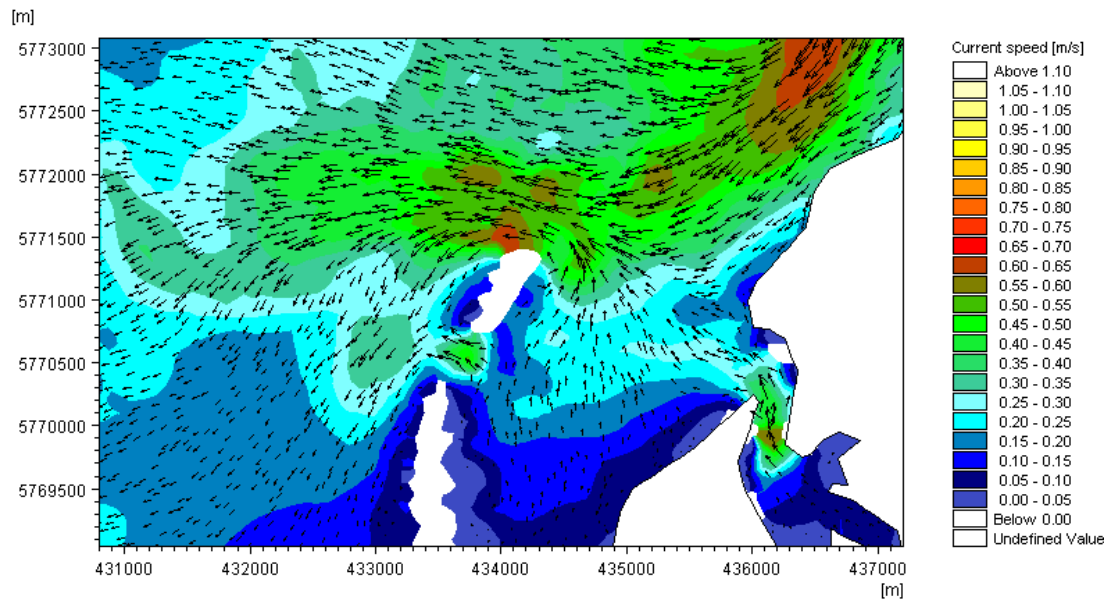


Figure 6.16 Mid ebb in drift aligned zone in Year 1(2014)

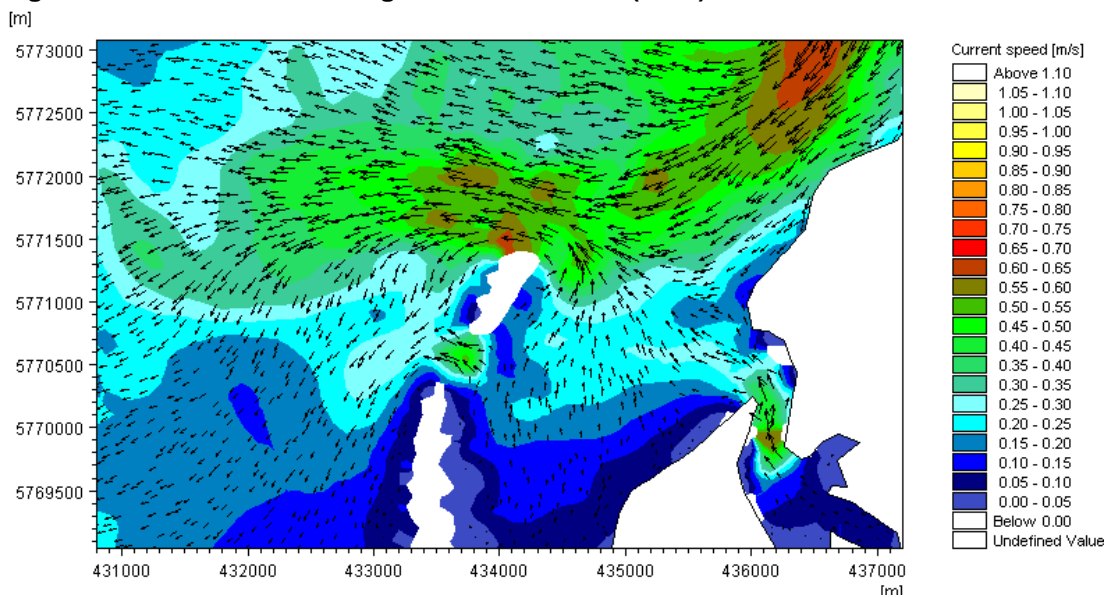


Figure 6.17 Mid ebb in drift aligned zone in Year 2(2015)

The accumulated sediment transport was represented in vector format at the end of each year long simulation. These vectors represent the total sediment load transported from each node. They were plotted on a background of bathymetry for year 1, figure 6.18, and year 2, 6.19. The sediment transport patterns from year 1 to year 2 did not change significantly with the exception of the island section and a small area to the south east of the ebb tidal delta.

An increase in accumulated sediment transport was visible at both locations from year 1 to year 2.

Generally, the sediment transport vectors followed similar patterns to that of the tidal current vectors. The sediment transport in the tidal inlet was dominated by ebb currents while the beach and ebb tidal bar was dominated by flood current driven sediment transport. The effect of wave direction was also visible with sediment transport vectors shifted slightly to the east compared to the tidal current vectors. This was due to the dominant westerly and north westerly wave directions driving sediment transport in this location.

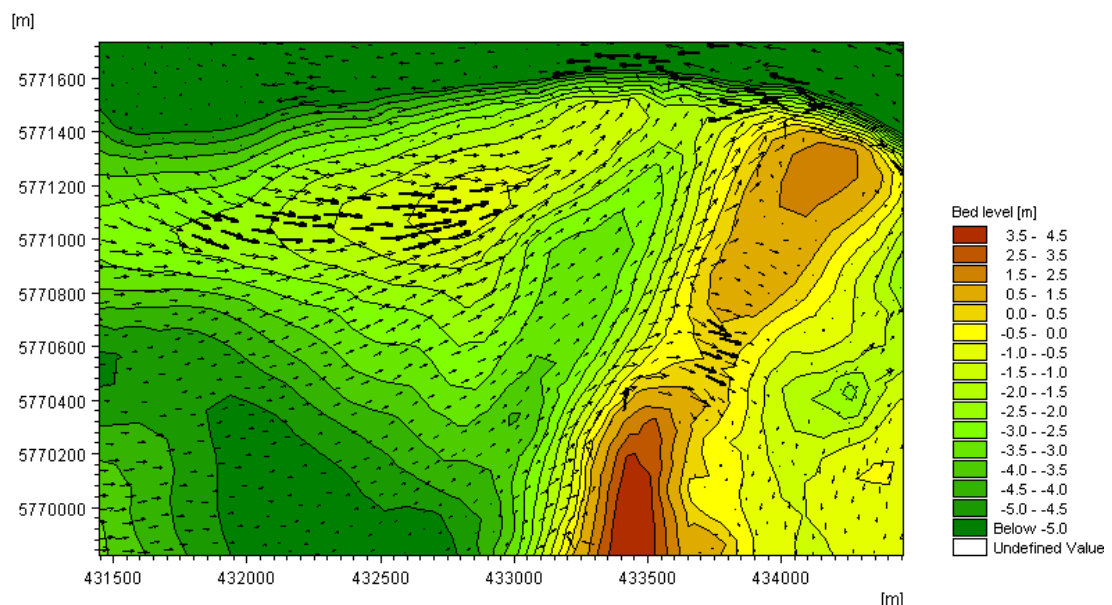


Figure 6.18 Accumulated Sediment transport vectors at end of Year 1(2014)

The sediment transport in the area seaward of the ebb tidal bar appears to have been wave dominated. The main body of the ebb tidal bar and the channel between ebb tidal delta and drift aligned zone was dominated by tidally driven sediment transport and sediment transport on the beach was dominated by both in various locations.

At the northern edge of the distal end of Rossbeigh, a large magnitude vector running in a north westerly direction was evident in contrast to the north easterly vectors in the vicinity. This transport vector was in response to the dominant north westerly wave condition that is responsible for erosion at high

tide. The tidal dominated sediment transport on the beach is visible in the breach area and at the edge of the island.

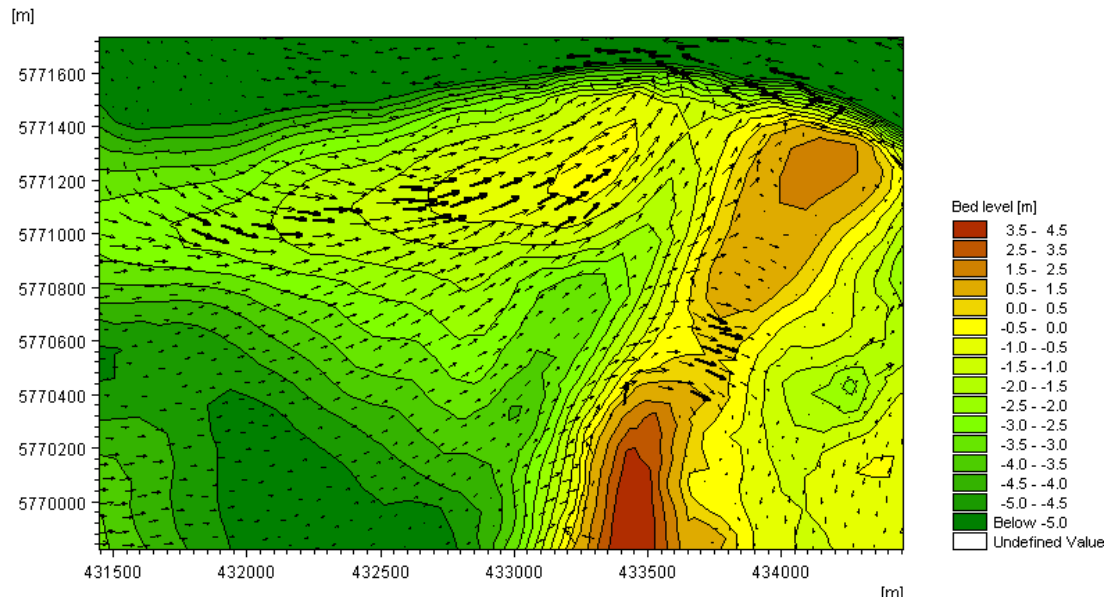


Figure 6.19 Accumulated Sediment transport vectors at end of Year 2(2015)

Similar to the validation of morphodynamic modelling on section 6.3.3, the volume of sediment movement was calculated by comparing volumes in the initial to end bathymetry. The change in volume at the end of year 1(2014) and at the end of year 2 (2015) was compared in Table 6.5. This was presented in terms of cut and fill.

The 3 areas examined were the channel, the upper swash and lower swash zones. The locations of where the volumes were extracted were shown previously in figure 6.6. The channel was subdivided into a sub tidal volume due to the dynamic nature of the sediment transport process in this area.

There was little variation in the morphological response between year 1 and year 2 in the lower part of the swash zone. The morphodynamic climate was accretive in nature with low amounts of sediment being removed and added.

Further up the swash zone greater volumes of sediment were moving in and out of the reference area. The rates of movement reduce by approximately 50% in both cut and fill from year 1 to year 2. The resultant morphodynamic

climate was erosive with over 9,000m³ being eroded in year one, but a large reduction to approximately 1,500m³ resultant erosion in year 2.

In the drift aligned zone, specifically in the channel, the general morphodynamic climate was accretive but with large volumes of sediment movement in both cut and fill in both years. Comparing the sub tidal section of the channel it was evident that the majority of the fill or accretion was occurring in the sub-tidal ebb tidal bar side of the channel.

Table 6.5 Volume calculations for Stage 1 simulations

Area	Year 1 (2014)			Year 2 (2015)		
	Cut (m ³)	Fill (m ³)	Balance (m ³)	Cut (m ³)	Fill (m ³)	Balance (m ³)
Channel	-84092	104176	20084	-90241	100084	9843
Channel Subtidal	-32502	86295	53794	-43445	81987	38542
Upper Swash	-47859	38736	-9122	-20724	19227	-1497
Lower Swash	-18190	27259	9070	-17959	27707	9747

A slowdown in accretion was noticeable from year 1 to 2 in the sub-tidal area but the volumes were large in both years (53,794 m³ and 38,542 m³). The erosion rates remain relatively constant from year 1 to 2 in the inter-tidal beach side of the channel.

6.5.3 Conclusions from Stage 1

The results of the modelling in Stage 1 provide an insight into the complexity of the morphodynamics of Rossbeigh. The relative stability in the swash aligned shoreline was reproduced in the simulations and was contrasted with the multi-mode sediment transport regime in the drift aligned zone.

Wave driven sediment transport appears to dominate seaward of the ebb tidal bar moving the sediment shoreward, Tidal current sediment transport dominates along the bar and into the channel with evidence of wave and tidally mixed sediment transport on the beach of the drift aligned zone.

The modelling has confirmed the presence of a north westerly wave direction acting at high tide in the drift aligned zone. The impact of this wave forcing on sediment transport was also observed. The bathymetry comparisons suggest that the ebb tidal delta is growing and beginning to join drift aligned beach, starting at the neck of the channel. Volume calculations confirm that the sub tidal section of the channel between ebb tidal bar and drift aligned zone is accreting while the beach continues to erode in the drift aligned zone.

The next stages of modelling are scenario based and focus on the longer term morphology of Rossbeigh. These scenarios are based on extrapolating morphodynamic trends identified in stage 1 modelling results.

6.6 Morphodynamic modelling – Stage 2

6.6.1 Stage 2 Approach

The second stage of morphodynamic modelling aims to predict the long term morphology of Rossbeigh. This scenario based modelling approach was focused on the morphodynamic interaction of the ebb tidal bar, channel and drift aligned zone.

It has been established from both Stage 1 modelling and successive bathymetry surveys that the ebb tidal bar was beginning to migrate shorewards. Good agreement between 6 month survey and 6 month simulation rates of migration in terms of sediment volume entering the channel area has been achieved in Section 6.3.3. The annual rate of increase in volume in the sub tidal zone from Stage 1 was found to be in the range of 38,000 m³ to 53,000 m³. A value lower than the mean was taken as the annual average rate of migration of 40,000m³.

To simulate a morphodynamic evolution period of ten years in the channel and ebb tidal bar, 400,000 m³ of sediment was artificially added to the model bathymetry for the end of year 2 in the stage 1 model (2015). This was achieved by locally changing the elevation value at the nodes in the model mesh. The bed levels at the ebb tidal bar boundary with drift aligned channel and the channel itself were raised to reflect the migration of the ebb tidal bar shorewards. To compensate for raising the bed level in the drift aligned zone channel, and ensure sediment was conserved within the coastal cell, an area seaward of the ebb tidal bar was reduced.

By adding 400,000 m³, the initial bathymetry for Stage 2 represents the year 2025 in morphological terms. A simulation time of 1 year with the same input parameters as Stage 1 and with the altered bathymetry was run. At the end of the Stage 2 simulation would theoretically represent 13 years of morphodynamic evolution from 2013. The Stage 2 results could also represent the coastal processes in Dingle Bay after a beach nourishment

campaign of 400,000 m³ undertaken after the March 2013 bathymetry survey.

The changes in bathymetry, wave, tidal and sediment transport patterns from Stage 2 modelling are discussed in the next section.

6.6.2 Stage 2 Results

The initial model bathymetry of Stage 2, figure 6.20, looks significantly different from the 2013 bathymetry of Stage 1, figure 6.8. The distinct channel between ebb tidal delta and drift aligned shore disappeared with a sub tidal flat in its place. This bathymetry plot shares characteristics with the satellite image of Rossbeigh in 2000 before breaching occurred, documented in Section 3.5.

Comparing the bathymetry from the beginning of Stage 2 to the end (2026), figure 6.21, the change evident after a 1 year simulation was the widening and growth of the drift aligned shoreline. The beach has widened significantly in the area north of the distal dune end where an inlet was forming in Stage 1. The sub tidal flats have also expanded in a southerly and westerly direction.

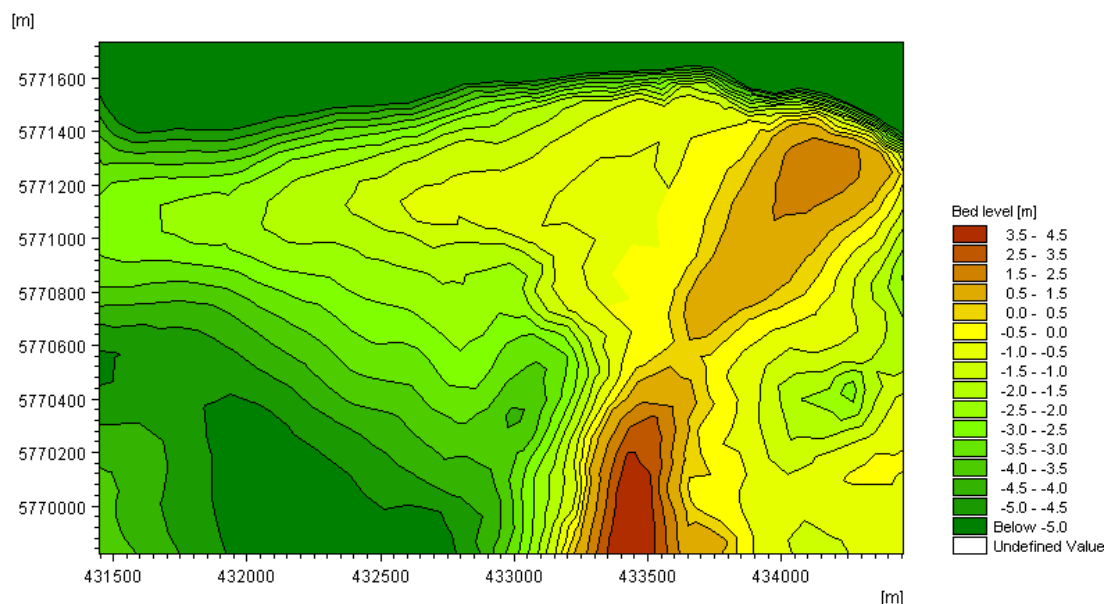


Figure 6.20 Bathymetry at start of Stage 2 (2025)

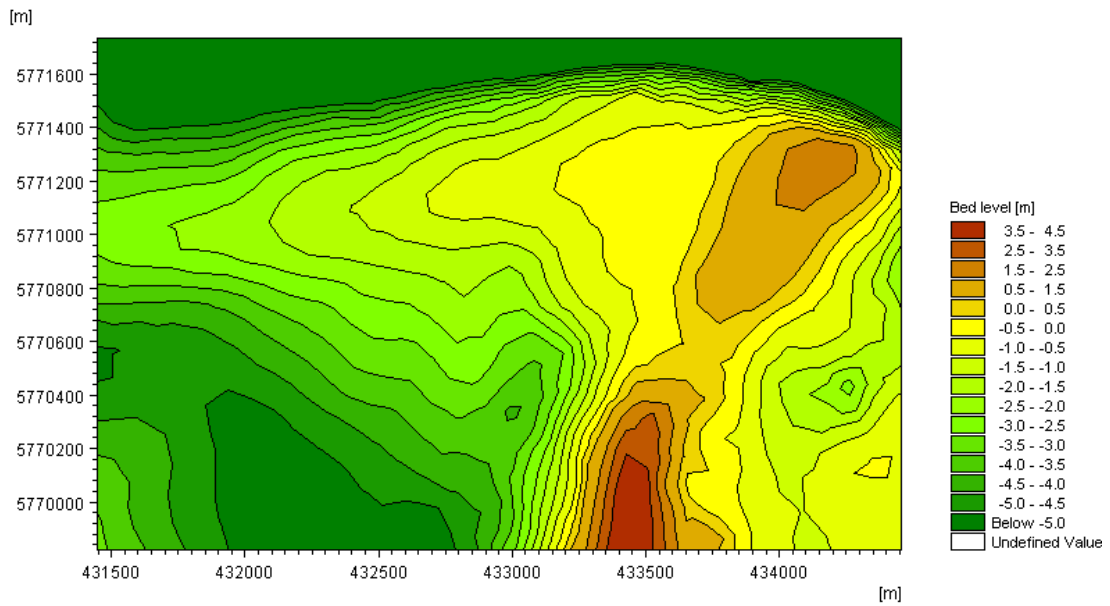


Figure 6.21 Bathymetry at end of Stage 2 (2026)

The significant wave height patterns at high tide during a storm event, figure 6.22, were similar to the stage 1 plots, figure 6.10 and figure 6.11. The wave heights were slightly reduced close to shore and in the vicinity of the sub tidal flat area where the drift aligned channel used to be. This was primarily due to the infilling of the channel. The reduction of depth close to the shoreline reduces the incident wave height

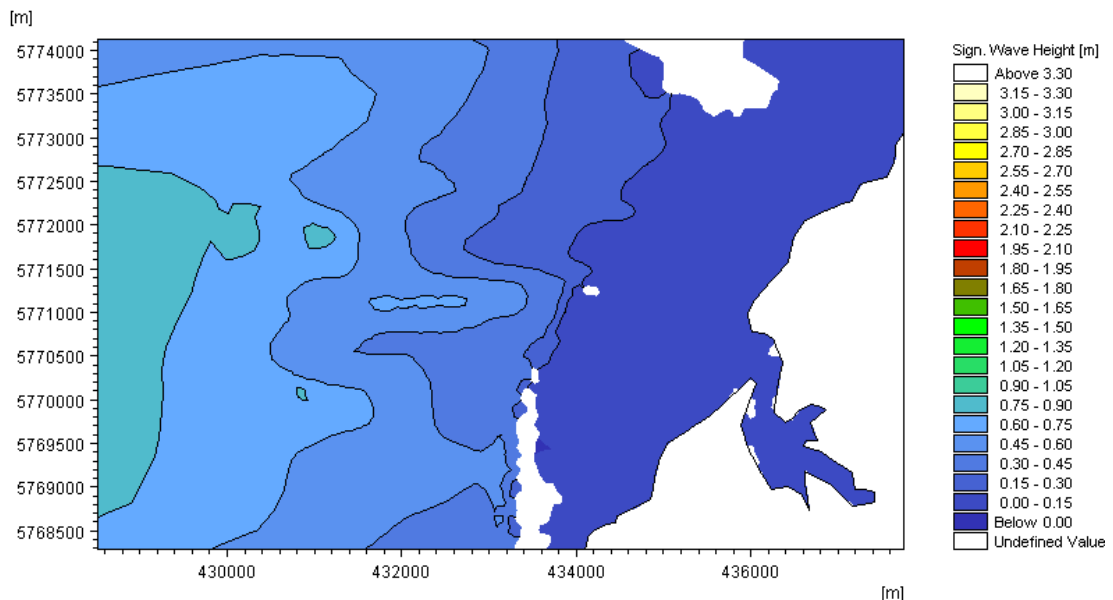


Figure 6.22 Significant wave height at high tide Stage 2 (2026)

The mean wave direction pattern, figure 6.23, during the same storm period was different from plots in Stage 1. The mean wave direction was similar

close to shore in the swash aligned zone but to the north of the island and along sub tidal flat the wave direction has altered compared to Stage 1. In this area the mean wave direction was from the 275°-300° sector in Stage 2 whereas in Stage 1 mean wave direction originated from the 250°-275° sector. This was as a result of the sub tidal flat replacing the drift aligned channel and in effect extending the influence of the ebb tidal delta in Stage 1 shore wards. This resulted in an increase in wave driven sediment transport potential in the direction of the drift aligned shoreline across the ebb tidal bar and Subtidal flat area.

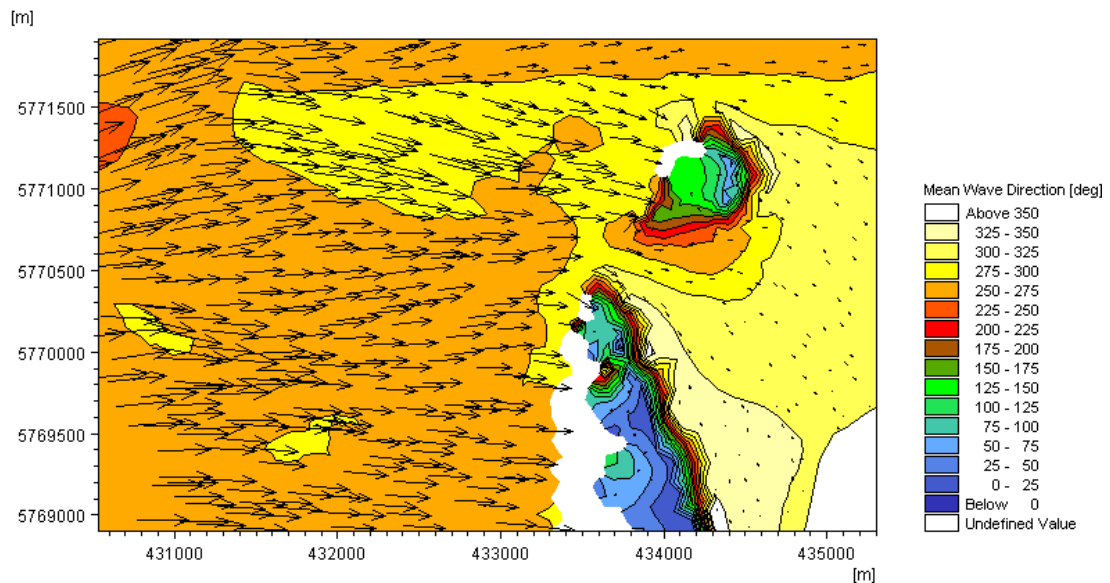


Figure 6.23 Mean wave direction at high tide Stage 2(2026)

The maximum mid flood current was plotted in figure 6.24. The maximum currents in the main tidal inlet channel and through the breach area remain similar to the Stage 1 simulation results. The only significant difference evident was a reduction in velocity where the channel between ebb tidal bar and drift aligned shore in Stage 1 exited into the main tidal inlet channel. This area has reduced from a maximum of 0.4 m/s Stage 1, figure 6.15, to 0.2 m/s in the Stage 2 simulation.

The maximum ebb current plot for stage 2 simulation, figure 6.25, was similar to the corresponding Stage 1 plots with the same exception described in the max flood plot.

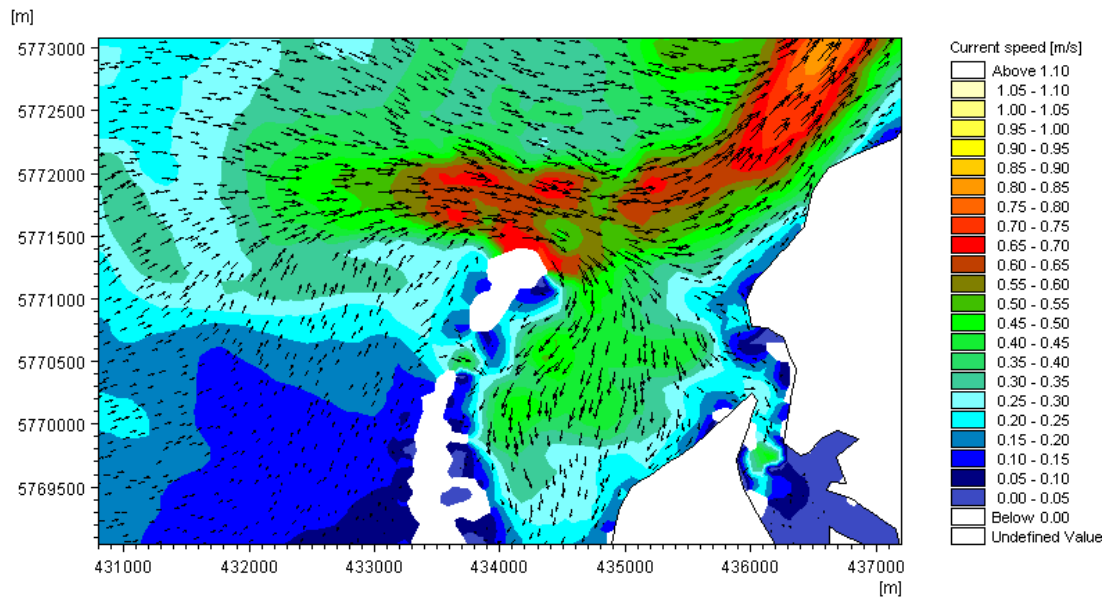


Figure 6.24 Mid flood Stage 2 (2026)

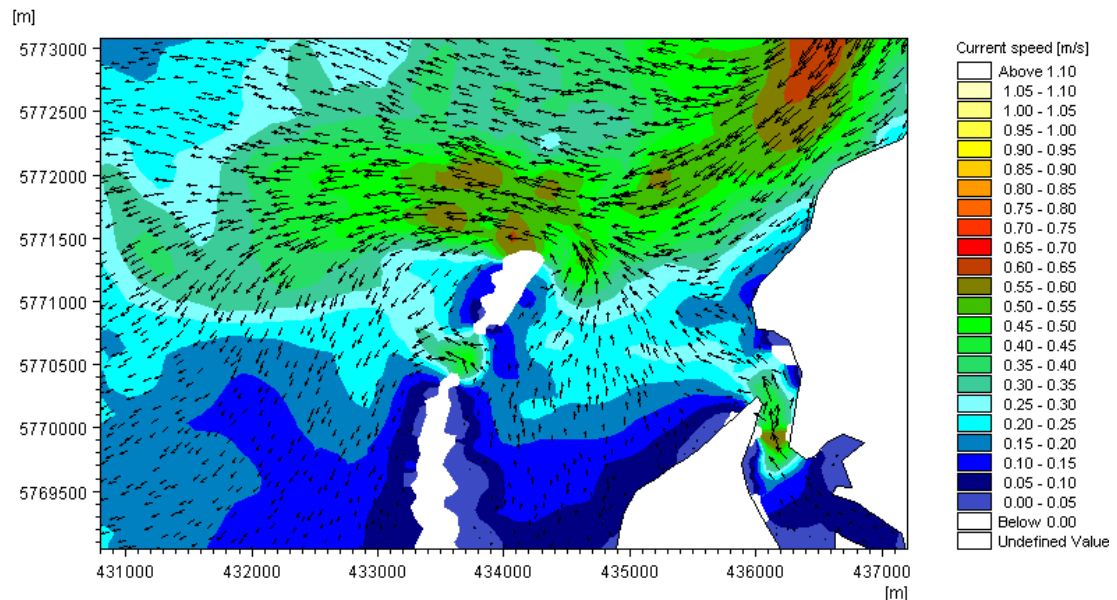


Figure 6.25 Mid ebb Stage 2 (2026)

Similar to Stage 1 the accumulated sediment transport was represented in vector format at the end of the year long simulation for Stage 2, figure 6.26. The sediment transport patterns in Stage 2 change significantly in the sub tidal flat area sea ward of the drift aligned shoreline. An increase in accumulated sediment transport was visible compared to Stage 1, figure 6.19, suggests that more sediment was moving into the channel in Stage 2.

A reduction in sediment transport vector magnitude was evident on the beach in front of the island section indicating a slowdown of sediment movement in this area.

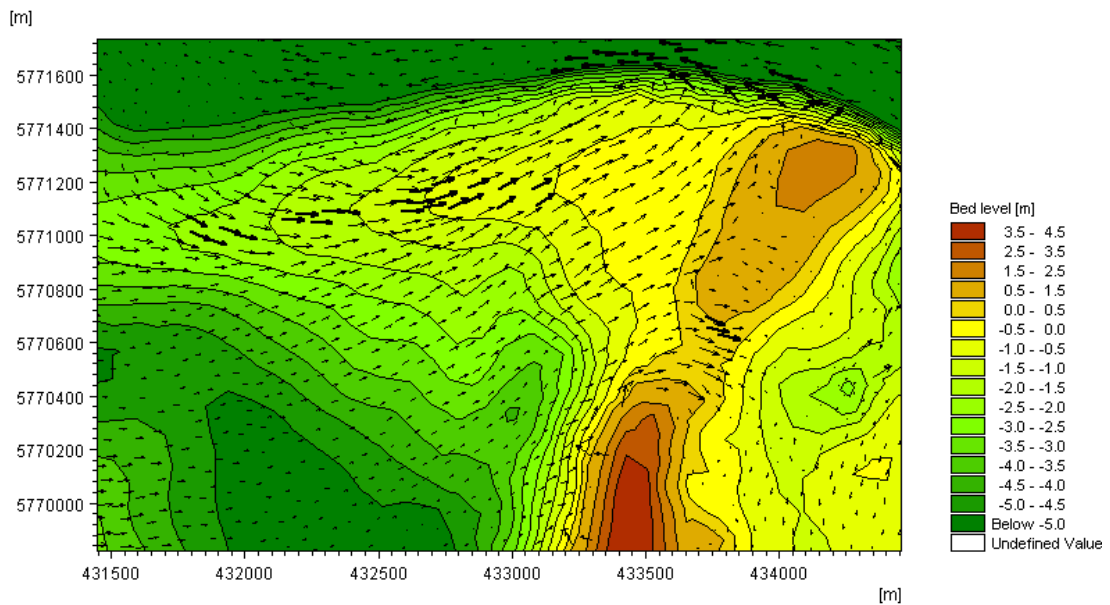


Figure 6.26 Cumulative sediment transport vectors at end of year 1 Stage 2(2026)

The volume of sediment movement in Stage 2 in the same locations as Stage 1 was compared in Table 6.6. There was little variation in the morphological response between Stage 1 and Stage 2 in the lower part of the swash zone. In the channel, large volumes of sediment movement in both cut and fill were observed. The resultant morphodynamic climate was erosive but the balance between cut and fill was much closer than in Stage 1 with only 5,419 m³ difference between cut and fill.

The sub tidal section of the channel appears to be reaching an equilibrium point with less than 2,000 m³ balance at the end of Stage 2. It was also evident that erosion was still occurring on the beach of the drift aligned zone but at a much reduced rate compared to Stage 1.

Table 6.6 Volume calculations for Stage 2 simulations

Area	Year 1 (2025-2026)		
	Cut (m ³)	Fill (m ³)	Balance (m ³)
Channel	-103063	97644	-5419
Channel Sub	-68034	66228	-1806
Upper Swash	-53568	44065	-9503
Lower Swash	-17766	28163	10397

6.6.3 Conclusions from Stage 2

The results of the Stage 2 modelling show that morphodynamic stability of Rossbeigh has been simulated utilising trends from Stage 1. The relative stability of both the swash aligned and drift aligned zones was observed at the end of Stage 2. To arrive at this stage of Rossbeigh's evolution 13 years of morphodynamic evolution from 2013 was simulated in total combining explicit and implicit methods of long term morphological modelling.

The dominant sediment transport patterns in Stage 2 vary little from the Stage 1 patterns, the exception being the areas where the bathymetry has been artificially elevated. This was undertaken to simulate 10 year evolution based on Stage 1 morphological trends.

At the end of Stage 2, sub tidal equilibrium in the drift aligned zone has been reached, however, regeneration of the dunes will not be initiated due to the erosion still occurring on the drift aligned beach. Further accretion in the sub tidal area between ebb tidal bar and drift aligned shore is required before aeolian driven dune regeneration can be initiated. As accretion continues in this area, it will become intertidal and provide the dry sediment required for aeolian driven dune recovery.

The next stage, Stage 3, of modelling examines a scenario that enables dune regeneration to begin.

6.7 Morphodynamic modelling – Stage 3

6.7.1 Stage 3 Approach

The final stage of morphodynamic modelling aimed to predict conditions necessary for dune regeneration to occur. As identified in Stage 2, a larger inter tidal area in front of the eroded drift aligned dunes is required before aeolian driven regeneration is initiated. To achieve this, the morphodynamic regime but sub tidal and intra-tidal in the drift aligned zone must become accretive in nature. This requires further elevation and expansion of the beach area in the drift aligned area. The Stage 3 model was run for 2 years.

This addition of sediment was justifiable morphologically as it follows the trends established in both Stage 1 and Stage 2. It was also a scenario that could be artificially induced. A beach nourishment programme could be implemented to speed up the evolution of Rossbeigh by infilling the channel between ebb tidal bar and drift aligned shoreline.

To create an accretive morphodynamic regime in the drift aligned zone a further 250,000 m³ of sediment was artificially added to the model bathymetry at the end of the Stage 2 model. The mesh nodes in the drift aligned zone were manually adjusted similar to the Stage 2 adjustment of bathymetry. The starting bathymetry of Stage 3 was representative of the year 2034. Stage 3 was run for 2 consecutive years.

The bathymetry at the end of Stage 3 was equivalent to a total of 23 years of evolution of Rossbeigh or the year 2036.

The changes in bathymetry, wave, tidal and sediment transport patterns are discussed in the next section.

6.7.2 Stage 3 Results

The initial model bathymetry of Stage 3 (2034), figure 6.27 looks similar to the final bathymetry of Stage 2 simulation but with a larger area in the drift aligned zone above the MWL of 0.0 OD Malin. The change visible after a 2

year simulation, figure 6.28, was the widening and growth of the drift aligned shoreline. Similar to Stage 2 the beach has widened further in the area north of the distal dune end where an inlet was forming in Stage 1. The drift aligned beach has continued to expand in a southerly and westerly direction. Erosion of the island was ongoing and only an area of less than 100 m² was above 3 m OD Malin at the end of year 2 (2036) in the simulation.

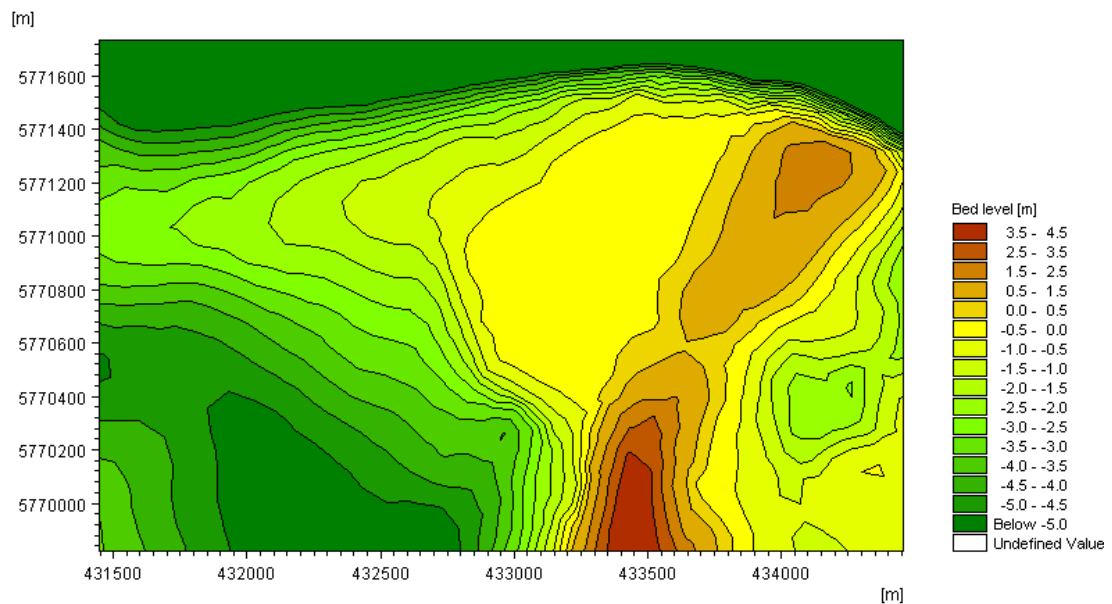


Figure 6.27 Bathymetry at Beginning of Stage 3(2034)

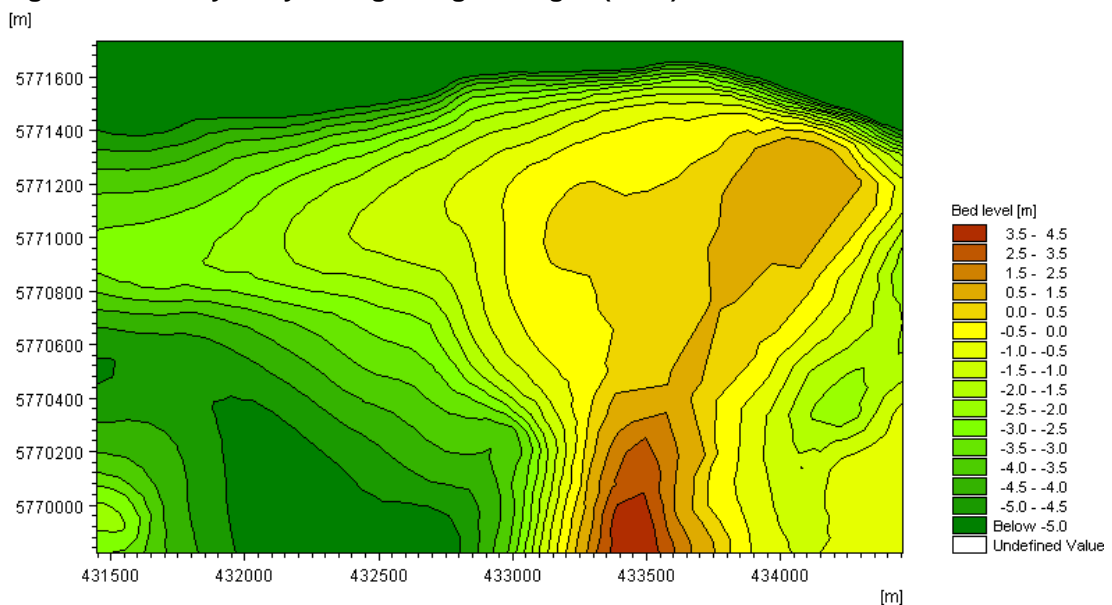


Figure 6.28 Bathymetry at end of Stage 3(2036)

The wave climate, figure 6.29 reduced again with the increase in bed level in the drift aligned zone compared to Stage 1 and 2. Examining the mean wave direction during a storm period figure 6.30 and figure 7.31, it is interesting

that the increased homogeneity of the drift align sub tidal region had the effect of turning the waves close to shore. The zone of influence of the ebb tidal bar was reduced. The 250°-275° sector wave direction was incident on a greater length of coastline in place of the 275°-300° sector.

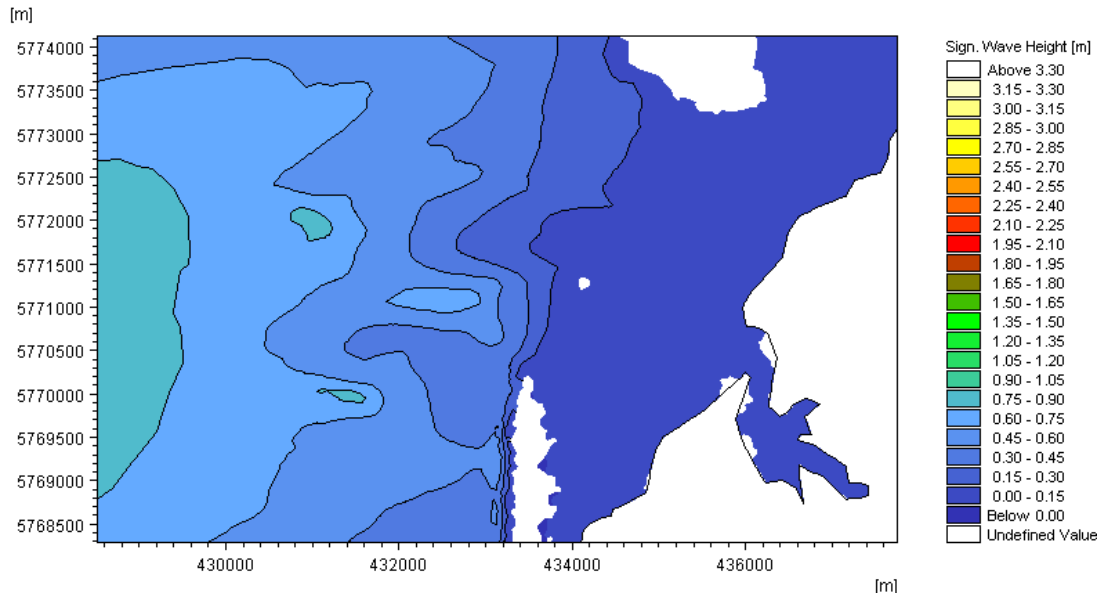


Figure 6.29 Significant wave height year 2 Stage 3(2036)

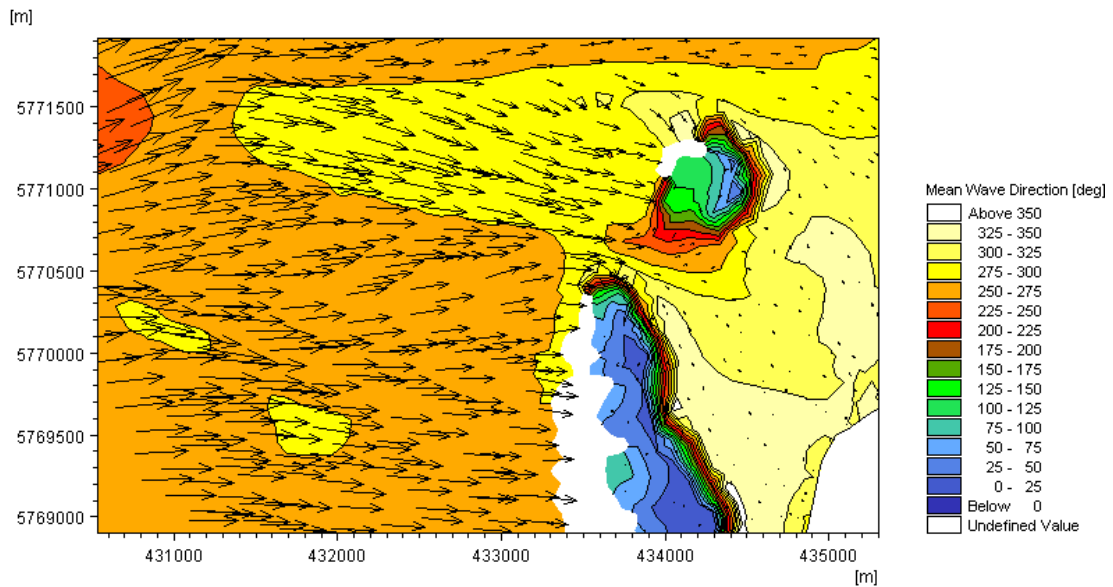


Figure 6.30 mean wave direction year 1 Stage 3(2035)

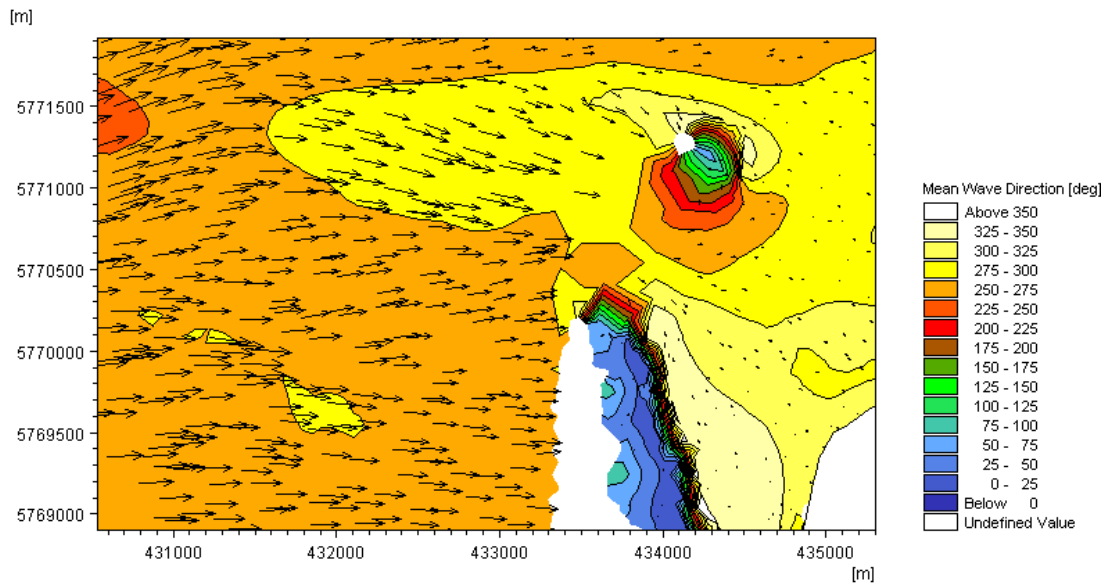


Figure 6.31 mean wave direction year 2 Stage 3 (2036)

The maximum mid flood current was plotted in figure 6.32 and figure 6.33 for year 1 and 2 in Stage 3 respectively and the maximum ebb current was plotted in figure 6.34 and figure 6.35. The maximum currents in the main tidal inlet channel and through the breach area remained similar to the Stage 1 and Stage 2 simulation results. There was a significant reduction in velocity in the area seaward of the original breach position for both max ebb and flood in year 1 compared to Stage 2. This reduction in year 2 of Stage 3 was even greater and the velocity reduced to almost 0 m/s for a large area seaward of the drift aligned shoreline.

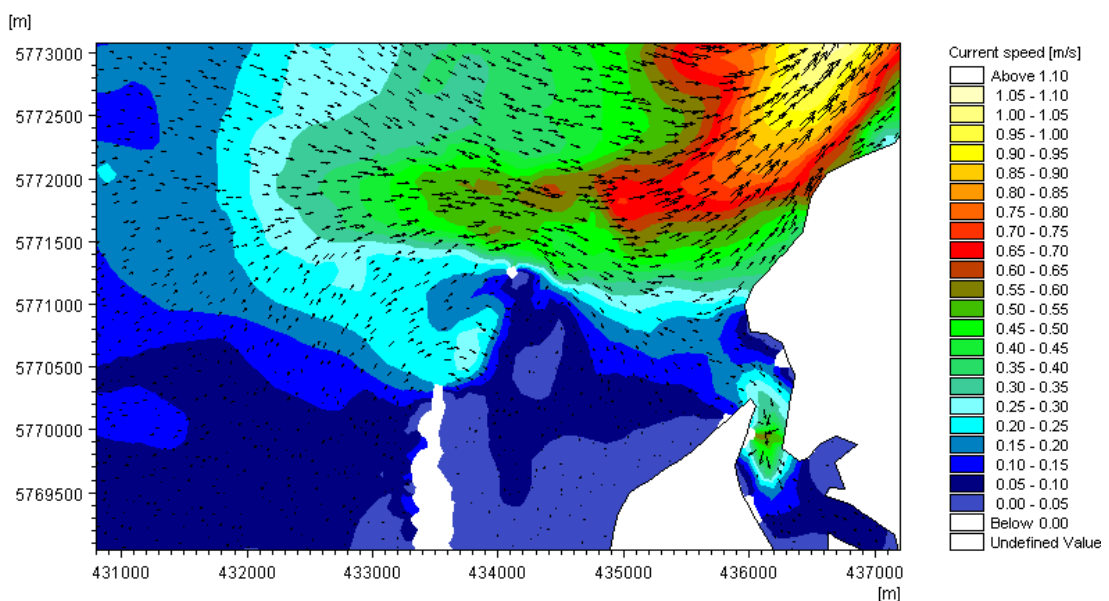


Figure 6.32 Mid flood year 1 Stage 3 (2035)

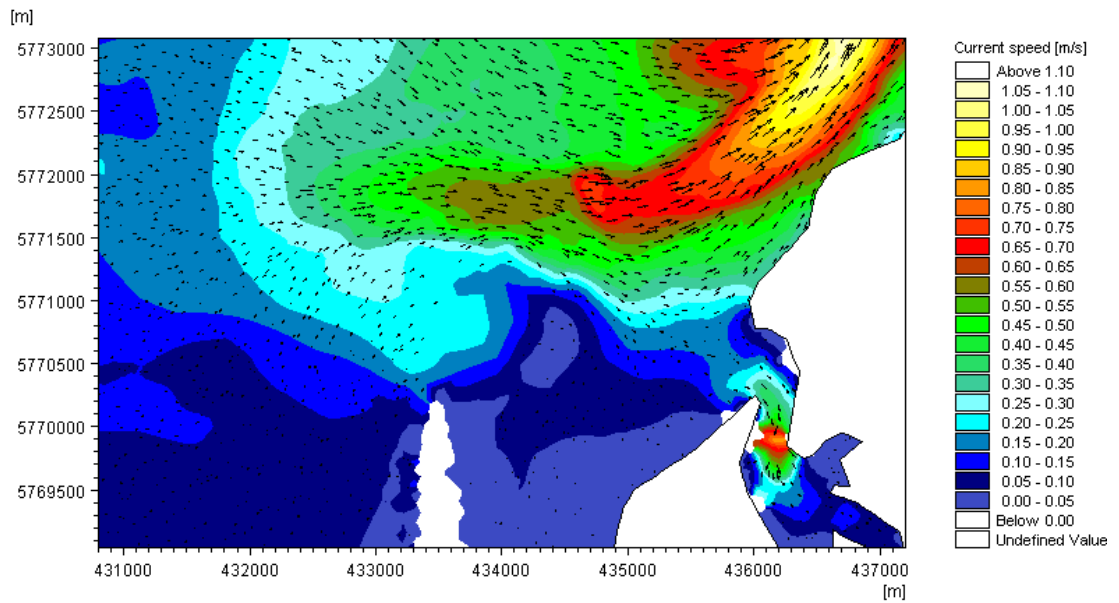


Figure 6.33 Mid flood year 2 Stage 3(2036)

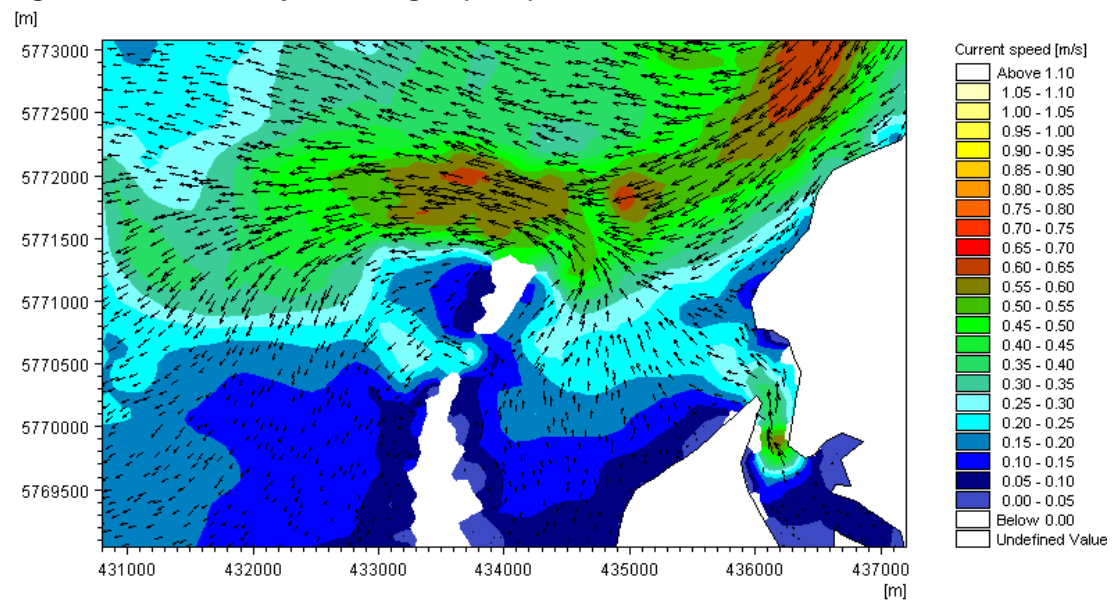


Figure 6.34 Mid ebb year 1 stage 3(2035)

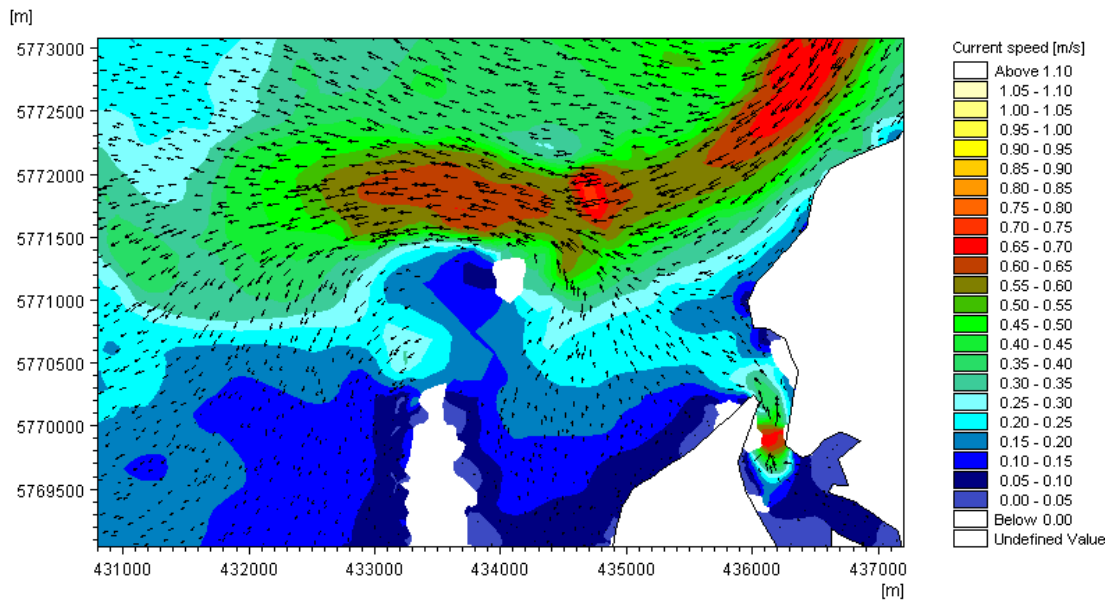


Figure 6.35 Mid ebb year 2 stage 3(2036)

The accumulated sediment transport was represented in vector format at the end year 1 and year 2 for Stage 3, figure 6.36 and figure 6.37. An increase in accumulated sediment transport was visible comparing year 1 Stage 3 (2035) to year 2 to Stage 3 (2036). The seaward transport vectors along the drift aligned dune were reduced significantly in Stage 3 suggesting wave driven transport has reduced with the addition of the sediment. The transport vectors across the infilled section were also reduced close to shore. A reduction in sediment transport vector magnitude was evident on the beach in front of the island section indicating a slowdown of sediment movement in this area.

A large decrease in sediment transport at the formative inlet in the drift aligned section was visible when comparing year 1 Stage 3 (2035) to year 2 Stage 3 (2036). There was minimal sediment transport in the area seaward of the original breach section, and a further reduction of erosive wave driven sediment transport was evident along the drift aligned dune line. However, an increase in sediment transport was visible further seaward where the bed level remains below MWL of 0.0m OD Malin. The transport direction seaward of the original Island section has become predominantly shore normal as opposed to previously being shore parallel.

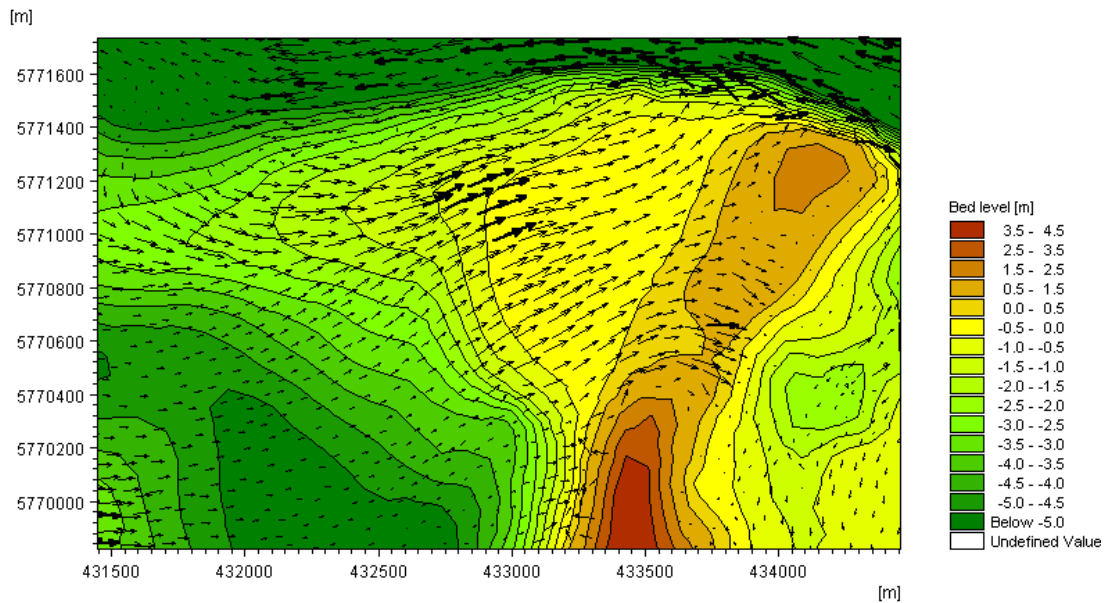


Figure 6.36 cumulative sediment transport vectors end of year 1 in Stage 3(2035)

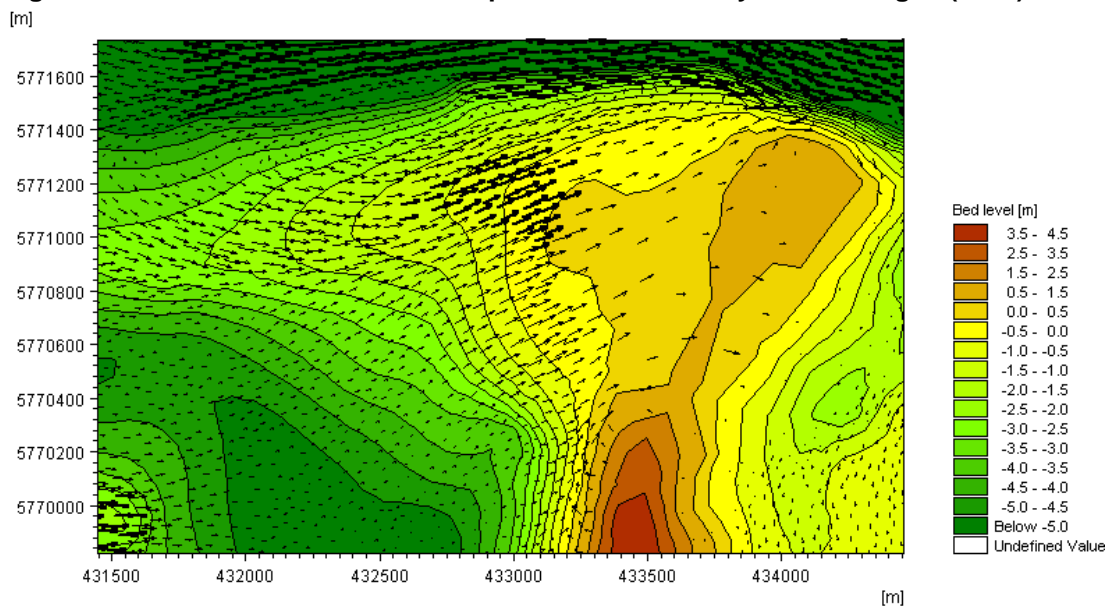


Figure 6.37 cumulative sediment transport vectors end of year 2 in Stage 3(2036)

The volume of sediment movement in Stage 3 in the same locations as Stage 1 and 2 is compared in Table 6.7. There was little variation in the morphological response between Stage 2 (2026) and year 1 in Stage 3 (2035) in the lower part of the swash zone. However, in year 2 Stage 3 (2036), the lower swash zone became significantly erosive in nature with a resultant loss of almost 30,000 m³. Similarly in the upper swash zone a larger increase in cut volumes and reduction in fill in year 2 was apparent in comparison with year 1. The increase in erosion in the swash aligned zone

when the drift aligned zone has become stable was indicative that a new stage in the long term evolutionary cycle is emerging in Inner Dingle Bay.

In the channel, the resultant morphodynamic climate was accretive but the balance between cut and fill became greater in year 2. The sub tidal section of the channel displays the greatest rates of accretion with approximately 55,000 m³ in year 2.

Table 6.7 Volume calculations for Stage 3 simulations

Area	Year 1			Year 2		
	Cut (m ³)	Fill (m ³)	Balance (m ³)	Cut (m ³)	Fill (m ³)	Balance (m ³)
Channel	-68892	70197	1305	-46775	96272	49496
Channel Sub	-39570	49868	10299	-26829	81956	55127
Upper Swash	-46936	50188	3252	-65832	9441	-56391
Lower Swash	-17172	24119	6947	-33987	4795	-29192

6.7.3 Conclusions from Stage 3

The Stage 3 modelling results indicated that a significant amount of sediment infilling in the channel will induce an accretive morphodynamic climate on the drift aligned beach of Rossbeigh. The amount of sediment required to trigger this change in morphodynamics has been approximated. The time scale for this volume to accrete naturally has also been quantified.

It was estimated that a total deposition of 650,000 m³ of additional sediment relative to the 2013 survey is required for dune regeneration in the drift aligned zone to initiate. An approximate timeframe for this deposition to occur naturally was approximated at 21 years. The in-filled model bathymetry is similar to the stable pre 2000 configuration of Rossbeigh.

The infilling of the channel reduces the erosive potential of both the tidal currents and waves. As a result the sediment transport patterns have altered to represent morphodynamic that is inherently beach nourishing as opposed to the present climate which is erosive.

6.8 Comparison with sediment trend analysis

6.8.1 General

As the GSTA sampling, discussed in Section 4.4, was undertaken during the Stage 1 modelling time period, direct comparisons of sediment transport results from both methods were possible. This presented a rare opportunity to assess the suitability of the GSTA method against a fully validated numerical morphodynamic model.

The modelled sediment transport regime was compared to the GSTA best case, FB+, figure 6.38. A corresponding plot of modelled accumulated sediment transport over the same time period as the GSTA is represented in figure 6.39.

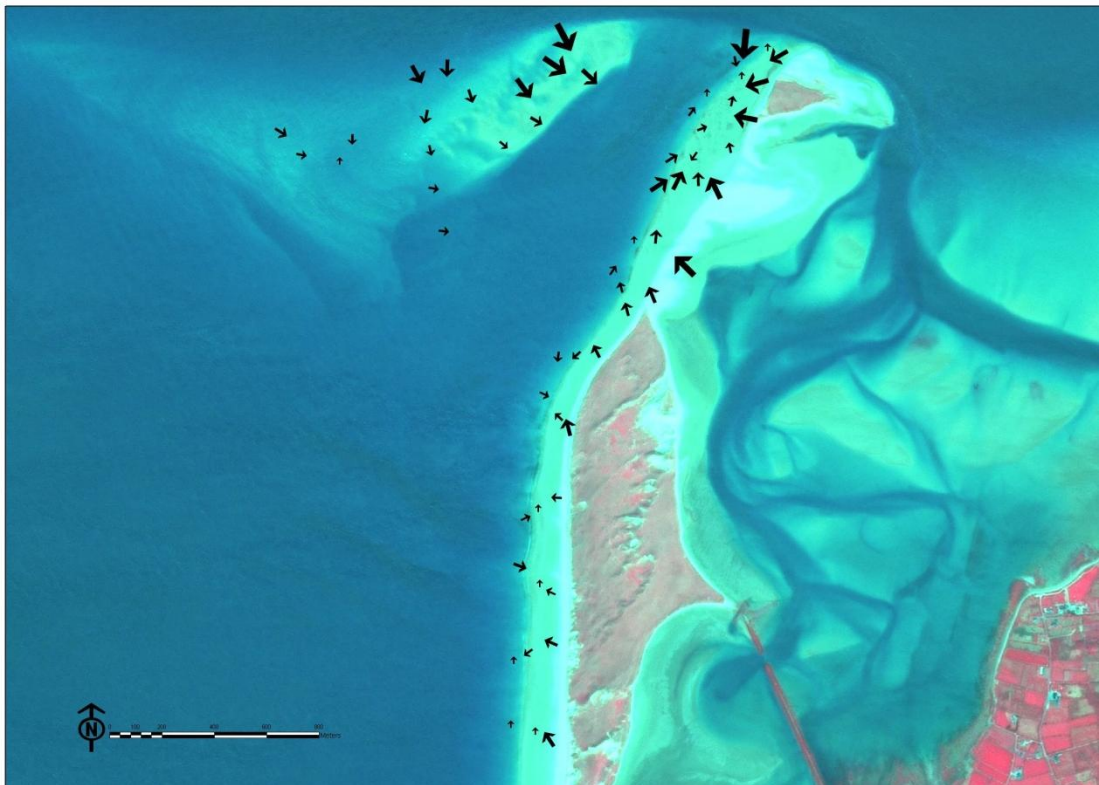


Figure 6.38 GSTA Fp + case

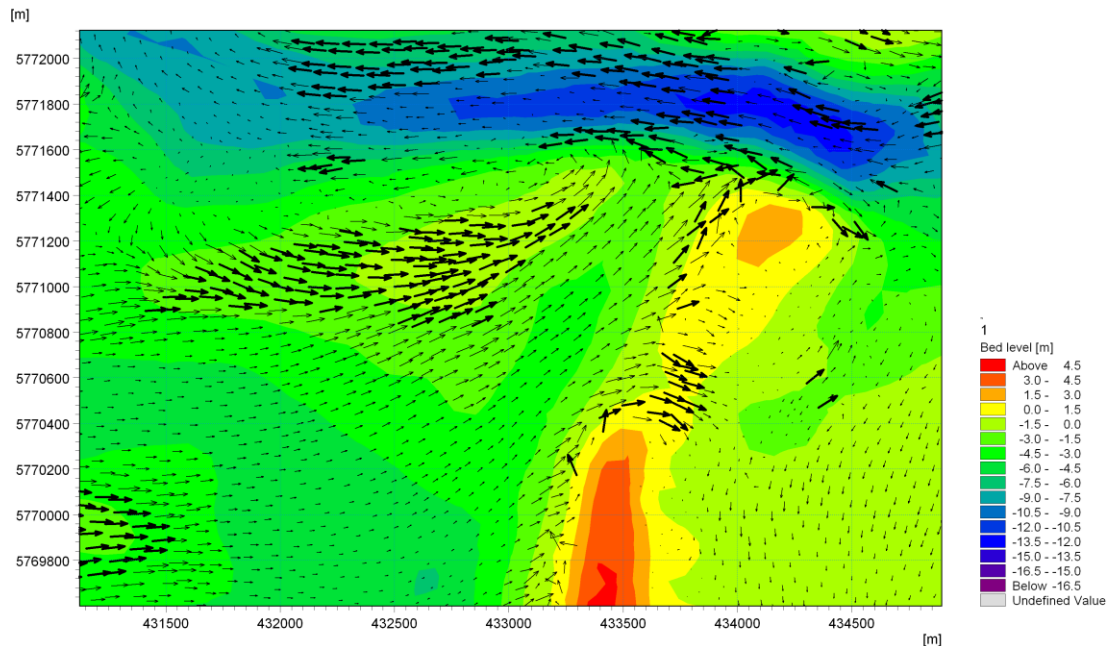


Figure 6.39 Simulated Accumulated Sediment transport vectors for GSTA comparison

6.8.2 Results

Comparing the trend analysis plot, figure 6.38, to the simulation, figure 6.39, it was evident that there were discrepancies between the two in certain areas of the coastal cell.

The direction of accumulated sediment transport on the ebb tidal bar differs in direction with the modelled. The modelled sediment transport vectors appeared to be driven in the same direction as peak tidal flood currents while the GSTA vectors follow a direct shore normal route. This suggests that the GSTA method showed a bias for wave dominated sediment transport in this area.

The other area of disagreement was at the breached inlet on the drift aligned beach. The model results show strong sediment transport going east wards through the breach but the GSTA trends were in the opposite direction showing sediment transport moving offshore in a westerly direction. This can be explained again by the mode of dominant sediment transport the GSTA method was biased towards. The GSTA adopted a wave dominant transport mode for this location, describing the sediment transport driven by wave erosive at the breach, while the model shows tidal current sediment transport through the breach was dominant.

Along the drift aligned dune section both GSTA and modelled sediment transport displayed alongshore and offshore wave dominated transport vectors. Although magnitude was notional in the GSTA analysis, the FB+ case tended to display wave driven sediment transport as the dominant mode along the entire dune line of the drift aligned beach where as the modelled transport vectors displayed intermittent wave dominant sediment transport.

An interesting feature was the agreement at the Island terminus, where the sediment transport vectors appeared to be acting against the flood tidal current patterns and moving in an ebb tidal direction. Given the agreement of both numerical modelling derived sediment transport vectors and the GSTA transport vectors it was possible that this location may be ebb tidally dominated. This was a significant finding; given the nature of the bar migration described in Section 6.5 and Section 4.3.6. The large sediment transport vectors explain why the ebb tidal bar migration was fastest at this location.

6.8.3 Conclusions on GSTA and Numerical Modelling Comparison

It was evident from the analysis in the previous section that the simulated and GSTA derived plots show good agreement. While discrepancies exist between the two the general trend of sediment transport in the study area described by numerical modelling results was reproduced by the GSTA method. This result provided further evidence there is merit in applying trend based methodologies to coastal sediment transport scenarios.

6.9 Conclusions

The main conclusions from the Morphological modelling focus on quantifying the dominant sediment transport patterns in the system and predicting the evolution of Inner Dingle Bay. Particular focus was given to the unstable erosive drift aligned section and ebb tidal bar of Rossbeigh.

A validated numerical model was created and successfully predicted short term evolution of the study area. This model was then utilised to simulate morphological change representing twenty years of evolution, implementing a novel form of morphological schematisation based scenario modelling. This scenario modelling provided quantities and a time frame for when Rossbeigh's breached area would begin to regenerate. Changing of the dominant modes of sediment transport was also identified.

The GSTA work in Section 4.4 was re-examined with comparative simulation results. Conclusions on the bias of the GSTA original results relating to wave dominated sediment transport were derived. A sediment transport trend originally thought erroneous was categorised as possible due to agreement of both numerical modelling and GSTA methodology.

The following conclusions on the evolution of the coastal system were made;

- Between 38,000 m³ and 53,000 m³ of sediment was shown to be migrating annually into the drift aligned and ebb tidal bar sub tidal region.
- Approximately 650,000 m³ of sediment deposition in the channel between ebb tidal bar and drift aligned shoreline of Rossbeigh is required before the dunes in the breached area begin to regenerate.
- It has been predicted that 23 years of evolution from 2013 is required for this amount of sediment to migrate shorewards to form an intertidal bar in front of the drift aligned shoreline of Rossbeigh. The bathymetry of Inner Dingle Bay in 2036 was generated in the final model run.
- Once a stable intertidal platform has established in the drift aligned shoreline of Rossbeigh, accretion rates increase and erosion in the

drift aligned reduces significantly resulting in an overall accretive environment.

7 Predicting the Evolution of Inner Dingle Bay

7.1 Introduction

This chapter focuses on the impacts and effects of the recorded and predicted morphological evolution documented in the preceding chapters. A summary of findings related to the evolution of Rossbeigh is presented and analysed. The timescale of the current evolutionary cycle is quantified combining aeolian and numerical modelling results. The flood risk in the area behind Rossbeigh Barrier associated with the breaching and evolution is also assessed along with possible intervention strategies and methodologies.

7.2. Summary of Findings

The analysis undertaken during this research has identified the key features of the current stage of evolutionary cycle of Inner Dingle Bay and specifically of Rossbeigh barrier beach. However, due to the paucity of historical data prior to the present breaching phase, it was difficult to identify what triggered the change from stable to dynamic erosive stages in the cycle. It is evident from the research that the removal of the ebb tidal swash platform between 2003 and 2004 and the simultaneous straightening of the tidal inlet channel; set in motion the erosive climate that led to breaching and erosion that followed.

The various methods of investigation have all yielded similar conclusions. The erosion in the drift aligned zone and growth of ebb tidal bar, its affect on wave direction and the migration of this ebb tidal bar shorewards were key features of the evolutionary process identified.

Using these results a stage by stage evolution cycle can be formulated and timescale quantified. A five stage conceptual model, figure 7.15, of the evolution of Inner Dingle Bay was developed and its key features are described as follows:-

- **Stage 1** -The identification of the removal of the wave breaking effect from the swash platform on the drift aligned zone of Rossbeigh from 2004 to 2008 can be considered Stage 1 of the cycle, this has been described in detail in Section 3.5.
- **Stage 2** -The reduction in area of the Island and growth of breach width due to erosion, establishment of channel between ebb tidal bar and drift aligned zone, migration of drift/swash hinge point and growth seaward of ebb tidal bar are all included in Stage 2
- **Stage 3** -The migration of the ebb tidal delta towards the drift aligned shore line, the complete erosion of the island, further widening of

breach and wave effects due to refraction over ebb tidal delta. Inlet channel meandering are all initiated in Stage 3.

- **Stage 4** -The welding of the ebb tidal bar, infilling of shore parallel channel, removal of island and slow down in dune retreat/breach width establishment of embryo dunes is represented in Stage 4.
- **Stage 5** -Aeolian regeneration, dune repair in drift aligned zone and re-emergence of a swash platform in the drift aligned shore as well as Inlet meander occur in Stage 5.

7.3 Critical Components to establishing Timescale of Evolutionary Cycle

Three critical components that contribute to evolutionary cycle described in Section 7.2 are discussed. These are;

- 1 the limit of the width of the breach/ dune edge erosion,
- 2 the rate of ebb tidal bar migration shore wards and
- 3 the rate of aeolian driven re-establishment of embryo dunes.

The various methods of measuring these three components undertaken over the course of this research are collated and compared in the following subsections.

7.3.1 Quantifying limits of Breach Width Erosion

The limits of breach width or median dune termination were plotted in Figure 7.1 by comparing the historical re- curves identified in Section 3.2, the dune vegetation line surveys measured in Section 3.3 and also the model generated bathymetry/topography presented in Section 6.7.

The historical limits of recurves were compared to the model generated final breach position when accretion is assumed to re commence, to establish a context for the current breaching.

The length and source of each width measurement was tabulated in Table 7.1. The HWM from 1977 was used as a reference for the Historical re- curves. It was considered that the extent of this line represents the northerly limit in Rossbeigh's evolution. The re-curves were identified as being either earlier northern limits of dune progression or southern limits to a historical breaching event.

Table 7.1 Median Termination widths

Phase	Breach Length (m)	Source	Year
Stable Dune Extent	-	HWM Photo	1977
Recent Breach +3year	650	Measured	2011
Initiation of Recovery	1,400	Simulated	2033
Historical Re-curve 1	1,500	Photo Identification	Unknown
Historical Re-curve 2	1,900	Photo Identification	Unknown

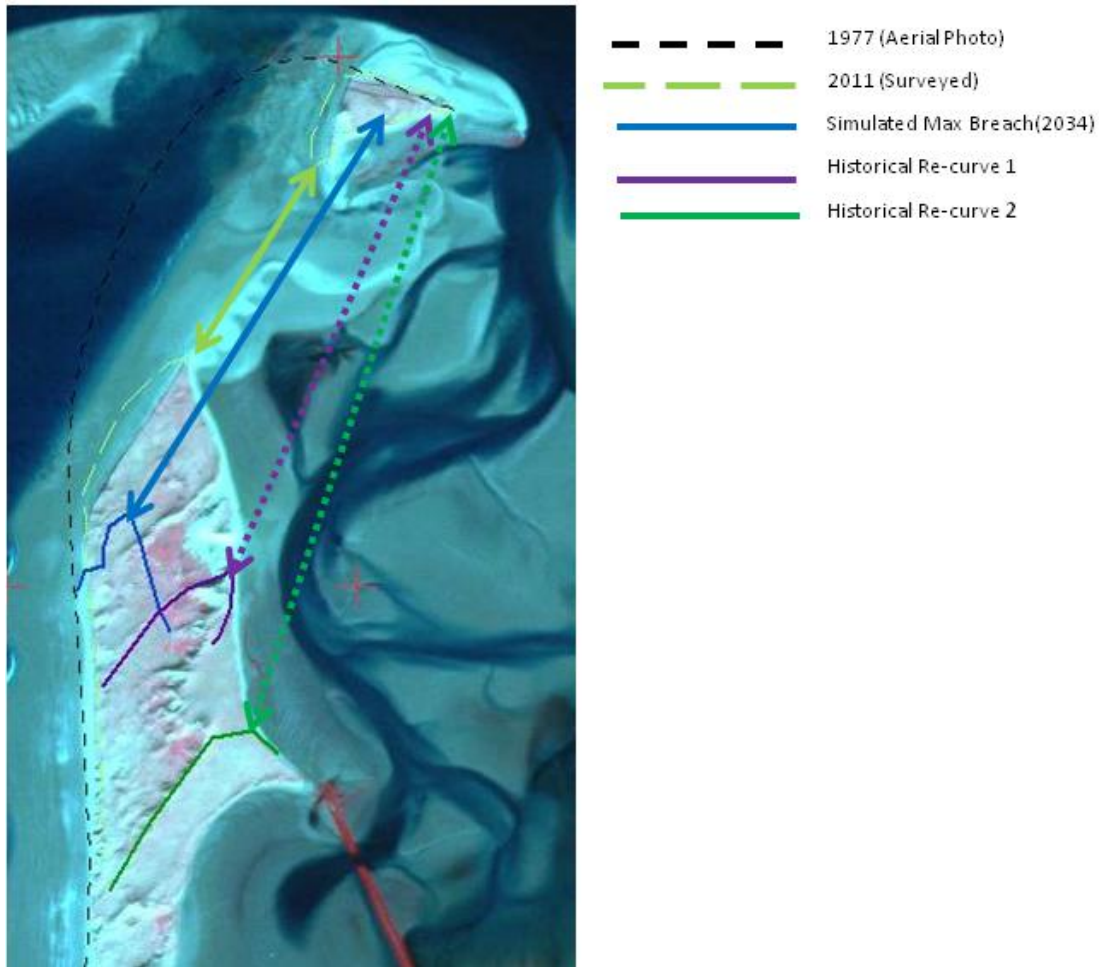


Figure 7.1 Breach width – Dune Termination points over time on Rossbeigh

A breach width of 650 m was measured in 2011 from the island section to the dune terminal section while the numerical modelling generated breach maximum width prior to Initiation of recovery phase was measured to be 1,400 m from the dune terminal end to the remaining Island section still above 3 m OD Malin.

It was apparent that the simulated breaching width of is almost double that of the measured breach in 2011, suggesting the breach widening rate will slow down considerably from 2011 to 2034. In 2013 (not shown), the breach was measured at 900 m representing a dune removal rate of 125 m width per year. Extrapolating this rate out it would only take 6 years for the breach to grow to the simulated dune line representing the beginning of regeneration phase and not 2034 as shown in numerical modelling, Section 6.7.

Several factors can explain the disparity of the timing, as the ebb tidal bar infills it is expected to reduce the rate of dune erosion, therefore direct extrapolation is not accounting for this slowdown. The dune cross-section increases in area moving south from the breach location. It would, therefore, take longer to remove a meter width than in the initial breaching location. It is likely that the timescale to arrive at the regeneration initiation phase is between 20 and 6 years as the modelling can be deemed overly conservative as detailed later in this chapter.

Although it was not possible to date the historical re-curves, Figure 7.1 presents a picture of the extent of the current breaching relates to these historical events. It is unclear if these re-curve were formed as part of the barrier's initial evolution north or as a result of breaching, either way it is evidence that the barrier previously expanded northward from these positions. This reinforces the theory that the dune system can recover and rebuild dune structure towards the 1977 position.

7.3.2 Ebb Tidal Bar migration and Channel Infilling.

The rate at which the ebb tidal bar is migrating towards the drift aligned shoreline has been identified as a key metric in estimating the progression of Rossbeigh's morphodynamic cycle to a regeneration stage. The rate of infilling of the channel between ebb tidal bar and drift aligned shore was noted in numerical modelling and bathymetric surveying, Section 6.5 and Section 4.3.6 respectively.

A qualitative rate of migration was also obtained from satellite imagery analysis from Section 3.5 and compared with the surveyed rates from Section 4.3.6, figure 7.2. The ebb tidal bar boundary was defined at the -2.0 m contour. This was identified from the survey cross-sections of Section 4.3.4 and Section 4.3.5. The sources of these contour lines are tabulated in Table 7.2

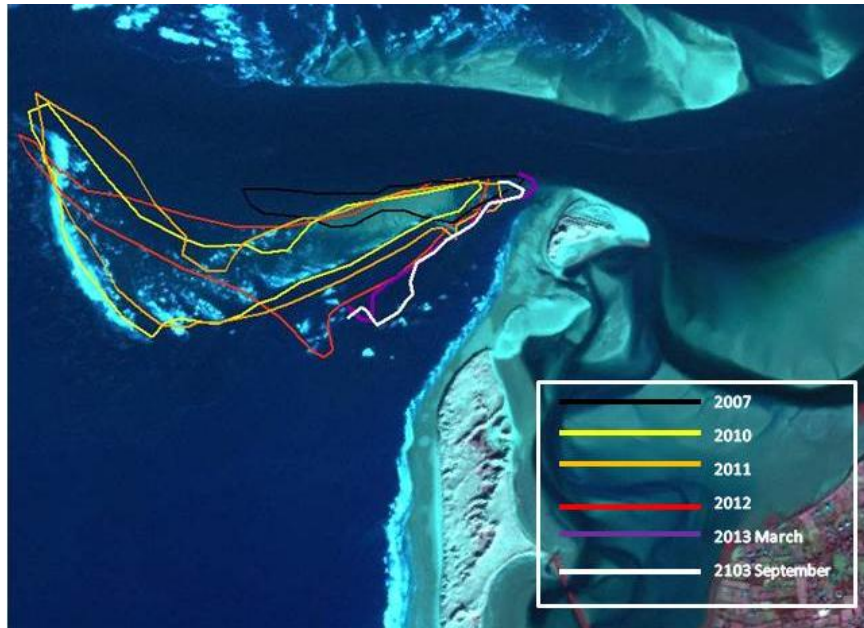


Figure 7.2 Ebb Tidal Bar migration

Table 7.2 Ebb Tidal Bar migration rate

Period	Source
2007	Satellite Imagery
2010	Satellite Imagery
2011	Satellite Imagery
2012	Satellite Imagery
2013 March	Bathy Survey
2013 September	Bathy Survey

It is apparent from figure 8.2, that the ebb tidal bar is moving shorewards. The bar migration was not uniform along the ebb tidal bar boundary. It has consistently migrated shorewards at the neck end of the channel, while large areas of the south eastern corner of the ebb tidal bar have advanced into the channel entrance in recent years.

The non-uniformities in the migration rates measured from survey and imagery were due to the non uniform forcings driving the migration. Comparing the rate of infilling of the channel, figure 7.3, was considered a more suitable method of quantifying the rate at which the ebb tidal bar migrates. This figure was ultimately used to estimate the amount of time it will take for the bar to weld with the drift aligned shore of Rossbeigh.

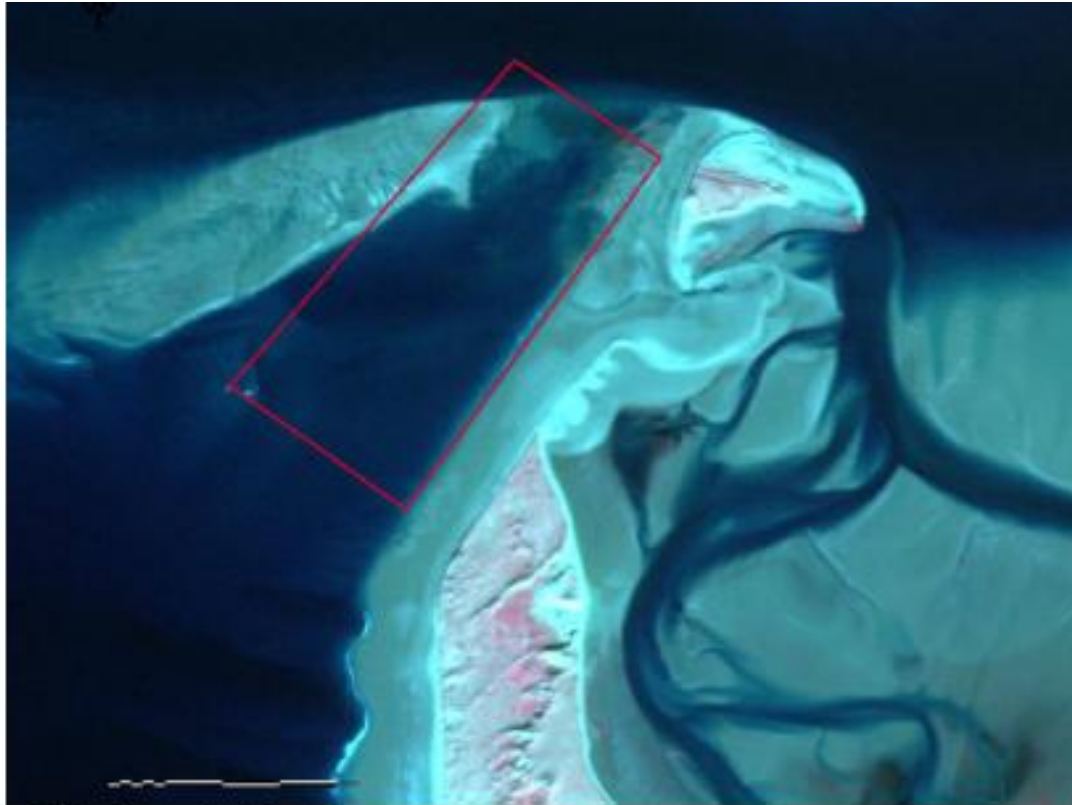


Figure 7.3 Channel area used in volume calculation

The rates of infilling per year were documented in Table 8.3. It was evident that the rates vary significantly with time period. The longer 18 month survey period results showed the channel eroding. The shorter 6 month survey period and 6 month simulation showed good agreement of approximately 100,000 m³ infilling per year. This was expected as both periods cover a summer season only. The infilling rate of the model was reduced when a full year was simulated and a further infilling rate was visible when a second year was simulated.

Table 7.3 Channel Infilling Rates

Period	Source	Cut (m ³)	Fill (m ³)	Balance (m ³)	Rate (m ³ / year)
Aug 2011-Mar 2013	Survey	138595	63243	-75352	-50235
Mar 2013- Sep 2013	Survey	60212	120106	59894	119788
Mar 2013+6 months	Model	-69210	114697	45487	90974
Mar 2013+1 year	Model	-84092	104176	20084	20084
Mar 2013+2 year	Model	-90241	100084	9843	9843

The erosion rates of the longer periods survey was in contrast with the other results. This was because the surveyed rate included two winter seasons and only one summer season. It was also from an earlier period in the

channel's evolution therefore direct comparison with the simulated rates could not be made. Another feature that disguises the channel infilling was the inclusion of the beach which was eroding constantly and therefore masking infilling rates due to bar migration.

It has been calculated that a further 650,000 m³ of sediment was required for the ebb tidal bar to weld to the shoreline to reflect bathymetry similar to the stable pre-breaching phase of Rossbeigh.

The timescale of when the channel fills with sediment and bar welding occurs calculated by the numerical modelling approach was estimated at approximately 23 years from 2013. However, from survey analysis and sediment trend analysis it was possible that this timescale maybe an over estimation.

An alternative method of calculating the time taken for ebb tidal bar welding to the drift aligned was using the surveyed rates of migration. The results for each survey, 6 month and 18 month, were added and divided by two to produce an average yearly infilling rate from 2011 to 2013. Using this method, the channel infilling rate was calculated to be approximately 35,000 m³/ year. This rate would result in bar welding occurring in 18 years from the base year of 2013.

However, this method of timescale calculation also discounts critical components such as the cumulative effect of bathymetry change on the accretion process. In the simulated results the rate was shown to vary year on year due to the constant updating of the bathymetry. Based on simulation results the rate of infilling reduces as the bar migrates shoreward. This is due to the increase in peak velocities as a result of the channel narrowing due to infilling and bar migration. Considering this it was deemed reasonable to state that infilling will take approximately 20 years from a base year of 2013.

7.3.3 Aeolian driven dune regeneration

The third factor to be considered was the quantification of aeolian transport driven dune regeneration. This mode of sediment transport only becomes a morphodynamic driver in Rossbeigh's evolution when the ebb tidal bar has welded to the drift aligned zone. The formation of an intertidal platform in the drift aligned zone provides the dry sediment necessary aeolian transport to have an effect. The intertidal platform also provides protection from wave breaking to embryo sand dunes. The timescale for the bar welding to occur has been estimated in the previous sections.

The potential for relatively rapid dune regeneration was demonstrated in Section 4.2.5 using sediment fencing. It was also noted that for long-term regeneration the upper beach must be sufficiently above the SHWL. The need for a stable beach to ensure aeolian transport establishes robust stable dunes was also apparent, when three months of build-up was removed in a single storm event.

The length of beach or fetch is a critical component when estimating the potential of aeolian driven dune regeneration. A study by De Vries et al. (2013) on the Dutch coast has shown that the optimum beach width is 200 m. However, it was also shown that beaches >300 m wide have little correlation between volume change and width, possibly due to damp pockets of sand resisting wind forcing. Delgado-Fernandez (2013) found that effective aeolian transport has speed limits, the optimum for transport of sand being low to medium speeds. During field tests it was found that critical shear velocity was between 4.7 m/s and 5.4m/s.

In terms of re-establishment rates, Priestas et al. (2010) recorded approximately 3-4 cm per month in the presence of vegetation, with transport dominant from offshore winds blowing over a back barrier wash over terrace. In Brittany, France, Suanez et al. (2011) recorded secondary embryo dunes growing at 4-4.5 cm per month. The volumes recorded varied -1 m³/m to 2 m³/m over a length of 650 m of dunes, between November 2008 to January 2009.

The aeolian transport measurements taken on Rossbeigh, detailed in Section 4.2.6, were analysed to establish a rate of dune re-establishment similar to the cases documented above. The first step was extrapolating out the field data to represent a typical year. The percentage occurrence, figure 7.4, from the nearest weather station, Valentia, was applied to the hourly measurements recorded in Table 4.1 in Section 4.2.6. Table 7.4 documents the yearly rate of aeolian sediment per direction in both recording locations on Rossbeigh's drift aligned shore. Only directions where sediment was accumulated in the traps were used in this calculation. The maximum rates were recorded for the South westerly directional segment.

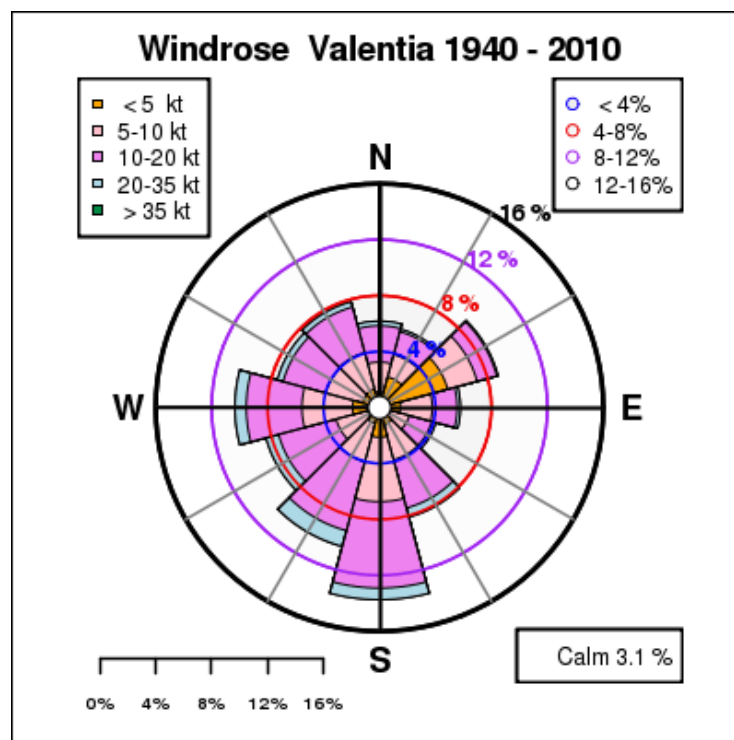


Figure 7.4 Windrose for Valentia Weather Station (Met Eireann)

Table 7.4 Yearly rate of aeolian sediment accumulation

Directional Segment	%occurrence	Collection Rate		Yearly Trap Collection Total	
		Station 1 (g/hr)	Station 2 (g/hr)	Station 1 (g/yr)	Station 2 (g/yr)
SSW	4%	118	-	41312	0
SW	7%	46	238	28207	145896
W	6%	9	7	4888	3679
NW	8%	8	13	5770	9321
NNE	2%	30	27	5335	4654
N	6%	-	11	0	5834

The yearly weight and volume per meter width of dune was calculated in Table 7.5. The yearly rate was recorded in Table 7.4 was multiplied by 50 to represent a meter width; (the trap width is 0.02 m). To calculate the volume, a density of 1600 Kg /m³ was used for dry sand. The total volumes for each station vary by a factor of 2. Station 1 closest to the Rossbeigh terminal dune was approximately half that of the Station 2 volume. This was expected as Station 2 was in a more exposed location with no natural sheltering from wind directions incident on Rossbeigh.

Table 7.5 Yearly Weight and Volume per m width of Dune

Direction	Yearly Weight per m width dune		Yearly Volume per m width dune	
	Station 1 (Kgs/m/yr)	Station 2 (Kgs/m/yr)	Station 1 (m ³ /m/yr)	Station 2 (m ³ /m/yr)
SSW	2065.61	0.00	1.29	0.00
SW	1410.36	7294.78	0.88	4.56
W	244.40	183.96	0.15	0.11
NW	288.50	466.03	0.18	0.29
NNE	266.74	232.72	0.17	0.15
N	0.00	291.71	0.00	0.18
Total	4275.61	8469.20	2.67	5.29

To estimate the annual and monthly dune height increase several assumptions were made. The major assumptions were that the initial surface was flat, the dune shape was prism shaped, and an angle of repose for the dune of 40 ° and, critically no erosion due to wind or wave action was considered. This gives embryo dunes of 3.55 m base width and a height of 1.50m for Station 1, and a base width of 5 m and height of 2.12 m for Station 2 after the first year of regeneration, as shown in Table 7.6.

Table 7.6 Calculation of monthly dune height increase

Station	1	2
Base width (m)	3.55	5
Area (m ²)	2.67	5.29
h/2 (m)	0.75	1.06
h (m)	1.50	2.12
Monthly height increase	0.13	0.18
Angle of Repose (deg)	40.3	40.2

The calculated rates were compared with rates from literature and measured rates from the sediment fencing trial detailed in Section 4.2.5, in Table 7.7. The calculated monthly height increases were higher than recorded previously in literature. The rates calculated from field data were also higher than accretion rate of the sediment fence location adjacent to the wind trap location 2, measured 1 year after fence installation.

The other sediment fencing rate which represents a month of accretion on a relatively flat beach, uninterrupted by storms was much larger than the largest calculated rate on Rossbeigh.

Table 7.7 Comparison of Dune Height increase rates

Type	Rate (m/month)
Rossbeigh Location 1	0.13
Rossbeigh Location 2	0.18
Priestas et al. (2009)	0.03-0.04
Suarez et al. (2011)	0.04-0.045
Sediment fencing ⁽¹⁾	0.083
Sediment fencing ⁽²⁾	1.0

⁽¹⁾Based on 1 year measurement including erosion and gravel accretion.

⁽²⁾Based on 1 month Summer measurement with no erosion.

It was clear from the field work and also the embryo dune development rate calculations that if the right conditions are present, dune regeneration will occur within 1-2 years to a level where vegetation can establish and bind the embryo dunes. A height range of 1.5 m to 2.12 m was estimated after one year of aeolian transport. This rate appears to be relative high compared to literature; this was likely due to the exclusion of aeolian erosion in the calculations. However, the results of the sediment fencing reinforce the theory that large rates of accretion were possible on Rossbeigh.

It should also be noted that the calculated rates were based on 2011 beach topography. This has a maximum fetch of approximately 100 m which was half the maximum fetch that positively effects accretion due to aeolian transport documented in literature. It has been established that for regeneration to initial, bar welding will occur, therefore providing twice the

fetch distance for aeolian transport during the dune embryo development stage.

7.4 Flood risk

As identified in Section 1.1, the increase in flooding in the low lying area behind Rossbeigh has been attributed to the erosion and breaching of the barrier in the local media. The flooding in the back barrier and lower Cromane in particular during high tides and storm surges has received national coverage.

In an attempt to quantify the effect the breaching of Rossbeigh has and will have in the future on the area behind the barrier beach, simulations representing three stages of Rossbeigh's evolution were modelled.

- 1 the pre-breach bathymetry and dune structure of approximately the year 2000
- 2 bathymetry and surveyed dune height from 2013 and
- 3 the simulated bathymetry from 2034 when regeneration will recommence.

The models were run for a spring tidal range with a moderate wind and a H_s of 4 m and T_p of 8 seconds to represent storm conditions. Water level output was recorded in 5 locations behind Rossbeigh, figure 7.5. These are shown in figures 7.6 and figures 7.7.

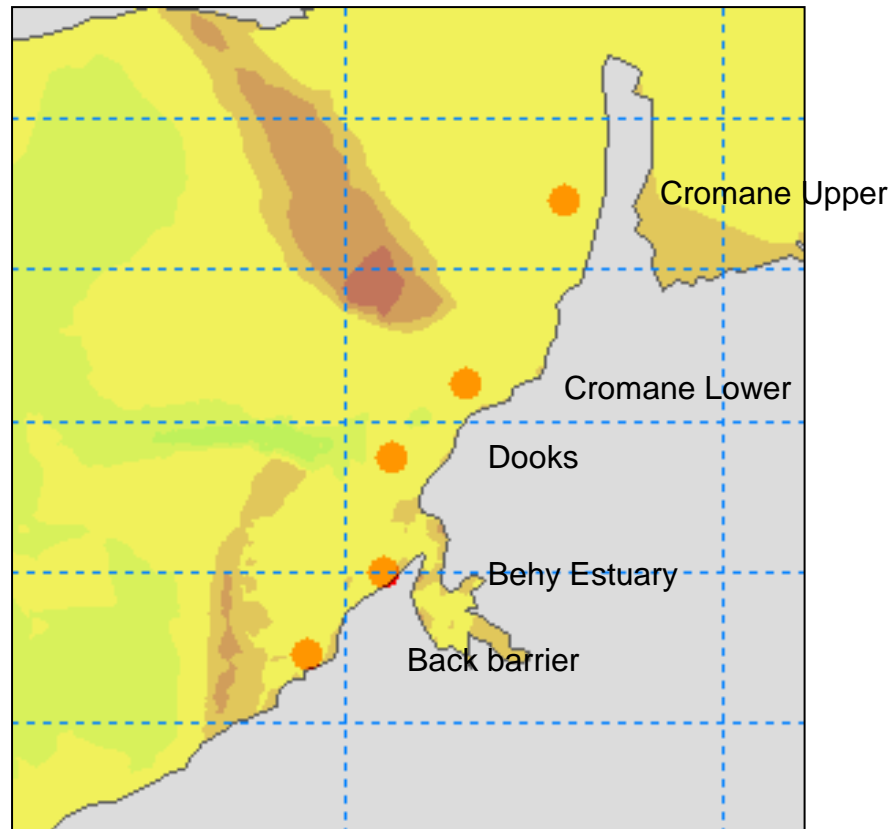


Figure 7.5 Simulated Data Locations

Four of the five locations showed very little difference in maximum water level at high tide. However, at Cromane Lower, figure 7.7, there was a significant increase (80 mm approx.) from the pre breach to current bathymetry (2013) and even larger increase for the future simulated bathymetry (130 mm). This suggests that flood risk is increasing as the erosion continues to alter the bathymetry of Rossbeigh, tidal Inlet and surrounding area. The tidal prism was greater in most locations when the 2000 bathymetry was compared with the present and future modelled bathymetry scenarios. In particular in the Behy Estuary and Back barrier locations and at the aforementioned Cromane Lower.

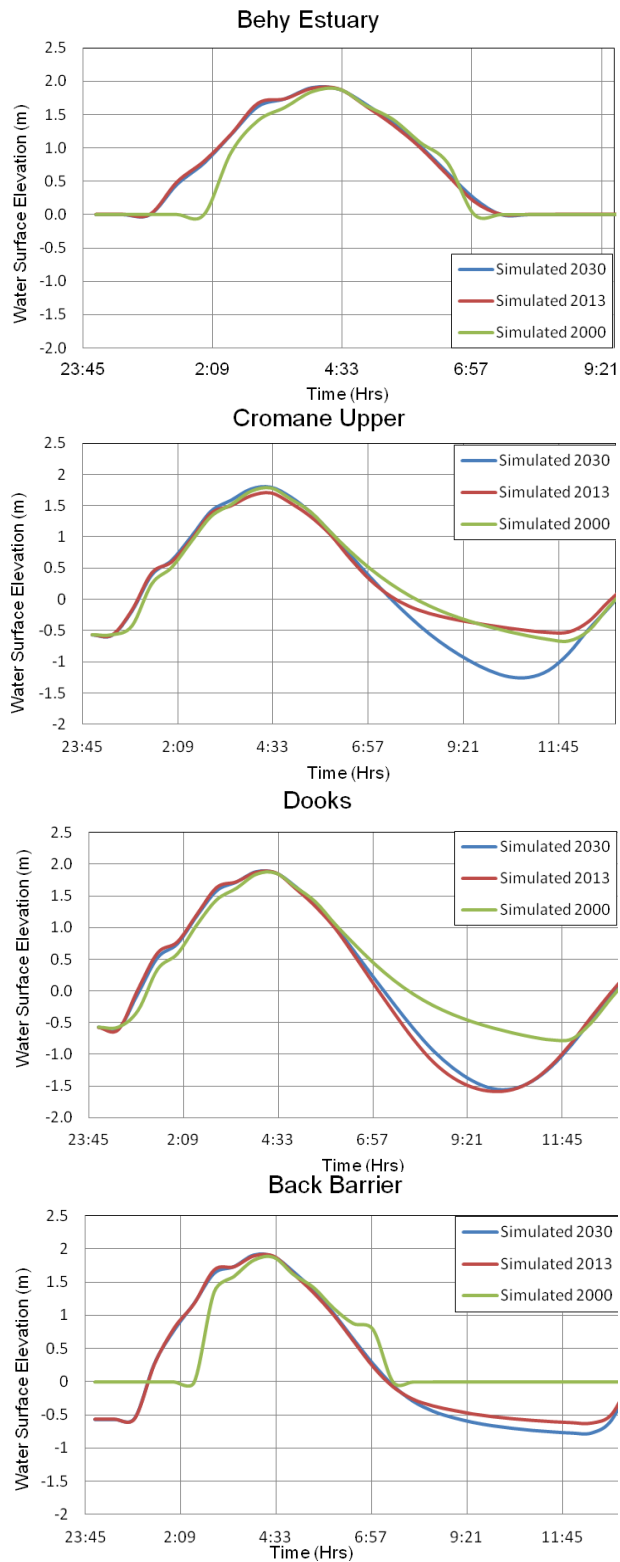


Figure 7.6 Simulated water level at Behy Estuary, Cromane Upper, Dooks, and Back Barrier

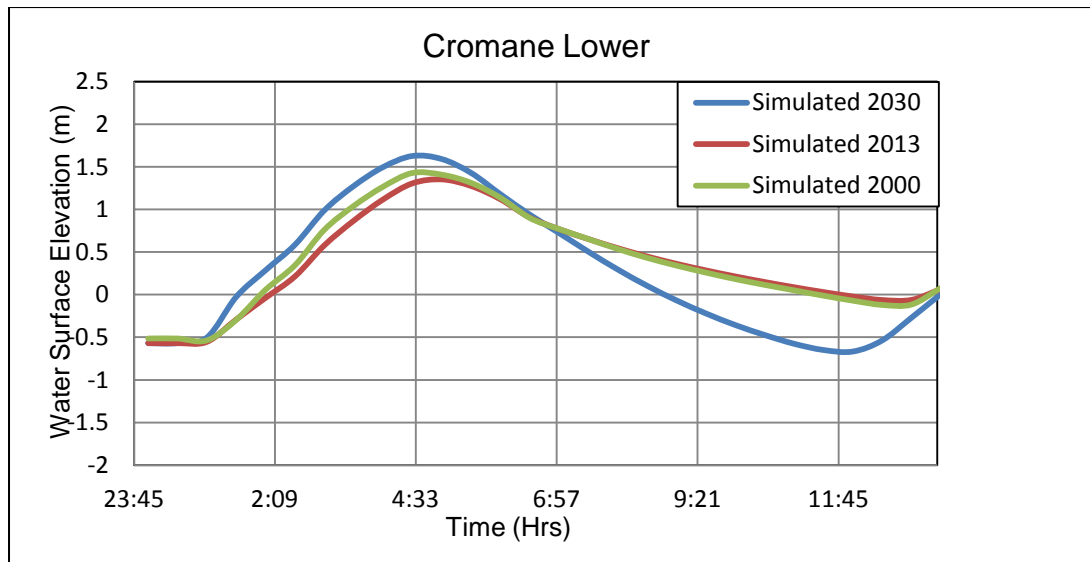


Figure 7.7 Simulated water level heights at Cromane Lower

Examining the plot of H_s at high tide for each model, figures 7.8-7.10, it was apparent that wave height has increased over time in the tidal inlet channel behind the barrier beaches, most notably in the channel between Cromane and Inch. The wave height increases in some locations from a range of 0.00 m-0.15 m to a range of 0.40 m – 0.60 m at high tide under storm conditions. The increase can be attributed to the lack of wave dissipation which was historically provided for by well-developed ebb tidal bars further offshore. The S shaped channel reduced the impact of large westerly swelling entering the inlet east of Rossbeigh.

The deepening of the tidal inlet channel in this area was another contributing factor to the increase in wave height. This deepening was caused by an increase in tidal currents which scour the channel bed. This increase in wave height was a significant factor to consider when evaluating the flood risk increase due to the erosion of Rossbeigh. It should also be taken into account when renovating flood defences in this area.

There was also a visible increase in wave height in the area directly behind Rossbeigh during the period from 2000 to the present 2013 bathymetry. This was due to waves propagating through the breach area. There was little change in the back barrier wave height distribution between the time periods from 2013 model to the 2030-35 model. It is evident from the 2030-2035 plot,

figure 7.10, that seaward of Rossbeigh's drift aligned zone, the newly emerged swash platform reduces the wave height incident on the beach at this location. The propagation distance of wave energy through the breach on Rossbeigh has also reduced slightly from 2013, figure 7.9 and 2030-2035, figure 7.10.

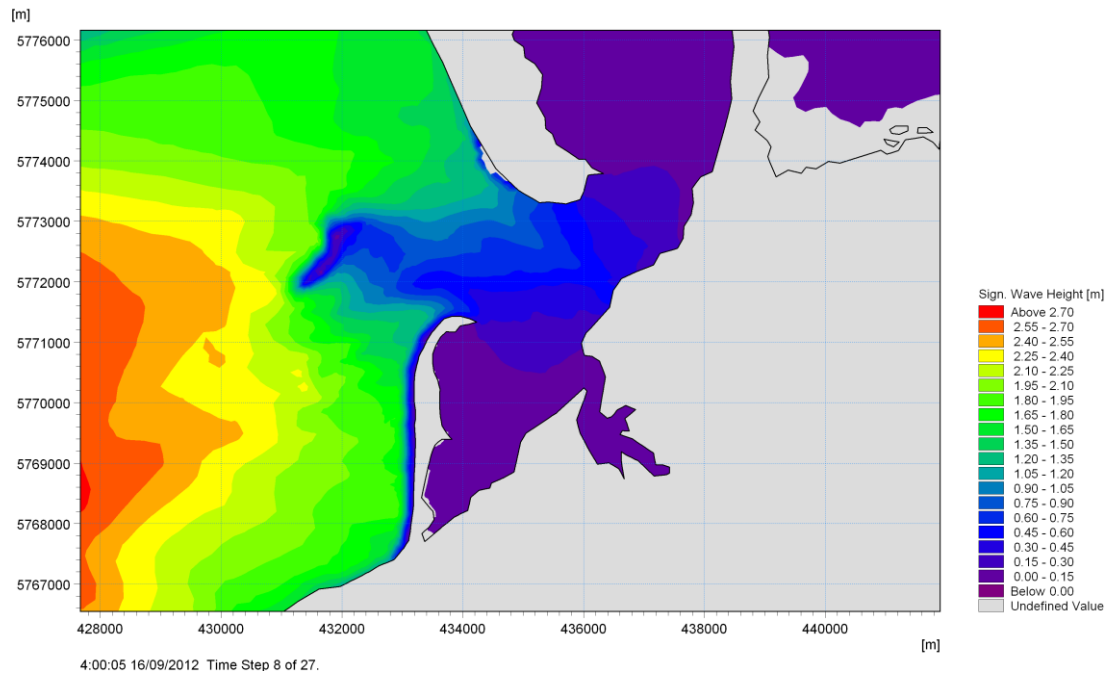


Figure 7.8 Hs at high tide for pre Breach bathymetry (2000)

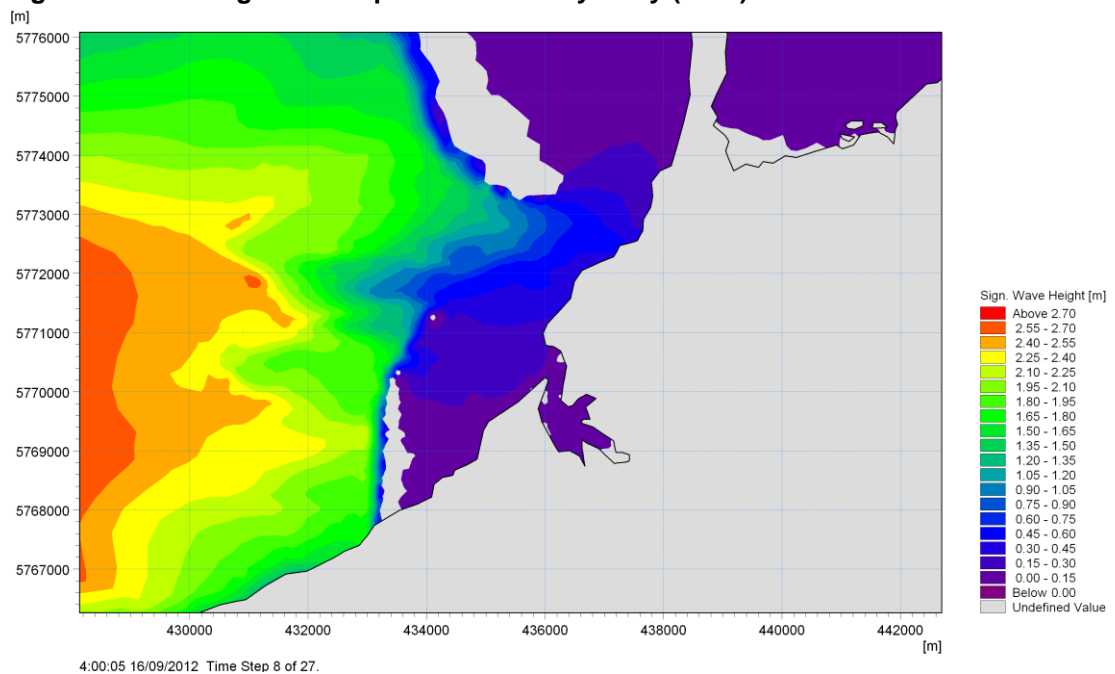


Figure 7.9 Hs at high tide for present bathymetry (2013)

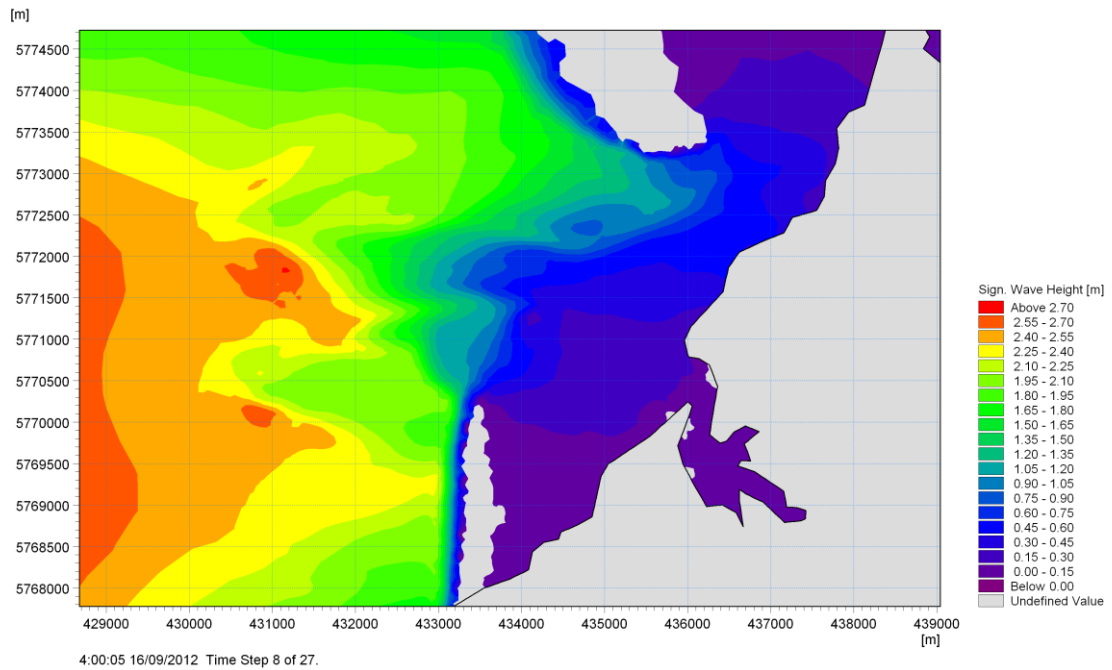


Figure 7.10 Hs at high tide for simulated future bathymetry (2030-2035)

It was apparent from this analysis that flood risk in low lying areas behind the barrier beaches was increasing with the continued erosion on Rossbeigh. The evolution of the ebb tidal bars and tidal inlet channel were also identified as driving factors behind the increase of wave height and tidal prism.

It has been shown that the area's most likely to be effected from the increases is the Lower Cromane area. The Back barrier and Behy Estuary locations display increased tidal prism, i.e. larger water volume moving during the tidal cycle. This was a result of erosion deepening the tidal inlet channel at these locations. However, as the max tidal height was not increasing, it is assumed that there is adequate storage in these areas to accommodate the extra flux of water.

7.5 Intervention Strategy

While the focus of this study was on gaining an understanding of the natural coastal processes driving the evolution of Rossbeigh and Inner Dingle Bay, consideration was also given to human intervention. This section details one possible strategy to return Rossbeigh to its pre breach stable state. The strategy was based on speeding up the natural evolution process described previously during this study.

A three stage process is proposed. The stages are:

1. Beach nourishment / Dredging
2. Sediment Fencing
3. Dune Vegetation Planting

7.5.1 Stage 1 – Beach Nourishment / Dredging

The migration of the ebb tidal bar toward the drift aligned shore of Rossbeigh and subsequent channel infilling has been identified as a key component of the recovery of Rossbeigh. It has been estimated it will take approximately 20 years for this to occur naturally, However, with human intervention this process could be speeded up. A beach nourishment scheme utilising dredged material from a borrow pit offshore of the ebb tidal bar was considered to be the most proficient method to speed up the natural migration pattern of ebb tidal bar.

The selection of a suitable borrow pit is critical to a successful nourishment scheme. Firstly the changes to the bathymetry of the borrow pit location due to dredging should not impact the morphological evolution. Secondly the borrow site material properties should match the nourishment location sediment properties as close as possible. Finally the distance from borrow pit to nourishment location should be kept to a minimum for two reasons, to ensure sediment property homogeneity and reduce pumping costs.

A borrow pit of over 1.5 Km x 2.0 Km, figure 7.11, was chosen as the most suitable location for the purposes of supplying sediment to the leading land

ward edge of the ebb tidal bar and the drift aligned shoreline. It is shallow sub tidal sand bank, that is the natural sediment source for the ebb tidal bar migration and is supplied by sediment deposition from the tidal inlet channel.

It was calculated that 650,000 m³ of dredged material would be required to fill the channel and weld the ebb tidal bar to the drift aligned shore of Rossbeigh to create a swash platform. To achieve this, an average dredged depth of 210 mm is required. However, depending on the retention rates on the beach, it is likely that an additional 30-50% dredge material would be needed. According to Mattis et al. (2004) who studied the dune recovery post nourishment on a beach in the Cacela Peninsula, Portugal, up to 32% of material was lost due to superficial drainage with another 33% lost after 25 months to erosion, figure 7.12.



Figure 7.11 Proposed borrow pit for beach nourishment of Rossbeigh

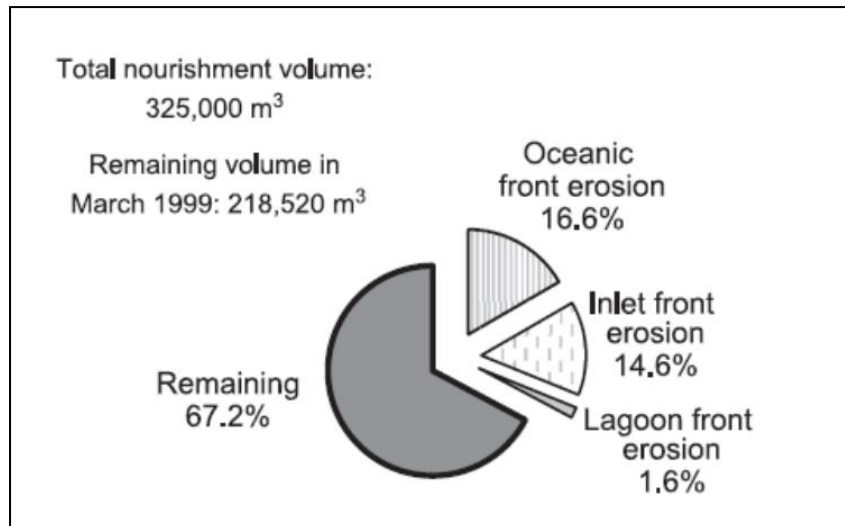


Figure 7.12 Percentage loss of dredged material (Matias et al. 2004)

The time to completion is dependent on the rate of infilling, the interaction of the fill material with tidal currents and the weather (wave) conditions. The rate of infilling depends on the type of dredging/pumping equipment used. Considering the shallow nature of the borrow pit, a barge mounted sand pump, deployed in summer time to minimise wave interference and over a neap tidal cycle would be suitable.

Due to the low head involved in dredging from the selected borrow pit (6-10 m) large pumping rates can be achieved with standard sand pumps. A typical rate is 700 m³/hour/pump. Assuming a 12 hour work day, this would take almost 80 days to complete using one pump and 20 days using four pumps. This would be achievable over a summer season. Alternatively a cutter suction dredger, figure 7.13 would complete the nourishment in several weeks but at a much higher cost.



Figure 7.13 Cutter suction dredger suitable for Rossbeigh beach nourishment

7.5.2 Stage 2 Sediment Fencing

The second stage of remediation is concerned with building the super tidal (above HWL) dune structure. When the intertidal zone of the drift aligned beach has stabilised and wave attenuation is occurring due swash platform as a result of the beach nourishment, the focus of regeneration is trapping wind-blown sediment. This has already been trialled with moderate success on Rossbeigh as documented in Section 4.2.5 and also earlier in this chapter, figure 7.14.

According to Table 8.7, the impact of sediment fencing on embryo dune growth is significant. During summer months with little wave erosive activity the dunes grew at a rate of up to 1 m/month. Installing two layers of the sediment fencing along the complete length of the breach and beyond to the Island section would be a cheap and effective method to accelerate embryo growth. Assuming stage one is completed over a 2 month period in late spring-early summer, the embryo dunes could effectively be 3-4 m high before winter storm driven erosion affects them with the aid of sediment fencing.



Figure 7.14 Aeolian fencing trials on Rossbeigh

7.5.3 Stage 3 Sediment Fencing

The final stage of the intervention strategy is planting suitable flora along the embryo dunes. This has two functions, the first is to anchor and bind the sediment into a fixed structure, the second is to enhance the capture ratio of aeolian sediment. The increased foliage on the dunes results on increased interference with wind flow resulting in a reduction in wind speed and increase in sediment deposition.

There are two types of vegetation suitable for dune re-establishment as recommended by An Taisce (2012). Lyme grass (*Leymus arenarius*) should be planted on the seaward facing dune edge below the Spring HWL. This can withstand total immersion in salt water. The planting of Marram grasses (*Ammophila arenaria*) is recommended above the water line as it can withstand salt spray but not total immersion in salt water. The recommended planting time for these grasses is September to April. This time frame suits the successive implementation of this stage immediately after stage 2.

7.5.4 Summary

While an outline method is provided above for the reestablishment of Rossbeigh to pre breach orientation, further analysis would be required to design a comprehensive recovery plan. The analysis presented herein has shown that such a recovery is possible within a short (6 month) time frame, providing that the right weather conditions occur and correct project planning and execution is undertaken.

However, considering the findings of this research particularly relating to Rossbeigh's long term evolutionary cycle, anthropogenic interference into the morphology is not advised. It has been established that Rossbeigh has previously been subject to severe erosion during its evolution. It has been shown through the present study that the Dunes have the potential to repair naturally with time. Any interference in this process could have significant impacts on the future morphology of the entire coastal cell.

7.6 Conclusion

In this chapter the results and conclusions of the preceding chapters were collated and combined to produce quantifiable conclusions on the evolution of Rossbeigh. A definitive conceptual model for the morphology of Inner Dingle Bay was identified and organised into 5 phases based on the data produced throughout this study. These phases are outlined in figure 7.15.

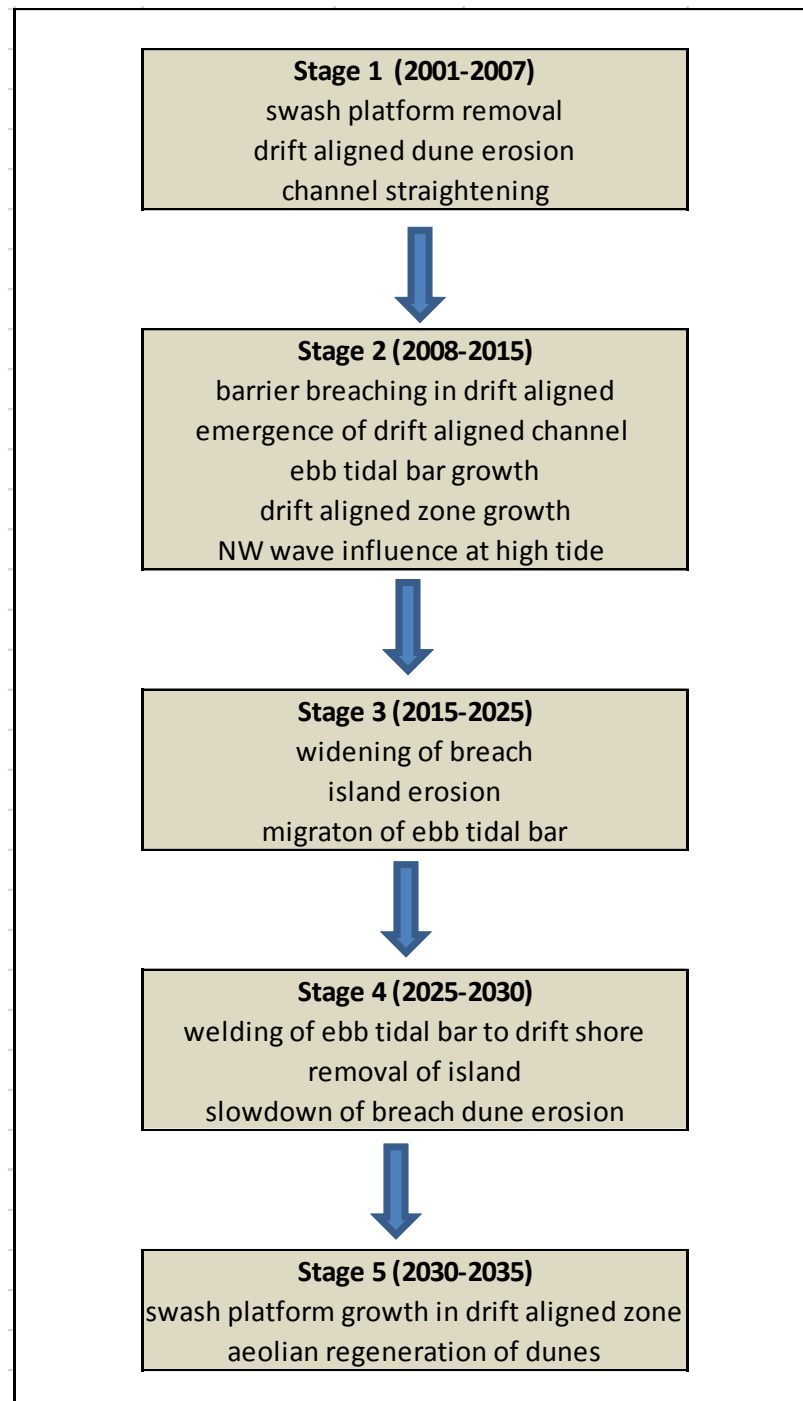


Figure 7.15 5 Phase evolution of Rossbeigh and Inner Dingle Bay

Three critical components of this model were identified as indicators of the evolutionary cycle, the maximum breach width, the migration time of the ebb tidal bar and aeolian regeneration of embryo dunes. Each of these components was assigned a timeline based on available information, data collected and literature from similar case studies.

The impact the breaching and evolution thereafter has on flooding in the low lying areas behind the barrier beach was examined and quantified. This was the first time a scientific study has identified a quantifiable change in water levels due to the breaching event in Rossbeigh and Inner Dingle Bay. An increase in wave height was also identified during the examination of the flood risk due to the evolution. This increases the threat of erosion in this area.

Finally, a methodology to accelerate the evolution of Rossbeigh and return it to its pre breach strategy was proposed. The strategy includes three stages, which if undertaken correctly would replenish the dunes and create a swash platform on Rossbeigh drift aligned shore in a 6 month time frame. This would provide a base for further natural dune reestablishment and beach growth. The intervention would also reduce the necessity for large flood defence schemes in the back barrier area, as storm wave heights and peak tidal elevations would be returned to stable pre breaching levels.

8 Conclusions

8.1 Introduction

The primary goals of this research as set out in Section 1.3 have been achieved. Through the use of field based and numerical research techniques, a clear understanding of the dynamics driving evolution in Inner Dingle Bay has been attained. This understanding has been distilled into a 5 phase conceptual model that outlines the future evolution of Rossbeigh and Inner Dingle Bay including the quantification of both timescales and sediment volumes.

A summary of conclusions is provided in this chapter, and the innovative aspects of the study are discussed. The characteristics of the coastal processes are also discussed. Conclusions on sediment transport characteristics and the long term evolution of the system are described in detail. Finally recommendations on further research and coastal protection works in Inner Dingle Bay are made and discussed.

8.2 Innovative Aspects of Study

To develop the understanding necessary to produce a conceptual model of Dingle Bay's evolution extensive field data and remotely sensed data collection was necessary. This comprised both experimental and established coastal monitoring methods. The study utilises novel sediment trend analysis, experimental HF Ocean radar technology and a new form of schematised long term morphological modelling.

- The design and commissioning of a surf zone survey craft was a major achievement of the field base research. This craft has provided bathymetry data from areas of unsuitable for traditional craft. Without the development of the nearshore survey craft detailed bathymetry of the ebb tidal bar and drift aligned channel would not have been possible. This data was essential in understanding the migration process of the ebb tidal bar.
- The performance of a HF ocean radar system to produce useful datasets in a dynamic narrow bay such as Dingle Bay was assessed during this research project. The success and limitations of this trial are discussed in Chapter 5. This includes an interpretation of results and discussion on errors. As a result of this radar trial a new method of wave radar data post processing analysis suitable for coastal applications was formulated and tested on the Dingle Bay dataset collected during the course of the radar trial.
- The successful application of GSTA to the complex beach system of Rossbeigh was a significant achievement. The validation of a new trend case makes the study important not only in terms of sediment transport in Inner Dingle Bay but also to the emerging field of sediment trends analysis.
- A robust 2-dimensional depth integrated hydrodynamic, fully coupled wave, sediment transport and morphological model has been created

and validated for Dingle Bay. This model has aided in the validation of the conceptual model presented in Chapter 4, provided data for the validation and troubleshooting for wave radar in Chapter 5 and is utilised to examine the flood risk in Chapter 7. However, the primary use of this model has been in the prediction of the morphodynamic evolution of Rossbeigh and Inner Dingle Bay utilising a new approach to long term modelling.

- Finally, this study has been the first of its kind to combine novel wave radar technology, aeolian transport measurement, grain size trend analysis, long term numerical morphological modelling, bathymetric profiling, satellite imagery analysis, wave and tidal current monitoring, sediment dye testing and sediment fencing to establish the evolution of a coastal system.

8.3 Characteristics of Governing Coastal Processes on Rossbeigh

A strong tidal flow combined with wave direction change at higher tidal elevations are found to be the main drivers of the erosion taking place on Rossbeigh. The following were found to be the main characteristics of these drivers:-

- The flood tidal currents flowing through a channel between the ebb tidal bar and drift aligned shoreline of Rossbeigh is the main pathway of sediment transport. The dune line is eroded at high tide by a wave forcing that is aligned at an angle to the typical shore normal wave direction. This wave angle is caused by refraction of the wave front due to a change in depth between tidal inlet channel and ebb tidal bar.
- As the ebb tidal bar grows in size, so does its influence on the wave direction incident at high tide in the drift aligned zone. As the bar widens the angled wave incident on the drift aligned shoreline increases in length. This increases the alongshore length of dune eroded at that angle. The result is the growth of the drift aligned zone of Rossbeigh at the expense of the stable swash aligned beach.
- When swash aligned erosion occurs usually during storm conditions, eroded sediment is deposited offshore in a shore normal direction, in calm weather this sediment is restored to the beach constituting a closed cycle. On the drift aligned shoreline, the eroded dune material is deposited in the intertidal zone, where tidal currents move it into the main tidal inlet channel on the flood tide and then offshore in the subsequent ebb tide. This results in a deficit in the local sediment budget and promotes the continuation of an erosive climate on the drift aligned shore.

8.4 Sediment Transport Pattern

To derive the sediment transport patterns in Dingle Bay, several techniques were utilised. These include interpreting bathymetric changes from surveys comparisons, grain size trend analysis based on sediment sampling, hydrodynamic field data collection and sediment transport modelling using numerical modelling software.

While there are some discrepancies between sources the general trends indentified by these sources agree on several fundamental features of the sediment transport regime:-

1. Sediment transport rates in the drift aligned zone are large relative to the swash aligned zone and generally in a shore parallel direction.
2. The ebb tidal delta is migrating shorewards with the area of the bar closest to the neck of the drift aligned channel migrating fastest.
3. Sediment deposition offshore is governed by the alignment of the main tidal inlet channel. The majority of the sediment eroded from the drift aligned shore is transported offshore and deposited seaward of the ebb tidal bar.
4. The shoreward migration of the ebb tidal bar is driven by the supply of sediment deposited offshore by the tidal inlet currents. Wave action is moving this deposited sediment shoreward and on to the ebb tidal bar.

The sediment deposited in the intertidal zone by wave action is then transported in a shore parallel direction off the beach and into the main tidal inlet channel. This sediment is then deposited further offshore. It has been shown in sediment transport simulations that the sediment deposited offshore is gradually moving onto the ebb tidal bar by wave action and tidal current. This sediment transport cycle is driving the growth of the ebb tidal bar, this growth is clearly visible in last decade since breaching processes initiated.

8.5 Long Term Behaviour

The long term behaviour of Inner Dingle Bay has been investigated by combining trends from successive bathymetric surveys with a numerical morphodynamic model. The simulations predicted that erosion on the dunes will continue for another 20 years approximately.

- This behaviour is governed by the tidal channel between the ebb tidal bar and drift aligned shoreline. A return to equilibrium on the drift aligned zone of Rossbeigh will not occur until this channel is infilled by the shoreward migration of the ebb tidal bar.
- Currents in the drift aligned channel are moving all eroded sediment offshore via the main tidal inlet channel, therefore removing the opportunity for the beach and dune to regenerate during calm weather.
- The infilling of the channel will occur when the welding of the ebb tidal bar to the drift aligned shoreline is completed. This bar will become an extended swash platform that forces waves to break further offshore from the dune line, therefore reducing erosion. This swash platform will also provide the sediment supply for embryo dune re formation. This evolution is described in a 5 stage conceptual model in Chapter 8.
- The simulations have predicted that the Island section of Rossbeigh will be eroded to below the high tide line before regeneration commences.
- The breach width will grow to 1.4 Km prior to the morphodynamic climate returning to an accretive nature.

8.6 Assessment of Experimental techniques

During the course of this research several experimental coastal research techniques were trialled. Two of these trials have yielded significant conclusions on the applicability of the techniques to a coastal system such as Dingle Bay. The techniques were HF Ocean Radar and grain size trend analysis.

The comprehensive 6 week trial of the WERA wave radar system in Dingle Bay provided mixed results. This trial was the first to be conducted at such a large bandwidth in a dynamic environment like Dingle Bay. The two station set-up yielded significant amounts of erroneous plots, with wave height plots largely incomprehensible and surface current plots showing large banding errors.

The errors prompted the development of a new post processing technique based on transect analysis of the entire data set one timestep at a time. This methodology reduced the amount of error in the plots, however, a persistent radial banding interference remained. This error rendered the conclusions drawn from the plots unreliable and not useful in morphodynamic analysis which was the original purpose of the HF Ocean Radar trial. In some instances the radar generated surface plots reflected several features identified in other monitoring techniques conducted during this research, however, given the erroneous nature of the majority of the plots no definitive conclusions could be derived from the dataset.

The trial has shown that while wave radar has the potential to monitor surface currents and waves on a large spatial resolution in a dynamic bay, further work is needed in both the set-up approach and post processing analysis of data.

The more successful trial of grain size trend analysis (GSTA) produced a viable result. The suitability of the FP+ scenario, as reported in Chapter 5, is the first time that this case has described the sediment transport climate of a

barrier beach - ebb tidal bar system. The magnitude and direction of the majority of transport vectors agree with surveyed transport trends and to a large extent with the numerically modelled sediment transport vectors.

The one exception being the general direction of the ebb tidal bar sediment transport, the numerical model appears to have a bias for tidal transport thus the majority of the vectors are angled in the direction of the main inlet channel. However, the GSTA FP+ cases show the main sediment trends on the ebb tidal bar are moving in a more shore normal direction towards the drift aligned shore line. This would suggest that the transport on the bar is dominated by the incident wave direction rather than the tidal current direction. This is confirmed by successive surveys of the bar and channel which suggests that the bar is migrating at present in the direction of the FP+ trend vectors.

This finding has also raised the issue of the validity of the timeline inferred from the numerical modelling. If the numerical model is underestimating the significance of wave action moving the sediment on the ebb tidal bar shoreward, the time to bar welding could be reduced and regeneration could initiate before the 20 year approximation of numerical simulations.

8.7 Further Research Recommendations

8.7.1 Field Data and Numerical Modelling

From the results of this study it is apparent that with regular data collection and robust numerical modelling it is possible to make predictions on the evolution of a coastal system. The accuracy of morphological predictions depends not only on the accuracy of the data but also on the amount of successive data sets acquired. It is recommended that seasonal surveys of both beach and bathymetry on Rossbeigh be conducted. Integrating this data with the numerical model will enable the monitoring of evolution on an ongoing basis and compare results with the work outlined in this study. This is essential for improving the accuracy of the simulations.

To further enhance the accuracy of morphological modelling, wave climate studies in Dingle should be continued. By building a dataset of wave and tidal current recordings a more comprehensive representation of the sediment transport forcings can be simulated.

8.7.2 Wave Radar

Despite the errors in wave radar trial's surface current and wave height data plots, the potential for Wave radar to provide accurate data sets of Dingle bay still exists. Post processing work is ongoing to eradicate the radial banding error that interfered with real data recordings. It is planned to develop a methodology to remove all sources of error using the transect method. However, the source of the radial banding is yet to be identified.

8.7.3 Intervention

The first step to take before any human intervention with a coastal system is to gain an understanding of the coastal processes driving sediment transport in the area of interest. This study contains a body of information that would constitute such an understanding. A description of the best strategy of interventions is also provided in Chapter 8. However, before any work is initiated in Rossbeigh or the surrounding area, a simulation of that work should be undertaken. This would not be an onerous undertaking given the

existence of a validated fully coupled sediment transport model of the entire area as a result of this research.

If a dredging nourishment programme is selected as a means of restoring Rossbeigh to a stable configuration. The impact of such work should be analysed comprehensively. An analysis of the wave and tidal current patterns, as well as of the sediment transport trends on pre and post dredged/nourished bathymetries is a relatively straightforward but a valuable undertaking.

8.7.4 Flood protection

Analysis undertaken as part of this research shows that the threat of increased flooding in storm conditions due to the evolution of inner Dingle Bay has increased. The reasons for this increase in flood risk are due to an increase in wave height in the back barrier area and an increase in maximum tidal height during spring tides. The increase in wave height is caused by a deepening of the inlet channel an issue that is not likely solved by the intervention strategy described above and in detail in Chapter 8.

Considering this, it is recommended that the historical dikes and flood defences in the area surrounding Cromane lower should be enlarged and strengthened. The extent and height of this flood defence renovation work could also be designed using the numerical model created for this research. The topography in the model can be augmented to represent numerous variations in flood defence heights and lengths to ensure the most effective and economic solutions is achieved.

8.8 Closure

This thesis has presented the results of a 4 year long study of a dynamically evolving coastal system. The coastal processes driving this evolution have been described and quantified using established and experimental methods. A timeline of the evolution of Inner Dingle Bay has been formulated based on the results of these methods. The dynamic evolution has been predicted to slow down over the next 20 years after which the coastal system will return to a slower morphodynamic phase of evolution.

References

- Austin M and Brown J, 2009 Macrotidal Rip Current Experiment: Circulation and Dynamics. *J. Coastal Res.*, SI 56, 24–28.
- Bagnold, R. A, "Experiments on a gravity-free dispersion of large solid spheres in a Newtonian fluid under shear", Royal Society London, Proceedings, Series A, v 225. pp. 49-63, 1954.
- Baldock T, Weir F, and Hughes M, "Morphodynamic evolution of a coastal lagoon entrance during swash overwash," *Geomorphology*, vol. 95, pp. 398-411, 2008.
- Balouin, Y. and. Howa H, "Sediment transport pattern at the Barra Nova inlet, south Portugal: a conceptual model." *Geo-Marine Letters* **21**(4): 226-235. 2001.
- Barrick D., "First-order theory and analysis of MF/HF/VHF scatter from the sea", *IEEE Transactions on Antennas and Propagation*, AP- 20, 2-10, 1972.
- Battjes, J.A.. Surf similarity, Proceedings of 14th Coastal Engineering Conference, Copenhagen, Denmark, American Society of Civil Engineers, New York, pp.466-480, 1974.
- Bertin X., Deshouillieres A., Allard J., Chaumillon E.,. A new fluorescent tracers experiment improves understanding of sediment dynamics along the Arcay Sandspit (France), *Geo-Marine Letters*, 27: 63–69, 2007
- Blott, S.J. and Pye, K. GRADISTAT: a grain size distribution and statistics package for the analysis of unconsolidated sediments. *Earth Surface Processes and Landforms* 26, 1237-1248, 2001.
- Boak E., Turner I, 2005. Shoreline Definition and Detection: A Review. *Journal of Coastal Research*, 688-703.
- Buynevich I and Donnelly J "Geological Signatures of Barrier Breaching and Overwash, Southern Massachusetts, USA," *Journal of Coastal Research*, pp. 112-116, 2006.
- Cayocca, F. Long-term morphological modeling of a tidal inlet: the Arcachon Basin, France, *Coastal Engineering*, Volume 42, Issue 2, Pages 115-142, 2001.

- Chadwick H, Gehrels W, Massey A, O'Brien D and Dales D, "A new analysis of the Slapton barrier beach system, UK," Proceedings of the ICE - Maritime Engineering, vol. 158, pp. 147 –161, 2005.
- Chadwick, A J, and Morfett, J C. Hydraulics in Civil and Environmental Engineering (3rd edition). Chapman & Hall (600 pp), 1998.
- CEM, Coastal Engineering Manual U.S. Army Corps of Engineers. Engineer Manual 1110-2-1100, U.S. Army Corps of Engineers, Washington, D.C. 2002.
- Coastal Engineering Research, C., United, S., Shore protection manual / [prepared for Department of the Army, US Army Corps of Engineers]. Dept. of the Army, Waterways Experiment Station, Corps of Engineers, 1984.
- Cochin, V et al.,. SURLITOP experiment in West Brittany: Results and validation. Proceedings of Radiowave Oceanography Workshop (ROW-6), Hamburg, Germany. 2006.
- Cope, S.N. Breaching of UK coarse clastic barrier beach systems: methods developed for predicting, breach occurrence, stability and flooded hinterland evolution. PhD Thesis, University of Portsmouth, 281p, 2004.
- ConScience, Concepts and Science for Coastal Erosion Management. http://www.conscience-eu.net/inch_beach/index.htm, 2010.
- Cooper J and Jackson D, "Geomorphology of a high-energy barrier island on the rocky west coast of Ireland," Journal of Coastal Research, pp. 6-9., 2011
- Cooper J, McKenna J, Jackson D and O'Connor M, "Mesoscale coastal behaviour related to morphological self-adjustment," Geology, vol. 35, pp. 187-190, February 1, 2007.
- Crombie D, "Doppler spectrum at sea echo at 13.56 Mc/s", Nature, 175, pp.681-682, 1955.
- Dean, R.G. "Heuristic Models of Sand Transport in the Surf Zone," Proceedings of the First Australian Conference on Coastal Engineering, Sydney, Aus., pp 208-214. 1973.
- De Chant LJ. The Venerable 1/7th Power Law Turbulent Velocity Profile: A Classical Nonlinear Boundary Value Problem and Its Relationship to

- Stochastic Processes. Applied Mathematics and Computation.161:463-474, 2005;
- Devoy, R.J.N., Delaney, C., Jennings, S., Controls on medium to long term organogenic salt marsh sedimentation under rising relative sea-level along the western European (East Atlantic) margin: evidence from Dingle Bay, western Ireland. . European Commissions Impacts Project Contract no EV5V-GT93-0266. 2006.
- Delgado-Fernandez, I, Jackson, D.W.T., Cooper, J.A.G., Baas, A.C.W., Beyers, J.H. and Lynch, K. Field characterization of three-dimensional lee-side airflow patterns under offshore winds at a beach-dune system. Journal of Geophysical Research – Earth Surface, 118. pp. 706-721. 2013.
- Deltares 2010a. Delft3D-FLOW. Simulation of multi-dimensional hydrodynamic flow and transport phenomena, including sediments – User Manual. Version 3.04, rev. 11114. Deltares, Delft, The Netherlands. 2010
- Deltares 2010b. Delft3D-WAVE. Simulation of short-crested waves with SWAN – User Manual. Version 3.04, rev. 11114. Deltares, Delft, The Netherlands. 2010.
- De Vriend, H. J., M. Capobianco, T. Chesher, H. E. De Swart, B. Latteux, and M. J. F. Stive, Approaches to long term modeling of coastal morphology: A review, Coastal Eng., 1993.
- De Vries, S., van Thiel de Vries, J., van Rijn, L., Arens, S., Ranasinghe, R. Aeolian sediment transport in supply limited situations, Aeolian Research, Volume 12, Pages 75-85, ISSN 1875-9637, 2013.
- DHI, 'MIKE 21: Sediment Transport and Morphological Modelling – User Guide', DHI Water and Environment, Hørsholm, Denmark, pp388. 2007.
- Dijkman, J, "Some Characteristics of the USP-61 and Delft Bottle." Delft University of Technology, Dep. of Civ.Eng., Int. Report No. 5-78, The Netherlands, ., 1978
- Duffy, M. J. and R. J. N. Devoy. 1998. Contemporary process controls on the evolution of sedimentary coasts under low to high energy regimes: western Ireland. Geologie en Mijnbouw 77 (3):333–349.

- Escoffier F, "The Stability of Tidal Inlets," *Shore and Beach*, vol. VIII, 1940.
- FitzGerald D, Kraus N, et al. Natural mechanisms of sediment bypassing at tidal inlets, US Army Corps of Engineers Vicksburg, MS. 2000.
- Giese G, Mague S, and Rogers S, "A Geomorphological Analysis of Nauset Beach/Pleasant Bay/Chatham Harbour For the Purpose of Estimating Future Configurations and Conditions," Provincetown Center for Coastal Studies 2009.
- Gourlay, M.R. Beach and dune erosion tests. Delft Hydraulics Laboratory, Report No. M935/M936, May 1968.
- Gracia, V., García, M., Grifoll, M. and Sánchez-Arcilla, A.,. Breaching of a barrier beach under extreme events. The role of morphodynamic simulations In: Conley, D.C., Masselink, G., Russell, P.E. and O'Hare, T.J. (eds.), *Proceedings 12th International Coastal Symposium (Plymouth, England)*, *Journal of Coastal Research*, Special Issue No. 65, pp. 951-956, ISSN 0749-0208. 2013.
- Hallermeier, R.J., Rhodes, P.E.. Generic treatment of dune erosion for 100-year event. 1988.
- Haza, A.C., T.M. Özgökmen, A. Griffa, A. Molcard, P.M. Poulain and G. Peggion,; Transport properties in small scale coastal flows: relative dispersion from VHF radar measurements in the Gulf of La Spezia. *Ocean Dynamics*, 60, 2010.
- Helley, E.J. and Smith, W., *Development and Calibration of a Pressure-Difference Bed Load Sampler*. U.S. Geological Survey Open File Report, Washington, USA. 1971
- Heron, M.L.; O'Shea, M.; Murphy, J.; Petersen, L.; Mollaghan, D.; Prytz, A., "Interpretation of VHF radar echoes from a complex flow field," *Oceans - San Diego, 2013* , vol., no., pp.1,4, 23-27 Sept. 2013.
- Herrling, G. and Winter, C.: Morphological and sedimentological response of a mixed-energy barrier island tidal inlet to storm and fair-weather conditions, *Earth Surf. Dynam.* 2013.
- Houser C, Hapke C, and Hamilton S, "Controls on coastal dune morphology, shoreline erosion and barrier island response to extreme storms," *Geomorphology*, vol. 100, pp. 223-240, 2008.

- Irish, J.L., White, T.E., 1998. Coastal engineering applications of high-resolution LiDAR bathymetry. *Coastal Engineering* 35, 47-71.
- Isla, F. and Bujalesky, G. Cannibalisation of Holocene gravel beach-ridge plains, northern Tierra del Fuego, Argentina, *Marine Geology*, Volume 170, Issues 1–2, 2000.
- Jackson D, Cooper J, and del Rio L, "Geological control of beach morphodynamic state," *Marine Geology*, vol. 216, pp. 297-314, 2005
- Kamphuis, J., 1991. Alongshore Sediment Transport Rate. *Journal of Waterway, Port, Coastal, and Ocean Engineering* 117, 624-640.
- Karunarathna, H., Reeve, D.E. and Spivack, M. Beach profile evolution as an inverse problem, *Continental Shelf Research*, Vol. 29, pp.2234-2239. 2009.
- KerrysEye. High Tides Bring Food Threat, *The Kerrys Eye* pp. 8. 2010.
- Kraus N, Militello A, and Todoroff G, "Barrier Breaching Processes and Barrier Spit Breach, Stone Lagoon, California," *Shore & Beach*, vol. 70, 2002.
- Kriebel, D.L., Dean, R.G. Numerical simulation of time-dependent beach and dune erosion. *Coastal Engineering* 9, 221-245. 1985
- Latteux, B. Techniques for long-term morphological simulation under tidal action, *Marine Geology*, Volume 126, Issues 1–4, Pages 129-141, 1995.
- MacMahan, J. ,Hydrographic surveying from personal watercraft. *Journal of Surveying Engineering* 127, 12-24. 2001.
- MacMahan, J. Thornton, E., Reniers, A, Rip current review, *Coastal Engineering*, Volume 53, Issues 2–3, 2006
- Mason, D.C. and Garg, P.K . Morphodynamic modelling of intertidal sediment transport in Morecambe Bay. *Estuarine, Coastal and Shelf Science*, 53, 79-92. 2001
- Masselink G and Short A, "The Effect of Tide Range on Beach Morphodynamics and Morphology: A Conceptual Beach Model," *Journal of Coastal Research*, vol. 9, pp. 785-800, 1993.
- Matias, A., Ferreira, Ó., Mendes, I., Dias, J., and Vila-Concejo, A., Artificial Construction of Dunes in the South of Portugal. *Journal of Coastal Research* 213, 472-481. 2004

- McComb, P.J. and Black K.P. Detailed observations of littoral transport using artificial sediment tracing, wave and circulation measurements and numerical model studies in a high-energy, rocky reef and black sand environment. *Journal of Coastal Research*. 21, 358-373. 2005.
- McLaren, P. An interpretation of trends in grain size measures *Journal of Sedimentary Research* June 1, 1981 51:611-624, 1981.
- Michel D and. Howa H, "Morphodynamic behaviour of a tidal inlet system in a mixed-energy environment," *Physics and Chemistry of The Earth*, vol. 22, pp. 339-343, 1997.
- Moore, L.J., 2000. Shoreline Mapping Techniques. *Journal of Coastal Research* 16, 111-124.
- Moni, A., S. Donne, C. Bean, D. Craig, M. Mollhoff, F. Hauser, A. Braiden, K. Lambkin, C. Creamer and M. White. Towards ocean wave energy-potential quantification from a terrestrially-based seismic observation system. 4th International Conference on Ocean Energy, Dublin, Ireland. 2012.
- Nickling, W.G., McKenna Neuman, C. Wind tunnel evaluation of a wedge-shaped aeolian sediment trap. *Geomorphology* 18, 333–345. 1997.
- Ohlmann, J.C., P.F. White, L. Washburn, E. Terrill, B. Emery, and M. Otero. Interpretation of coastal HF radar derived surface currents with high-resolution drifter data. *Journal of Atmospheric and Oceanic Technology* 24:666–680. 2007.
- Orford, J.D., Carter, R.W.G. And Jennings, S.C. Control Domains and Morphological Phases in Gravel-dominated Coastal Barriers., *Journal of Coastal Research*, 12, 589-605. 1996.
- O'Shea M., Murphy J. and Sala, P., 2011. Monitoring the morphodynamic behaviour of a breached barrier beach system and its impacts on an estuarine system. OCEANS'11 IEEE Conference, Santander, Spain.
- Panigrahi, Ananth P, Umesh P, Coastal morphological modelling to assess the dynamics of Arklow Bank, Ireland, *International Journal of Sediment Research*, Volume 24, Issue 3, Pages 299-314, 2009
- Petitjohn, F.G., Ridge, J.D.,. A textural variation series of beach sands from Cedar point. *Ohio J. Sediment. Petrol.* 2 (2), 76–88. 1938.

- Poizot E, Mear Y, Thomas M, Garnaud S. The application of geostatistics in defining the characteristic distance for grain size trend analysis. *Comput Geosci* 32(3):360–370. 2006.
- Poizot E, Méar Y. ECSedtrend: a new software to improve sediment trend analysis. *Comput Geosci* 34(7):827–837. 2008
- Poizot E, Anfuso G, Méar Y, Bellido C. Confirmation of beach accretion by grain-size trend analysis: Camposoto beach, Cádiz, SW Spain. *Geo-Mar Lett* 33(4):263–272. 2013
- Poulos, S., Ballay, A.,. Grain-size trend analysis for the determination of non-biogenic sediment transport pathways on the Kwinte Bank (southern North Sea), in relation to sand dredging. *J. Coast. Res.* 51, 87–92. 2010.
- Priestas AM, Fagherazzi, S. Morphological barrier island changes and recovery of dunes after Hurricane Dennis, St. George Island, Florida. *Geomorphology*. 2010
- Pye K and Blott S, "Progressive breakdown of a gravel-dominated coastal barrier, dunwich-walberswick, suffolk, U.K.: Processes and implications," *Journal of Coastal Research*, vol. 25, pp. 589-602, 2009.
- Roelvink, J.A. Coastal morphodynamic evolution techniques, *Coastal Engineering*, 53, 277-287. 2006.
- Saini, S., Jackson, N.L., Nordstrom, K.F. Depth of activation on a mixed sediment beach. *Coastal Engineering*, 56, 788-791. 2009.
- Sala, P.,. Morphodynamic Evolution of a Tidal Inlet Mid-bay Barrier System. Cork, Ireland: University College Cork, Master's thesis. 2010.
- Sanderson P and Eliot I "Compartmentalisation of beachface sediments along the south-western coast of Australia," *Marine Geology*, vol. 162, pp. 145-164, 1999.
- Smyth TAG, Jackson DWT, Cooper JAG. Computational Fluid Dynamic modelling of Three-Dimensional airflow over dune blowouts. *Journal of Coastal Research* **SI 64** : 314-318. 2011.
- Soulsby, R.L., Dynamics of marine sands—A manual for practical applications: London, Thomas Telford Publications, 249 p. 1997.

- Stéphan, P. Les fleches de galets de Bretagne: morphodynamiques passée, présente et prévisible. Laboratoire Géomer, Université de Bretagne Occidentale. PhD: 2009.
- Stumpf, R.P., Holderied, K., Sinclair, M., 2003. Determination of water depth with high-resolution satellite imagery over variable bottom types. *Limnology and Oceanography* 48, 547-556.
- Suanez S., Cariolet J.M., Cancouët R., Ardhuin F. et Delacourt C. Dune recovery after storm erosion on a high energy beach: Vougot beach, Brittany (France). *Geomorphology* ,2011.
- SWAN User Manual, Delft University of Technology, 2006.
- Terchunian A and Merkert C, "Little Pikes Inlet, Westhampton, New York," *Journal of Coastal Research*, vol. 11, pp. 697-703, 1995.
- Unesco-IHE, Deltares, TU Delft. XBeach model description and manual, 2009.
- van Son R, M A de Schipper R, de Vries S and Duijnmayr K. Monitoring bathymetric changes at storm scale, Technical Application. Delft University of Technology. 2010
- van Rijn, L.C.,. Principles of coastal morphology. Aqua Publications: Amsterdam.1998
- van Rijn, L.C., .Prediction of dune erosion due to storms. *Coastal Engineering* 56, 441-457.2009.
- Vial, T.,. Monitoring the Morphological Response of an Embayed High Energy Beach To Storms and Atlantic Waves. Cork, Ireland:University College Cork, Master's Thesis. 2008.
- Vila-Concejo, A., Ã. Ferreira, et al. "The first two years of an inlet: sedimentary dynamics." *Continental Shelf Research* **23**(14â€“15): 1425-1445. 2003.
- Vila-Concejo, A., Ã. s. Ferreira, et al. "Tracer studies on the updrift margin of a complex inlet system." *Marine Geology* **208**(1): 43-72. 2004.
- Walstra D, van Rijn L, van Ormond M, Briere C, and Talmon A, "The Effects of Bed Slope and Wave Skewness on Sediment Transport and Morphology," New Orleans, Louisiana, 2007.
- Weir F, "Berm Morphodynamics Fronting Coastal Lagoons," in *School of Geosciences*. vol. PhD Sydney: University of Sydney, 2007, p. 172.

- WHITE, T. E. Status of measurement techniques for coastal sediment transport. *Coastal Engineering*,35, 17–45. 1998..
- Xie, D.; Wang, Z.; Gao, S. & de Vriend, H. J. Modelling the tidal channel morphodynamics in a macro-tidal embayment, Hangzhou Bay, China. *Continental Shelf Research*, Vol.29, pp. 1757-1767. 2009.